AN ABSTRACT OF THE THESIS OF

Laura J. Snow for the degree of Master of Science in Oceanography presented on January 24, 2003
Title: Hydrothermal Links Between Ocean Plateau Formation and Global Anoxia at the Cenomanian-Turonian Boundary

Redacted for Privacy

Abstract approved: _____
Robert A. Duncan

The Cretaceous was a period of extreme climatic conditions accompanied by major perturbations in ocean-atmosphere biogeochemical cycles. One of the most intriguing features is the sporadic interruption of normal marine pelagic sediment deposition by organic rich sediments deposited during oxygen-deficient conditions (ocean anoxic events - OAEs). A current model for the abrupt onset and conclusion of these events relates increased trace metal delivery to the ocean during volcanic activity associated with ocean plateau construction, to the eventual depletion of oxygen and deposition of organic rich sediments. A majority of the trace metals are most likely released in eruption related "event plumes", degassed magmatic fluids mixed with seawater, rather than typical hydrothermal activity dominated by water/rock exchange. An important aspect of volcanic "event plumes" is that trace element concentrations are controlled by volatility into magmatic gases rather than solubility in water-rock reactions and therefore, the abundance pattern of released elements is fundamentally distinct from background hydrothermal venting.

This study specifically evaluates a proposed link between "event plumes" associated with the construction of the Caribbean ocean plateau and OAE2 at the Cenomanian/Turonian (C/T) boundary (~93 Ma) by examining five globally distributed C/T boundary sedimentary sections for major, minor and trace elemental abundance patterns. Resulting trace metal anomalies are evaluated in terms of their timing and relationship to the other major biogeochemical perturbations at this time.

After normalizing element concentrations to Zr to remove the effect of variable terrigenous input to these sediments, an interval of metal anomalies, at approximately the same stratigraphic location, is present in four of the five sites. I interpret the presence of metal abundance anomalies, and their stratigraphic position relative to events associated with OAE2, to suggest that hydrothermal activity could be the causative agent in pushing the ocean abruptly into anoxia. Also, the changes in trace metal patterns and intensities at all five sites are consistent with a source of metals being the Caribbean ocean plateau and modeled late-Cretaceous surface circulation.

Hydrothermal Links Between Ocean Plateau Formation and Global Anoxia at the Cenomanian-Turonian Boundary

by
Laura J. Snow

A THESIS
submitted to
Oregon State University

in partial fulfillment of
the requirements for the
degree of

Master of Science

Presented January 24, 2003
Commencement June 2003

Master of Science thesis of Laura J. Snow presented on January 24, 2003.

APPROVED:

Redacted for Privacy

Major Professor, representing Oceanography

Redacted for Privacy

Dean of the College of Oceanic and Atmospheric Sciences

Redacted for Privacy

Dean of the Graduate School

I understand that my thesis will become part of the permanent collection of Oregon State University libraries. My signature below authorizes release of my thesis to any reader upon request.

Redacted for Privacy

Laura J. Snow, Author

ACKNOWLEDGEMENTS

First of all, I would like to thank my advisor Bob Duncan for making this work possible, as well as providing lots of support and feedback through the whole process. Thanks to Gary Klinkhammer and Jim McManus for serving on my committee and providing great feedback as well. A big thank you to Andy Ungerer, Bobbi Conard, Dale Hubbard and Brian Haley for teaching me the ways of the lab, the microwave, and the mass spectrometer, and providing lots of entertainment throughout the entire process. Thanks to Tim Bralower, Maya Elrick, Andy Bowman and Linda de Romero for willingly sharing samples and data.

Thanks to Irma for getting me here to Oregon and for Sue and Linda for all the chats. Thanks to Heather and Matt for being some of the best roommates I could have and for putting up with my "sue-isms". Thanks to all the people I played soccer, frisbee and softball with. You kept me in shape, sane and made my time here in Oregon that much more enjoyable.

Lastly, I would like to thank Sadie (the dog) for providing stress relief and being a great hiking partner and my family, for just being a great family full of love and support.

CONTRIBUTION OF AUTHORS

Dr. Robert Duncan was involved in the design and writing of this thesis. Dr. Tim Bralower, Dr. Maya Elrick, Andrew Bowman and Linda De Romero assisted with sample collection and shared unpublished data from their research.

TABLE OF CONTENTS

TABLE OF CONTENTS (Continued)

Page

TABLE OF CONTENTS (Continued)

Page

LIST OF FIGURES

LIST OF FIGURES (Continued)

Figure Page

LIST OF FIGURES (Continued)

Figure Page

LIST OF TABLES

LIST OF APPENDICES

Hydrothermal Links between Ocean Plateau Formation and Global Anoxia at the Cenomanian-Turonian Boundary

Chapter 1: The Black Shale – Ocean Plateau Connection

Introduction

Earth's climate during the Cretaceous period (144 - 65 Ma by the Harland et al., 1990 time scale) was significantly different from that of the present. This time interval is often referred to as the "greenhouse world" because CO_2 levels were higher (ranging from 3-12 times pre-industrial pCO_2; Berner, 1994) and temperatures on land and in the ocean were much warmer than today. In fact, oxygen isotope data indicate that deep ocean temperatures were up to 10-12°C warmer than today (Brass et al., 1982). The Cretaceous was also characterized by a general absence of polar ice caps, reduced temperature gradients from the equator to the poles, higher sea levels due to a combination of a lack of glacial ice as well as thermal uplift of the sea floor, and increased rates of volcanic activity (Schlanger et al., 1981). The surfacing and melting of a mantle "superplume" in the Pacific basin has been credited by Larson (1991 a, b) as the cause for a 50-100% increase in ocean crust production and the formation of a number of rapidly-erupted Large Igneous Provinces (LIPs) on land and in the ocean basins (e.g. Duncan and Richards, 1991; Coffin and Eldholm, 1994).

One of the most intriguing features of the Cretaceous is the interruption of normal marine sediment deposition by a number of distinct, ocean-wide anoxic episodes (Schlanger and Jenkyns, 1976; Jenkyns, 1980; Arthur et al., 1990). These

intervals are characterized by finely laminated, organic rich sediments deposited in oxygen-deficient conditions, accompanied by a distinct positive $\delta^{13}C$ isotopic excursion in both carbonate and organic carbon sediment fractions. Schlanger and Jenkyns (1976) termed these periods "Oceanic Anoxic Events" (OAEs) and, over the past three decades, the origin of these black shales and the geological and climatic processes that brought them about has received much attention. However, despite extensive research in this area, there is still considerable debate about the causes of these OAEs.

In the past ten years, increasingly precise radiometric dating of mid- to late-Cretaceous LIPs, particularly oceanic plateaus, indicates that these major volcanic events correlate with ocean-wide anoxic events (Larson, 1991b; Erba, 1994; Bralower et al., 1997). Leary and Rampino (1986) also noticed a correlation between mass extinctions, ocean anoxic events and flood basalt volcanism. Does this temporal coincidence mean that these phenomena are related? If so, what signals might we look for in the sedimentary sections to mark the presence and effects of the significant volcanic activity? Orth et al. (1993) found high abundances of trace metals in a number of sedimentary sequences deposited about the time of the Cenomanian/Turonian (C/T) boundary, ~93 Ma, and attributed them to increases in volcanic activity during this time. It has been suggested by a number of people that hydrothermalism associated with large-scale submarine volcanic events was partly responsible for the decreased levels of O_2 and deposition of black shales (e.g., Vogt, 1989; Orth et al., 1993; Erba, 1994). More recently,

Sinton and Duncan (1997) hypothesized that metal-rich, eruption-related hydrothermal "event plumes" attending ocean plateau construction may have promoted black shale events. However, an actual causal relationship between these two, if it exists, is still unclear.

The main goal of this study is to expand on Sinton and Duncan's (1997) hypothesis and better determine a specific link between anoxic events and LIP-generated hydrothermal "event plumes" during the Cretaceous. To accomplish this, I have measured the distribution of major, minor and trace element abundances, specifically examining evidence for trace metal abundance anomalies in pelagic carbonate and black shale sequences from a number of sites around the world. An important aspect of "event plume" hydrothermalism is that the chemical exchange of elements to seawater from erupted magmas is controlled by volatility during high temperature degassing of magmas as well as low temperature water-rock solubility. Therefore, the abundance pattern of elements released to seawater is different from those derived from typical steady-state hydrothermal vents, providing us with a suite of elements diagnostic of "event plume" activity. The stratigraphic position of any trace metal abundances will determine the timing of any "event plumes" with respect to the onset of anoxia, as well as to other biogeochemical responses (e.g. species contraction or expansion, seawater carbon and strontium isotopic changes). Also, by looking at the abundance patterns and global distribution of these trace elements, information will be gained about the source and global dispersal of "event plume" hydrothermal activity.

Background

Global Anoxic Events

There is considerable evidence of intermittent widespread episodes of anoxia throughout the Cretaceous oceans (Figure 1) (Schlanger and Jenkyns, 1976). However, the cause for these periods of global anoxia is a highly debated topic. In the present ocean, two different marine environments give rise to anoxia and the deposition of organic carbon rich, anaerobic sediments. The first is expanded and intensified oxygen minimum zones underlying highly productive upwelling areas (e.g., Gulf of California). Due to the high rain of organic matter from productive surface waters, water column oxygen contents are drawn down leading to rapid burial of organic matter and high sediment accumulation rates. The second is stagnant, semi-enclosed basins with restricted circulation (e.g. the Black Sea). Here, oxygen levels are low enough that remineralization is reduced and more organic material from the photic zone can be deposited. Restricting oxygen-rich ocean waters from entering the basin keeps oxygen levels low enough that even a small amount of primary production can lead to anoxia. However, Cretaceous black shale sequences are not confined to isolated basins cut off from oxygenated bottom water or to upwelling areas. Instead, these organic carbon rich sediments are found in sequences from ocean plateaus, ocean basins, and continental margins as well as shallow and shelf seas. The global extent of these events suggests that they were not formed by local conditions (restricted circulation/upwelling conditions) but were instead produced by some global condition. The global

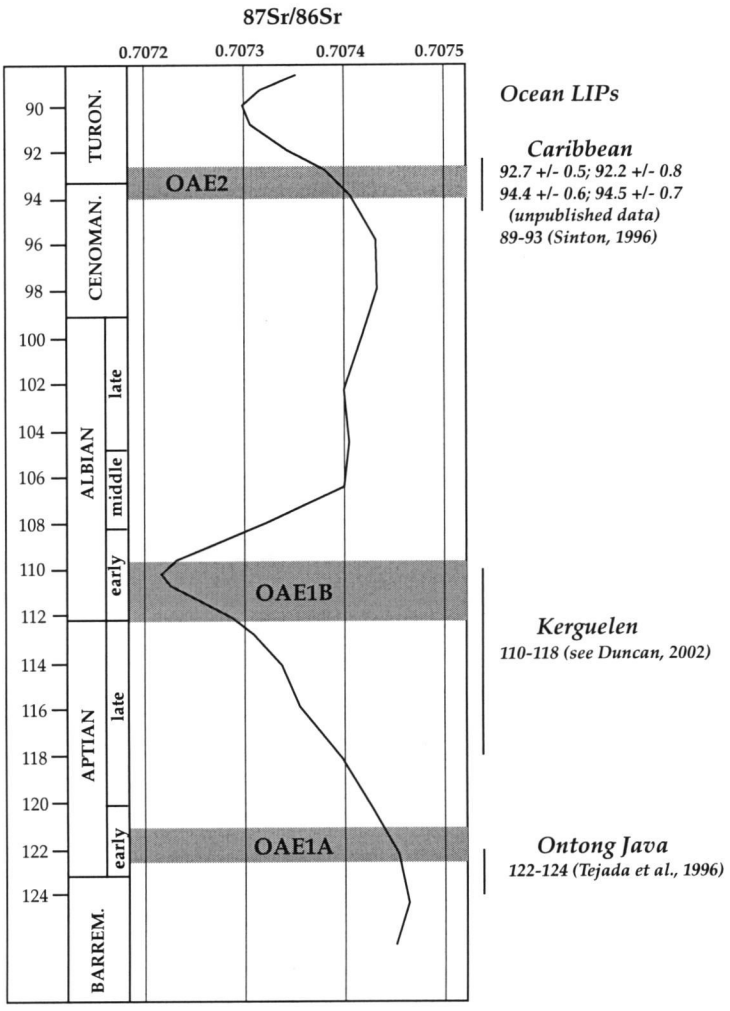

Figure 1. Mid-Cretaceous Sr-isotope stratigraphy shows several departures to lower values which have been related to hydrothermal inputs to the oceans. The two decreases pictured here correlate approximately with ocean anoxic events (OAE) 1 and 2, found globally and defined by biostratigraphic and C-isotopic data, and organic carbon contents. Given the long residence time of Sr in the oceans, abrupt inputs of unradiogenic Sr will be broadened to intervals at least 3 m.y. in duration. The timing of major ocean plateau construction correlates closely with the onset and greatest development of the Sr-isotopic lows, and maybe the source for the unradiogenic Sr, rather than pulses or new arrangements of spreading ridges. Amended from Bralower et al. (1997), with Sr-isotopic evolution curve from Howarth and McArthur (1997); time scale from Gradstein et al. (1995) and Channel et al. (1995). New age determinations from the Caribbean plateau are ^{40}Ar-^{39}Ar total fusion ages for lava flows from Haiti and Curacao.

occurrence implies some fundamental change in ocean circulation and/or the production and preservation of organic material (Sarmiento et al., 1988).

Two processes have been proposed for black shale formation during the Cretaceous. The first is higher productivity. Schlanger and Jenkyns (1976) first suggested this process because ocean conditions during the mid to late Cretaceous were favorable for high production within the marine ecosystem. Sea level was higher, increasing the area of shallow banks with large influxes of terrestrial nutrients, as was global mean temperature, both promoting primary productivity. Large inputs of organic carbon to deep waters could have increased the extent and intensity of the oxygen minimum zone, inducing black shale deposition.

The second process proposed for black shale formation is a global stagnation of ocean circulation. Ocean stagnation during the Cretaceous could have been produced by a number of mechanisms. The increased global temperatures during this time could have inhibited cold bottom water formation in high latitudes, reducing the supply of oxygenated bottom water to the oceans (Schlanger and Jenkyns, 1976). Inhibiting bottom water circulation by density stratification can also reduce oxygen. Ocean temperatures were much warmer than present; studies suggest that temperatures of bottom water were as high as 15°C (Douglas and Savin, 1975; Saltzman and Barron, 1982). Because the solubility of oxygen in water drops off considerably as temperatures increase, the warm ocean temperatures during the Cretaceous resulted in lower concentrations of O_2 throughout the water column.

However, these two explanations do not seem to satisfactorily explain the presence of global anoxic periods during the mid to late Cretaceous. For instance, black shale deposits correlate with periods of high species mortality at what seem to be excellent conditions for marine life (Kaufmann, 1986; Larson,1991a, b). Also, if anoxia were due to higher sea levels and warmer climate, then why isn't the whole mid to late Cretaceous sediment record characterized by black shales (Herbin et al., 1986)? Instead, Cretaceous black shale episodes have a very abrupt onset and conclusion, suggesting some other intermittent forcing behind these events, possibly pushing an already low oxygenated ocean over into an anoxic state.

One factor not examined by most studies is the impact of volcanic activity in the form of Large Igneous Provinces (LIPs), in particular submarine ocean plateaus, on climate and ocean chemistry. Vogt (1989) explored the possibility that the demise of Pacific carbonate bank communities during the mid and late Cretaceous reflect local volcanogenic hydrothermal upwelling of anoxic nutrient rich waters. Sinton and Duncan (1997) expanded this idea to look at the effects of trace metal loading on the ocean during volcanic activity associated with ocean plateau construction.

Large Igneous Provinces

Large Igneous Provinces (LIPs) are massive emplacements of intrusive and extrusive rock erupted over a geologically short period (a few million years) (Coffin and Eldholm, 1994). These include continental flood basalts, oceanic

plateaus and volcanic rifted margins. LIPs apparently originate by processes unrelated to those of steady-state plate tectonics, such as subduction related volcanic arcs and sea-floor spreading, but are related to surfacing and melting mantle plumes at the beginning stage of hotspot activity (Morgan, 1971, 1981; Richards et al., 1989). Compared to the relatively steady-state production of crust at seafloor spreading centers, oceanic plateaus are enormous volumes of magma erupted over time scales of 10^5-10^6 years. It is speculated that magmatism occurs in short, large-volume pulses with flows erupting over periods of days to decades, which is consistent with a flood basalt origin (Courtillot and Besse, 1987; Richards et al., 1989). For brief periods (~1 Ma), submarine oceanic plateau formation probably involved crustal accumulation rates in excess of total mid-ocean ridge rates of production (Duncan and Richards, 1991; Larson, 1991a, b). During the Cretaceous, a number of these ocean plateaus formed, including the Ontong Java Plateau (early Albian), the Kerguelen Plateau (early Aptian), and the Caribbean Plateau (C/T boundary). What were the environmental consequences, on ocean chemistry, the atmosphere and life on Earth, of these large outpourings of magma over such short time periods (days to decades)? Since there are no modern analogues for LIPs, one must look in the sedimentary record and the hydrothermally altered rocks of buried plateaus for any clues for the consequences of plateau formation.

The sedimentary record reveals that the formation of these ocean plateaus during the Cretaceous correlates closely with a number of global ocean phenomena.

The Sr isotope composition of seawater shows a number of distinct decreases in the $^{87}Sr/^{86}Sr$ values during the early Albian and from the C/T boundary through the upper Turonian (Figure 1). The onset and greatest development of these Sr-isotopic lows correlate with the timing of the major ocean plateau construction. Seawater $^{87}Sr/^{86}Sr$ values record a balance between the proportions of strontium in seawater contributed by hydrothermal activity ($^{87}Sr/^{86}Sr$ ~0.704), the weathering of old sialic rocks of the continental crust ($^{87}Sr/^{86}Sr$ ~0.720), and the weathering of marine carbonate rocks ($^{87}Sr/^{86}Sr$ ~0.708). Because of this, it has been proposed that the drop in seawater Sr isotope values seen are most likely the result of an increased flux of hydrothermal Sr into the ocean, due to increased ocean crustal formation, rather than a decrease in the chemical weathering of continental rocks (McArthur et al., 1994; Ingram et al., 1994; Jones et al., 1994; Bralower et al., 1997).

The source of the unradiogenic Sr may be coming from ocean plateau eruptions rather than pulses or new arrangements of spreading ridges. The fact that these negative anomalies in the seawater Sr isotope evolution extend well beyond the times of LIP eruption is due to the long residence time of Sr in the ocean (~5 Ma). The formation of ocean plateaus also correlates approximately with OAE 1 and 2 (Schlanger and Jenkyns, 1976), a number of defined Cretaceous extinction events in groups such as the calcareous nannofossils (Erba, 1994), radiolarians (Erbacher et al., 1996), deep-dwelling planktonic and benthic foraminifera (Kaiho et al., 1993; Kaiho and Hasegawa, 1994; Kaiho, 1998), and molluscs (Kuhnt and

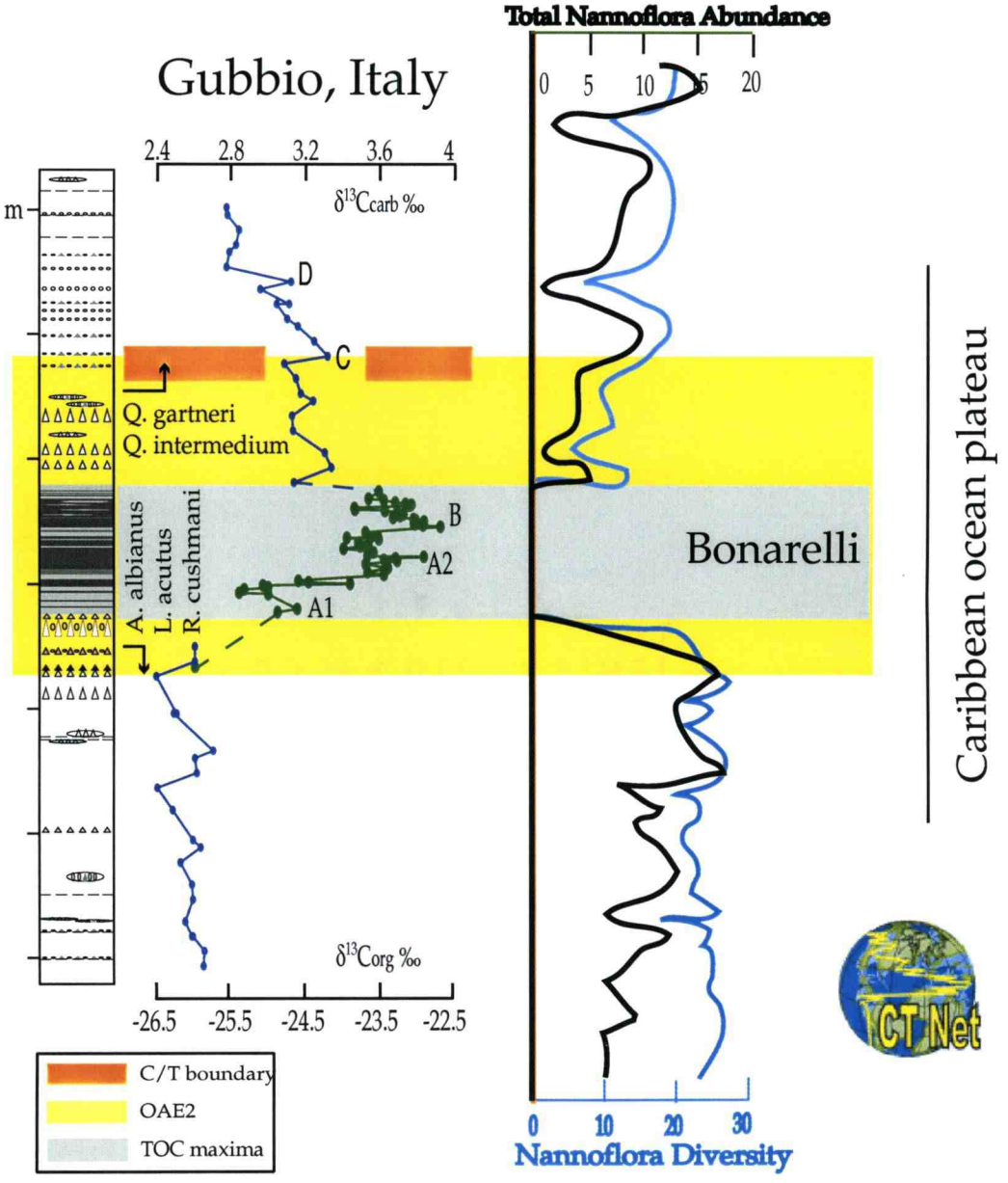

Figure 2. Figure showing timing of positive $\delta^{13}C$ global excursion, abundances in nannoflora communities, formation of the Caribbean ocean plateau, and OAE2 in a sedimentary sequence from Gubbio, Italy. Figure from C/T NET.

Wiedmann, 1995), along with the well-documented positive $\delta^{13}C$ excursions (Schlanger et al., 1987) (Figure 2).

The positive carbon-isotope excursion is widely interpreted as the response of the ocean to enhanced preservation and burial of organic carbon in sediments (Jenkyns, 1980; Arthur et al., 1987). Biologically synthesized organic matter is enriched in ^{12}C (lighter isotope) and so its removal by burial could cause the ocean to be richer in ^{13}C, producing a more positive $\delta^{13}C$ signal. Although these oceanic events have similar timing to the formation of ocean plateaus, the relationship between them, if it exists, is still unclear.

Sinton and Duncan (1997) proposed that there was indeed a relationship between ocean plateau formation and other global ocean phenomena, in particular anoxia, during the mid to late Cretaceous. They proposed that metals released during hydrothermalism associated with single large ocean plateau eruptions were oxidized, consuming O_2 in ocean waters. Using approximate concentrations of metal species from ~350°C vent fluids from Von Damm (1995) and a lava volume of 10,000 km^3, Sinton and Duncan calculated the amount of O_2 utilized if all material released was oxidized. According to their calculations, approximately 6% of the total dissolved O_2 in today's ocean located beneath the mixed layer would be consumed. However, considering O_2 concentrations were probably much lower during the Cretaceous, this could have been a much larger proportion of the ocean. Also, due to buoyancy considerations, these hydrothermal plumes were most likely carried to the ocean surface bringing nutrients and metals with them. This large

influx of nutrients in the form of biolimiting metals may have increased primary production, or eventually lead to massive kills as metal concentrations reached levels toxic to marine organisms (e.g., Erickson and Dickson, 1987), both promoting the consumption of O_2.

Recent experiments (Coale et al., 1996) in ocean areas with high nutrients but low production, known as high nutrient low chlorophyll (HNLC) regions, have shown that Fe is a limiting nutrient. The introduction of Fe to these regions can actually stimulate phytoplankton blooms. Fe and other trace metals (such as Cu, Zn, Co, Mo, Na, Mg and V) are important for such aspects as the growth of all photosynthetic organisms (Sunda and Huntsman, 1996) and therefore are essential for maintaining primary production. It has been suggested that an increasingly stratified water column during the Cretaceous limited the availability of nutrients and trace metals to the oceanic photic zone (Leckie et al., 2002). Hence, surface production is the expected result of adding massive amounts of nutrients, Fe and other bio-limiting metals into ocean surface waters during the Cretaceous. The increased rain of organic carbon from the photic zone would have increased the consumption of O_2 in ocean waters. This reduction in O_2 would have expanded the oxygen-minimum zone, allowing for the deposition of organic-rich sediments.

The combination of oxidation of released volcanic materials and increased production may have periodically had a large enough effect to cause global anoxia. These processes would have been especially effective in Cretaceous waters, considering that they were already poorly oxygenated because of the warmer

temperatures, which may have favored the formation of warm salty bottom waters in the tropics rather than cold deep waters at the poles (Brass et al., 1982).

Hydrothermal Activity and Oceanic LIPs

Since there are no modern day equivalents of LIP eruptions, understanding the hydrothermal processes associated with ocean plateau volcanism is very challenging. However, ocean plateaus appear to be the submarine equivalents of continental flood basalt provinces (Sinton et al., 1998). Therefore, volcanism most likely occurred as a series of intermittent but large magmatic events. Individual lava flows could have been up to thousands of km^3 in volume each. For example, single flows of the Columbia River basalt province erupted over a few years were as large as 1500 km^3 (Ho and Cashman, 1997) and flowed for hundreds of kilometers from the source (Swanson et al., 1975). Considering that ocean lithosphere is thinner and denser than continental crust, even larger volumes of magma could be expected to rise to the Earth's surface in ocean basins. Therefore, it is possible that individual flows from ocean plateau eruptions were much larger (maybe even up to 10,000 km^3 modeled by Sinton and Duncan, 1997).

It has been known for sometime that hydrothermal venting at MOR's occurs as steady-state hydrothermal plumes associated with the convection of seawater through hot rock (Corliss et al., 1979). However, with the discovery of large event plumes over the southern Juan de Fuca Ridge in 1986, it was realized that a portion of heat flux from MOR's is released episodically in larger, discrete plumes, termed "event plumes" rather than just by continuous steady state vents (Figure 3) (Baker

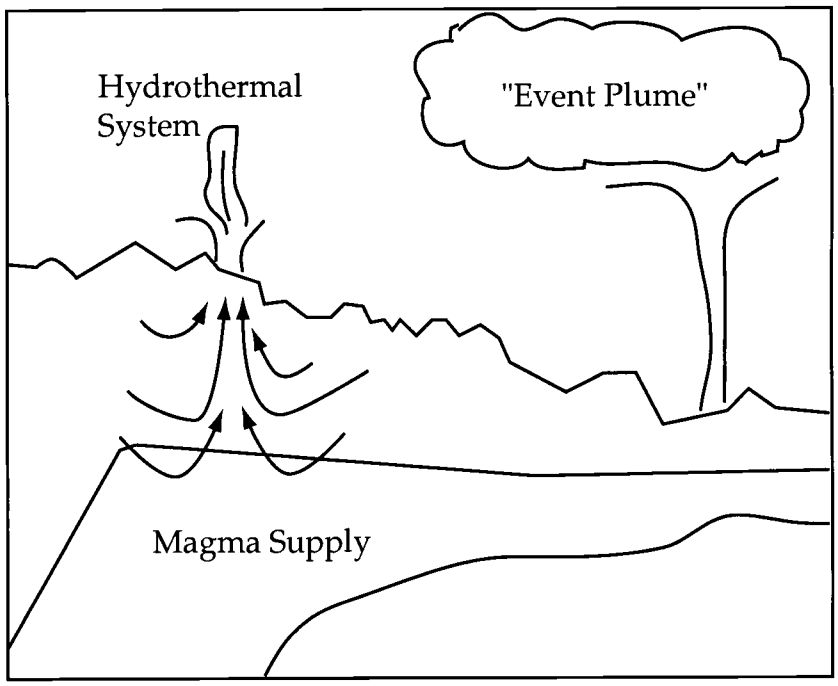

Figure 3. Cartoon summarizing the different methods of heat flux and metal flux from ocean plateau eruptions. Figure derived from Lupton et al. (1999).

et al., 1987). Differing $^{3}He/\Delta T$ ratios in event plumes compared to steady state plumes suggest these two develop from different mechanisms (Lupton et al., 1999). Event plumes are most likely generated by a distinct eruption or dike injection of some sort. According to this idea, the entry of magma increases the permeability of the ocean crust, allowing a sudden, massive release of hot, mature, buoyant fluid to escape (Lupton et al., 1999). This newly created dike or lava flow then interacts with seawater to produce the typical steady-state hydrothermal vents. It is likely that both types of seawater-basalt interactions occurred with ocean plateau formation during the Cretaceous; event plumes during eruption of single flows and steady-state hydrothermal activity dominated by water/rock reactions during cooling of intrusions.

Considering both event plume and steady-state hydrothermal activity, the former has a much more pronounced impact on the surrounding environment, especially for shorter periods of time. Eruption related event plumes can in fact be quite large. The 1986 plume, due to an eruption on the Juan de Fuca ridge, was 20 km in diameter, 600 m thick, rose to about 800 m above the seafloor and, contained about 10^{17} J of excess heat, equivalent to the annual thermal output of a typical ridge crest hydrothermal system (Baker et al., 1989). Vogt (1989) argued that hydrothermal event plumes produced from an eruption of 15 ± 4 km^3 would have sufficient energy to bring bottom water to the ocean surface from 3 km deep (typical spreading ridge axial depths). Considering that LIPs could be built from much larger single eruptions (up to 10,000 km^3) at much shallower depths (~1 km),

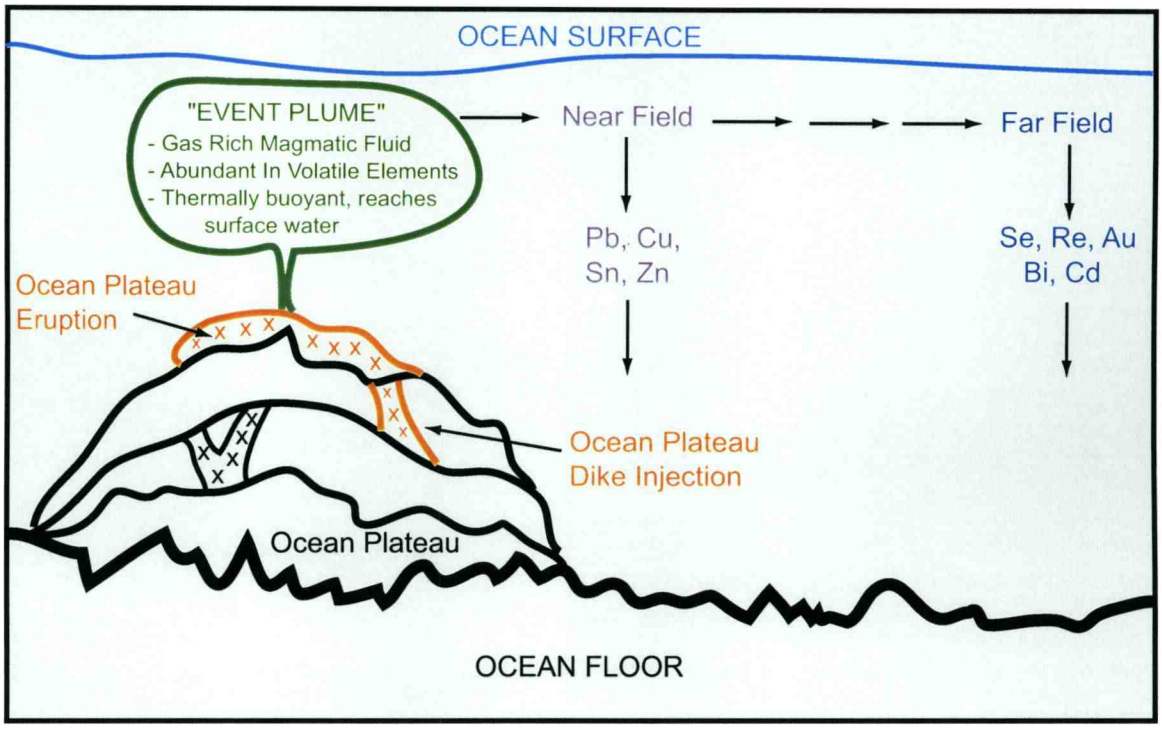

Figure 4. Schematic drawing showing what occurs during an ocean plateau eruption. A large eruption or dike injection releases a gas rich magmatic fluid abundant in volatile elements. This megaplume has enough heat and energy, and comes from a shallow enough depth, that it reaches the ocean surface and is caught in surface circulation. Metals will then fractionate and precipitate out depending on their reactivity (residence times). Those that precipitate out close to the source are termed "near field" elements and those that precipitate out far from the source are termed "far field" elements.

degassed magmatic fluids, mixed with warmed ambient seawater, undoubtedly had enough buoyancy to rise to the surface (Figure 4). Thus they would bring metals to the surface where they could be transported rapidly throughout the ocean. Such metals would enter into a variety of chemical exchanges (many biologically mediated) and ultimately be removed from the surface as sinking particles that accumulated as sediments.

An important aspect of this model is that the chemical exchange of elements to seawater during eruption of large lava flows is controlled by the volatility-exchange between basalts and very high temperature gas-rich magmatic fluids (Rubin, 1997). The compositions of degassing fluids, and therefore the abundance pattern of elements released to seawater in the form of an eruption event plume, are fundamentally different from those derived from the solubility-driven exchange between hot water and rock (e.g. typical high temperature, steady-state hydrothermal vents) (Bowers et al., 1985). Rubin (1997) estimated that the general predicted element enrichment pattern in a magmatic fluid is: main group elements > transition metals > alkaline earths ~ alkali metals > rare earths and actinides. For marine hydrothermal processes, it is nearly the opposite, alkaline earths ~ alkali metals > transition metals > rare earths and actinides > main group elements (Figure 5). For example, many volatile transition metals and main group metals such as Hg, Bi, Se, Cd, and As are expected to be much more prevalent in degassed effluents ("event plumes") whereas the concentrations of Fe, Al, Zn, Mn, Ir, the

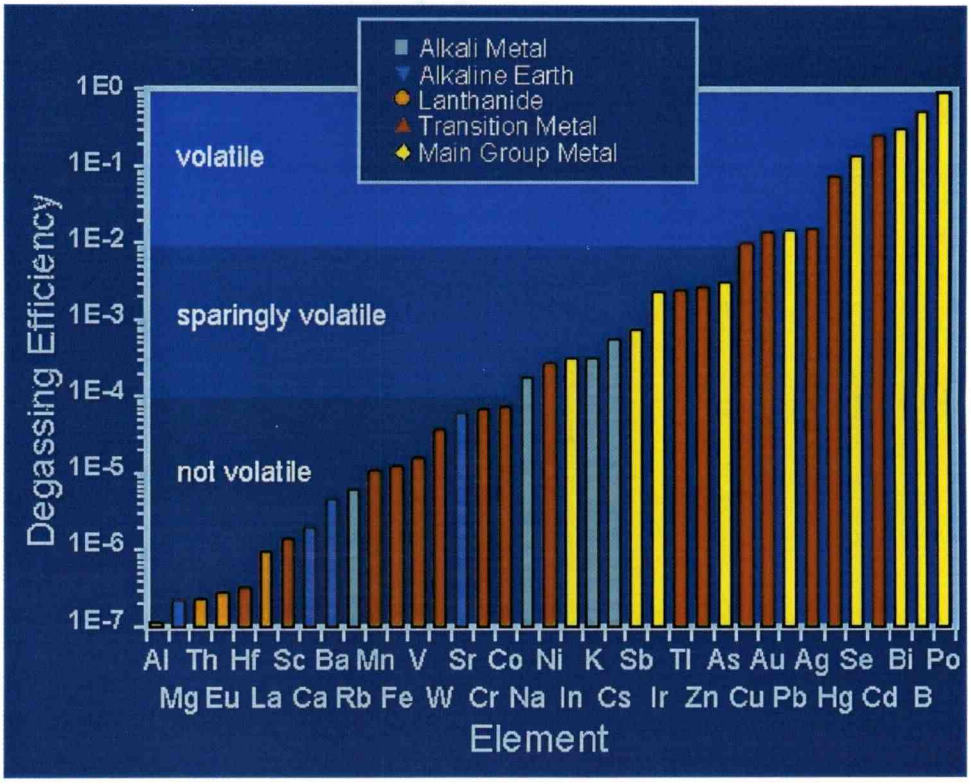

Figure 5. Degassing efficiency for a suite of elements. Elements with a large degassing efficiency are more volatile and therefore will be enriched in degassed magmatic fluids whereas those elements with a small degassing efficiency are less volatile and will be enriched in solubility-controlled hydrothermal reactions. Figure from Rubin (1997).

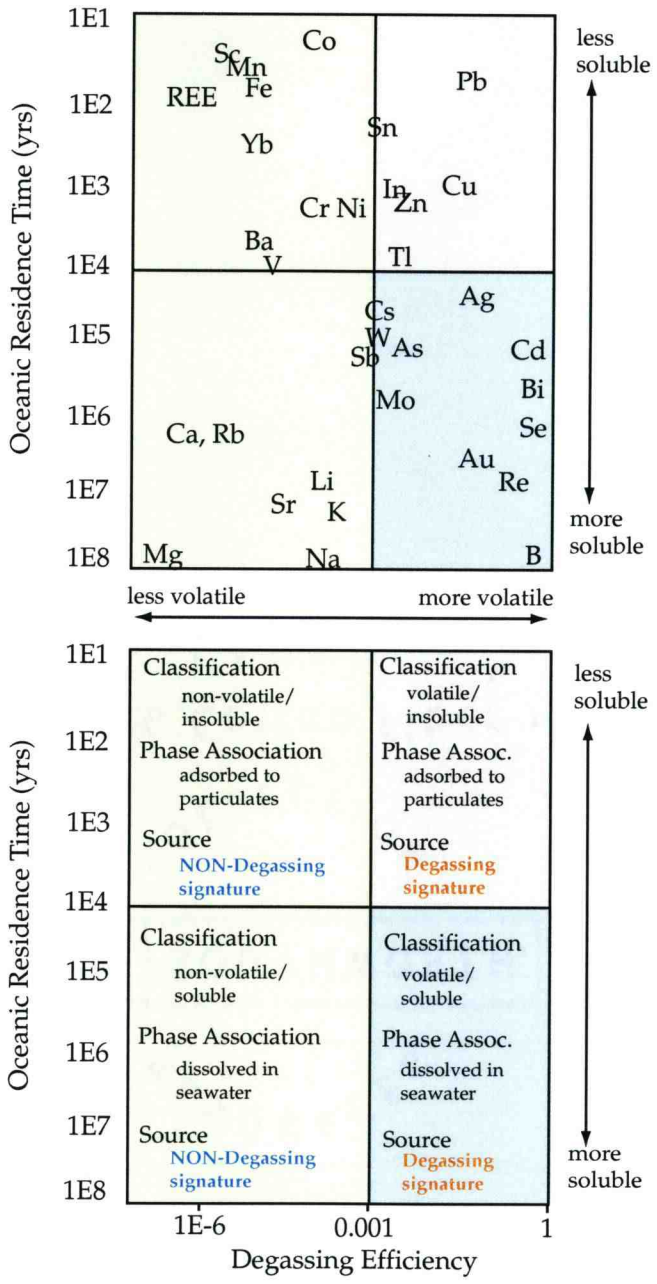

Figure 6. A diagrammatic representation of the volatility of elements into degassed magmatic fluids and residence time of elements in seawater (after Rubin, 1997). This matrix is useful in determining a source for elements enriched in pelagic sediments and distinguishing near-field and far-field signatures. Elements in yellow boxes tend to be more enriched in steady-state hydrothermal activity whereas elements in blue and pink boxes tend to be more enriched in "event plumes".

lanthanides, alkali metals and alkaline earth elements are 10-10^4 greater in hydrothermal fluids (steady-state vents) (Figure 6).

Therefore, these different chemical signatures could provide a way to distinguish between metal enrichments produced by eruption related event plumes and those by hydrothermal vents. Rubin (1997) suggested looking at variations in Mo, W, Se, Hg, Cd, As, Cu, Re, Tl and Bi. Abundance patterns of these selected trace metals plus others recorded in pelagic sediments have the potential to tell us if the ocean was affected by intermittent hydrothermal vents or eruption related plumes.

Metal Abundance Anomalies

In 1993, Orth et al. reported two closely spaced metal abundance peaks just below the C/T boundary from a number of sites in the Western Interior Basin of North America and around the world. These metal anomalies seem to correlate well with a number of mollusk, planktonic and benthic foraminifera extinctions (Eicher and Worstell, 1970; Hart and Bigg, 1981; Elder, 1987), the well-documented positive $\delta^{13}C$ excursion in the late Cenomanian, and OAE 2 commonly know as the "Bonarelli Level" of Italy (Arthur and Premoli-Silva, 1982) and the "Black Band" of England (Leary et al., 1989).

Elements that showed enrichment patterns in Orth et al.'s (1993) study are Sc, Ti, V, Cr, Mn, Co, Ni, Pt and Au. The authors attribute these metal abundance peaks to new or increased activity in spreading center or hotspot activity in the eastern Pacific basin. However, their suggested source of metals does not explain

the sharp onset, brevity and magnitude of these metal abundances. Instead, Sinton and Duncan (1997) concluded that the metal peaks of the late Cretaceous are not a result of continuous magmatic activity, but rather to abrupt and distinct hydrothermal "event plumes" released in conjunction with the rapid formation of the Caribbean Plateau. Metals contained in these hydrothermal fluids are suggested to be related to the drawdown in seawater oxygen concentrations, and therefore to increases in the accumulation and preservation of organic carbon-rich sediments we see around the C-T boundary. As mentioned above, this can happen by two mechanisms: (1) the consumption of dissolved O_2 in ocean waters by the reduction of reduced materials vented during the plateau eruptions, and (2) the influx of bio-limiting nutrients (e.g., Fe, Co, Mn, Cu, Zn, Se) (Martin and Fitzwater, 1988; Martin and Gordon, 1988) from thermally buoyant hydrothermal plumes reaching the ocean surface initially increasing primary production and then eventually leading to mortality and extinctions as metal concentrations reached toxic levels. The increased rain of organic matter to the deep ocean could have exhausted O_2 concentrations for brief intervals.

If we look at the relative abundance of these metal anomalies with respect to geographic location (Figure 7), we see that the strongest signals are in the south-central and southern regions of the Western Interior of the United States. The intensities drop off sharply to the north and more gradually to the east and west. Orth et al. (1993) attribute this distribution pattern to a source of metals to the

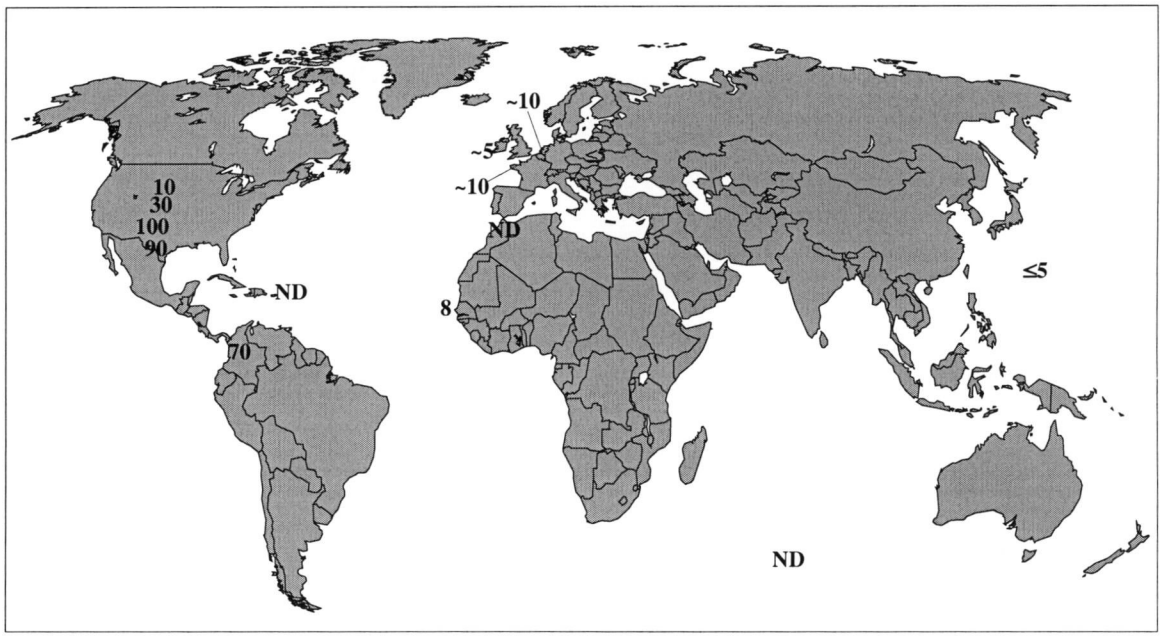

Figure 7. Relative global distributions of elemental anomalies measured by Orth et al. (1993) with the site of greatest deposition assigned a value of 100; ND = anomalies not detected. Strongest signals are in the south-central and western interior seaway of the United States and northern Columbia. Intensities drop off sharply to the north and more gradually to the east and west.

south, perhaps from or via the proto-Gulf of Mexico/Caribbean area or far eastern Pacific.

This Study

Although a comprehensive investigation of trace metals at all of the OAEs throughout the Cretaceous is needed to evaluate the proposed link between ocean plateau "event plumes" and ocean anoxic events, my study will specifically concentrate on the OAE 2 at the C/T boundary in the late Cretaceous. This prominent black shale layer has been correlated with the construction of the Caribbean ocean plateau (Sinton and Duncan, 1997). I will investigate this relationship through the following:

(1) In Chapter 2, I examine a C/T boundary section from Rock Creek Canyon, Pueblo, Colorado for major, minor and trace elemental abundances and discuss the results and their significance in terms of the timing and relationship to other biogeochemical changes (e.g. carbon isotopes, lithologic and biostratigraphic data).

(2) In Chapter 3, I present major, minor and trace element abundances for other C/T boundary sections from other parts of the world. Specifically, these are the Bass River borehole (ODP Leg 174AX) from the New Jersey Coastal Plain, ODP Site 1138 on the Kerguelen Plateau, the Totumo-3 well core from northern Venezuela, and the Baranca el Cañon section from southwest Mexico. I examine this global array of sites for any gradients in trace metal

abundance signals and changes in trace metal pattern between distal and proximal locations relative to the Caribbean ocean plateau.

(3) In Chapter 4, I combine all C/T boundary sections to produce general conclusions about the relationship between ocean plateau formation and major anoxic event OAE2.

Although this study will examine the specific relationship between the "Bonarelli" black shale layer (OAE2) and the Caribbean ocean plateau, the rationale and analytical strategy should be applicable to other suspected connections between submarine volcanic activity and ocean anoxia (e.g. Ontong Java Plateau with the "Selli" black shale level (OAE 1a) at ~122 Ma).

Chapter 2: Trace Elemental Abundances in the Rock Creek Canyon, Pueblo, Colorado Marine Sedimentary Section and their Relationship to Ocean Plateau Construction and OAE2

Abstract

It has been recently recognized that the formation of the Caribbean ocean plateau correlates closely in time with Ocean Anoxic Event 2 (OAE2), which bracketed the Cenomanian/Turonian (C/T) boundary at around 93 Ma (Gradstein et al., 1995). These two features also correspond with an increase in carbon isotopic composition and a decrease in the strontium isotopic compositions of seawater. Hydrothermalism associated with large-scale submarine volcanism may have been responsible for these C/T boundary ocean conditions. However, a causal relationship among these signals, if it exists, is still unclear.

To determine a specific link between "event plume" activity from Caribbean ocean plateau eruptions and OAE2, I determined the distribution of major, minor and trace element abundances in a high density sampling of the Rock Creek Canyon marine sedimentary section (Pueblo, Colorado), above and below the C/T boundary. After normalizing element concentrations to Zr to remove the variable contribution of terrigenous material to these sediments, an interval of metal abundance anomalies can be seen. A weaker, lower set of metal anomalies lies about four meters below the C/T boundary and coincides with the beginning of the rapidly increasing positive $\delta^{13}C$ isotope excursion. A stronger, upper set of metal anomalies lies about two meters below the C/T boundary and falls just below the long duration of constantly positive $\delta^{13}C$ values. Both metal anomaly peaks fall

roughly in the same stratigraphic location as high rates of speciation and extinction in foraminifera, radiolaria and molluscs. The presence of metal abundance anomalies, well developed in both the low and high volatility elements, strongly supports the hypothesis that intermittent hydrothermal activity, both water/rock solubility dominated and "event plume" dominated, introduced a large concentration of trace metals into the Cretaceous ocean at the same time changes in benthic species, organic carbon preservation, and burial of isotopically light carbon occurred. The stratigraphic position of this interval of trace metal anomalies with events associated with OAE2 suggests that hydrothermal activity could be the causative agent in pushing the ocean abruptly into anoxia.

Introduction

The mid to late Cretaceous period is characterized by many extreme climatic and ocean conditions including a number of distinct, world wide ocean anoxic events (OAEs). Although a number of suggestions have been made about the cause of these events, there is still considerable debate. One of the most extensive and best expressed of these events occurred at the Cenomanian/Turonian boundary (C/T), which has been dated 93.5 ± 0.2 Ma by the Gradstein et al. (1995) time scale and can be considered the type example (Wignall, 1994). This OAE correlates closely in time with the formation of a massive volcanic ocean plateau that now constitutes the core of Caribbean plate. This study investigates a proposed causal relationship between the two phenomena – extraordinary submarine volcanic activity and ocean-wide anoxia.

To assess a proposed connection between these two Cretaceous phenomena, I have investigated the pelagic sediment record for elements diagnostic of "event plume" hydrothermal activity. For the most comprehensive analysis of this interval, I have chosen the Rock Creek Canyon section for its accessibility and well documented and defined lithologic and biostratigraphic descriptions. In particular, I have analyzed bulk rock samples from the Rock Creek Canyon section for a broad spectrum of trace metal abundances. The appearance of metal signals could indicate "event plume" hydrothermal activity and the stratigraphic position of these trace metal anomalies might determine their timing relative to ocean anoxic events, biotic responses, and the positive shift in δ^{13} C.

The Caribbean Ocean Plateau

The late Cretaceous experienced a major pulse of LIP activity, including the formation of the Caribbean ocean plateau. This ocean plateau has been proposed to be the product of the onset of the Galapagos hotspot (Duncan and Hargraves, 1984) and is a good choice for studying LIPs. First, the Caribbean ocean plateau can be easily sampled because of uplift and exposure of predominantly tholeiitic pillow basalt sequences around the tectonized margins of the plateau, whereas other LIPs are still under the ocean and thick pelagic sediments, inaccessible except by deep ocean drilling. Samples from the Caribbean plateau have been dated (using ^{40}Ar-^{39}Ar radiometric dating methods) and indicate that the main pulse of volcanism occurred between 92-88 Ma (Sinton, 1996). More recently, sections have been re-analyzed and have yielded dates that are slightly older, ranging from 94-92 Ma

(Duncan, unpublished data, 2002), revealing a close correlation with the timing of OAE2. However, early eruptive products and much of the internal structure of deep ocean plateaus have not been sampled, so some volcanic activity occurred some undetermined time earlier as well.

The core of the Caribbean plate, divided into the Columbian and Venezuelan basins, and numerous tectonically uplifted sections along the plate margins represent the bulk of the Caribbean ocean plateau that has been wedged between North America and South America (Burke et al.,1978; Duncan and Hargraves, 1984). Based on the combined volume of the Columbian and Venezuelan basins, the Caribbean plateau is estimated to be about 5-10 x 10^6 km^3, but could be quite larger if on-land sections and the unknown amount of obducted and subducted parts were included (Larson, 1991b; Sinton, 1996). Rather than continuous effusion, emplacement probably occurred in discrete, large-scale events, in as short a period as a few days with volumes up to 1500 km^3 (Swanson et al., 1975).

Rocks of the Caribbean plateau are predominantly characterized by a combination of thick, pillow and massive basaltic flows and sills, erupted in a submarine environment, onto or intruding foraminiferal limestone (Sinton, 1996). Composition of the magma is predominantly tholeiitic, but includes some high-Mg lavas and alkali basalts. The Caribbean ocean plateau exhibits varying degrees of low-grade alteration associated with hydrothermal processes. Some basalts show signs of chlorite, celadonite, zeolite and secondary oxide phases, but most samples

have relatively pristine pyroxene and pristine to partially altered plagioclase (to clays).

Study Site

Geological Setting – Rock Creek Canyon

During the Cretaceous, the Rock Creek Canyon (Figure 8) section of Colorado was part of a shallow inland sea called the U.S. Western Interior Seaway (WIS). Because of the warmer temperatures characteristic of the Cretaceous, there was no polar ice and sea levels during this time were much higher. In fact, the WIS extended across more than 30° latitude and more than 2000 km (Hay et al., 1993) wide from the Gulf of Mexico coast to the Arctic Ocean with depth ranging to about 1500 m (Sageman and Arthur, 1994). Sedimentation in this area was dominated by deposition of siliciclastic input from the uplifted fold and thrust basin to the west and more fine-grained, carbonate rich input from the east (Kauffman, 1984). One of the most studied rock formations of the Cretaceous WIS is the Greenhorn Formation (e.g., Dean and Arthur, 1998; Pratt et al., 1993). Deposition of this formation began just prior to the peak high sea level event of the C/T boundary.

The Bridge Creek Limestone and Hartland Shale units of the Greenhorn Formation are marked by the development of interbedded, light colored, highly bioturbated limestone and finely laminated dark colored marlstone or calcareous shale. This can be seen clearly in the sediments of the Rock Creek Canyon section

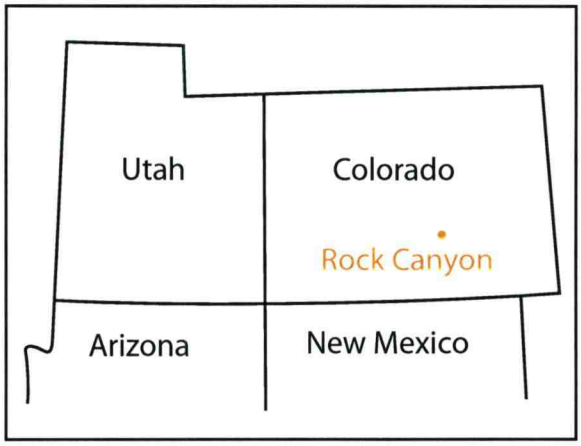

Figure 8. Map showing location of the Rock Creek Canyon, Pueblo, Colorado section.

(Figure 9). The dark color of the marlstones and shales is due to higher concentrations of organic material whereas the lighter limestones contain more carbonate-rich sediments. The limestone–shale couplets have been interpreted by many to reflect climate-driven changes in productivity, clastic dilution and benthic oxygenation (e.g., Barron et al., 1985; Pratt, 1984; Pratt et al., 1993).

The sequences of the Cretaceous WIS are among some of the best-studied C/T boundary samples in the world due to the abundance of well-exposed and easily accessible outcrops. The Rock Creek Canyon section provides high-resolution biozones and well-defined lithologic changes. The Rock Creek Canyon section also presents a number of well-dated bentonite layers (Obradovich, 1993; Kauffman et al., 1993) providing excellent time constraints. For this project, sampling at Rock Creek Canyon extended from the uppermost part of the Hartland Shale through to the lower Bridge Creek Limestone, spanning about eight meters below and six meters above the C/T boundary.

Carbon Isotope Excursion

The OAE2 is characterized by a global positive $\delta^{13}C$ shift in both carbonate and organic carbon fractions brought about by a major shift in the global carbon budget (Figure 10). This excursion has been suggested to most likely result from the increased burial of isotopically light organic matter ($\delta^{13}C$ in the range of -15 to -30 ‰) under anoxic conditions and is clearly expressed in the Rock Creek Canyon section (Figure 11) (Pratt et al., 1993). I made sure to sample the Rock Creek Canyon section below and through this entire isotopic excursion to determine the

Figure 9. Photograph of sedimentary sequence at Rock Creek Canyon, Pueblo, Colorado. Layers of finely laminated dark colored marlstones and shales are interbedded with sequences of light colored, highly bioturbated, thick limestones.

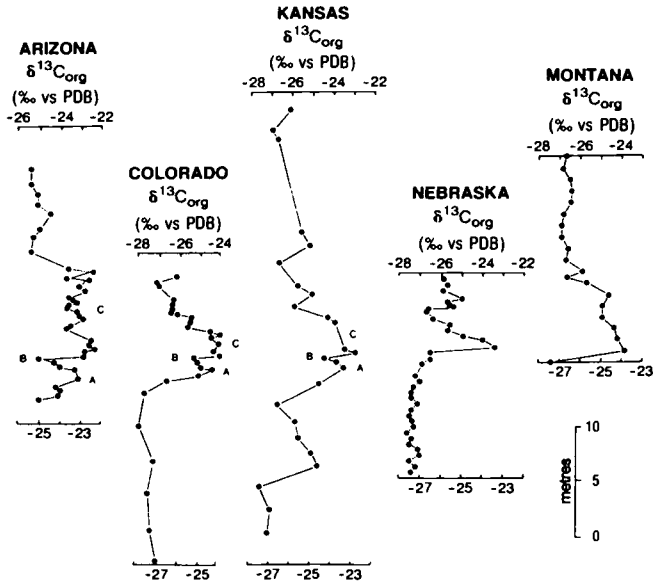

Figure 10. Comparison of carbon-isotopic profiles from outcrops spanning the C/T boundary. The distinct global positive carbon isotopic shift can be seen in all of these sections. Figure from Pratt et al. (1993).

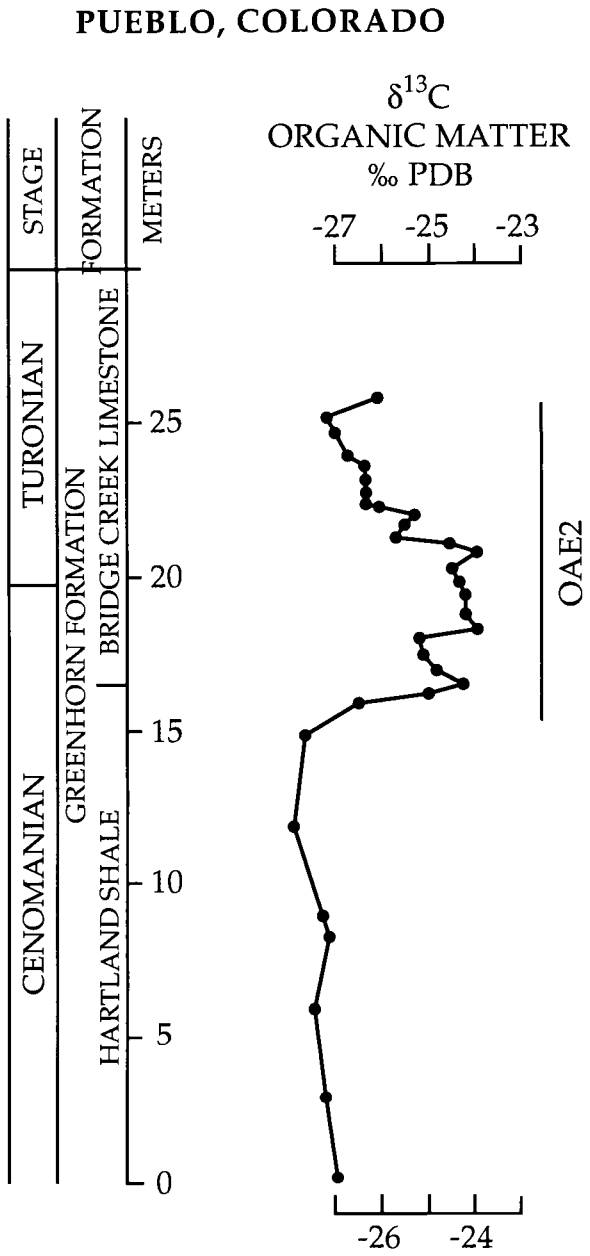

Figure 11. Carbon isotopic profile for the Hartland Shale and Bridge Creek Limestone Members of the Greenhorn Formation at Rock Creek Canyon, Colorado. The distinct positive carbon isotopic profile begins at about 15 m and ends at about 25 m. Figure from Pratt et al. (1993).

position of metal anomalies with respect to changes in the $\delta^{13}C$ curve.

Methods

Sample Collection

Samples from the Rock Creek Canyon section in Pueblo, Colorado were collected and measured with reference to a prominent, basal limestone, indicated by the numbered marker beds of Cobban and Scott (1972), and taken as the 0 cm position for this study. Samples were taken every 30 cm from 4 m below the basal limestone, then every 10 cm starting 1.5 m above the basal limestone, then about every 2 cm around the C/T boundary from 1.5 m to 3 m above the basal limestone, every 10 cm from 3 m to 4.2 m above the basal limestone, and every 50 cm from 4.2 m to 10 m above the basal limestone.

Sample Preparation

Samples were prepared for digestion and analysis using the following method. Whole rock samples were first washed thoroughly with deionized water to remove any loose material. Samples were then broken with a hammer into smaller pieces (ranging from 1" to 3"). The smaller pieces were further crushed in an alumina jaw rock crusher to coarse size. This crushed material was then powdered using a ball mill and mortar and pestle. All material was then sieved using a 100 μm plastic sieve to achieve a uniform sized powder ready for dissolution.

Sample Digestion

All samples were digested in XP 1500 plus vials using a CEM Mars 5 microwave in the following manner. Each microwave "batch" contained 12 samples. One Teflon vial is designated solely for the pressure-temperature (P/T) control, which records the temperature and pressure of the vials during the procedure, and the other 11 are designated for actual samples. For each "batch", I added approximately 35 ± 2 mg of a powdered sample to the P/T control vial and approximately 25 ± 2 mg of sample to the other 11 vials. To each is then added, carefully and slowly using a pipette, 5 ml of 40% omni trace HF, 1 ml of 6M redistilled HCL and 3 ml of trace metal grade 16N HNO_3. XP 1500 vent fittings that have had new safety membranes installed are now screwed on tightly and sample vials capped with XP 1500 plus load disks. Vials are covered with Kevlar sleeves and placed in MARS 5 XP 1500 plus support modules. To prevent venting of acid fumes into the microwave cavity, the top screws of the support modules are tightened using a torque wrench. Support modules are then placed in a turntable base in the microwave and both the pressure sensor (ESP-1500) and temperature sensor (ESP-300 plus) are inserted.

Each set of 12 samples was then run on a "XP 1500 Shale" digestion program with the following protocol. Samples are first heated over 15 minutes to a temperature of ~210°C and pressure of 130 psi. Once samples reach this temperature and pressure, they are maintained here for 60 minutes. When the program is finished, samples are allowed to cool down to near room temperature

before being removed from support modules. Samples are now ready for the evaporation sequence.

The following steps occurred in the evaporation technique. XP 1500 vent fittings are loosened to release pressure (there may be a small amount of venting acid fumes). Each sample vial is removed from the support module and Kevlar sleeve and placed in the evaporation turntable. Digestion caps are replaced with evaporation caps that have Teflon vent tube and air filter installed. Evaporation caps are aligned in such a manner that the filters are on the left-hand side of the central opening. Samples are then placed in the microwave and attached to the evaporation manifold by affixing the vacuum take-off tubing. The vacuum manifold has three scrubbers where number one contains 4% boric acid, number two contains 5% NaOH and number three contains distilled H_2O. Evaporated acid is drawn into these containers to neutralize HF. A vacuum pump is turned on prior to evaporation to verify that scrubbers are bubbling. For the first evaporation step, samples are run on " Evap Mixed Acid – 1500" program. Samples are heated up to a plateau temperature and held here until the temperature drops, meaning the sample has evaporated to a bead of liquid, and the microwave is turned off. After samples have cooled down to room temperature, 5 ml of trace metal grade 8N HNO_3 is added to each. The above process is then repeated using an "Evap HNO_3 – 1500" program. Samples are once again cooled to room temperature, 5 ml of 8N HNO_3 is added and the procedure is repeated once more. After this third evaporation step, the P/T sample is discarded. To the others, 10 ml of distilled 2N

HNO_3 is added and the content of each vial are carefully poured into an acid-cleaned, weighed, labeled 15 ml Nalgene bottle. Samples are then ready to run on mass spectrometer. Standard reference materials and analytical blanks are prepared according to the same procedure. For a list of standard reference materials with accepted elemental abundances and average analytical blank levels, see Appendix 1.

Sample Analyses

Trace and minor element concentrations were determined simultaneously using inductively coupled plasma mass spectrometry (a VG PQ-Excell ICP-MS in the W.M. Keck Collaboratory) at Oregon State University. Sample solutions, external standard reference materials, and procedure blanks are first diluted by 25x (0.2 ml of sample solution to 5 ml of 1% 3 x quartz-distilled HNO_3). To each is added a known amount of internal standard (In-115 and Re-187) to correct for factors such as instrument drift, loss of sensitivity, and matrix effects. Once this is done, samples and standards are ready to be run on the ICP-MS. Sample sets are analyzed in this order: first a procedure blank followed by all external standard reference materials, then an acid blank (for extra wash out time) followed by samples in which between every 10 samples is placed a reference standard material run as an unknown. At the end of each procedure is placed a set of blind duplicate samples (in this case there were three sediment samples from the CISMON Core, Italy) followed with another procedure blank and all external standards.

ICP-MS results are reported in "analyte integrated counts per second" (ICPS) (corrected for instrument variability via internal standard) and are converted to "analyte dilution concentrations" (e.g. ppt, ppb, ppm) through calculations from standard curves. Based on the elemental ICPS for known concentrations of standard reference materials, the elemental ICPS for given samples are assigned a concentration value. The elemental concentration values of the liquid are then corrected for dilution to yield elemental concentrations in the solid rock sample. Based on the analysis of blind duplicates and standards the average error for most elements for ICP-MS analyses is about 10% (2σ), depending on the element analyzed (Table 1). However, some elements have slightly higher errors. Group one, which includes Sc, V, Ni, Sn, Sb, Cs and Bi, exhibited errors of about 15% and group two, which includes, Ag, Au and Se, about 21%. Because of this larger instrumental uncertainty, inferences from this last group of elements should be treated with more caution. Analytical errors may also be introduced because only two internal standards were used during analyses (three to four is the norm). This aspect should also be kept in mind when looking at the data.

Major element concentrations were determined using inductively coupled plasma-atomic emission spectrometry (ICP-AES in the W.M. Keck Collaboratory) at Oregon State University. Sample solutions, external standard reference materials, and procedure blanks are diluted 100x (0.1 ml of sample solution to 10 ml of 1% 3 x distilled HNO_3) before being run. No internal standard is added for

Table 1. Mean and 2σ standard deviation for ICP-MS analyses of a blind standard and blind duplicates. All concentrations are ppm. (Continued).

Element	MAG-1 Accepted Values	MAG-1 Mean	MAG-1 2σ	CS 16-268 Mean	CS 16-268 2σ	CS 16-168 Mean	CS 16-168 2σ	CS 15-55 Mean	CS 15-55 2σ
Sc	17	14.7	4.5	2.5	0.25	1.4	0.24	8.7	0.98
V	140	139	41	14.6	1.7	7.5	1.8	53	6.6
Cr	?	97.1	13.0	33.9	3.2	18.6	3.0	315	34.2
Co	20	21.1	3.8	38.1	8.7	7.1	1.1	9.7	1.0
Ni	53	50.6	16.2	127	36.9	44.6	10.0	105	11.6
Cu	30	27.0	6.6	166	42.1	11.7	2.6	31.4	4.6
Zn	130	136	31	49	6.4	12.4	2.6	48.0	5.6
As	9.2	9.9	2.4	3.3	0.90	0.69	0.39	1.4	0.13
Se	?	4.2	1.8	1.2	0.67	0.87	0.69	3.1	0.70
Rb	150	149	34	13.8	2.4	7.2	1.5	56.0	7.3
Sr	150	147	27	482	50	418	85	225	23
Y	28	26.9	5.9	21.5	2.2	16.1	3.2	32.1	2.8
Zr	130	124	19.6	13.3	1.9	7.8	3.9	79.8	8.8
Mo	1.6	1.3	0.36	0.70	0.16	0.22	0.14	0.39	0.20
Ag	0.08	0.30	0.12	0.11	0.06	0.06	0.06	0.14	0.05
Cd	0.2	0.74	0.20	0.62	0.12	0.31	0.10	0.29	0.04
Sn	3.6	3.5	1.07	0.32	0.09	0.15	0.04	1.0	0.16
Sb	0.96	0.97	0.32	0.32	0.08	0.09	0.037	0.34	0.05
Cs	8.6	8.0	2.34	0.91	0.10	0.41	0.13	3.6	0.30
W	1.4	1.6	0.45	0.22	0.03	0.10	0.02	0.95	0.13
Au	0.0024	0.11	0.053	0.02	0.008	0.011	0.000	0.03	0.006
Tl	?	0.66	0.15	0.10	0.01	0.054	0.011	0.31	0.04
Pb	24	26.5	6.2	8.5	0.88	2.6	0.49	10.3	1.1
Bi	0.34	0.28	0.097	0.03	0.01	0.024	0.011	0.20	0.03
Th	12	12.1	1.9	1.0	0.09	0.54	0.12	5.7	0.49
U	2.7	2.9	0.48	0.30	0.04	0.33	0.06	1.6	0.18

ICP-AES. Sample sets are analyzed in this order: first a procedure blank followed by all external standard reference materials, then an acid blank (for extra wash out time) followed by samples. A reference standard material is run as an unknown between every 10 samples. Each procedure then ends with a set of blind duplicate samples and a procedure blank followed by all external standards. Results for ICP-AES are reported in intensities, which is proportional to the amount (concentration) of that element in the analyzed sample. Element compositions of a given sample are quantified relative to reference standards. Finally, the elemental concentration values of the liquid are corrected for dilution to yield elemental concentrations in the solid rock sample. Based on the analysis of blind duplicates and standards, the average error for ICP-AES analyses generally ranged from 3 to 8%, depending on the element analyzed (Table 2).

Results

28 trace and minor elements were measured on a VG PQ-ExCell ICP-MS and eight major elements were measured on an ICP-AES at Oregon State University for the Rock Creek Canyon section (for results see Appendix 2). All elemental concentrations were normalized to Zr. The only significant source of Zr to pelagic sediments is from terrigenous material, thus normalizing to Zr removes the effect of variable terrigenous elemental components to these sediments (Milnes and Fitzpatrick, 1989). It should be noted that problems may arise with normalizing to Zr. The major source of Zr in these sediments is in zircons, which are very difficult to fully dissolve. Therefore, there is a chance that all of the Zr is

Element	MAG-1 Accepted Value	MAG-1 Mean	MAG-1 2σ	CS 16-268 Mean	CS 16-268 2σ	CS 16-168 Mean	CS 16-168 2σ	CS 15-55 Mean	CS 15-55 2σ
Al	86810.8	89089.4	10277.1	8748.2	551.7	4198.2	3597.6	40126.7	4085.4
Ba	480.0	499.6	84.7	493.8	58.4	185.0	12.8	1000.6	128.1
Ca	9792.2	9864.5	1288.1	323468	17308	336489	35232	7990.9	989.5
Fe	47566.2	47921.6	3288.8	5096.7	738.6	3224.6	384.3	21286	1690.1
K	29471.9	30530.8	4547.0	4631.5	14796.3	1780.1	5613.7	11391.3	454.7
Mg	18093.5	18459.1	2733.7	4322.5	656.4	3326.1	628.4	11366.6	1094.3
Mn	759.0	727.9	56.3	386.7	36.2	420.4	83.3	89.5	10.5
Na	28415.3	28300.5	2091.8	1222.7	185.9	738.9	757.2	5460.7	830.3
P	698.4	754.8	640.7	165.5	662.3	156.3	625.3	132.8	531.3
Tl	4496.1	4201.9	236.1	490.8	85.3	285.3	27.4	2200.5	209.8

Table 2. Mean and 2σ standard deviation for ICP-AES analyses of a blind standard and blind duplicates. All concentrations are ppm.

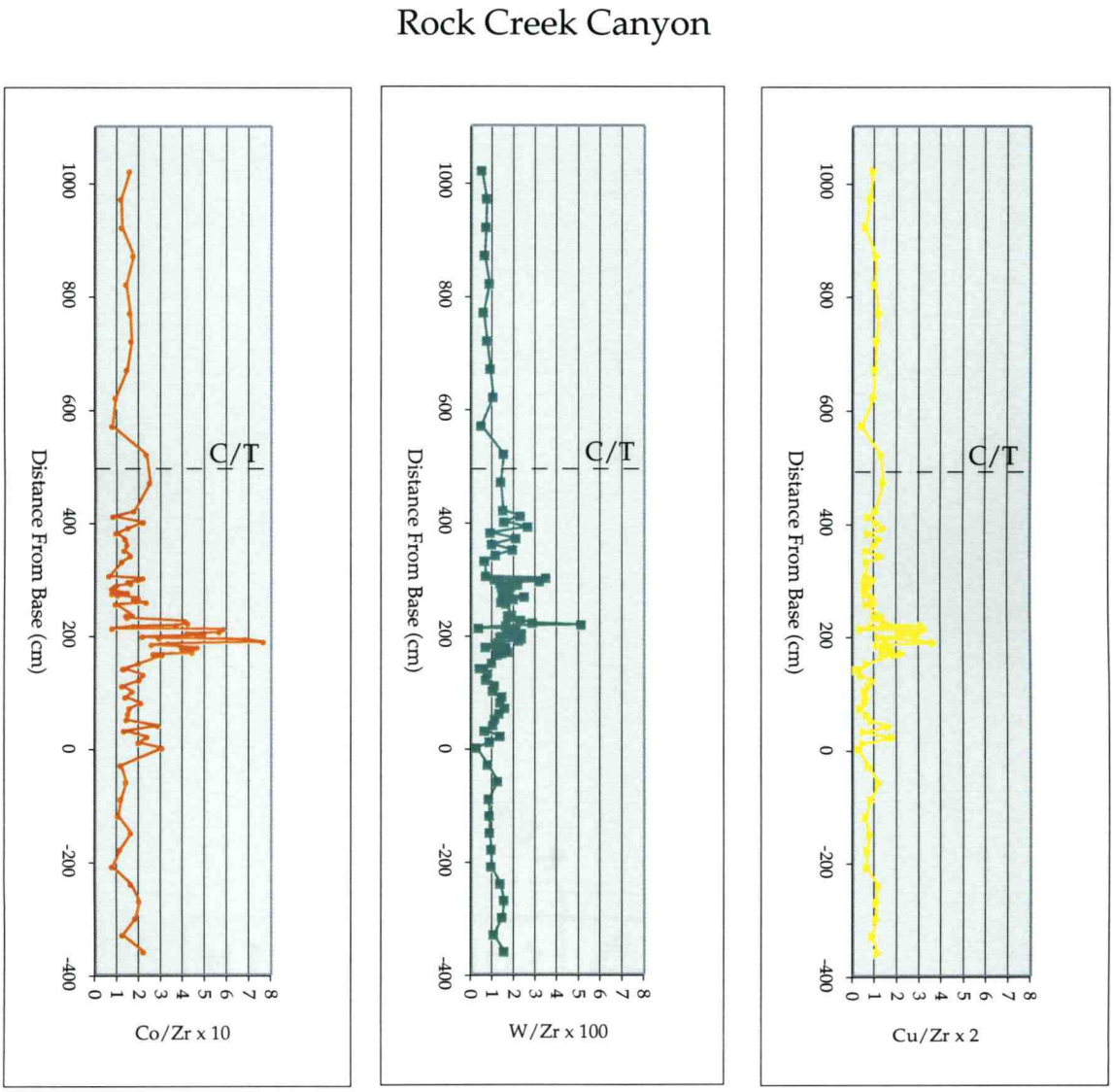

Figure 12. Co, Cu and W as Zr-normalized metal abundances for the Rock Creek Canyon section. An interval of high metal abundances can be seen below the C/T boundary shown as dashed line.

not being measured. However, an external reference material with a similar matrix as my samples shows that all of the Zr is being fully dissolved (Table 1), which makes me fairly confident that all of the Zr in these samples was in solution. Also, the behavior of Zr in the oceans is not well known, but displays a non-nutrient behavior with concentrations increasing with depth (Nozaki, 2001), indicating possible flux from sediments. This makes it difficult to determine if Zr measurements accurately represent terrigenous input. However, for this study, I assume all of the Zr is from terrigenous material.

A 2.5 m interval of Zr-normalized metal abundance anomalies can be seen in the Rock Creek Canyon section, between ~0 cm and 250 cm above the basal limestone (Figure 12 and Appendix 2). Within this interval are several distinct peaks with much higher abundances. The largest of these metal abundance peaks spans about 115 cm and is centered about 2 m above the basal limestone. There is a precursor of weaker metal abundances that spans 80 cm centered around the basal limestone (Figure 12). The upper anomaly is especially well developed in Mn, Ba, Y, Au, and Sr, and more weakly in Sc, As, Bi, Ag, Na, Cr, Co, Ni, Cu, Cd, Fe, V, Se, W, Pb, Mg and Ti. The lower anomaly is well developed in Mn, Na, Ba, Cr, Co and Sc, but is also seen in Sr, Y, Cu, Ag, W, Ni, Bi, Fe, Se, V, Au, As, Pb, Mg, Ti, and Cd. This interval of metal anomalies lies close below the C/T boundary, the stronger metal abundance area about 2 m below and the weaker abundance area about 4 m below.

Discussion

According to Sinton and Duncan's (1997) model, an increase in trace metals to the ocean from "event plumes" from volcanic eruptions of the Caribbean ocean plateau may have either (1) increased primary production by the introduction of biolimiting trace metals (such as Fe, Zn, Cu) as in HNLC regions in today's oceans, and/or (2) increased trace metal concentrations to toxic levels, causing an increased flux of organic carbon to bottom waters and reduction of O_2 levels, possibly leading to expansion of the oxygen minimum zone and ocean anoxia. If this "event plume" activity is the case, an increase in trace metals to ocean waters should be reflected in ocean sediments accumulating at these times. There are certain metals specifically associated with "event plume" activity, giving us a diagnostic suite of elements to look for in these sediments. According to Rubin (1997), metals concentrated in hydrothermal plumes generated by eruptions are those that are more volatile in a magmatic degassing fluid, such as B, Bi, Cd, Se, Hg, Ag, Pb, Au, Cu, As, Zn, Tl, In, Re, Sn and Mo (Figures 5 and 6). Elements that are less volatile, such as Fe, Mn, Ba, V, Sr, Sc, Co, Cr, Ni and Rb would more likely be found in higher concentrations in water/rock exchange reactions of typical steady-state hydrothermal vents. Elemental abundance patterns at Rock Creek Canyon show a stratigraphic interval of increased abundances in both the non-volatile and volatile elements. The presence of metal anomalies indicates concentrations of metals in the ocean, or at least at this site, were increased by some mechanism other than influx of terrigenous sediment, possibly the release of

metals in "event plumes". I interpret the anomalies at Rock Creek Canyon, in both the non-volatile and volatile elements, to indicate that this area of the world experienced the effects of both "event plumes" and increased hydrothermal venting.

An important aspect of many trace metals is that once they enter the ocean environment, they become biologically reactive (used in metabolic processes) and chemically reactive (used in inorganic reactions) and will be removed from seawater by scavenging particulate matter. Depending on how reactive they are, some will be scavenged very quickly whereas others will remain in ocean water much longer. An element's reactivity can mathematically be represented by its mean oceanic residence time (total mass dissolved in oceans/rate of supply or removal). Elements that are more reactive and are removed quickly have shorter residence times, whereas those elements that are less reactive and stay in ocean waters longer have longer residence times. In Figure 6 I have compiled a graph of most trace metals (adapted from Rubin, 1997) showing their volatility versus their mean oceanic residence times to get a better idea of what elements might be released by "event plumes" and what happens to them once they are in the ocean.

When we look at the results from Rock Creek Canyon according to this volatility vs. residence time figure, we can see some important features (Figure 13). For interval of metal abundance anomalies, elements that are less volatile and have shorter residence times are generally more enriched (abundances above background levels) compared with elements that are more volatile and/or have longer residence

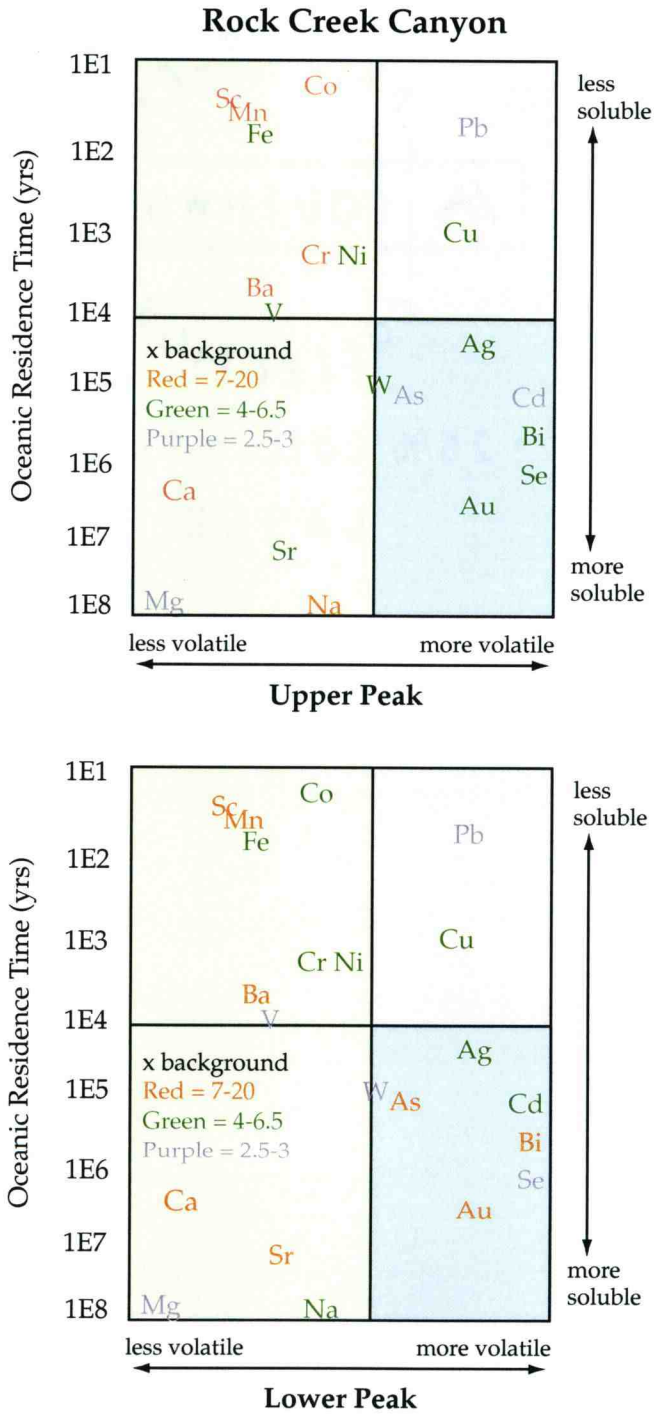

Figure 13. Rock Creek Canyon results according to the volatility vs. residence time figure.

times. For the lower (precursor) abundance anomaly peak, the less volatile, more reactive elements range about 7-18 times above background levels and for the stronger, upper abundance anomaly peak, are about 8-20 times above background levels. An enrichment in the less volatile elements indicates that Rock Creek Canyon was affected by water/rock exchange hydrothermal activity. This hydrothermal activity occurred on an intermittent timescale and therefore is associated with plateau construction rather than "steady-state" hydrothermal activity associated with mid ocean ridge spreading centers. Both the lower and upper abundance peaks also show enrichments in elements that are more volatile with a wide range of residence times. These elements are present at about 2-6 times background levels. The presence of the more volatile elements suggests that Rock Creek Canyon felt effects of "event plume" activity as well. These volatility vs. residence time data seem to be consistent with the location of Rock Creek Canyon in relationship to the suspected source of "event plumes". Assuming the source of event plumes was the Caribbean ocean plateau (over the Galapagos hotspot at 93 Ma), the Rock Creek Canyon was around 5000 km from this source (distance based on reconstructed plate position to ~90 Ma from Wignall, 1994). Thus, it is not surprising to see enrichments in elements found in both water/rock hydrothermal exchange activity and "event plume" activity, but also to see a change in element enrichment factors based on residence time. That is, metal anomalies are more pronounced in those elements that are more reactive (will be pulled out of ocean water faster), termed near-field elements, compared to those

elements that are less reactive (will remain in ocean waters longer), termed far-field elements. Eruptions on ocean plateaus could have been up to thousands of km^3 in volume, producing enough water/rock hydrothermal activity and "event plume" effluents to affect a site at a distance of 5000 km.

It should be noted that the elemental abundance pattern at Rock Creek Canyon does not exactly follow the volatility/solubility vs. mean oceanic residence time predicted pattern. This pattern is based on today's values, and although oceanic residence times in the Cretaceous may have been similar, they were probably slightly different, and therefore, may have resulted in a different abundance pattern. For example, behavior of some elements could significantly change with a change in ocean chemistry via O_2 draw down. This would vary their position on Rubin's diagrammatic representation of the different pathways an element in a submarine eruption can take based on oceanic residence time and volatility. For example, if ocean waters became dysoxic/anoxic, Fe and Mn would become significantly more soluble, increasing their residence times. This possible change in an elements behavior should be kept in mind when looking at results according to Rubin's volatility vs. residence time matrix.

Also, some of the major and minor element abundances that produce big anomalies, such as Na, Mg, Sr and Ca, are major constituents of seawater and an injection of a metal rich "event plume" would probably not significantly change their concentration in seawater. Therefore, it seems likely that something other than increased hydrothermal metal release is occurring that might cause these

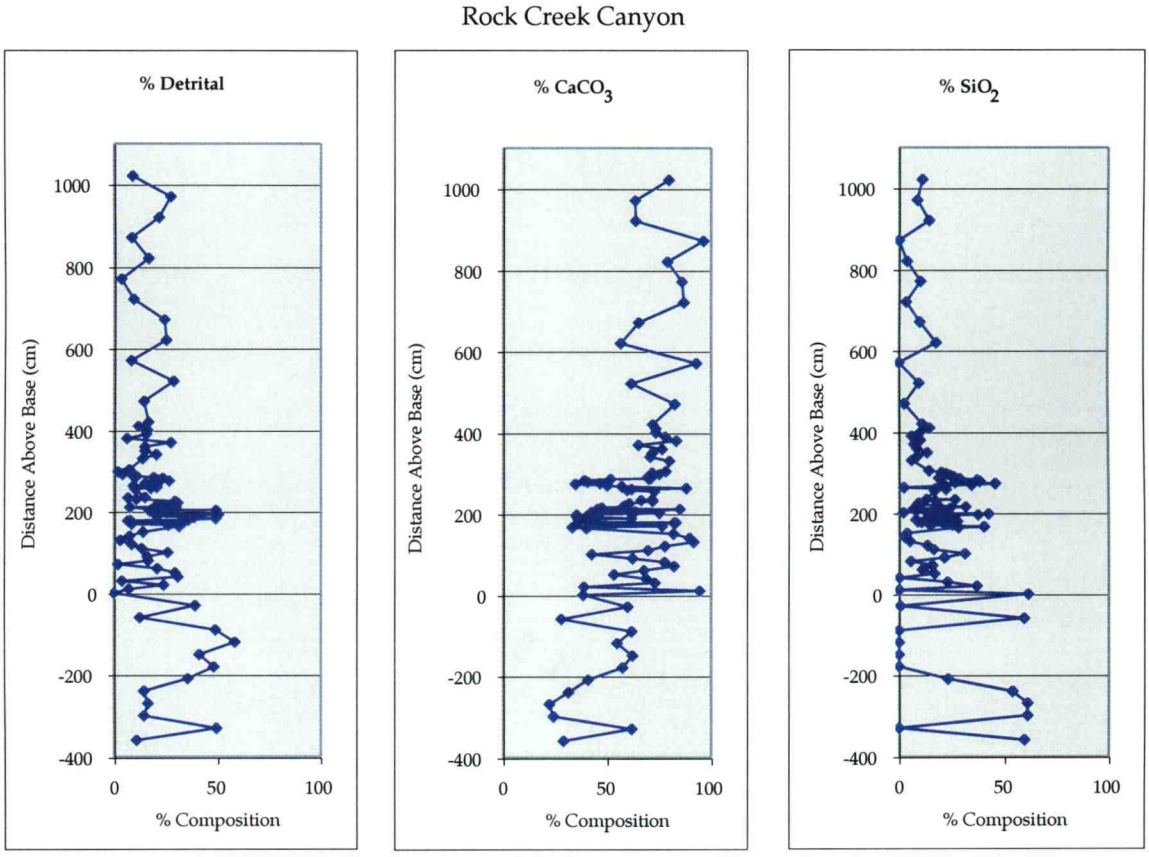

Figure 14. Compositional make-up of Rock Creek Canyon sediments.

elements to have higher concentrations in seawater at this time. These are precisely the elements that are the major dissolved ions in seawater. One possible explanation is that excess CO_2 from volcanism may have increased acidity of precipitation and enhanced continental weathering and increased the elemental concentrations in river water (Table 3), especially the major components such as Mg, Na, K, Ca, Rb, and Sr, and thus their supply to ocean waters. This increased weathering may explain why Na, Mg, Sr, and Ca have such high abundances above background values but are not predicted from the volatility vs. oceanic residence time pattern.

Metal Anomalies in Relation to Bulk Sediment Composition

Although elemental concentrations have been normalized to Zr to remove the terrigenous component of these sediments, it is important to look at the compositional make-up of these sediments to make sure there is not a large flux of detrital material in the same place as the metal anomalies. The detrital fraction is calculated from Al concentrations, assuming that Al_2O_3 makes up about 17% of typical shale composition (Gromet et al., 1984). The $CaCO_3$ fraction is calculated from Ca concentrations, assuming that all of the Ca is from $CaCO_3$ and the SiO_2 fraction is calculated by subtracting the detrital and carbonate fractions from 100%. The variability in the fractions of these three components in Rock Creek Canyon can be seen in Figure 14. There is a slight increase in the detrital component of the sediments at the same position as the stronger, upper anomaly peak. However, the increased trace metal concentrations span about 115 cm and the increased detrital

Element	Average Black Sea Sediments	Average Gulf of California Sediments	Average Early Jurassic Black Shales	Average C/T Black Shales	Average Deep Sea Clays	Average Metal Source Potential of Deep Sea Clays
Ag	0.3	0.2		3.3	0.2	0.1
Ba		566	191	771	580	
Cd	1	2.5	2.7	16	0.225	0.1
Co	28	6.6	21	34	19	40
Cr		44	65	263	90	
Cu	58	27	72	218	39	100
Mn		193	908	282	850	
Mo	29	11.9	19	39	2.6	5
Ni	76	38	101	201	68	
Pb	18	17	59	15.3	20	
Sb		2		10	1	1
Sr		167	1721	223	230	
V	106	101	163	790	130	50
Zn	106	88	285	975	115	50

Table 3. Average trace metal composition of modern Black Sea sediments, upwelling sediments from the Gulf of California, early-Jurassic black shales from SW Germany, C/T black shales and deep-sea clays and an estimate of the metal source potential of deep-sea clays. All concentrations are ppm. It can be seen that the trace metal chemistry of C/T black shales is distinct when compared to other anoxic sediments and also can not be explained by leaching of deep-sea clays. All data from Brumsack (1986) except for average deep-sea clays data which is from Colley et al. (1984).

composition only spans about 50 cm. There is no increase in the detrital component of the Rock Creek Canyon sediments around the location of the lower, weaker metal abundance anomalies. Lastly, there is a large flux of detrital material in this core at –130 cm. However, in the element/Zr panels, there are no metal abundance anomalies, which is encouraging that normalizing to Zr has taken out the terrigenous elemental components.

Metal Anomalies in Today's Ocean Anoxic Places

Significant metal anomalies do exist in these sediments, thus it is important to consider whether or not these trace metal abundances result from an actual increase in metal concentrations in the ocean, caused by increased hydrothermal input, or are the result of some other process, such as accelerated accumulation by increased productivity, sediment diagenesis, or metal scavenging and particle transport to the ocean floor during anoxic events. It can be seen from modern ocean anoxic sediments (such as the Black Sea and Gulf of California) that some trace metals do accumulate at greater rates compared to oxic sediments. However, Brumsack and Thurow (1986) compared trace metal chemistry of Cenomanian/Turonian black shales and early Jurassic black shales from southwest Germany with modern upwelling-related sediments from the Gulf of California, to show that the pattern of trace element abundances of the C/T black shales is quite distinct (Table 3). In their study, C/T black shales showed an extremely high enrichment of trace metals (particularly in Cd, Ag, Zn, Sb, Mo, Cu and V) not typical of the early Jurassic black shales or upwelling-related organic-rich

sediments. Considering the low trace metal content of plankton (for compilation see Brumsack, 1983), it seems unlikely that high biological productivity could concentrate enough metals to account for the extreme trace metal content of C/T black shales (Brumsack and Thurow, 1986). Another aspect to consider is that metal anomalies in these C/T sediments may be a result of diagenetic metal accumulation. According to Brumsack and Thurow (1986), based on the metal source potential of deep-sea clays, the element enrichment pattern of C/T black shales cannot be explained by this process either. They suggest that the enrichment factor of C/T shales is higher than that which can come from reasonable amounts of diagenetically released metals (Table 3) and therefore these metal anomalies are probably not a result of diagenetic accumulation.

Intervals of complete stagnation, as would occur in anoxic basins, may have been able to trap metals from seawater to produce high abundances in sediments. However, C/T black shales also show a significant enrichment of trace metals compared to Black Sea sediments (a present day stagnant basin) (Table 3). Therefore, if stagnation conditions could trap significant amounts of metals to produce these C/T signals, it would be expected that the metal anomalies would fall within the stagnant, anoxic sediments. However, the metal anomalies for the Rock Creek Canyon section actually fall stratigraphically below the worldwide OAE2, and thus do not fall within maximum anoxic conditions. If the C/T trace metal anomalies are due solely to either simply higher productivity induced (e.g.,

upwelling) anoxia, stagnant basin anoxia, or sediment diagenetic conditions, it is expected that similar anomaly patterns would be seen in all black shales.

Position of Metal Anomalies, Carbon Isotopes and Species Mortality in the Rock Creek Canyon Section

There are a number of ways to distinguish the onset and duration of OAE2, but probably the best and most universally utilized is the pronounced global carbon isotope excursion. The onset of OAE2 is recognized by the shift towards more positive $\delta^{13}C$ values. This indicates that marine organic matter (more negative $\delta^{13}C$ values) is removed from the carbon reservoir (i.e., buried). The slower regeneration of light carbon (i.e., increased burial), due to low levels of benthic oxygen in expanding oxygen minimum zones (Arthur et al., 1987; Schlanger et al., 1987; Pratt et al., 1993), leaves the ocean more enriched in heavy carbon, producing the more positive $\delta^{13}C$ values. As this process continues through the duration of the ocean anoxic event, the ocean becomes increasingly more positive. The conclusion of OAE2 is recognized by the shift in the carbon isotope curve back to more negative (i.e., background) $\delta^{13}C$ values. This shift indicates that light organic matter is once again being recycled into the ocean, due to the presence of oxygen and thus respiration. Bulk sedimentation rates for the Rock Creek Canyon section have been determined from evolutive harmonic analysis and stratigraphic modeling by Meyers et al. (2001). Based on their average sedimentation rates, OAE2 lasted about 600 k.y.

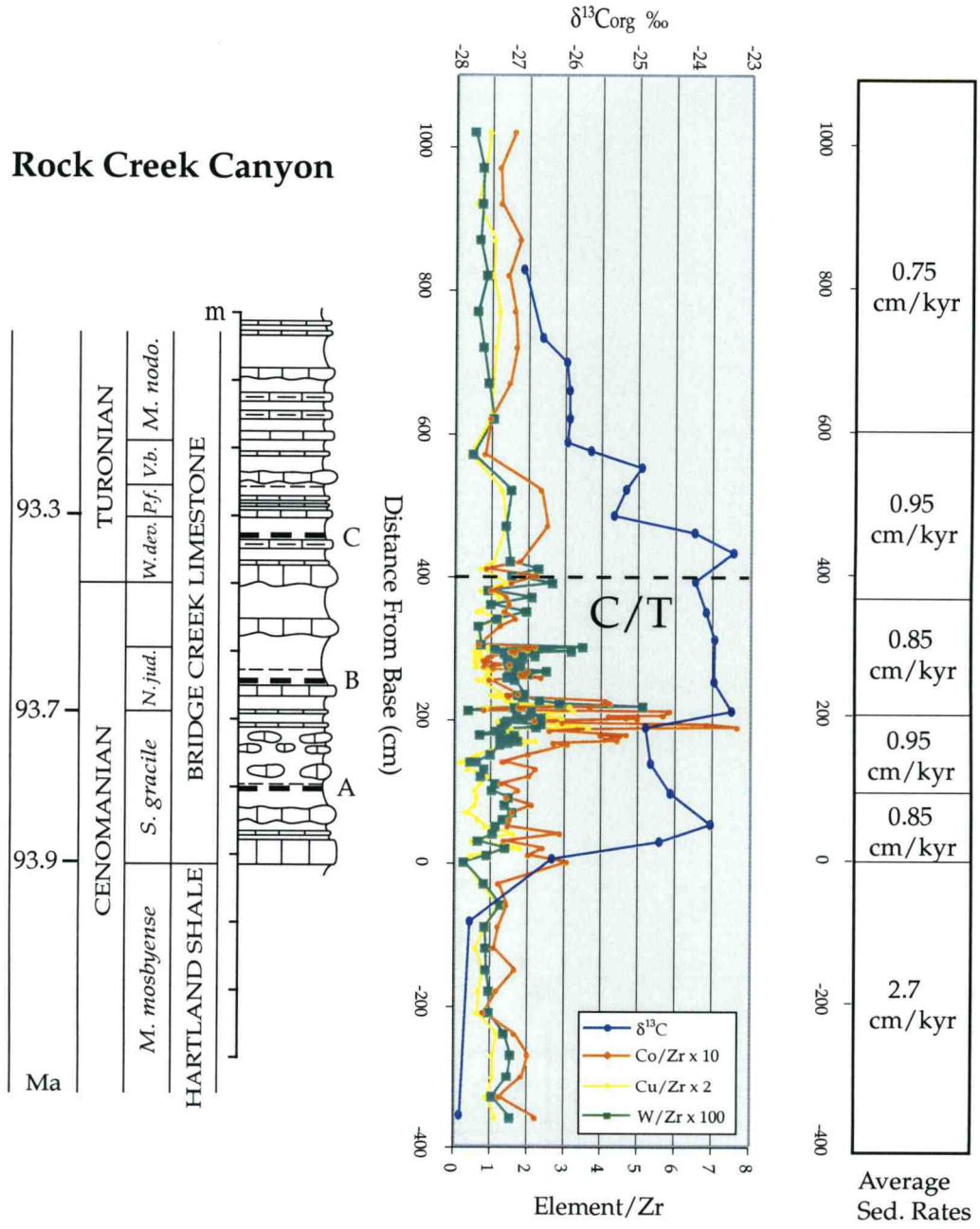

Figure 15. Position of Rock Creek Canyon metal abundance anomalies with respect to the carbon isotopic curve. Carbon data from Pratt et al.(1993). Time scale from Kauffman et al. (1993) and sedimentation rates from Meyers et al. (2001). C/T boundary shown as dashed line.

To determine the relationship between the metal anomalies in the Rock Creek Canyon section and the onset and duration of OAE2, it is important to examine their timing relative to the carbon isotope curve (Figure 15). All time estimates are based on average sedimentation rates from Meyers et al. (2001). The lower weaker interval of metal abundance anomalies falls at approximately the time when the $\delta^{13}C$ curve just begins to shift towards more positive values, at the onset of OAE2. The upper, stronger interval of metal abundance anomalies occurs above the initial shift towards more positive $\delta^{13}C$ values, but at approximately the onset of the main duration of the $\delta^{13}C$ positive event. Both metal anomalies last about 120 k.y, which suggests that volcanic activity occurred over a similar time period. This timing is consistent with the speculated eruption history of ocean plateaus, which is that magmatism occurs in short, large volume pulses erupting in periods of days to decades, over a total duration of 10^5-10^6 years. The stratigraphic position of these metal anomalies, the lower peak at ~160 k.y. below and the upper peak right at the main C/T OAE event, gives a good indication of the timing of events, which is that the metal anomalies, indicating an "event plume" eruption, occur before the main onset of OAE2. The OAE then lasts about 600 k.y. before oxygen is restored and $\delta^{13}C$ returns to background values. The position and timing of these anomalies supports the hypothesis that "event plumes", associated with eruptions on the Caribbean ocean plateau, may be directly related to the reduction of O_2 levels, possibly leading to ocean anoxia.

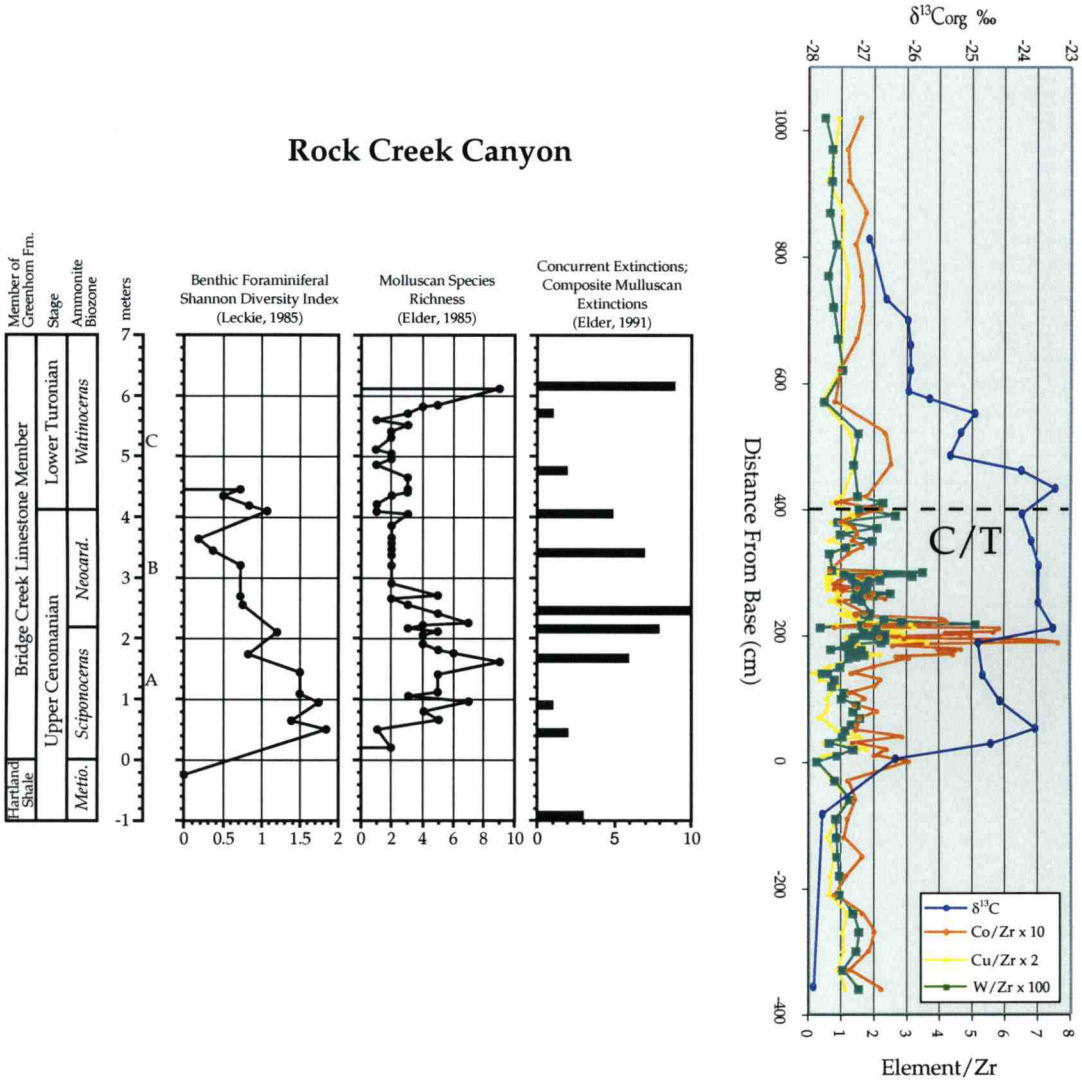

Figure 16. Position of Rock Creek Canyon metal abundance anomalies with respect to evolutionary turnover (speciation and extinction). Ammonite biostratigraphy, lithostratigraphy and bentonite beds from Elder (1985) and Elder and Kirkland (1985). Figure from Leckie (1989).

Another important relationship to investigate is the position of the metal anomalies with respect to species mortality. The release of high abundances of trace metals to the ocean surface has the potential to increase primary production and/or produce mass mortality from toxic metal concentrations. Therefore, looking at the biostratigraphic data can give yet another indication of the order of events during this period. It has been documented that major species perturbations, particularly in radiolaria, calcareous nannoplankton (Bralower, 1988) and deeper-dwelling planktic foraminifera, occurred during the main OAE2 event and have been attributed to the expansion of the oxygen minimum zone (Leckie, 1985, 1989). However, more noteworthy is a study conducted by Leckie et al. (1998) of planktonic and benthic foraminiferal assemblages in rocks from several sections of the southwestern U.S. Western Interior Seaway, including the Rock Creek Canyon section. The interval of metal anomalies we see in this section seems to fall in the same position as an interval for which Leckie et al. (1998) noticed accelerated rates of evolutionary turnover (speciation and extinction) in plankton and benthic foraminifera, radiolaria and mollusks (Figure 16), about 2 m below the C/T boundary. According to Leckie et al. (2002), changing nutrient availability and water column stratification, possibly related to elevated rates of hydrothermal activity, were likely the major factors responsible for high species turnover during the OAE2. Increased rates of speciation and extinction may be a result of biolimiting trace metals entering the ocean, stimulating production or leading to toxicity. Also, excess CO_2 from volcanism may have resulted in increased

Element	Average River Water Concentration Today (mg/kg)
Na	6.3
Mg	4.1
K	2.3
Sr	0.07
B	0.01
Li	0.003
Mo	0.0006
As	0.002
V	0.0009
Ni	0.0003
Zn	0.02
Cu	0.007
Cs	0.00004
Cr	0.001
Sb	0.00007
Se	0.00006
Cd	0.00001
Ag	0.0003
Pb	0.002
Sn	0.00004
Ca	15
Co	0.0001
Ba	0.08
Mn	0.007
Fe	0.04
Rb	0.001

Table 4. Today's average river concentrations from Taylor and McLennan (1985).

continental weathering, leading to excess runoff of nutrients, and other elements in river water (Table 4), and increased production and species turnover. Conversely, excess CO_2 may have lowered seawater pH and reduced carbonate availability, a necessary component in calcium carbonate used by many planktonic organisms to form their hard parts, stressing and leading to the loss of calcareous plankton (Leckie et al., in press). An increased supply of nutrients may in fact have had an indirect negative effect on some species. Habitat expansion of previously nutrient-limited organisms may have resulted in major changes to ecosystems. Erba (1994) suggested this as a partial cause to the early Aptian "nannoconid crisis", in which a group of heavily calcified calcareous nannoplankton experienced major perturbations, and the same may have been true in producing the demise of species around OAE2.

Summary and Conclusions

In this chapter, I examined a C/T boundary section from Rock Creek Canyon, Pueblo, Colorado for major, minor and trace elemental abundances. The C/T boundary of the late Cretaceous is synchronous with OAE2 and with the massive volcanism that built the Caribbean ocean plateau at around 93 Ma. It has been suggested by Sinton and Duncan (1997) that these events are related because of their temporal coincidence. In particular, they proposed that metal rich, eruption related hydrothermal "event plumes" accompanying ocean plateau construction may have pushed the ocean temporarily into anoxia. If this hypothesis is true, high metal abundances, marking the presence of ocean plateau "event plumes", should

be present in sedimentary sections around the C/T boundary. The stratigraphic position of metal abundance anomalies indicates the timing of "event plumes" with respect to the onset of anoxia and other indicative biogeochemical responses.

Trace, minor and major element analyses demonstrate an interval with two distinct abundance peaks. The lower, weaker anomaly, especially well developed in Mn, Ba, Y, Au and Sr, lies about four meters below the C/T boundary and the upper, stronger anomaly, well developed in Mn, Na, Ba, Cr, Co and Sc, lies about two meters below the C/T boundary. The two anomalies show increased abundances in both the non-volatile (concentrated in water/rock solubility reactions) and volatile (concentrated in gas rich magmatic fluids) elements, suggesting this area may have felt affects of both eruption related "event plumes" as well as eruption related water/rock hydrothermal exchange. Both metal peaks are more abundant in the less volatile, more reactive elements, such as Sc, Co, and Mn and Fe, and less abundant in the more volatile, less reactive elements such as Se, Cd, W, Au and Bi. Assuming the source of "event plume" metals was the Caribbean ocean plateau, the Rock Creek Canyon is in fairly close proximity to this source and therefore, it is expected to be rich in more volatile and less volatile elements as well as near-field and far-field elements, with near-field being more dominant.

An important aspect of these metal abundance anomalies is that the lower peak of metal abundances occurs right at the beginning of OAE2, as defined by the initial positive increase in $\delta^{13}C$ values, and that the upper peak of metal abundances

occurs right at the onset of the main duration of OAE2, defined by constantly positive $\delta^{13}C$ values. This stratigraphic position indicates that "event plumes" lead to ocean anoxia. The synchronous position of the lower abundance anomaly with the first signs of a positive shift in $\delta^{13}C$ values suggests that this first "event plume" injection may have consumed enough oxygen to shift the ocean into anoxia. The position of the stronger upper metal anomaly right before the main duration of OAE2 suggests that this larger event may have consumed enough oxygen in an already partially anoxic ocean to maintain these conditions for a significant period. The synchroneity of the lower metal abundance anomaly and high rates of speciation and extinction in foraminifera, radiolarians and mollusks, as reported by Leckie et al. (in press), seems to strengthen the argument that "event plumes" carried biolimiting and/or toxic concentrations of metals into the ocean. Increased productivity resulted in an increasing supply of organic carbon to the deep ocean, thus exhausting oxygen supplies and bringing about the demise of benthic species. The collapse of planktic species was most likely brought about by the stress induced by major environmental perturbations, shrinking or loss of ecological habitats, increased predation, increased pCO_2 and river runoff, and possible metal toxicity (Erba, 1994; Leckie et al., 2002).

Due to the stratigraphic location of these metal anomalies, falling at the onset of the $\delta^{13}C$ positive shift and the OAE2, I interpret that metals released in an "event plume", during an eruption on the Caribbean ocean plateau, may have consumed enough oxygen by either the reduction of reduced material and/or the

influx of biolimiting trace metals. Thus, it seems highly reasonable that there is indeed a relationship between ocean plateau formation and anoxia during the mid to late Cretaceous.

Chapter 3: The Global Distribution of Metal Anomalies around the Cenomanian/Turonian Boundary. Evidence for the Ocean Plateau Formation – Global Anoxia Connection

Abstract

Initial volcanism that formed a large part of the Caribbean ocean plateau appears to have coincided with ocean anoxic event 2 (OAE2), which occurred close to the Cenomanian/Turonian (C/T) boundary (~93 Ma). Increased trace metal delivery to the surface ocean during volcanic activity associated with this ocean plateau has been suggested as the cause for the depletion of seawater oxygen concentration and deposition of organic rich sediments. An interval of trace metal anomalies can be seen in pelagic carbonate and black shale sequences of the Rock Creek Canyon section, Pueblo, Colorado at the onset of the $\delta^{13}C$ global positive event. In interpret the presence of these metal anomalies and their stratigraphic position as indicating a relationship between ocean plateau formation and ocean anoxia.

To further strengthen the argument for a direct connection between ocean plateau formation and ocean anoxia, I determined the distribution of major, minor and trace element abundances in pelagic carbonate and black shale sequences from an additional four globally distributed sites (Bass River, New Jersey; ODP Site 1138, central Kerguelen Plateau; Baranca el Cañon, Mexico; and Totumo, Venezuela). After normalizing element concentrations to Zr to remove the effect of variable terrigenous input to these sediments, an interval of metal anomalies, at approximately the same stratigraphic location, is present in all five sites. The

changes in the trace metal patterns and intensities among these sites is consistent with modeled late-Cretaceous surface circulation and a source of metals being the Caribbean ocean plateau.

Introduction

To further determine a connection between formation of the Caribbean ocean plateau and OAE2, it is important to investigate other Cenomanian/Turonian (C/T) pelagic sediment records for signs of submarine volcanic activity. In particular, I have chosen a set of four globally distributed sections (Figure 17): the Bass River Borehole, New Jersey; ODP Leg 183, Site 1138, central Kerguelen Plateau; the Baranca el Cañon section, Mexico; and the Totumo-3 Well core, Venezuela to analyze bulk sediments for trace metal abundance patterns. Again, the appearance of metal anomalies indicates "event plume" activity and the stratigraphic position of metal anomalies determines the timing of "event plume" activity relative to other biogeochemical responses.

Another important aspect to consider in this study is variation in the patterns and intensity of trace metal abundance signals in the five globally distributed sites relative to the proposed source of metals (Caribbean ocean plateau). Vogt (1989) argued that hydrothermal megaplumes from submarine eruptions ~ 15km^3 volume had enough thermal buoyancy to rise to the surface. Considering that single lava flows from ocean plateaus were much larger, eruptions could have produced "event plumes" that easily spread through the water

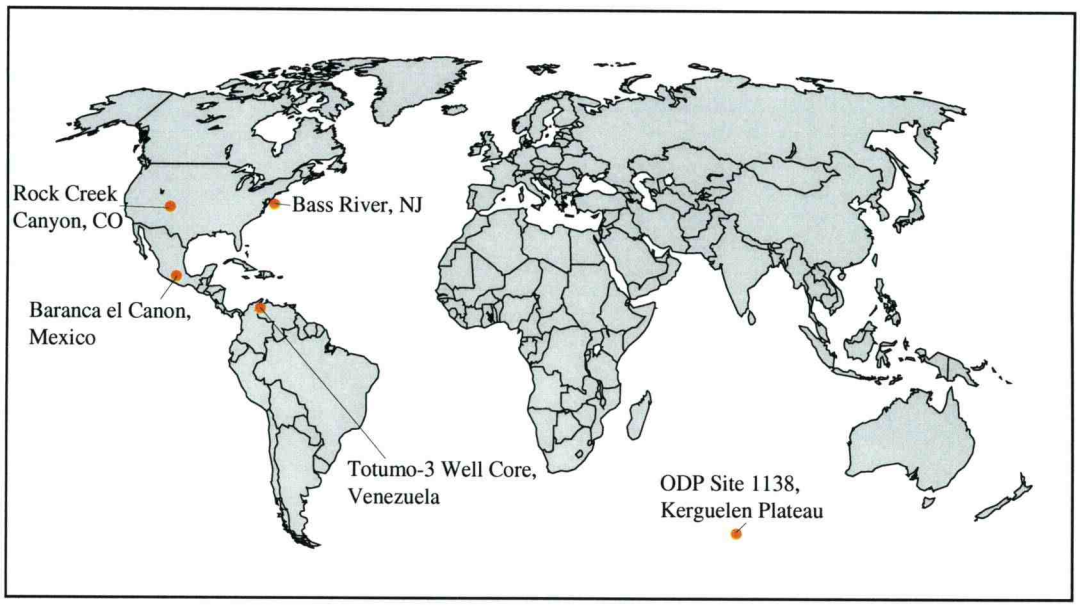

Figure 17. Map showing location of the five globally distributed sites.

column and up to the sea surface. Metals and warmed ambient seawater would then be transported throughout the ocean by surface circulation while metals were being removed from seawater by particle scavenging. Those elements with longer residence times (less reactive) are expected to remain in ocean waters longer than those elements with shorter residence times (more reactive). I am investigating if changes in trace metal patterns and abundances are consistent with modeled late-Cretaceous ocean circulation and with Rubin's (1997) general predicted element enrichment pattern based on element volatility and residence times.

Cretaceous Ocean Circulation

Early modeling (Luyendyk et al., 1972; Gordon, 1973; Haq, 1984) of the circulation of the mid-Cretaceous oceans applied present day wind stress profiles or oceanic circulation patterns and biogeography patterns to mid-Cretaceous paleocontinental reconstructions. These models simulate a circumglobal current flowing westward through the Pacific Ocean and the Tethys Ocean. Most of these reconstructions suggest that much of the Pacific surface circulation was similar to the present day, just simply in a larger ocean. More recent models of Cretaceous ocean circulation (Barron and Peterson, 1989, 1990) include atmospheric forcing (temperature, precipitation-evaporation, and wind stress) from mid-Cretaceous atmospheric general circulation models. These models also predict that much of the Pacific circulation was similar to the modern day, with the exception of the Cretaceous analogue of the Oyashio current, which means a westward flowing equator current, counter-clockwise circulation in the southern hemisphere, and

clockwise circulation in the northern hemisphere. However, in contrast to the westward-flowing circumglobal current flowing through the Tethys Ocean, these models simulate a clockwise circulation with easterly flow along the northern margin and westerly flow along the southern margin (Figure 18).

Global, atmospheric, general circulation models have also been run for circulation within the U.S. Western Interior Seaway and indicate a strong counter-clockwise gyre controlling surface flow over the whole north-south extent of the seaway and linking tropical Tethyn waters in the south to cold Boreal waters in the north (Slingerland et al., 1996; Kump and Slingerland, 1999).

Examining models of the simulated mid-Cretaceous surface circulation can give a rough estimate of where "event plume" metals could migrate. Assuming the Caribbean Plateau is the source of "event plumes" (and other hydrothermal activity), and was formed in approximately the present location of the Galapagos hotspot (around 2°S, 90°W), metal rich plumes may have been entrained in waters moving westward into the Pacific Ocean or moving north and northeast into the Western Interior Seaway and Tethys Ocean, according to the current models of late-Cretaceous surface circulation.

Study Sites

Bass River Borehole (ODP Leg 174AX), NJ

The Bass River borehole (ODP Leg 174AX) was drilled on the New Jersey Coastal Plain, USA and recovered approximately 200 ft of upper Cenomanian to

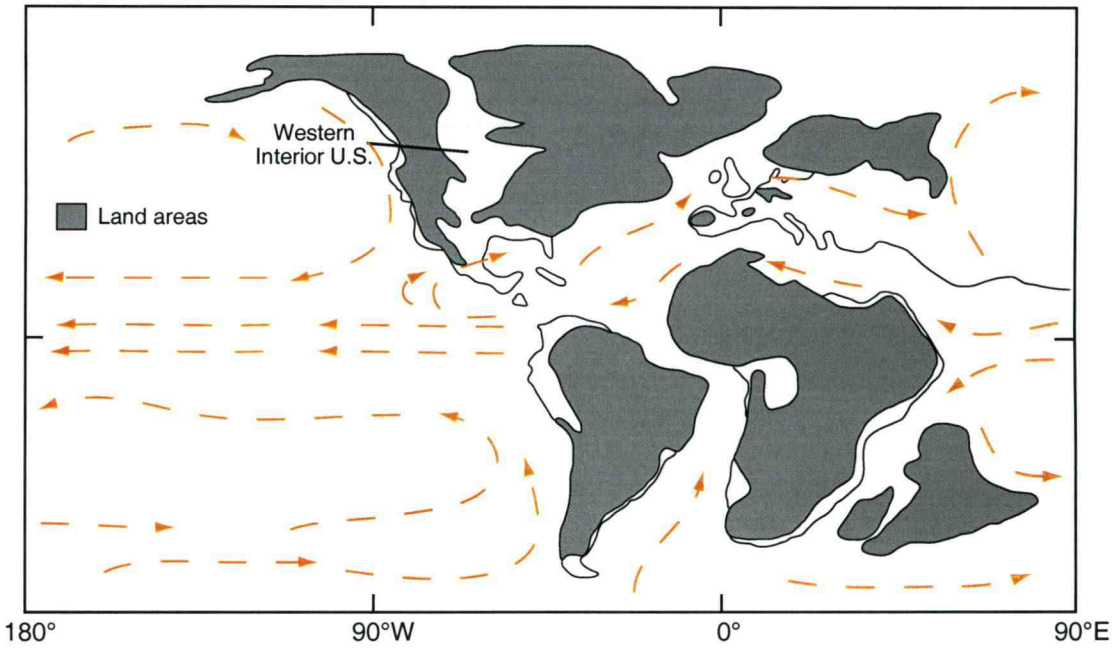

Figure 18. Simulated late-Cretaceous surface circulation on reconstructed plate positions, from Wignall (1994), illustrated by streamlines, which follow the flow, taken from Barron and Peterson (1990). Streamlines show the westward-flowing circumglobal current and the clockwise circulation through the Tethys Ocean. Detailed circulation for the U.S. Western Interior Seaway indicates a strong counter-clockwise gyre linking Tethyn waters to Arctic waters (Slingerland et al., 1996; Kump and Slingerland, 1999).

lower Turonian strata, including the Bass River sequence that spans the C/T boundary. Sugarman et al. (1999) place the C/T boundary for this section at 1935.5 ft (590.6 m) below sea floor. Benthic foraminifera from this core indicate that the entire section was deposited in a shallow shelf marine environment with sedimentation rates ranging from 2.35 to 3.07 cm/k.y. (Sugarman et al., 1999). Samples for this study were taken from the lower part of the Bass River sequence, which consists predominantly of very dark gray laminated, fossiliferous silty clay. Samples were collected approximately every five inches from a sample depth of 1950 ft to 1941 ft below sea floor and approximately every three inches from a sample depth of 1941 ft to 1925 ft below sea floor.

The carbon isotopic record for the Bass River borehole shows the familiar positive increase starting below the C/T boundary. These increased $\delta^{13}C$ values continue into the lower Turonian, in association with high values of organic carbon in the sediments as well. The $\delta^{13}C$ profile from the Bass River borehole can be correlated with the global carbon burial event recorded at the Rock Creek Canyon section and in high resolution C/T sections in Europe (e.g. Pomerol, 1983; Gale et al., 1993; Jenkyns et al., 1994).

ODP Leg 183, Site 1138, Central Kerguelen Plateau

ODP cores 1138A-69R and 70R were taken on the central Kerguelen Plateau (53° 33'S, 75° 58'E). The top of core 69R, Sections 1 through 5, consists of light to dark gray chalk interbedded with very dark gray to black shale. Section

5 contains a 1-m thick black, organic-rich claystone that is unburrowed and displays faint horizontal laminae (Coffin et al., 2000). This lowermost Turonian section marks the main OAE2 event and confirms that this ocean anoxic event was experienced in the Cretaceous high-latitude Indian Ocean. The bottom of core 69R, Section 6, and top of core 70R, Section 1, consists of a reddish brown to light gray glauconite-bearing calcareous sandstone (Coffin et al., 2000). These sediments were probably deposited in a nearshore shelf region of a subsiding volcanic edifice during the major Cretaceous transgression (Wise et al., 2002). Samples were taken approximately every 20 cm in core 69R, Sections 1 through 4, and every 10 cm in core 69R, Sections 5-6, and core 70R, Section 1. Carbon isotope data are not yet available for these samples (Wise and Meyers, in preparation, 2002).

Baranca el Cañon, Mexico

The Baranca el Cañon section is located in southwest Mexico (northern Guerrero State) and comprises upper Cenomanian and lower Turonian strata. The upper Cenomanian consists of shallow-marine limestones of the Morelos Formation which is part of the Guerrero-Morelos carbonate platform (Aguilera-Franco et al., 2001). Rocks are characterized by 0.3-1.5m thick limestone beds with mollusc fragments and benthic foraminifera (Aguilera-Franco et al., 2001). The Mexcala Formation represents the lower Turonian and is characterized by open-marine limestones. The Morelos and Mexcala Formations together represent the maximum development of the Guerrero-Morelos Platform and the transition

from a shallow-marine to a deeper-marine environment due to drowning and burial of the platform as a result of tectonic and eustatic sea level change (Hernandez-Romano et al., 1997). This site does not contain any black shale sediments, indicating the shallow ocean waters at this location were oxic throughout the C/T boundary. Samples are approximately every half-meter from 47 m to 83 m above the base and span the C/T boundary. The Baranca el Cañon carbon isotopic profile contains the positive $\delta^{13}C$ excursion characteristic of many other C/T boundary sections throughout the world (Elrick and Molina, 2002). Previous studies (Hernandez-Romano et al., 1997 and Aguilera-Franco et al., 2001) suggest that the C/T boundary lies at the Morelos-Mexcala contact. However, given the observed C-isotope profile, the C/T boundary lies well below this contact (Elrick and Molina, 2002).

Totumo-3 Well Core, Venezuela

The Totumo-3 Well core was drilled in the Maracaibo Basin, located in northwestern Venezuela, and spans the upper Cenomanian to Campanian of the well-known La Luna Formation. This formation is characterized by thin-bedded, laminated, organic-rich black shales interbedded with limestone and chert (Martinéz and Hernandez, 1992) which were deposited in a hemipelagic to pelagic environment, in water depths of approximately 200-300 m (Peréz-Infante et al., 1996). High organic carbon content and lack of benthic foraminfera suggest that sediments were deposited in an anoxic environment. However, occasional bivalve fragments indicate at least brief periods of benthic oxygenation (Davis et al.,

1999). Samples were collected from the base of the La Luna Formation through the C/T boundary and are taken approximately every 0.5 m. The C/T boundary is located 15 m above the base of the La Luna Formation (de Romero et al., 2002). The organic carbon fraction of samples from the Totoumo-3 Well core exhibit the $\delta^{13}C$ positive signal (de Romero, personal communication, 2002) typical of the C/T boundary globally.

Sample Preparation and Analyses

Methods for preparation, digestion and elemental analyses for these four sites are the same as those described in Chapter 2. Based on the analysis of blind duplicates and standards, the average error for ICP-MS trace and minor element concentrations is about 10% and for ICP-AES major element concentrations ranges from 3 to 8%, depending on element analyzed (Table 1 and 2).

Results

28 trace and minor elements were measured on a VG PQ-ExCell ICP-MS and eight major elements on an ICP-AES at Oregon State University for, the Bass River Borehole, ODP Leg 183, Site 1138, the Baranca el Cañon sections, and the Totumo-3 Well core (for results see Appendix 3). All elemental concentrations were normalized to Zr.

Bass River Borehole, (ODP Leg 174AX), NJ

Very weak abundance anomalies in V, Cu, As, Pb, Sb, Fe and Bi can be seen at depths of 1945, 1941 and 1935 feet below sea floor (fbsf) and lie about 10

ft, 6 ft and 0 ft below the C/T boundary (Figure 19). However, these anomalies are not very distinct and are not present in any other elements.

ODP Leg 183, Site 1138, Central Kerguelen Plateau

A 3.5 m interval of Zr-normalized metal abundance anomalies can be seen in this section from the central Kerguelen Plateau between 655.5 mbsf and 659 mbsf (Figure 20). Within this interval are several peaks with much higher abundances. These are especially well developed in As, Se, Rb, Mo, Cd, U, and Bi, but are also seen in V, Zn, Cs, Sb, Y, Cr, Ag, Fe, Ba, Tl, Mg, Co, Ni, Cu, Sc, Mn and Sn. The most enriched part of the interval of metal anomalies falls 1-3 m below the tentative placement of the C/T boundary.

Baranca el Cañon, Mexico

A 10 m interval, between 50 and 60 m above the base, and a weaker 11 m interval, between 71 and 82 m above the base, of Zr-normalized metal abundance anomalies can be see in the Baranca el Cañon, Mexico section (Figure 21). The lower interval of metal peaks is well developed in Ag, Mo, Au, Na, Sb, Zn, Se, Y but also seen in V, Ba, Fe, As, Cu, U, Cr, Mn, Mg, Sc, Ni, Th, Co, Sr, Cs, W, Ti and Pb. The upper interval of metal abundance anomalies is well developed in Ba, Cu, Cr, W, U, Zn, Sb and Ni and more weakly in Co, Sr, Na, Mg, Mn, As, V, Pb, Ti, Se, Sc, Y, Ag, and Cs. The lower interval of metal anomalies falls below the Morelos-Mexcala contact.

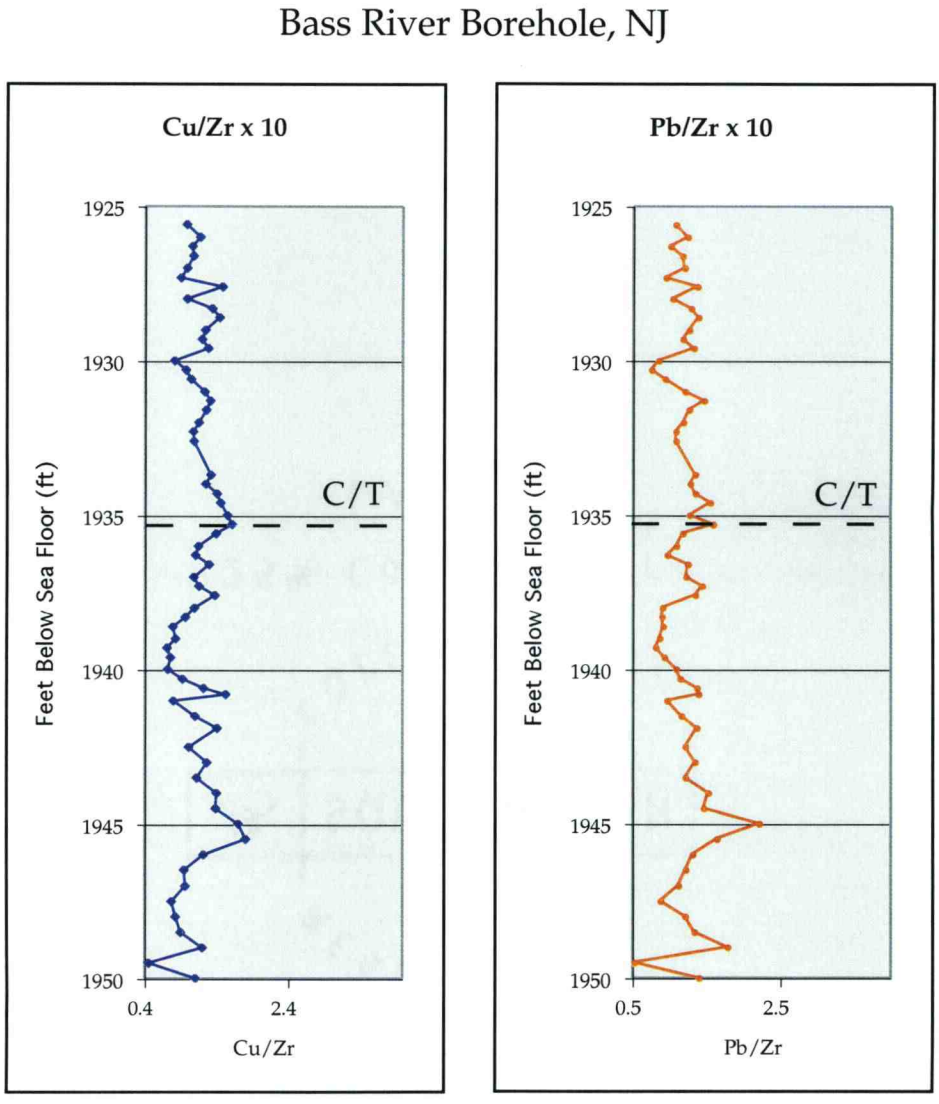

Figure 19. Cu and Pb as Zr-normalized metal abundances for the Bass River Borehole. Intervals of very weak high metal abundances can be seen at 1945 fbsf, 1941 fbsf and 1935 fbsf. C/T boundary show as dashed line from Sugarman et al. (1999).

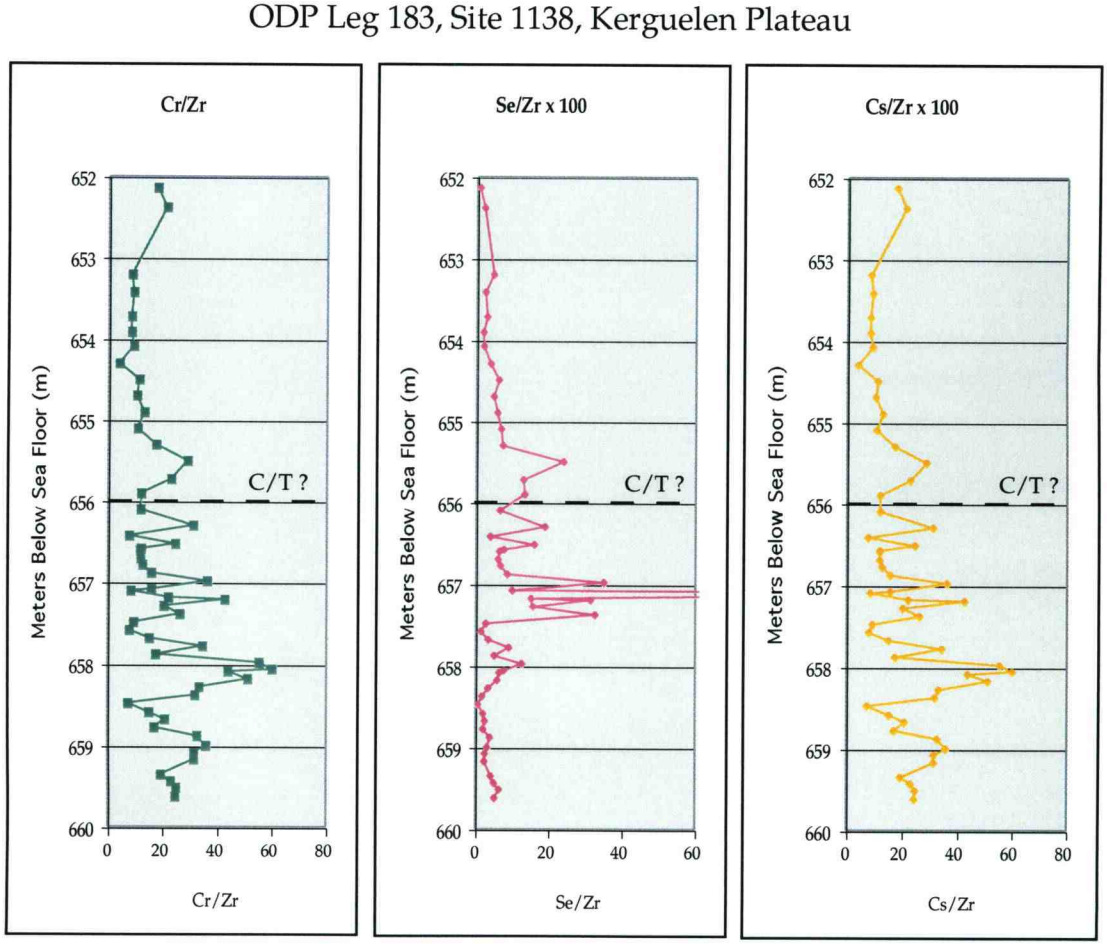

Figure 20. Cr, Se and Cs as Zr-normalized metal abundances for ODP Site 1138, central Kerguelen Plateau. An interval of high metal abundances can be seen below the tentative position of C/T boundary, show as dashed line, from Coffin et al. (2000).

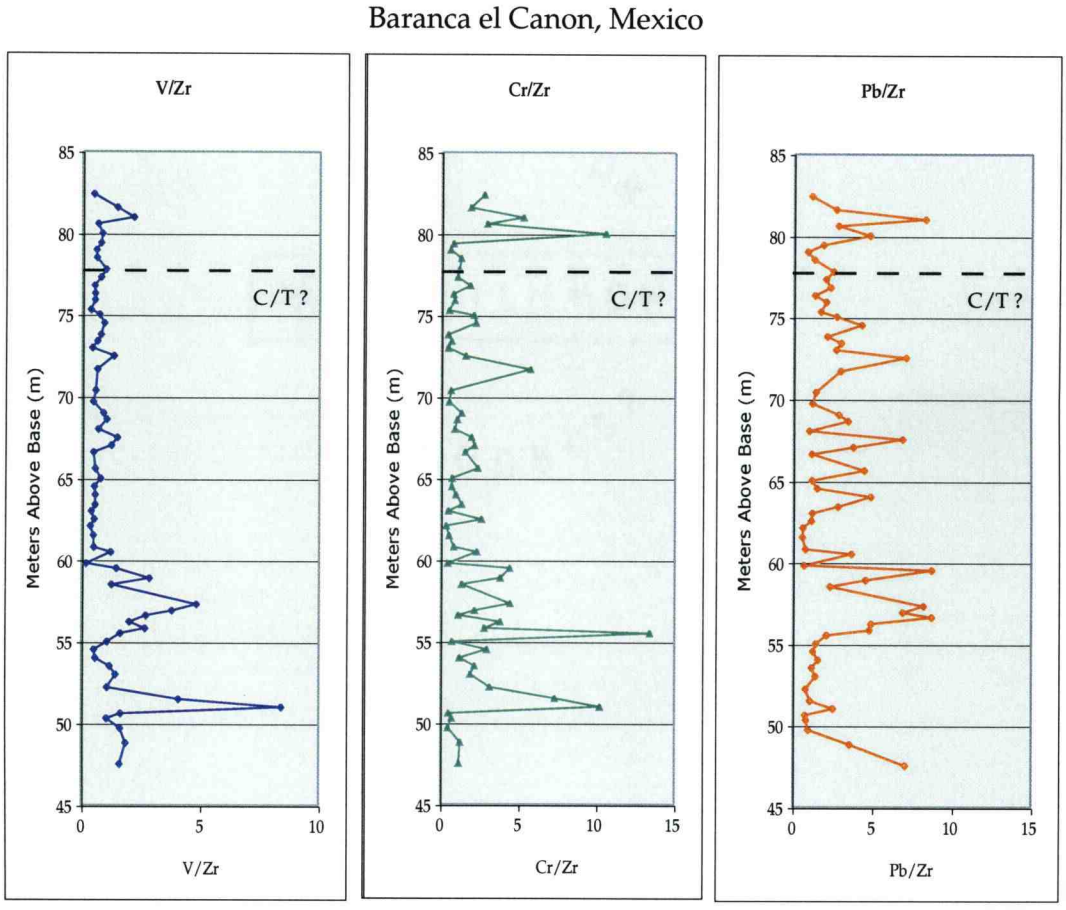

Figure 21. V, Cr and Pb as Zr-normalized metal abundances for Baranca el Cañon, Mexico. Intervals of high metal abundances can be seen.

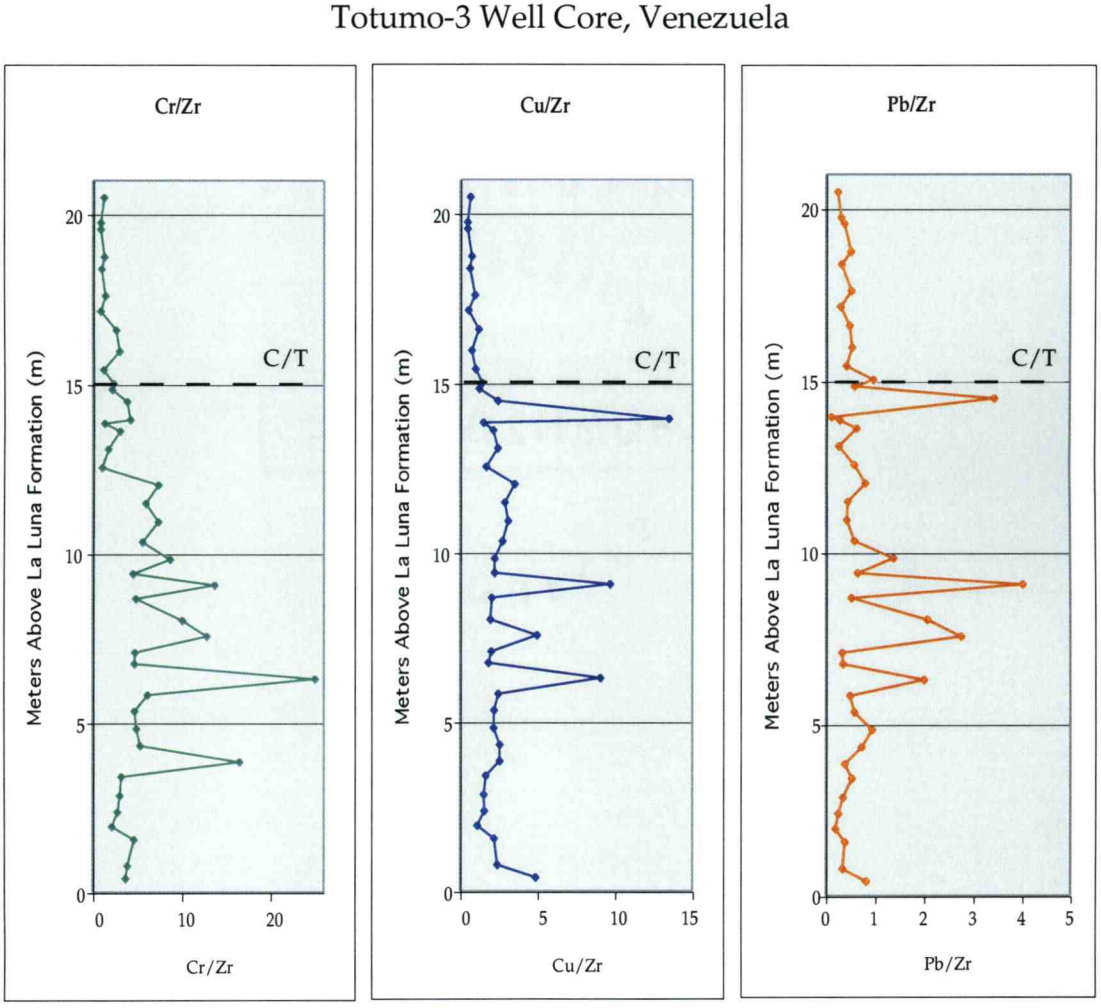

Figure 22. Cr, Cu and Pb as Zr-normalized metal abundances for the Totumo-3 Well core. An interval of high metal abundances can be seen below the position of the C/T boundary shown as dashed line from de Romero et al. (2002).

Totumo-3 Well Core, Venezuela

A 10 m interval, between 4 m and 14 m above the base of the La Luna formation, of Zr-normalized metal abundance anomalies can be seen in the Totumo-3 Well core (Figure 22). The interval of metal anomalies is well developed in Au, Cd, Ag, Sr, Mg, Ba, Zn, U, Co, Pb and Na and more weakly in Ni, Y, Sb, Mn, V, Se, Cr, Mo, Tl, As, Fe, Cu, Ti, Sc, W and Rb. The strongest part of the interval of metal anomalies lies about 5 m below the C/T boundary (which is at 15 m above the base of the La Luna formation).

Major Elements

Major element concentrations are used to determine the compositional make-up of the sediments. The detrital, $CaCO_3$ and SiO_2 fractions for each of the four sites were calculated the same way as described in Chapter 2. The variability in the fractions of these three components in Bass River (Figure 23) shows sediments are dominated by the detrital fraction with small contributions from the $CaCO_3$ and SiO_2 fractions. This is consistent with a shallow shelf environment with large fluxes of continental material. Sediments from ODP Site 1138 are more abundant in the SiO_2 fraction toward the bottom of the core. Up-core, the sediments are more abundant in the detrital and $CaCO_3$ fractions (Figure 24). Lastly, the variability in these three components in Baranca el Canon and the Totumo-3 Well core show that the sediments at these two sites are mostly

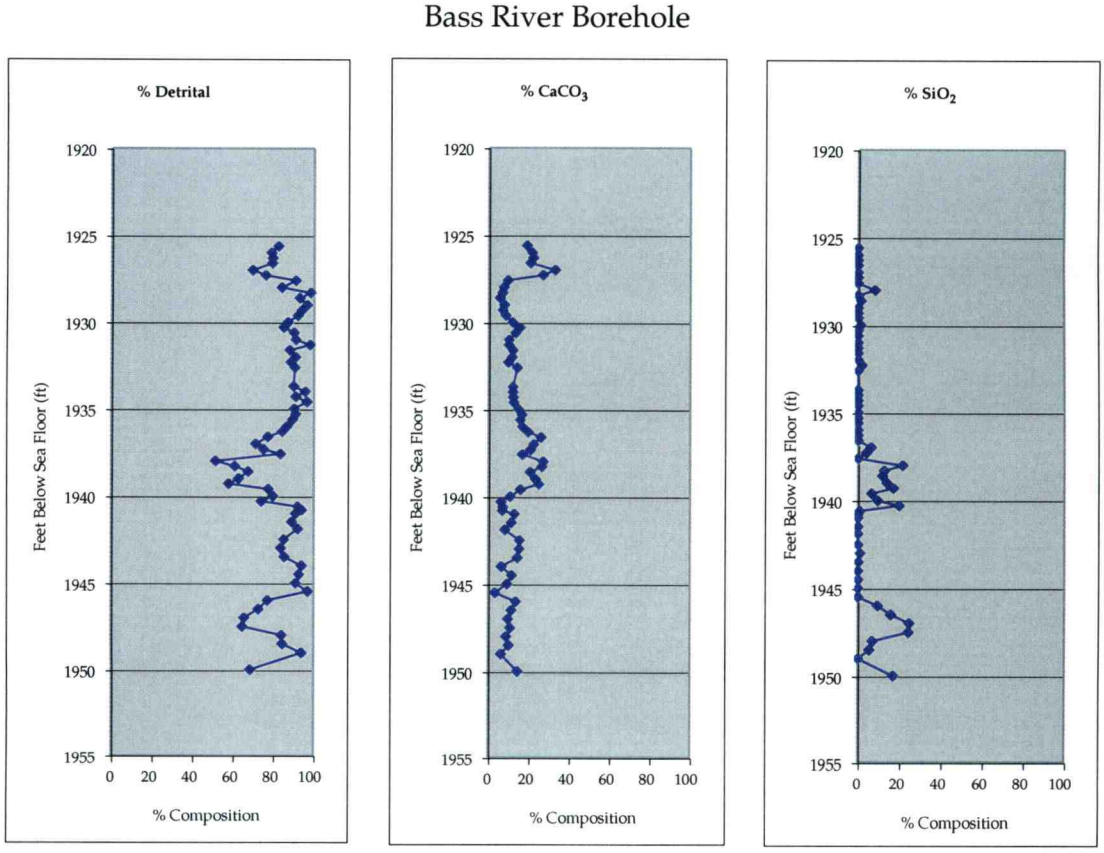

Figure 23. Compositional make-up of Bass River sediments.

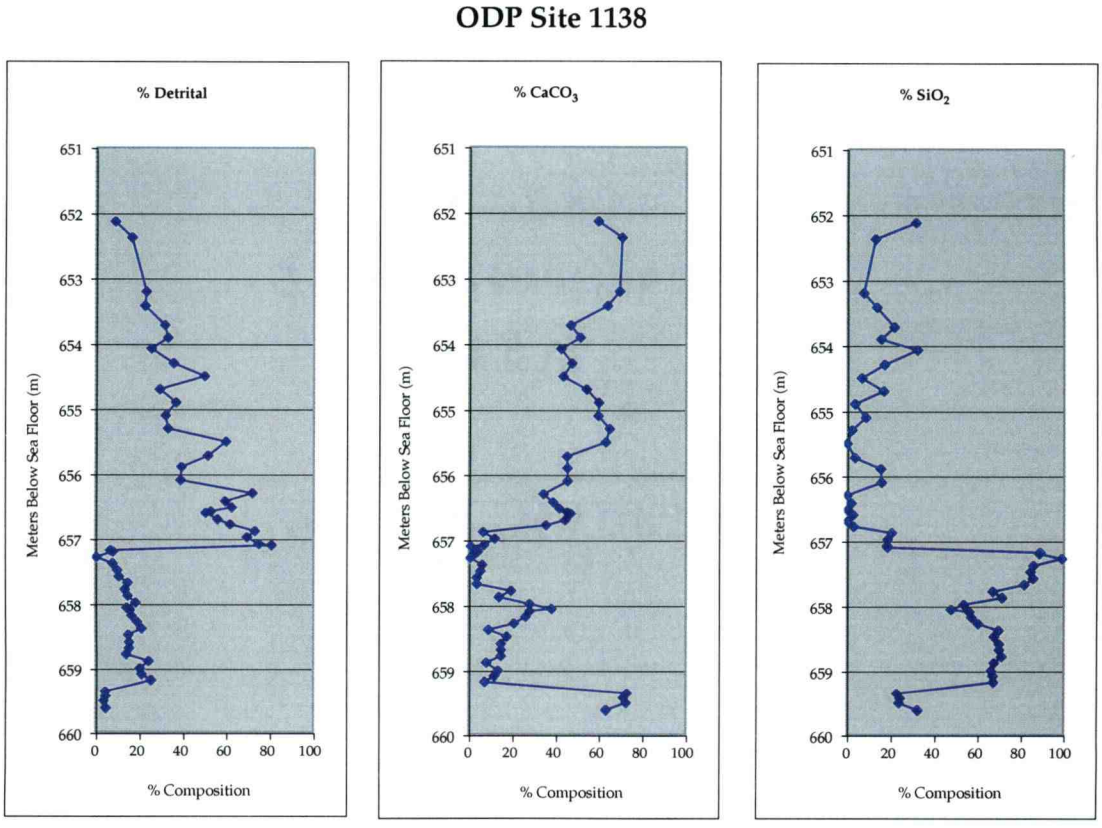

Figure 24. Compositional make-up of ODP Site 1138 sediments.

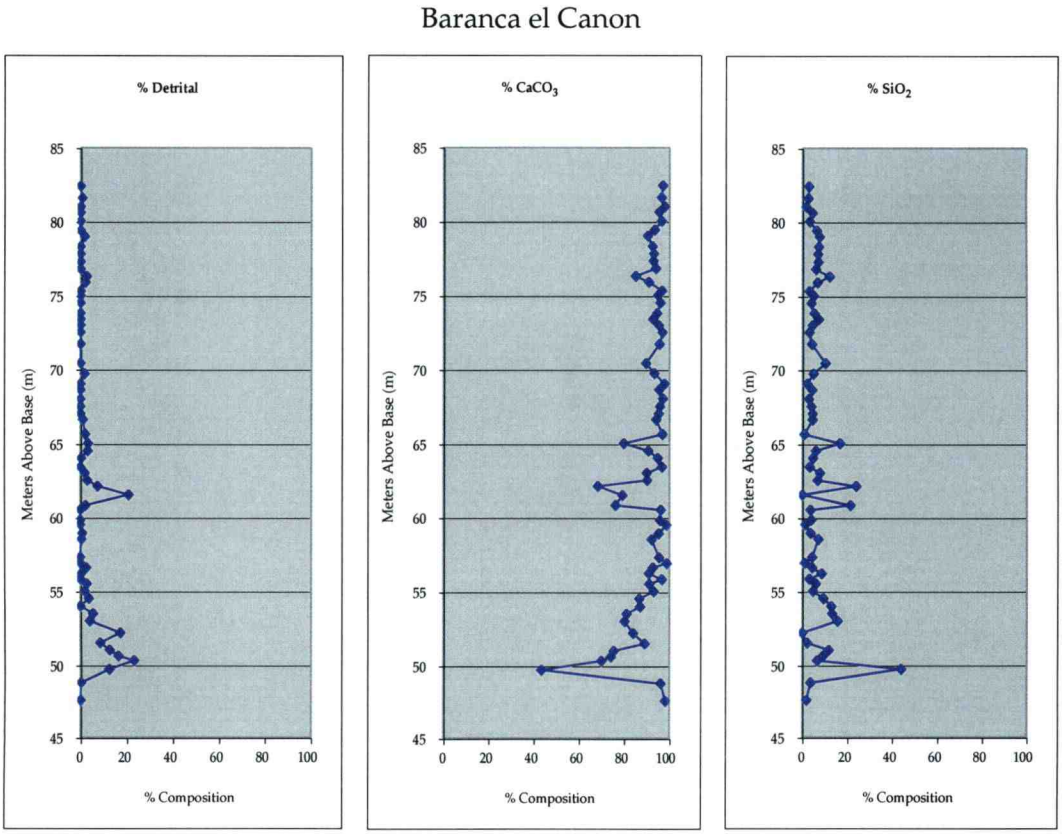

Figure 25. Compositional make-up of Baranca el Cañon sediments.

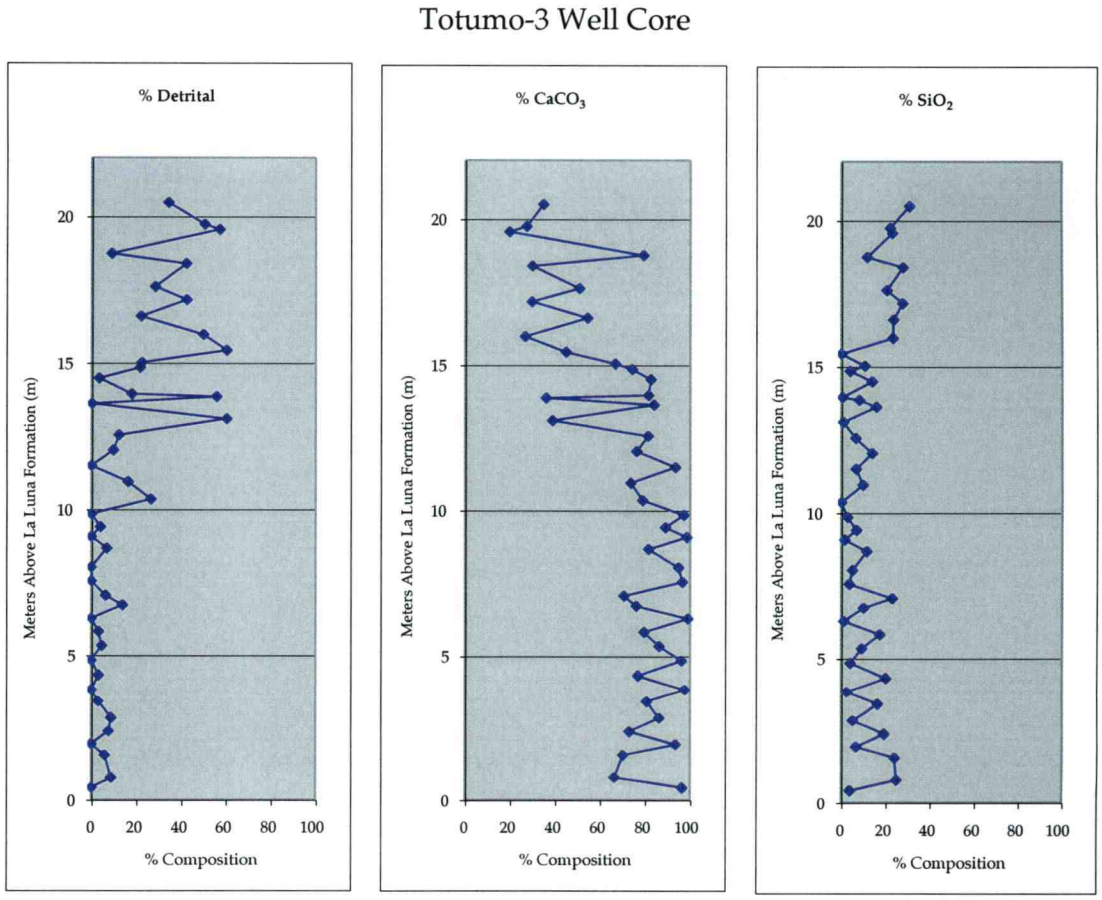

Figure 26. Compositional make-up of Totumo-3 Well core sediments.

carbonates, although the upper most section of the Totumo-3 Well core has slightly more of a detrital fraction (Figures 25 and 26). The compositional make-up and the location of metal anomalies in these sediments encourages us that normalizing to Zr has taken out the terrigenous elemental component.

Discussion

If an increase in trace metals to the ocean from eruptions of the Caribbean ocean plateau is directly related to reduction of oxygen concentrations, this large influx of trace metals should be reflected in sediments accumulating at these times. In Chapter 2, sediments from the Rock Creek Canyon section, Pueblo, Colorado show two intervals of metal abundance anomalies, both in the non-volatile and volatile elements, suggesting that this region (Western Interior Seaway) experienced the effects of both magmatic degassing "event plumes" and increased hydrothermal venting. Elemental abundance patterns for the Bass River Borehole, ODP Site 1138, the Baranca el Cañon section, and the Totumo-3 Well core also show intervals of increased metal abundances just prior to the C/T boundary. These intervals of metal anomalies are abundant in both the non-volatile and volatile elements.

When we look at the results for each of the five sites according to the matrix of element volatility versus mean oceanic residence time, some interesting trends develop. For the Bass River Borehole (Figure 27), the only elements that exhibit anomalies, ranging from 2–3 times background levels, are those that are volatile, except for V and Fe, which are slightly less volatile but also less enriched

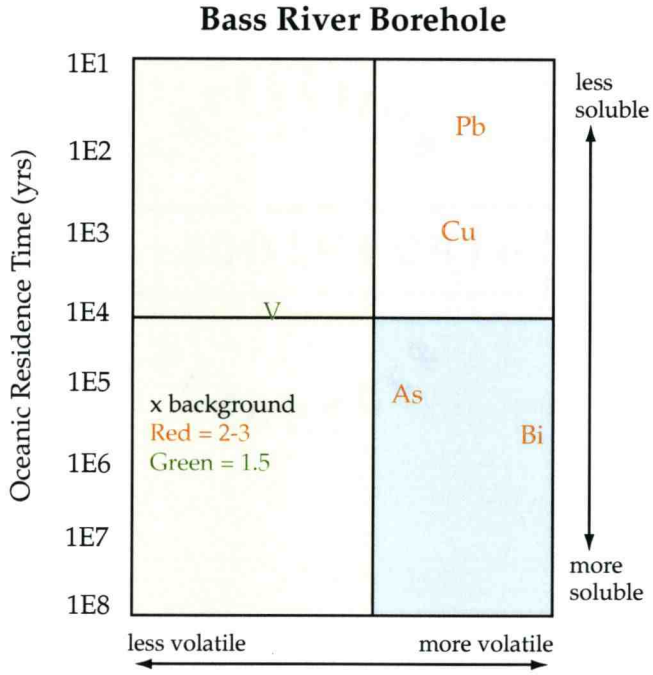

Figure 27. Bass River Borehole results according to the volatility vs. residence time figure.

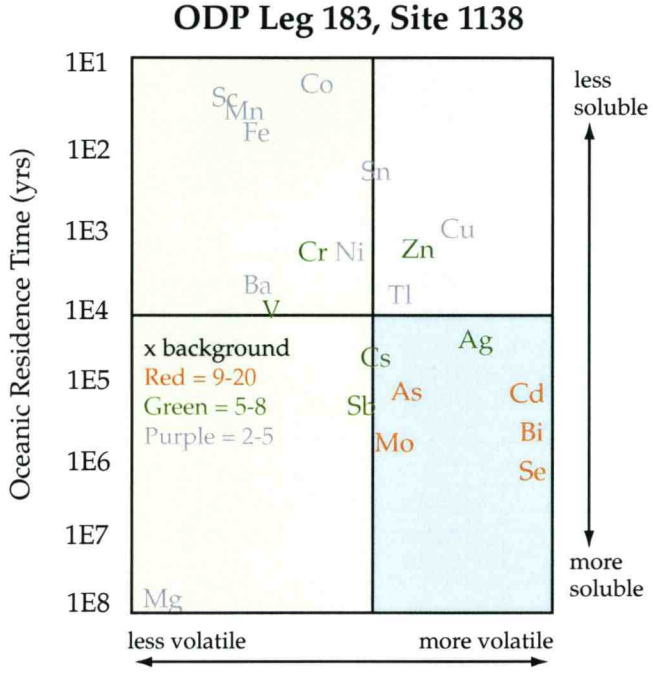

Figure 28. ODP Site 1138 results according to the volatility vs. residence time figure.

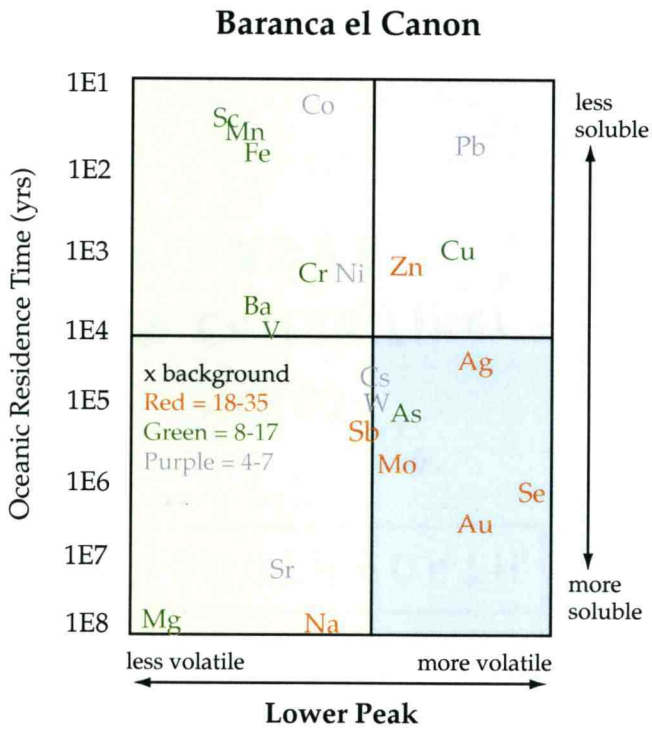

Figure 29. Baranca el Cañon results according to the volatility vs. residence time figure.

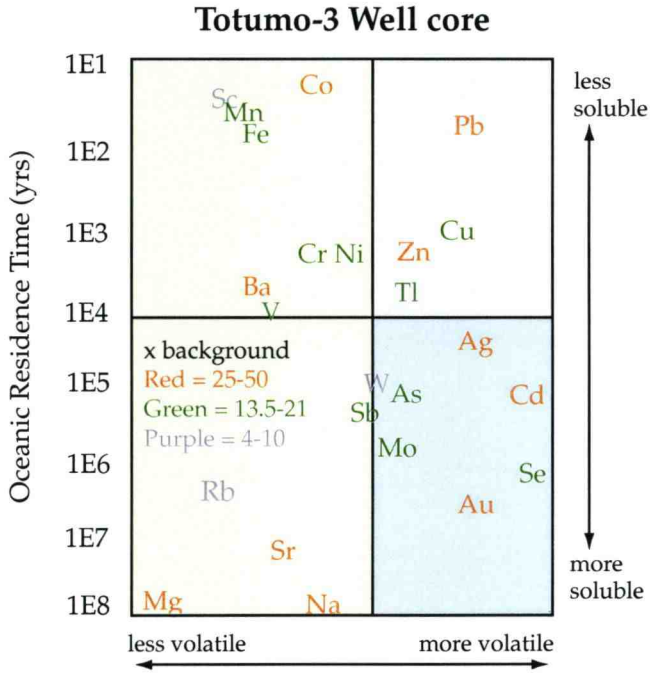

Figure 30. Totumo-3 Well core results according to the volatility vs. residence time figure.

(only 1.5 times above background levels), compared to the other elements. A weak enrichment in the more volatile elements suggests that the Bass River Borehole was probably only slightly affected by "event plume" activity. For the interval of metal abundance anomalies in ODP Leg 183, Site 1138 (Figure 28), elements that are more volatile and have longer residence times are more enriched (9-20 times background levels) compared with elements that are less volatile and those that are volatile but more reactive (2-8 times background levels). A strong enrichment in the more volatile elements, but also an enrichment in the less volatile elements, suggests that the Kerguelen plateau area of the ocean strongly felt effects of "event plume" activity but felt effects of hydrothermal activity as well. For the Baranca el Cañon section and the Totumo-3 Well core (Figures 29 and 30), the intervals of metal abundance anomalies are in both the volatile and less volatile elements. Neither category of elements seems generally more enriched than the other. This elemental make-up suggests that both "event plume" activity and hydrothermal activity affected the Baranca el Cañon section and the Totumo-3 Well core.

Strength of Metal Anomalies compared with Distance from Source and Cretaceous Surface Circulation

Considering that metal rich "event plumes" associated with formation of the Caribbean ocean plateau reached the ocean surface and were transported globally through wind-driven circulation, we would expect to see a fractionation in elements according to their residence times and the distance of the site from the

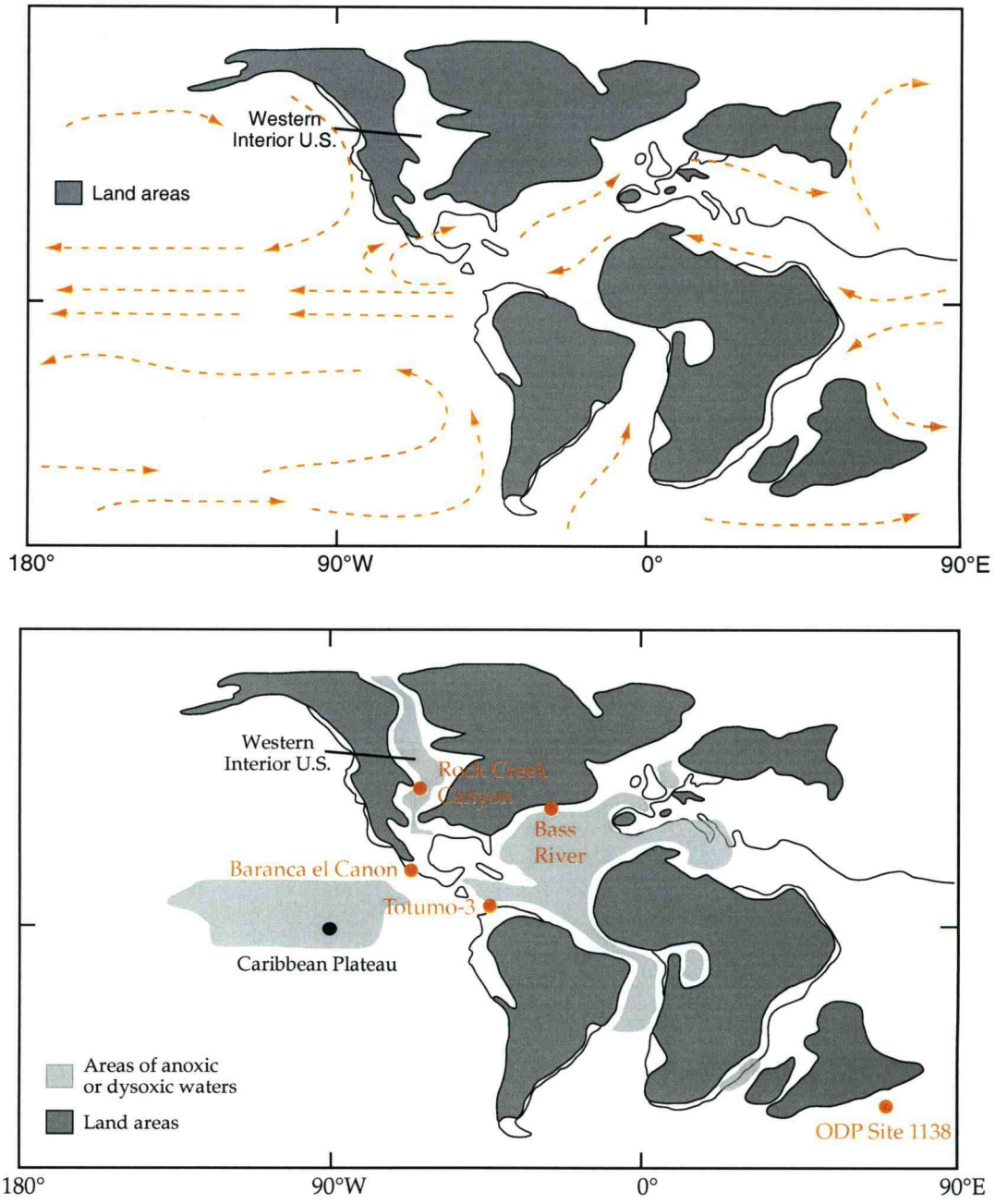

Figure 31. Map of reconstructed plate positions at ~90 Ma from Wignall (1994) showing the distance of each site from the Caribbean ocean plateau. Simulated late-Cretaceous surface circulation shown in the top panel for reference.

source of "event plumes". Based on reconstructed plate positions at ~90 Ma (Figure 31) from Wignall (1994), and assuming the source of "event plumes" is the Caribbean ocean plateau, Rock Creek Canyon is approximately 5000 km, Bass River is approximately 7000 km, ODP Site 1138 is approximately 12,000 km, Baranca el Cañon is approximately 3000 km, and the Totumo-3 Well core is approximately 4000 km away from the source (based on absolute distance). Based on these distances, those elements with shorter residence times (i.e. Cu, Pb, Zn, Sc) are expected to be relatively more enriched (abundances above background levels) in those sites closer to the source, such as Baranca el Cañon and Totumo-3, and those elements with longer residence times (i.e. Bi, As, Se, Cd) are expected to be relatively more enriched in those sites further from the source, such as Bass River and ODP Site 1138.

Although there are exceptions, in general, element abundance anomalies for all five sites follow the above pattern. For example, Cu and Pb anomalies (shorter residence times) are strong in the sites closest to the source and then decrease as distance from the source increases, whereas the strength of the Bi and As anomalies (longer residence times) are variable with distance from source (Figure 32). Exceptions to this pattern are the Bass River site and the Totumo-3 well core. In the Bass River site, some elements with shorter and longer residence times do not show anomalies that do occur at ODP Site 1138, even though Bass River is closer to the Caribbean ocean plateau than ODP Site 1138. If an element can reach the Kerguelen Plateau 12000 km away, why couldn't it reach Bass River

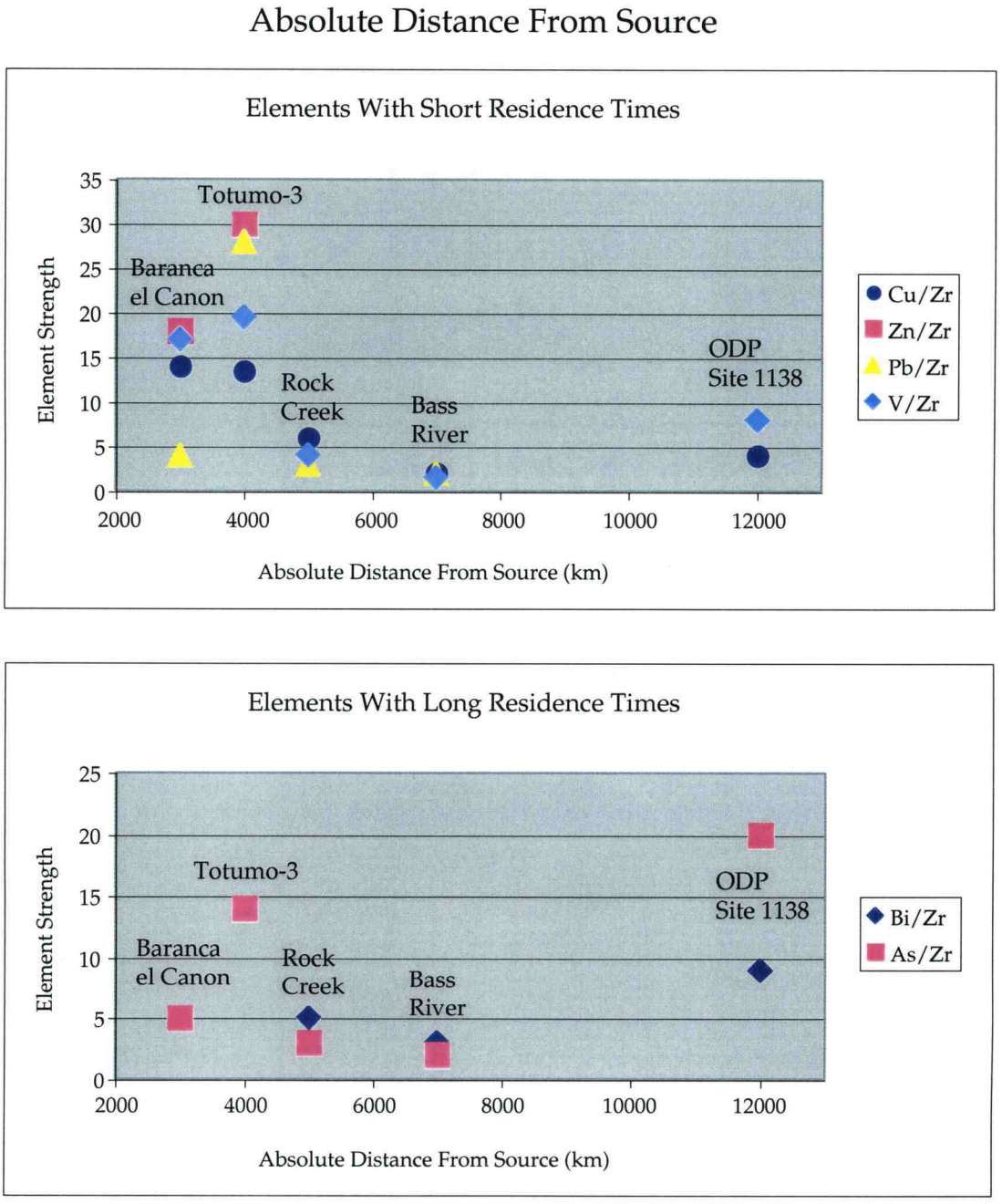

Figure 32. Diagram showing site distance from the Caribbean ocean plateau and the strength of element anomalies at each site. Elements with shorter residence times in top panel and longer residence times in bottom panel.

at 7000 km away? The explanation to this question probably lies in the Cretaceous surface circulation.

Current models predict very sluggish easterly flow along the northern margin of the Tethys Ocean, where the Bass River site was located. Therefore, to reach the Bass River site, surface waters would first flow westward from the Caribbean ocean plateau, then across the Pacific into the Tethys Ocean. In fact, based on actual travel distance, Bass River is 33,000 km away and ODP Site 1138 is 23,000 km away. Any metal rich "event plume" water travelling to Bass River would be greatly diluted and metal concentrations would have much longer to be scavenged out, and so it is not surprising to see very weak metal abundance anomalies at this site. If we look at the distance of sites from the source based on the actual travel distance (flow line), elemental abundance anomalies follow the predicted element enrichment pattern based on element volatility versus mean oceanic residence time much better (Figure 33).

For the Totumo-3 Well core, all of the elements are generally much more enriched than in the other sites, even though it is not the closest to the source either by absolute distance or circulation distance. However, it is important to note that eruptions on the Caribbean ocean plateau may have been as large as 10,000 km^3 (and flowed 100–1000 km^3) and that we do not know their exact extent, volume, or emplacement rate of them. Therefore, depending on the exact eruption location, the Totumo-3 Well core may have been very close to the source. This may explain why elemental abundance anomalies are so strong at this location.

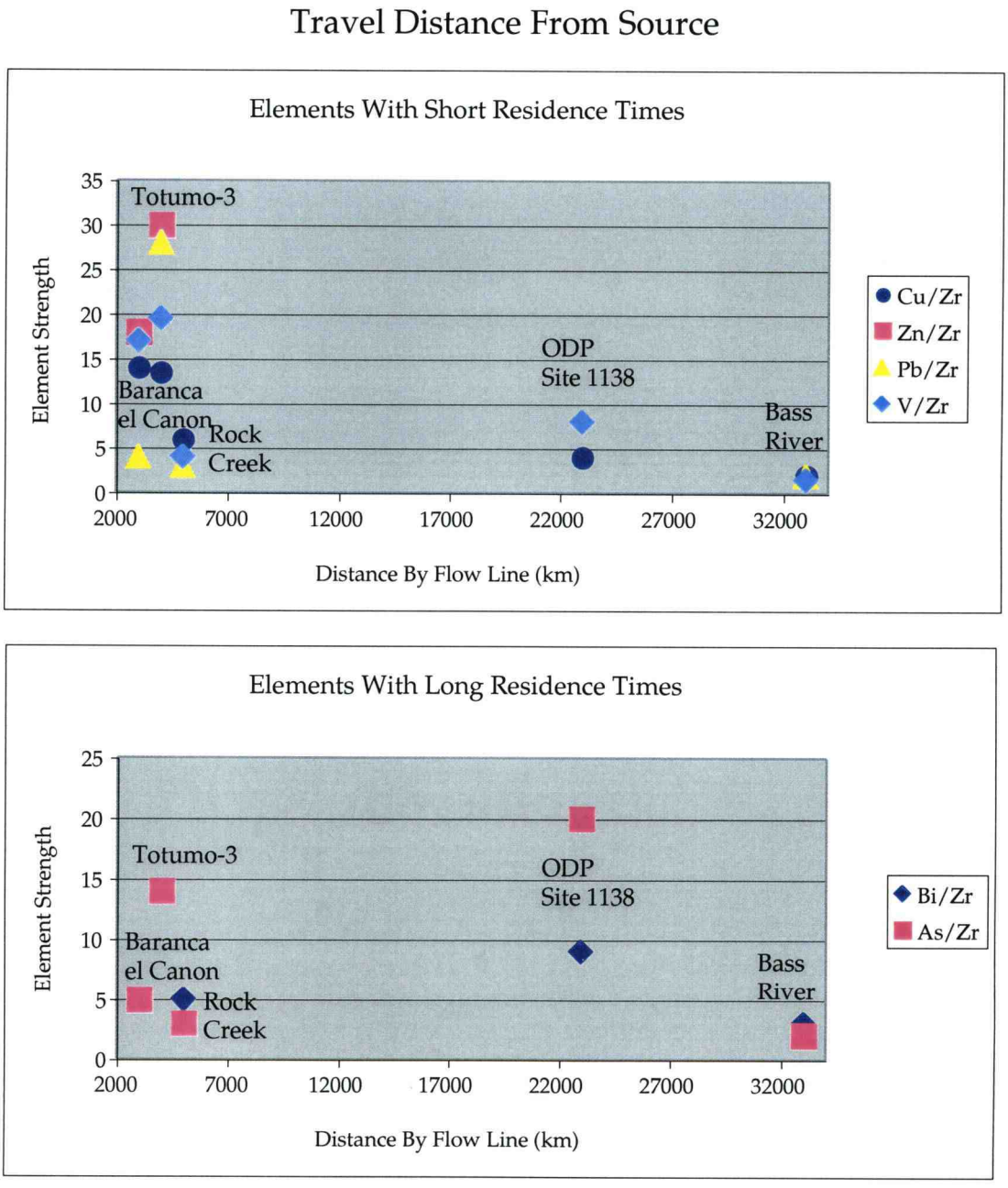

Figure 33. Diagram showing site distance from the Caribbean ocean plateau, based on travel distance, and the strength of element anomalies at each site. Elements with shorter residence times in top panel and longer residence times in bottom panel.

Position of Metal Anomalies and Carbon Isotopes

Since the pronounced global carbon isotope excursion around the C/T boundary is a good way to distinguish the onset and duration of OAE2, and to correlate widely distributed C/T sections, it is important to look at the position of metal anomalies in these five sites compared to their carbon isotopic profiles (Figure 34). For the Bass River Borehole, the very weak metal abundance anomalies at 1945 and 1941 fbsf fall just below the rapid rises in the $\delta^{13}C$ curve towards more positive values, at the onset of OAE2. It should be noted that the organic carbon isotope curve for the Bass River Borehole does not show the normal shift in $\delta^{13}C$ values back to background values (pre-OAE2). It has been suggested that sedimentation rate is very high in this core and so the sampled interval does not capture this shift back to more negative values (Bralower, personal communication, 2002). However, the $\delta^{13}C$ curve determined from carbonate for the whole core does show a decrease to background values at 1905 fbsf (Sugarman et al., 1999), and so these samples miss this decrease. Sugarman et al. (1999) estimate the duration of OAE2 at Bass River to be ~500k.y.

For the Baranca el Cañon section, the stronger interval of metal abundance anomalies falls just at the main rise to positive values in the $\delta^{13}C$ excursion. A brief positive $\delta^{13}C$ excursion occurs below this main global event but samples were not collected below this, and therefore we do not know if any metal anomalies occur before the main excursion. The weaker interval of metal anomalies in the Baranca el Cañon section actually fall slightly above the C/T boundary and as the

$\delta^{13}C$ values start to return to background values, which suggests these metal anomalies are not related to the main OAE2 event. For the Totumo-3 Well core, the maximum metal abundance peaks (ranging 6-10 m above the base of the La Luna Formation), fall just below and at the start of the main rise in $\delta^{13}C$ values. There is also a minor shift toward more $\delta^{13}C$ positive values below this main event, and it looks like there may be an abundance anomaly at this point (e.g. Cr at 4 m, Cu at 0 m Figure 22). However, samples were not available below the earliest peak and so it cannot be determined if there were any precursor metal anomalies. There are no carbon isotope data available yet for ODP Site 1138, so unfortunately the position of the metal anomalies with respect to the global $\delta^{13}C$ excursion cannot be determined. However, obvious metal abundance anomalies occur 1-3 m below the approximate C/T boundary, and certainly could correlate with peaks in other sections. The stratigraphic position of these intervals of metal anomalies in the Bass River Borehole, the Baranca el Cañon section (except for the higher interval of abundance anomalies), and the Totumo-3 Well core, as in the Rock Creek Canyon section, support the idea that "event plume" and hydrothermal activity are integral to OAE2 events, particularly the removal and sequestering of isotopically light carbon. The data are consistent with trace metal reduction of ocean oxygen concentrations, possibly leading to ocean anoxia.

Another important aspect is the position of the interval of metal anomalies in each of the five sites in relationship to each other. In Rock Creek Canyon, the initial shift towards more positive $\delta^{13}C$ values occurs around 0 cm above the basal

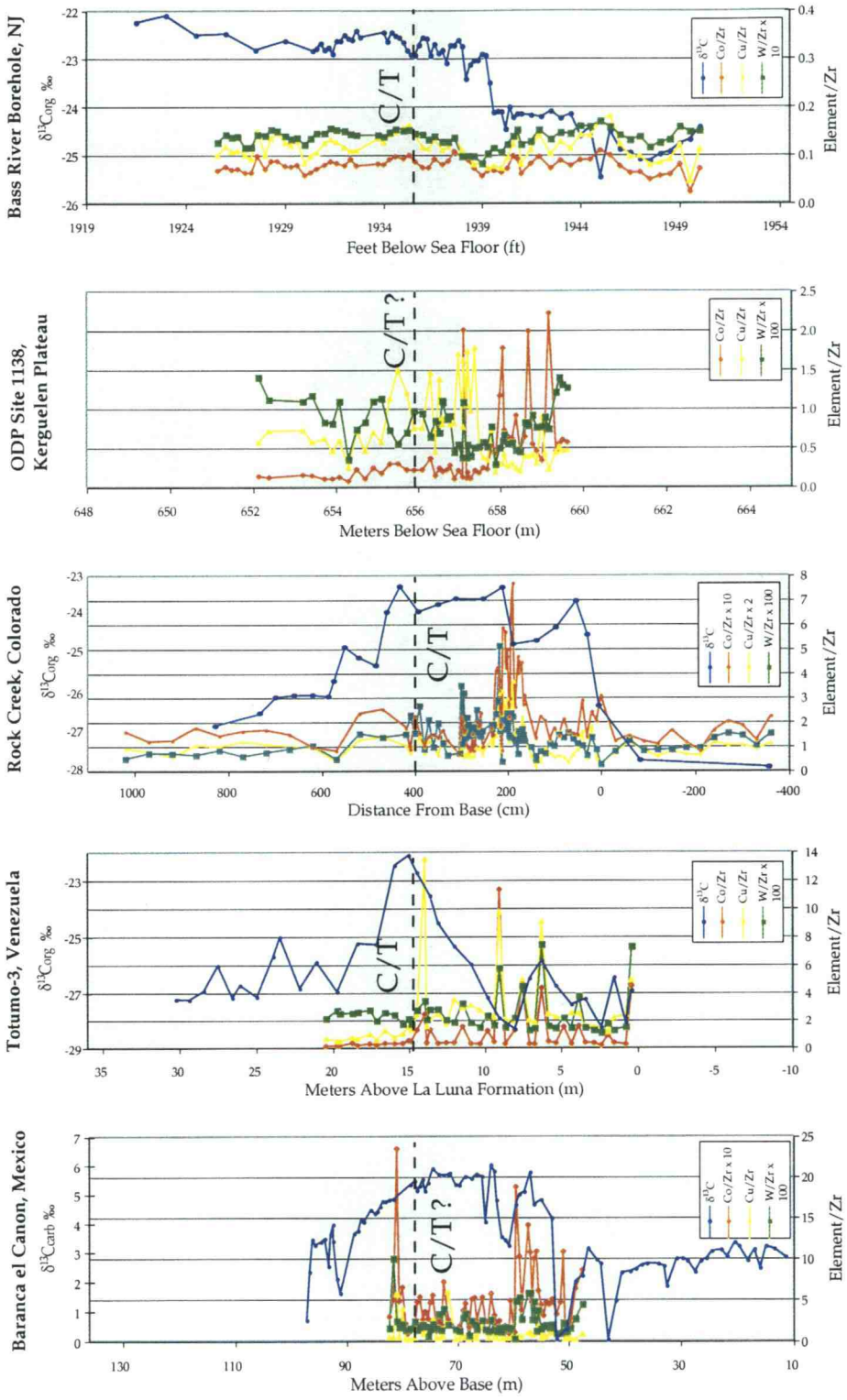

Figure 34. Position of metal abundance anomalies in all five sites correlated using their carbon isotopic profiles. Carbon data for; Baranca el Canon from Elrick and Molina (2002), for Totumo-3 from de Romero et al. (2002), for Rock Creek from Pratt et al. (1993), and for Bass River from Bralower and Bowman (2002). Sites are arranged in decreasing trace metal abundance concentration from left to right. Metal anomalies fall roughly in the same stratigraphic positions.

limestone, and the main duration of the $\delta^{13}C$ positive event begins at 200 cm above the basal limestone, where we see the main metal abundance anomalies. Metal abundances for the Bass River Borehole, the Baranca el Cañon section and the Totumo-3 Well core are matched to Rock Creek Canyon by the shape of their carbon isotope profiles (Figure 34). First, the weak metal abundance anomalies at 1945 fbsf in the Bass River section fall in the same stratigraphic position as the lower, weaker area of metal abundance anomalies in Rock Creek Canyon. Sampling in the Baranca el Cañon section and Totumo-3 Well core does not go low enough to determine if there is a precursor interval of weak metal abundance anomalies at these sites as well. Second, the weak metal anomalies at 1941 fbsf in the Bass River section, the lower interval of metal anomalies in the Baranca el Cañon section, and the interval of metal anomalies at the Totumo-3 well core fall in almost the same stratigraphic position as the upper, stronger interval of metal abundance anomalies in Rock Creek Canyon. Since there are no carbon data yet available for the ODP Site 1138 section, I assume the maximum abundance peaks fall in the same location as the other sites and match the abundance curves this way. The position of the metal abundances relative to the other sites seems to match well with the tentative placement of the C/T boundary at ODP Site 1138. The global correlation of the position of the metal anomalies gives further evidence that much of the surface ocean experienced large influxes of trace metals, mainly at the beginning but intermittently through OAE2, through hydrothermal activity associated with eruptions on the Caribbean ocean plateau.

Depositional Environment of Sedimentary Sections

As was discussed in Chapter 2, sediments deposited in ocean anoxic environments today, such as the Black Sea and Gulf of California, do show a higher concentration of trace metals compared to sediments deposited in oxic environments. However, Brumsack and Thurow (1986) showed that the pattern of trace metal abundances in C/T black shales is quite distinct compared to other anoxic sediments, and therefore, can not be explained by upwelling related anoxic conditions, or by diagenetic leaching from deep sea clays. The intervals of metal abundance anomalies in the Baranca el Cañon further support Brumsack and Thurow's (1986) conclusions. This section consists of sediments deposited in a shallow-marine environment where waters were always oxygenated, as is illustrated by the absence of laminated, black shales. Intervals of metal anomalies in this oxic environment indicate that ocean chemistry changed just prior to the C/T boundary, in accordance with a global $\delta^{13}C$ excursion. Therefore, it seems reasonable that anoxia resulted from, rather than promoted the trace metal abundance anomalies, which are most likely the result of metals released in "event plume" activity during Caribbean ocean plateau eruptions.

Summary and Conclusions

In this chapter, I examined five globally distributed C/T boundary sections (Rock Creek Canyon, Bass River Borehole, ODP Site 1138, Baranca el Cañon, and Totumo-3 Well core) for major, minor and trace elemental abundances to gain additional information on the proposed connection between metal rich, eruption

related magmatic degassing "event plumes" and associated hydrothermal activity, and ocean anoxia. The appearance of anomalously high metal abundances marks the presence of ocean plateau "event plumes" and the stratigraphic position of these anomalies indicates the timing of "event plume" activity. In this chapter, I also looked at the variation in trace metal patterns and intensities among all five sites to determine if: (1) the changes in metal abundance gradients relative to the proposed source of metals (the Caribbean ocean plateau at ~ 90°W, 2°S) follow the predicted enrichment pattern based on volatility and residence time, and (2) if these patterns are consistent with models of late-Cretaceous surface circulation.

Trace, minor and major element analyses demonstrate intervals of high metal abundances in all sites. When the shape of the carbon isotope curves for each site are matched up to each other (with the exception of ODP Site 1138, awaiting $\delta^{13}C$ data), the anomaly in the Bass River Borehole falls in the same stratigraphic position as the lower metal abundance interval at Rock Creek Canyon. Samples for the three other sites do not go low enough to capture any potential anomalies at this stratigraphic level. The lower interval of metal anomalies in Baranca el Cañon and the interval of metal anomalies in the Totumo-3 Well core fall in the same position as the upper interval of metal abundances in the Rock Creek Canyon section. The fact that the intervals of metal anomalies in these sites occur in the same stratigraphic position, and that these metal anomalies fall just at or slightly before the main shift to more positive carbon isotope values,

further supports the idea that metals released in event plume activity may lead to temporary periods of ocean anoxia.

The elemental abundance patterns for all five sites can potentially provide information on the proposed source of metal rich event plumes. Based on the predicted volatility and residence time separation of elements, the less volatile and reactive volatile elements are expected to be more enriched in the sites closer to the source, whereas the less reactive volatile elements are expected to be more enriched further from the source. In general, the element abundance patterns of these sites follow this prediction. Based on flow distance, Baranca el Cañon, the Totumo-3 Well core, and Rock Creek Canyon, 3000 km, 4000 km, and 6000 km away from the source, are more enriched in elements with shorter residence times compared to the sites further away. On the other hand, ODP Site 1138, which is approximately 23,000 km away from the Caribbean ocean plateau, is more enriched in elements with longer residence times compared to the sites much closer. Metal abundance anomalies at the Bass River section, which is approximately 33,000 km away from the source, are very weak to mostly absent. The gradients in elemental abundances are consistent with the position of the sites from the proposed source, indicating that the Caribbean ocean plateau is a logical source of the metal rich event plumes. These abundance patterns are also consistent with late-Cretaceous surface circulation models.

Chapter 4: Summary of Conclusions, and Future Research Directions

Primary Results

The primary goal of this thesis was to better determine a specific link between ocean anoxic events and ocean plateau (LIP) generated hydrothermal activity during the Cretaceous by examining the relationship between OAE events and trace metal abundance anomalies in widely distributed late-Cretaceous marine sediments. Here I summarize the primary conclusions of this thesis and suggest areas of future research needed to supplement this work.

In Chapter 2, I determined major, minor and trace elemental abundances in bulk rock samples from a high resolution sampling of the C/T boundary Rock Creek Canyon section, Pueblo, Colorado. This marine sedimentary section was chosen for its accessibility and well-defined biozones, carbon isotopic profile, and lithologic changes. After normalizing element concentrations to Zr to remove the variable contribution of terrigenous material to these sediments, an interval of metal abundance anomalies with several distinct peaks is seen. The positions of these metal peaks coincide with an interval of rapidly increasing $\delta^{13}C$ isotope values, at the start of a global carbon isotopic excursion, and high rates of speciation and extinction in foraminifera, radiolarians and molluscs. The chemical pattern of these element abundance peaks indicates that trace metals were introduced into the Cretaceous ocean by both water/rock solubility dominated and magmatic degassing "event plume" dominated activity. The presence and stratigraphic location of the interval of metal abundance anomalies suggests that

hydrothermal activity associated with the formation of the Caribbean ocean plateau could be directly related to OAE2.

In Chapter 3, I described major, minor and trace elemental abundances in bulk rock samples from an additional four globally distributed, C/T boundary marine sedimentary sections. After normalizing element concentrations to Zr, all five sites show intervals of metal abundance anomalies, some sites with several distinct peaks within the intervals, that coincide with areas of rapidly increasing $\delta^{13}C$ isotope excursions (except for ODP Site 1138, awaiting carbon isotopic data). Using the $\delta^{13}C$ profiles, metal abundance peaks for each site were matched to the Rock Creek Canyon section, revealing the position of metal abundance intervals with respect to the global ocean signal. The anomalies in the Bass River Borehole fall in the same stratigraphic position as the lower metal abundance interval at Rock Creek Canyon. The lower interval of metal abundance anomalies in Baranca el Cañon and the interval of metal abundance anomalies in the Totumo-3 Well core fall in the same position as the upper interval of metal abundances in the Rock Creek Canyon section. The presence and stratigraphic location of metal abundance intervals further supports the evidence from Chapter 2 that hydrothermal activity associated with the formation of the Caribbean ocean plateau could be directly related to OAE2.

In Chapter 3, I also examined changes in patterns and intensities of trace metal abundances relative to the source (Caribbean ocean plateau) in all five sites to determine if they are consistent with the general predicted metal enrichment

pattern and modeled late-Cretaceous surface ocean circulation. The metal enrichment pattern of these five sites reveal that elements with shorter residence times are more enriched in sites closer to the source and that the more volatile elements with longer residence times are more enriched in sites farther from the source. The gradients in elemental abundances agree with the proposed source of metals and with modeled late-Cretaceous ocean surface circulation.

Future Research

Although this research strongly supports a link between hydrothermal activity associated with formation of the Caribbean ocean plateau and OAE2, there is still a considerable amount of research to be completed to strengthen this connection.

(1) Ocean surface circulation models predict a strong westward equatorial flow in the Pacific, so elemental abundances are expected to be strong in these areas. Therefore, it would be very useful to measure the element abundances in high-resolution sections "downstream" from the Caribbean ocean plateau, particularly in the equatorial Pacific. However, much of the late-Cretaceous Pacific ocean floor has been subducted, leaving the most promising location as shallow rises, plateaus, and seamounts in the western Pacific.

(2) The Cretaceous period is characterized by a number of other distinct ocean-wide anoxic episodes approximately synchronous with ocean plateau formation. However, each of these OAEs has slightly different characteristics illustrating the complex nature of these interactions. Since this particular project

focuses only on the relationship between OAE2 and the Caribbean ocean plateau, it would be extremely helpful to better determine a specific link between the other OAEs and ocean plateau generated hydrothermal "event plume" activity, such as OAE1a and the Ontong Java plateau in the early Aptian. This could be accomplished by examination of trace metal abundance anomalies in pelagic sediments deposited at the times of OAE1a, the "Selli" black shale.

(3) It would be extremely valuable to show that elements producing significant metal abundance anomalies in C/T boundary sediments are the same elements that have been lost from the Caribbean ocean plateau through some kind of hydrothermal alteration. By comparing the bulk composition of altered lavas to the composition of unmodified magmas, the flux of elements due to degassing and seawater/rock exchange can be determined. However, in order to determine the flux of elements from Caribbean ocean plateau lavas, the composition of unaltered lavas needs to be determined. One means by which the primary composition of parental melts can be determined is from melt inclusions trapped in crystals that form early in the history of the magmagenesis. These inclusions trap melts before they have experienced degassing and alteration with seawater and therefore provide a starting inventory of trace metal concentrations. Elemental concentrations in melt inclusions could be determined using an electron or ion microprobe. Comparing the primary lava composition to altered Caribbean plateau lava composition, such as with a normalized element pattern plot, will help determine the loss of elements. This flux of elements due to degassing and

water/rock exchange can then be compared to the pattern of anomalies in pelagic sediments.

(4) It would be very useful to continue radiometric dating of lavas from the Caribbean ocean plateau. With more accurate age determinations, the volume and emplacement rate of the Caribbean ocean plateau can be better constrained. This will help in allowing a better understanding of oceanic responses, such as changes in ocean chemistry and biota mass extinction events, to eruption events.

(5) Isotopic studies for selective elements in anomalous intervals may also be extremely helpful. For example, the isotopic composition of Pb is characteristic of ocean plateau formation, MORB, continental runoff, etc. Each source will have a different Pb isotopic signature, which may help in determining the source of elements that make-up abundance anomalies in these sediments.

BIBLIOGRAPHY

Aguilera-Franco, N., Hernandez-Romano, U. and Allison, P.A. (2001). Biostratigraphy and environmental changes across the Cenomanian-Turonian boundary, southern Mexico. *J. South Am. Earth Sc.*,14: 237-255.

Arthur, M.A. and Premoli-Silva, I. (1982). Development of widespread organic carbon-rich strata in the Mediterranean Tethys, in *Nature and Origin of Cretaceous carbon-rich facies*. Eds: Schlanger, S.O. and Cita, M.B. Academic Press, London: 7-54.

Arthur, M.A., Jenkyns, H.C., Brumsack, H.J. and Schlanger, S.O. (1990). Stratigraphy, geochemistry, and paleoceanography of organic carbon-rich Cretaceous sequences, in *Cretaceous Resources, Events and Rhythms*. Eds: Ginsburg, R.N. and Beaudoin, B. Kluwer Academic, Norwell, MA: 75-119.

Arthur, M.A., Schlanger, S.O. and Jenkyns, H.C. (1987). The Cenomanian-Turonian Ocean Anoxic Event II, paleoceanographic controls on organic matter production and preservation, in *Marine Petroleum Source Rocks*. Eds: Brooks, J. and Fleet, A., Geol. Soc. London. Spec. Publ., London, 24: 399-418.

Baker, E.T. (1994). A 6-year time series of hydrothermal plumes over the Cleft segment of the Juan de Fuca Ridge. *J. Geophy. Res.*, 5: 319-337.

Baker, E.T., Massoth, G.J. and Feely, R.A. (1987). Cataclysmic hydrothermal venting on the Juan de Fuca Ridge. *Nature*, 329: 149-151.

Baker, E.T. et al. (1989). Episodic venting of hydrothermal fluids from the Juan de Fuca Ridge. *J. Geophy. Res.*, 94: 9237-9250.

Barron, E.J. and Peterson, W.H. (1989). Model simulation of the Cretaceous ocean circulation. *Science*, 244: 684-686.

Barron, E.J. and Peterson, W.H. (1990). Mid-Cretaceous ocean circulation: Results from model sensitivity studies. *Paleoc.*, 5: 319-337.

Barron, E.J., Arthur, M.A. and Kauggman, E.G. (1985). Cretaceous rhythmic bedding sequences: A plausible link between orbital variations and climate. *Earth Plan. Sci. Lett.*, 72: 327-340.

Berner, R.A. (1994). Geocard II: A revised model of atmospheric CO_2 over Phanerozoic time. *Am. J. Sci,* 294; 56-91.

Bowers, T.S., Von Damm, K.L. and Edmond, J.M. (1985). Chemical evolution of mid-ocean ridge hot springs. *Geochem. Cosmochim. Acta.*, 49: 2239-2252.

Bralower, T.J. (1988). Calcareous nannofossil biostratigraphy and assemblages of the Cenomanian-Turonian boundary interval: Implications for the origin and timing of oceanic anoxia. *Paleoc.*, 3: 275-316.

Bralower, T.J., Fullagar, P.D., Paull, C.K., Dwyer, G.S. and Leckie, R.M. (1997). Mid-Cretaceous strontium-isotope stratigraphy of deep-sea sections. *Geol. Soc. Am. Bull.* 109: 1421-1442.

Brass, G.W., Southam, J.R., and Peterson, W.H. (1982). Warm saline bottom water in the ancient ocean. *Nature*, 296: 620-623.

Brumsack, H.J. (1983). A note on Cretaceous black shales and recent sediments from oxygen deficient environments: paleoceanographic implications, in *Coastal Upwelling, Its Sediment Record.* Eds: Suess, E. and Thiede, J., NATO Advanced Research Institute, Plenum, NY: 471-483.

Brumsack, H.J. and Thurow, J. (1986). The geochemical facies of black shales from the Cenomanian-Turonian boundary event (CTBE), in *Biogeochemistry of black shales.* Eds: Degens, E.T. et al., SCOPE/UNEP Sonderbd., Mitt. Geool. Paleontt. Inst. Hamburg, 60: 247-265.

Burke, K.P., Fox, P.J. and Sengor, A.M.C. (1978). Buoyant ocean floor and the evolution of the Caribbean. *J. Geophys. Res.*, 83: 3949-3954.

Bush, A.B.G., and Philander, G.H. (1997). The late Cretaceous: Simulation with a coupled atmosphere-ocean general circulation model. *Paleoc*, 12: 495-516.

Channel, J.E.T., Erba, E., Nakanishi, M. and Tamaki, K., (1995). Late Jurassic-Early Cretaceous time scales and oceanic magnetic anomaly block models, in *Geochronology. Time Scales and Global Stratigraphic Correlation*, Eds: Berggren, W.A., et al., SEPM Special Publication, 54: 51-63.

Coale, K.H. and 18 others (1996). A massive phytoplankton bloom induced by an ecosystem-scale iron fertilization experiment in the equatorial Pacific Ocean. *Nature*, 383: 495-501.

Cobban, W.A. and Scott, G.R. (1972). Stratigraphy and ammonite fauna of the Graneros Shale and Greenhorn Limestone near Pueblo, Colorado. *U.S. Geol. Survey, Professional Paper*, P-0645:108.

Coffin, M.F. and Eldholm, O. (1994). Large igneous provinces: crustal structure, dimensions and external consequences. *Rev. Geophys.*, 32: 1-36.

Coffin, M.G., Frey, F.A., Wallace, P.J., Antretter, M.J., Arndt, N.T., Barling, J., Boehm, F., Borre, M.K., Coxall, H.K., Damuth, J.E., Delius, H. Duncan, R.A., Inokuchi, H., Keszthelyi, L., Mahoney, J.J., Moore, C.L., Muller, R.D., Neal, C.R., Nicolaysen, K.E., Pringle, M.S., Reusch, D.N., Saccocia, P.J., Teagle, D.A.H., Wahnert, V., Weis, D.A.M., Wise, S.W. and Zhao, X. (2000). Kerguelen Plateau-Broken Ridge: A Large Igneous Province, Proc. *ODP, Initial Reports*, 183: College Station, TX (Ocean Drilling Program): 1-190.

Courtillot, V. and Besse, J. (1987). Magnetic reversals, polar wander, and core-mantle coupling. *Science*, 237: 1140-1147.

Corliss, J.B., Dymond, J., Gordon, L.I., Edmond, J.M., Von Herzin, R.P., Ballard, R.D., Green, K., Williams, D., Bainbridge, A., Crane, K., and Van Handel, T.H. (1979). Submarine thermal springs on the Galapagos Rift. *Science*, 203: 1073-1083.

Davis, C., Pratt, L., Sliter, W., Mompart, L., and Murat, B. (1999). Factors influencing organic carbon and trace metal accumulation in the Upper Cretaceous La Luna Formation of the western Maracaibo Basin, Venezuela. *Geol. Soc. Am., Special Paper*, 332: 203-230.

Dean, W.E. and Arthur, M.A. (1994). The Cretaceous Western Interior Seaway Drilling Project, An overview (abs.): *Am. Association of Petr. Geol. Annual Meeting, Abstracts with Programs*, 3:134.

de Granciansky, P.C. and Poag, C.W. (1985). Geologic history of Goban Spur, Northwest Europe continental margin, *Initial Rep. Deep Sea Drill. Proj.*, Part 180: 1187-1216.

de Romero, L.M., Truskowski, I.M., Bralower, T.J., Odreman, O., and Zachos, J.C. (2002). An integrated calcareous microfossil biostratigraphic and carbon isotope stratigraphic framework for the La Luna Formation, Venezuela. Abstract: *Workshop on Cretaceous Climate and Ocean Dynamics*, 16.

Douglas, R.G. and Savin, S.M. (1975). Oxygen and carbon isotope analyses of Tertiary and Cretaceous microfossils from Shatsky Rise and other sites in the North Pacific Ocean. *Init. Rep. Deep Sea Drill. Proj.*, 32:509-520.

Duncan , R.A., and Hargraves, R.B. (1984). Plate tectonic evolution of the Caribbean region in the mantle reference frame. *Geol. Soc. Am. Mem.* 16: 81-93.

Duncan, R.A. and Richards, M.A. (1991). Hotspots, mantle plumes, flood basalts, and true polar wander. *Rev. Geophys.*, 29: 483-501.

Eicher, D.L. and Diner, R. (1985). Foraminifera as indicators of water mass in the Cretaceous Greenhorn sea, in *Fine-grained deposits and biofacies of the Cretaceous Western Interior Seaway: Evidence of cyclic sedimentary processes.* Eds: Pratt, L.M, Kauffman, E.G. and Zelt, F.B., Field Trip Guidebook No. 4: Soc. Econ. Paleontol. Mineral., Tulsa: 38-48.

Eicher, D.L. and Worstell, P. (1970). Cenomanian and Turonian foraminifera from the Great Plains, United States. *Micropaleo.,* 16: 269-324.

Elder, W.P. (1985). Biotic patterns across the Cenomanian-Turonian boundary near Pueblo, Colorado, in *Fine-grained deposits and biofacies of the Cretaceous Western Interior Seaway: Evidence of cyclic sedimentary processes.* Eds: Pratt, L.M, Kauffman, E.G. and Zelt, F.B., Field Trip Guidebook No. 4: Soc. of Econ. Paleontol. Mineral.,Tulsa: 157-169.

Elder, W.P. (1987). The paleoecology of the Cenomanian-Turonian (Cretaceous) stage boundary extinctions at Black Mesa, Arizona. *Palaios*, 2:24-40.

Elder, W.P. and Kirkland, J.I. (1985). Stratigraphy and depositional environments of the Bridge Creek Limestone member of the Greenhorn formation at Rock Canyon anticline near Pueblo, Colorado. in *Fine-grained deposits and biofacies of the Cretaceous Western Interior Seaway: Evidence of cyclic sedimentary processes.* Eds: Pratt, L.M, Kauffman, E.G. and Zelt, F.B., Field Trip Guidebook No. 4: Soc. of Econ. Paleontol. Mineral.,Tulsa: 122-134.

Elrick, M.B., and Molina, R.S. (2002). Cycle stratigraphy and chemostratigraphy of Cenomanian-Turonian (Late Cretaceous) shallow-through deep-marine carbonates and siliciclastics, southern Mexico. Abstract: *Workshop on Cretaceous Climate and Ocean Dynamics*, 19.

Erba, E. (1994). Nannofossils and superplumes: The early Aptian "nannoconid crisis". *Paleoc.*, 9: 483-501.

Erbacher, J., Thurow, J., and Littke, R. (1996). Evolution patterns of radiolaria and organic matter variations: a new approach to identify sea level changes in mid-Cretaceous pelagic environments, *Geo.,* 24: 499-502.

Erickson, D.J. III and Dickson, S.M. (1987). Global trace-element biogeochemistry at the K/T boundary: Oceanic and biotic response to a hypothetical meteorite impact. *Geo.*, 15: 1014-1017.

Gale, A.S., Jenkyns, H.C., Kennedy, W.J., and Corfield, M. (1993). Chemostratigraphy versus biostratigraphy: data from around the Cenomanian-Turonian boundary. *J. Geol. Soc. London*, 150: 29-32.

Gordon, W.A. (1973). Marine Life and ocean surface currents in the Cretaceous: *J. Geo.*, 81: 269-284.

Gradstein, F.M., Agterberg, F.P., Ogg, J.G., Hardenbol, J., van Veen, P., Thierry, J. and Huang, Z., (1995). A Triassic, Jurassic and Cretaceous time scale, in *Geochronology. Time Scales and Global Stratigraphic Correlation*. Eds: Berggren, W.A., et al., SEPM Spec. Publ., 5: 95-126.

Gromet, L.P., Dymek, R.F., Haskin, L.A. and Korotev, R.L. (1984). The "North American shale composite": Its compilation, major and trace element characteristics. *Geochem. Cosmochim. Acta,* 48: 2469-2482.

Haq, B.U. (1984). A synoptic overview of 200 million years of ocean history in *Marine Geology and Oceanography of the Arabian Sea and Coastal Pakistan.* Eds: Haq, B.U. and Milliman, J.D., Van Nostrand Reinhold, New York: 201-231.

Harland, W.B., Armstrong, R.L., Cox, A.V., Craig, L.E., Smith, A.G. and Smith, D.G. (1990). *A geologic time scale.* Cambridge University Press, Cambridge, England: 263.

Hart. M.B. and Bigg, P.J. (1981). Anoxic events in the late Cretaceous chalk seas of North-West Europe in *Microfossils of Recent and Fossil Shelf Seas.* Eds: Neale, J.W. and Brasier, M.D., Horwood, Chichester: 171-185.

Hauff, F., Hoernle, K., van den Bogaard, P., Alvarado, G. and Garbe-Schonberg, D. (1999). *Age and geochemistry of basaltic complexes in western Costa Rica: Contributions to the geotectonic evolution of Central America.*

Hay, W.W., Eicher, D.L., and Diner, R. (1993). Physical oceanography and water masses in the Cretaceous Western Interior Seaway, in *Evolution of the Western Interior Basin.* Eds: Caldwell, W.G.E. and Kauffman, E.G., Geological Association of Canada, Special Paper, 39: 297-318.

Herbin, J.P, Montadert, L., Muller, R., Gomez, R., Thurow, J., and Wiedmann, J. (1986). Organic-rich sedimentation at the C-T boundary in oceanic and coastal basins in the North Atlantic and Tethys in *North Atlantic Paleoceanography.* Eds. Summerhayes, C.P. and Shackleton, N.L., Blackwell, Oxford: 389-422.

Hernandez-Romano, U., Aguilera-Franco, N., Martinez-Medrano, M., and Barcelo-Duarte, J. (1997). Guerrero-Morelos Platform drowning at the

Cenomanian/Turonian boundary, Huitziltepec area, Guerrero State, southern Mexico. *Cret. Res.*, 18: 661-686.

Ho, A. and Cashman, K. (1997). Temperature constraints on the Ginkgo Flow of the Columbia River Basalt Group. *Geo.*, 25: 403-406.

Howarth, R.J. and McArthur, J.M. (1997). Statistics for strontium isotope stratigraphy: A robust LOWESS fit to the marine Sr-isotope curve for 0 to 206 Ma, with look-up table for derivation of numeric age. *J. Geo.*, 105: 441-456.

Ingram, B.L., Coccioni, R., Montanari, A. and Richter, F.M. (1994). Strontium isotopic composition of mid-Cretaceous seawater. *Science*. 264: 546-550.

Irving, E., North, F.K., and Couillard, R. (1974). Oil, climate and tectonics. *Canadian J. of Earth Sci.*, 11: 1-17.

Jenkyns, H.C. (1980). Cretaceous anoxic events: From continents to oceans. *J. Geol. Soc. London*, 137: 137-188.

Jenkyns, H.C., Gale, A.S. and Corfield, R.M. (1994). Carbon and Oxygen-isotope stratigraphy of the English Chalk and Italian Scaglia and its paleoclimatic significance. *Geol. Mag.*, 131: 1-34.

Jones, C.E., Jenkyns, H.C., Coe, A.L. and Hesselbo, S.P. (1994). Strontium isotopic variations in Jurassic and Cretaceous seawater. *Geochim. Cosmochim. Acta.*, 58: 3061-3074.

Kaiho, K. (1998). Phylogeny of deep-sea calcareous trochospiral benthic foraminifera: evolution and diversification. *Micropaleontol.*, 44: 291-311.

Kaiho, K., and Hasegawa, T. (1994). Cenomanian benthic foraminiferal extinctions and dysoxic events in the northwestern Pacific Ocean margin. *Palaeogeogr., Palaeoclimatol., Palaeoecol.*, 111: 29-43.

Kaiho, K., Fujiwara, O., and Motoyama, I. (1993). Mid-Cretaceous faunal turnover of intermediate water benthic foraminifera in the northwestern Pacific Ocean margin. *Micropaleontol.*, 23: 13-49.

Kauffman, E.G. (1984). Paleobiogeography and evolutionary response dynamic in the Cretaceous Western Interior Seaway of North America, in *Jurassic-Cretaceous Biochronology and Paleogeography of North America.* Eds: Westermann, G.E.G., Geological Association of Canada, Special Paper, 27: 273-306.

Kauffman, E.G. (1986). High-resolution event stratigraphy: Regional and global Cretaceous bio-events in *Global Bio-Events: A Critical Approach.* Eds: Walliser, O.H., Berlin, Springer-Verlag: 279-335.

Kauffman, E.G., Sageman, B.B., Elder, W.P., Kirkland, J.I., and Villamil, T. (1993). Cretaceous molluscun biostratigraphy and biogeography, Western Interior Basin, North America. in *Evolution of the Western Interior Basin.* Eds: Caldwell, C.G.E., and Kauffman, E.G., Geol. Association of Canada, Special Paper, 39: 397-434.

Kuhnt, W. and Wiedmann, J. (1995). Cenomanian-Turonian source rock: Palaeobiogeographic and paleoenvironmental aspects in *Palaeogeography, Palaeoclimatology and Source Rocks* . Eds: Huc, A.Y., AAPG Studies in Geology, 40: 213-231.

Kump, L.R. and Slingerland, R.L. (1999). Circulation and stratification of the early Turonian Western Interior Seaway: Sensitivity to a variety of forcings. *Geol. Soc. Am., Special Paper*, 332: 181-190.

Larson, R.L. (1991a). Latest pulse of Earth: Evidence for a mid-Cretaceous superplume. *Geo*, 19: 547-550.

Larson, R.L. (1991b). Geological consequences of superplumes. *Geo*, 19: 963-966.

Leary, P.N and Rampino, M.R. (1986). A multi-causal model of mass extinctions: Increase in trace metals in the oceans in *Global Bio-Events: A Critical Approach.* Eds: Walliser, O.H. Berlin, Springer-Verlag: 45-55.

Leary, P.N., Carson, G.A., Cooper, K., Hart, M.B., Horne, D., Jarvis, I., Rosenfeld, A. and Tocher, B.A. (1989). The biotic response to the late Cenomanian anoxic event; integrated evidence from Dover, SE England. *J. Geol. Soc. London*, 146: 311-317.

Leckie, R.M. (1985). Foraminifera of the C-T boundary interval, Greenhorn Formation, Rock Canyon Anticline, Pueblo, Co. in *Fine-grained Deposits and Biofacies of the Cretaceous Western Interior Seaway: Evidence of Cyclic Sedimentary Processes.* Eds: Pratt, L.M, Kauffman, E.G. and Zelt, F.B., Soc. Econ. Paleontol. Mineral. Field Trip Guide 4: 38-48.

Leckie, R.M. (1989). An oceanographic model for the early evolutionary history of planktonic foraminifera. *Palaeogeogr., Palaeoclimatol., Palaeoecol.*, 73: 107-138.

Leckie, R.M., Bralower, T.J. and Cashman, R. (2002). Oceanic anoxic events and plankton evolution: Biotic response to tectonic forcing during the mid-Cretaceous, *Paleoc.*, in press.

Leckie, R.M., Yuretich, R.F., West, O.L.O., Finkelstein, D., and Schmidt, M. (1998). Paleoceanography of the southwestern Western Interior Sea during the time of the Cenomanian-Turonian boundary (Late Cretaceous), in *Stratigraphy and Paleoenvironments of the Cretaceous Western Interior Seaway, USA*. Eds: Dean, W.E. and Arthur, M.A., SEPM, Concepts in Sedimentol. Paleontol., 6: 101-126.

Lilley, M.D., Feely, R.A. and Trefry, J.H. (1995). Chemical and biochemical transformations in hydrothermal plumes in *Seafloor Hydrothermal Systems: Physical, Chemical, Biological, and Geological Interactions*. Eds. Humphris, S.E. Zierenberg, R.A., Mullineaux, L.S. and Thomson, R.E., AGU Monography 91, Washington, D.C., American Geophysical Union: 369-391.

Lupton, J.E., Baker, E.T. and Massoth, G.J. (1999). Helium, heat and generation of hydrothermal event plumes at mid-ocean ridges. *Earth Plan. Sci. Lett.* 171: 343-350.

Luyendyk, B.D., Forsyth, D. and Phillips, J. (1972). An experimental approach to the paleocirculation of oceanic surface waters. *Geol. Soc. Am. Bull.*, 83: 2649-2664.

Martin, J.H. and Fitzwater, S.E. (1988). Iron deficiency limits phytoplankton in the North-east Pacific subarctic. *Nature*, 331: 341-343.

Martin, J.H. and Gordon, R.M. (1988). Northeast Pacific iron distribution in relation to phytoplankton productivity. *Deep Sea Res.*, 35: 177-196.

Martinéz, J.I. and Hernandez, R. (1992). Evolution and drowning of the Late Cretaceous Venezuelan carbonate platform. *J. South Am. Earth Sci.*, 5: 197-210.

McArthur, J.M., Kennedy, W.J., Chen, M., Thirlwall, M.F. and Gale, A.S. (1994). Strontium Isotopic stratigraphy for the Late Cretaceous Time: direct numerical calibration of the Sr isotope curve based on the US Western Interior. *Palaeogeogr., Palaeoclimatol., Palaeoecol.* 108: 95-119.

Meyers, S. R., Sageman, B.B. and Hinnov, L.A. (2001). Integrated quantitative stratigraphy of the Cenomanian-Turonian Bridge Creek limestone member using evolutive harmonic analysis and stratigraphic modeling. *J. Sedimentary Res.*, 71: 628-644.

Milnes, A.R. and Fitzpatrick, R.W. (1989). Titanium and zirconium minerals in *Minerals in Soil Environments*. Eds: Dixon, J.B. and Weed, S.B., Soil Science Society of America, Madison, Wisconsin, 23: 1131-1205.

Morgan, W.J. (1971). Convection plumes in the lower mantle. *Nature*, 230: 42-43.

Morgan, W.J. (1981). Hotspot tracks and the opening of the Atlantic and Indian oceans, in *The Sea, The Oceanic Lithosphere*, Eds: Emiliani, C.: 443-487.

Mortimer, R.N. (1986). Stratigraphy of the upper Cretaceous White Chalk *of Sussex. Proc. Geol. Assoc.*, 97: 97-139.

Nozaki, Y. (2001). Elemental distribution overview in *Encyclopedia of Ocean Sciences*. Academic Press.

Obradovich, J.D. (1993). A Cretaceous timescale: *Geol. Association of Canada Special Paper*. 39: 379-396.

Orth, C.J., Attrep, M.J., Quintana, L.R., Elder, W.P., Kauffman, E.G, Diner, R. and Villamil, T. (1993). Elemental abundance anomalies in the late Cenomanian extinction interval: a search for the source(s). *Earth Plan. Sci. Lett.* 117: 189-204.

Perez-Infante, J., Farrimond, P., and Furrer, M. (1996). Global and local controls influencing the deposition of the La Luna Formation (Cenomanian-Campanian), western Venezuela. *Chem. Geo*, 130: 271-288.

Pindell, J.L and Barrett, S.F. (1990). Geological evolution of the Caribbean region: A plate tectonic perspective in *The Caribbean Region*, Eds: G. Dengo, J.E. Case, Geol. Soc. Am., Vol H: *405-433*.

Pratt, L.M. (1984). Influence of paleoevnironmental factors on the preservation of organic matter in middle Cretaceous Greenhorn Formation near Pueblo, Colorado. *Amer. Association. Of Petr. Geol. Bull.*, 68: 1146-1159.

Pratt, L.M., Arthur, D.A., Dean, W.E. and Scholle, P.A. (1993). Paleooceanographic cycles and events during the late Cretaceous in the Western Interior Seaway of North America, in *Evolution of the Western Interior Basin* Eds: Caldwell, W.G.E. and Kauffman, E.G., St.John's, Geol. Association of Canada Special Paper, 39: 333-354.

Pomerol, B. (1983). Geochemistry of the late Cenomanian-early Turonian chalks of the Paris Basin: manganese and carbon isotopes in carbonates as paleoceanographic indicators. *Cret. Res.*, 4: 85-93.

Rea, D. and Vallier, T. (1983). Two Cretaceous volcanic episodes in the western Pacific Ocean. *Geol. Soc. Amer. Bull.*, 94: 1413-1416.

Richards, M.A., Duncan, R.A. and Courtillot, V.E. (1989). Flood basalts and hotspot tracks: Plume heads and tails. *Science,* 246: 103-107.

Rubin, K. (1997). Degassing of metals and metalloids from erupting seamount and mid-ocean ridge volcanoes: Observations and predictions. *Geochim. Cosmochim. Acta*, 61: 3525-3542.

Sageman, B.B. and Arthur, M.A. (1994). Early Turonian paleogeographic/ paleobathymetric map, Western Interior, U.S. in *Mesozoic Systems of the Rock Mountain Ranges*, USA. Eds: Caputo, M.V., Peterson, J.A. and Franczyk, K.J., SEPM, Rocky Mountain Section: 457-470.

Sageman, B.B., Rich, J., Arthur, M.A., Birchfield, G.E. and Dean, W.E. (1997). Evidence for milankovitch periodicities in Cenomanian-Turonian lithologic and geochemical cycles, Western Interior U.S.A. *J. Sed. Res.*, 67: 286-302.

Saltzmann, E.S. and Barron, E.J. (1982). Deep circulation in the Late Cretaceous: oxygen isotope paleotemperature from Inoceramus remains in D.S.D.P. cores. *Palaegeogr., Palaeoclimatol., Palaeoecol.*, 40: 167-181.

Sarmiento, J.L., Herbert, T.D. and Toggweiler, J.R. (1988). Causes of anoxia in the world oceans. *Global Geochemical Cycle.* 2: 115-128.

Schlanger, S.O. and Jenkyns, H.C. (1976). Cretaceous oceanic anoxic events: Causes and consequences. *Geol. Mijnbouw*, 55: 179-184.

Schlanger, S.O., Jenkyns, H.C. and Premoli-Silva, I. (1981). Volcanism and vertical tectonics in the Pacific Basin related to the global Cretaceous transgressions. *Earth Plan. Sci. Lett.*, 52: 435-449.

Schlanger, S.O., Arthur, M.A. Jenkyns, H.C., and Scholle, P.A. (1987). The Cenomanian-Turonian ocean anoxic event: Stratigraphy and distribution of carbon-rich beds and the marine $\delta^{13}C$ excursion: *Geol. Soc. Lon. Spec. Pub.* 26: 371-399.

Sinton, C.W. (1996). A tale of two large igneous provinces: Geochronological and geochemical studies of the North Atlantic Volcanic Province and the Caribbean ocean plateau. PhD Thesis. Oregon State University.

Sinton, C.W. and Duncan, R.A. (1997). Potential links between ocean plateau volcanism and global ocean anoxia at the Cenomanian-Turonian boundary. *Econ. Geol.* 92:836-842.

Sinton, C.W., Duncan, R.A., Storey, M., Lewis, J. and Estrada, J.J. (1998). A oceanic flood basalt province within the Caribbean Plate. *Earth Plan. Sci. Lett.* 155: 221-235.

Slingerland, R.L., Kump, L.R., Arthur, M.A., Sageman, B.B., and Barron, E.J. (1996). Estuarine circulation in the Turonian Western Interior Seaway of North America. *Geol. Soc. Am. Bull.,* 108: 941-952.

Stein, M. and Hoffman, A.W. (1994). Mantle plumes and episodic crustal growth. *Nature*, 372: 63-68.

Sunda, W.G. and Huntsman, S.A. (1996). Antagonisms between cadmium and zinc toxicity and manganese limitation in a coastal diatom. *Lim. And Ocean.*, 41: 373-387.

Sugarman, P.J., Miller, K.G., Olsson, R.K., Browning, J.V., Wright, J.D., De Romero, L.M., White, T.S., Muller, F.L. and Uptegrove, J. (1999). The Cenomanian/Turonian carbon burial event, Bass River, NJ, USA: Geochemical, paleoecological, and sea-level changes. *Jour. Of For. Res.*, 29: 438-452.

Swanson, D.A., Wright, T.L. and Helz, R.T. (1975). Linear vent systems and estimated rates of magma production and eruption for the Yakima basalt on the Columbia Plateau. *Am. J. of Sci.*. 275: 877-905.

Taylor, S.R. and McLennan, S.M. (1985). *The continental crust: it's composition and evolution: an examination of the geochemical record preserved in sedimentary rocks.* Blackwell Scientific, Palo Alto, California.

Von Damm, K.L. (1995). Controls on the chemistry and temporal variability of seafloor hydrothermal fluids in *Seafloor Hydrothermal Systems: Physical, Chemical, Biological, and Geological Interactions*. Eds. Humphris, S.E. Zierenberg, R.A., Mullineaux, L.S. and Thomson, R.E., AGU Monography 91, Washington, D.C., American Geophysical Union: 222-247.

Vogt, P.R. (1989). Volcanogenic upwelling of anoxic, nutrient-rich water: A possible factor in Carbonate-bank/reef demise and benthic faunal extinctions? *Geol. Soc. Am. Bull.*, 101: 1225-1245.

Weissert, H., McKenzie, J.A. and Channel, J.E.T. (1985). Natural variations in the carbon cycle during the Early Cretaceous in *The Carbon Cycle and Atmospheric*

CO_2: Natural Variations Archean to Present. Eds: Sundquist, E. and Broeker, W.S., Amer. Geophys. Union, Washington, DC: 531-545.

Wignall, P.B. (1994). *Black Shales*: Oxford University Press, Oxford: 127.

Wise, S.W., McArthur, J.M., Meyers, P.A., Hohr, B.A., Petrizzo, M.R., and Wahnert, V. (2002). Cenomanian-Turonian Oceanic Anoxic Event (OAE2) at 53° south latitude: A progress report. Abstract: *Workshop on Cretaceous Climate and Ocean Dynamics*, 90.

APPENDICES

APPENDIX 1

List of standard reference materials with accepted elemental abundances and average analytical blank.

Element	W-1	GSP-1	G-2	AGV-1	SDO-1	SCO-1	SGR-1	Blank
								(ppm)
(Wt %)								
Al2O3	14.99	15.16	15.39	17.15	12.27	13.7	6.52	-0.016
CaO	10.94	2.04	1.96	4.94	1.05	2.62	8.38	-0.018
Fe2O3	1.46	1.75	2.66	6.77	9.34	5.13	3.03	-0.0067
K2O	0.639	5.51	4.48	2.92	3.35	2.77	1.66	
MgO	6.62	0.988	0.75	1.53	1.54	2.72	4.44	0.0040
MnO	0.168	0.04	0.03		0.042			0.0009
Na2O	2.13	2.8	4.08	4.26	0.38	0.9	2.99	0.0037
P2O5	0.14	0.28	0.14	0.5	0.11	0.21	0.328	
TiO2	1.07	0.656	0.48	1.05	0.71	0.63	0.253	0.0034
(ppm)								(ppb)
Sc	35	6.2	3.5	12.2	13.2	11	4.6	-0.010
V	264	53	36	121	160	130	130	0.005
Cr	114	13	8.7	10.1	66.4	68	30	0.44
Co	47	6.6	4.6	15.3	46.8	11	12	0.017
Ni	75	8.8	5	16	99.5	27	29	0.21
Cu	113	33	11	60	60.2	29	66	0.017
Zn	84	104	86	88	64.1	100	74	0.080
As	?	?	?	0.88	68.5	12	67	-0.088
Rb	21.4	254	170	67.3	126	110	?	0.022
Sr	193	234	478	662	75.1	170	420	-0.10
Y	22.6	26	11	20	40.6	26	13	-0.011
Zr	99	530	309	242	165	160	53	0.57
Mo	?	?	?	2.7	134	1.4	35	0.067
Cs	0.9	1.02	1.34	1.28	6.9	7.8	5.2	0.098
Ba	160	1310	1882	1226	397	570	290	0.11
Pb	7.8	55	30	36	27.9	31	38	0.087
Th	2.6	106	24.7	6.5	10.5	9.7	4.8	-0.001
U	0.6	2.54	2.07	1.92	48.8	?	5.4	-0.005

APPENDIX 2

The following are the Zr-normalized data for the Rock Creek Canyon Section.

Sample	45Sc/Zr	51V/Zr	53Cr/Zr	59Co/Zr	60Ni/Zr	65Cu/Zr
1020	0.07	1.71	0.40	0.16	0.91	0.46
970	0.06	1.13	0.33	0.12	0.51	0.39
920	0.06	1.46	0.36	0.12	0.45	0.29
870	0.11	2.66	0.44	0.18	1.30	0.53
820	0.10	1.65	0.44	0.14	0.63	0.50
770	0.11	3.65	0.56	0.16	1.71	0.60
720	0.09	2.54	0.53	0.17	1.12	0.54
670	0.07	2.05	0.46	0.15	0.94	0.51
620	0.07	1.85	0.48	0.10	0.80	0.47
570	0.04	0.54	0.17	0.08	0.11	0.20
520	0.08	1.04	0.52	0.23	0.51	0.64
470	0.10	0.83	0.39	0.25	0.64	0.69
420	0.08	0.77	0.42	0.18	0.37	0.52
410	0.08	0.82	0.34	0.09	0.38	0.36
400	0.09	0.85	0.48	0.22	0.44	0.54
390	0.10	1.01	0.45	0.15	0.93	0.69
380	0.08	0.93	0.27	0.10	0.49	0.36
370	0.07	0.85	0.44	0.14	0.45	0.60
360	0.08	0.90	0.39	0.15	0.52	0.51
350	0.08	0.76	0.33	0.13	0.33	0.31
340	0.08	0.85	0.38	0.16	0.53	0.63
330	0.05	0.54	0.26	0.12	0.26	0.34
304	0.06	0.41	0.48	0.07	0.37	0.31
300.5	0.13	0.69	0.42	0.22	0.97	0.47
297.5	0.09	0.44	0.44	0.20	0.51	0.47
294.5	0.08	0.52	0.31	0.15	0.92	0.27
291	0.08	0.46	0.57	0.16	0.54	0.35
288	0.10	0.65	0.81	0.10	0.40	0.29
286.5	0.13	0.83	0.75	0.09	0.30	0.38
285	0.10	0.87	0.90	0.09	0.26	0.30
282	0.08	0.88	0.51	0.08	0.16	0.27
279	0.09	0.87	0.46	0.08	0.19	0.30
275.5	0.09	0.90	0.51	0.15	0.23	0.29
273	0.09	0.85	0.47	0.08	0.19	0.29
270	0.10	0.95	0.54	0.11	0.23	0.43
267	0.12	0.91	0.55	0.20	0.45	0.46
263	0.09	1.04	0.61	0.18	0.24	0.45
260	0.10	0.86	0.45	0.19	0.57	0.44
258	0.09	0.91	0.57	0.23	0.47	0.50
255	0.13	0.95	0.46	0.10	0.48	0.32
235	0.24	1.64	0.87	0.17	0.41	0.65
234	0.22	1.37	0.59	0.14	0.60	0.50
231	0.25	1.63	0.82	0.15	0.35	0.56
226	0.20	1.31	0.88	0.41	1.09	0.70
221.5	0.26	1.52	1.13	0.42	0.94	0.80

Sample	45Sc/Zr	51V/Zr	53Cr/Zr	59Co/Zr	60Ni/Zr	65Cu/Zr
218	0.36	2.56	1.60	0.37	0.69	1.57
216	0.09	0.97	0.73	0.18	0.35	0.43
212	0.03	0.50	0.14	0.08	0.12	0.18
211	0.57	2.60	1.50	0.59	1.26	1.62
205	0.51	1.68	1.26	0.57	1.48	1.05
204	0.32	2.49	2.12	0.42	0.99	1.13
202	0.46	1.96	1.52	0.47	1.46	1.46
201	0.50	1.97	1.51	0.50	1.14	1.08
197.5	0.24	1.55	0.90	0.22	0.69	0.59
195	0.24	1.67	1.26	0.29	0.77	0.75
193	0.31	1.95	1.97	0.69	1.56	1.42
188.5	0.44	2.12	1.85	0.77	1.70	1.82
186	0.24	1.53	1.36	0.34	0.80	0.77
183	0.21	1.31	1.64	0.26	0.96	0.56
178	0.29	1.51	2.12	0.47	1.25	0.84
177	0.41	2.50	3.49	0.40	1.93	0.88
176.5	0.18	1.30	1.96	0.45	1.36	0.67
171	0.24	1.49	3.23	0.41	1.32	0.79
169	0.40	3.04	4.16	0.44	1.96	1.11
166.5	0.31	1.97	2.78	0.27	0.91	0.94
164	0.19	1.41	2.27	0.31	0.94	0.70
150	0.09	0.68	0.26	0.20	0.81	0.32
140	0.06	0.59	0.11	0.13	0.99	0.08
140	0.07	0.58	0.22	0.14	0.49	0.15
130	0.09	0.76	0.14	0.22	2.00	0.18
120	0.08	0.62	0.35	0.20	0.85	0.46
110	0.10	0.83	0.35	0.13	0.74	0.36
100	0.07	0.96	0.48	0.17	0.44	0.28
90	0.10	0.90	0.63	0.14	0.64	0.31
80	0.31	1.12	1.25	0.21	1.27	0.28
70	0.30	0.96	0.84	0.16	1.17	0.17
60	0.10	0.88	0.61	0.15	0.65	0.32
50	0.09	0.85	0.44	0.15	0.51	0.42
40	0.10	0.81	0.47	0.29	0.85	0.81
30	0.07	0.63	0.13	0.14	1.26	0.25
20	0.23	1.41	1.17	0.24	0.79	0.89
10	0.06	0.67	0.29	0.20	1.35	0.23
0	0.14	0.70	0.45	0.31	1.18	0.14
-30	0.08	1.15	0.68	0.12	0.51	0.36
-60	0.12	1.89	0.89	0.14	0.67	0.60
-90	0.09	2.80	0.75	0.12	0.83	0.41
-120	0.09	2.26	0.69	0.11	0.60	0.29
-150	0.10	2.22	0.70	0.17	0.73	0.39
-180	0.10	2.26	0.77	0.12	0.64	0.34
-210	0.09	2.54	0.78	0.08	0.67	0.32
-240	0.13	3.75	1.08	0.16	1.03	0.58
-270	0.14	4.54	1.22	0.20	1.14	0.53
-300	0.11	4.22	1.09	0.18	1.08	0.53
-330	0.10	3.53	0.79	0.13	0.87	0.45
-360	0.12	4.08	1.13	0.22	1.01	0.57

Sample	66Zn/Zr	75As/Zr	77Se/Zr	85Rb/Zr	86Sr/Zr	89Y/Zr
1020	1.06	0.24	0.05	0.50	59.1	0.34
970	1.47	0.25	0.04	0.48	13.2	0.19
920	0.54	0.11	0.06	0.54	11.0	0.17
870	1.25	0.29	0.20	0.45	76.1	1.20
820	0.77	0.36	0.04	0.68	44.2	0.36
770	0.83	0.18	0.19	0.62	114.8	0.54
720	1.29	0.22	0.10	0.55	58.4	0.33
670	1.28	0.22	0.15	0.64	15.0	0.19
620	1.34	0.19	0.05	0.64	10.1	0.15
570	0.52	0.16	0.06	0.44	15.5	0.19
520	0.60	0.22	0.06	0.59	13.3	0.22
470	0.78	0.27	0.05	0.51	53.7	0.29
420	0.48	0.14	0.07	0.48	27.4	0.22
410	0.54	0.12	0.06	0.65	23.3	0.24
400	0.65	0.27	0.07	0.59	39.5	0.31
390	0.83	0.24	0.05	0.64	57.8	0.40
380	0.39	0.47	0.08	0.42	80.4	0.48
370	1.01	0.23	0.06	0.64	18.8	0.18
360	0.65	0.28	0.04	0.47	54.7	0.36
350	0.37	0.06	0.04	0.60	22.7	0.29
340	0.99	0.41	0.06	0.42	29.8	0.38
330	0.40	0.06	0.02	0.31	20.0	0.36
304	1.18	0.03	0.13	0.32	48.3	1.11
300.5	0.23	0.10	0.03	0.57	97.6	1.10
297.5	0.11	0.06	0.08	0.37	111.0	1.31
294.5	0.37	0.05	0.04	0.44	108.7	1.24
291	0.39	0.05	0.06	0.38	109.2	1.15
288	0.33	0.04	0.02	0.51	33.5	0.40
286.5	0.37	0.07	0.02	0.58	28.0	0.36
285	0.45	0.04	0.02	0.63	10.2	0.18
282	0.52	0.07	0.02	0.62	6.6	0.16
279	0.39	0.04	0.01	0.66	6.5	0.15
275.5	0.52	0.07	0.02	0.65	8.0	0.19
273	0.48	0.07	0.01	0.69	7.2	0.17
270	0.46	0.03	0.01	0.71	11.5	0.18
267	0.76	0.10	0.02	0.70	15.7	0.25
263	0.53	0.02	0.06	0.73	12.4	0.22
260	0.75	0.18	0.02	0.67	18.3	0.28
258	0.55	0.10	0.02	0.67	19.8	0.27
255	0.42	0.03	0.02	0.77	46.4	0.47
235	0.49	0.06	0.02	0.72	25.0	0.37
234	0.26	0.03	0.01	0.80	32.9	0.42
231	0.60	0.04	0.02	0.74	31.3	0.39
226	0.52	0.23	0.02	0.76	25.1	0.31
221.5	1.58	0.11	0.02	0.65	15.9	0.27

Sample	66Zn/Zr	75As/Zr	77Se/Zr	85Rb/Zr	86Sr/Zr	89Y/Zr
218	0.82	0.07	0.00	0.57	9.9	0.27
216	0.53	0.08	0.02	0.69	12.4	0.22
212	0.48	0.18	0.03	0.41	13.1	0.18
211	0.89	0.08	0.04	0.34	33.7	1.38
205	1.11	0.13	0.02	0.76	21.4	0.63
204	0.82	0.15	0.03	0.42	7.3	0.23
202	0.46	0.12	0.03	0.72	25.1	0.62
201	1.03	0.13	0.05	0.75	25.3	0.61
197.5	0.31	0.09	0.03	0.79	9.1	0.24
195	0.67	0.11	0.03	0.76	12.4	0.28
193	1.24	0.18	0.03	0.58	7.5	0.25
188.5	0.93	0.25	0.04	0.72	25.3	0.61
186	0.71	0.09	0.02	0.46	5.3	0.15
183	0.79	0.13	0.03	0.49	7.7	0.19
178	0.67	0.06	0.04	0.24	19.7	0.91
177	0.74	0.02	0.01	0.39	20.6	1.22
176.5	1.01	0.12	0.04	0.57	10.2	0.31
171	0.89	0.10	0.04	0.58	7.7	0.27
169	1.01	0.05	0.04	0.33	16.3	1.09
166.5	0.86	0.05	0.01	0.60	5.7	0.17
164	0.69	0.07	0.03	0.56	7.0	0.25
150	0.42	0.15	0.03	0.55	35.2	0.29
140	0.20	0.02	0.01	0.35	43.0	0.25
140	0.40	0.05	0.03	0.31	45.4	0.26
130	0.19	0.08	0.07	0.50	101.3	0.35
120	0.89	0.15	0.06	0.48	45.1	0.41
110	0.63	0.12	0.07	0.75	32.3	0.46
100	0.57	0.10	0.03	0.78	7.2	0.18
90	0.81	0.03	0.03	0.79	11.4	0.28
80	1.12	0.09	0.09	0.65	25.8	1.32
70	0.72	0.02	0.07	0.55	24.4	1.34
60	0.97	0.03	0.04	0.73	16.7	0.39
50	0.88	0.18	0.05	0.80	12.0	0.25
40	1.29	0.60	0.10	0.67	36.2	0.53
30	0.34	0.06	0.05	0.40	53.5	0.52
20	0.62	0.16	0.05	0.68	12.9	0.30
10	0.42	0.07	0.05	0.40	87.3	0.27
0	0.60	0.00	0.10	0.32	72.0	0.35
-30	0.79	0.27	0.03	0.64	17.5	0.25
-60	1.42	0.21	0.00	0.77	19.3	0.29
-90	1.32	0.27	0.07	0.83	16.6	0.22
-120	0.92	0.22	0.04	0.90	14.2	0.19
-150	1.25	0.21	0.03	0.93	16.6	0.22
-180	1.21	0.20	0.06	1.02	13.6	0.21
-210	1.13	0.17	0.01	0.97	12.3	0.20
-240	1.80	0.26	0.03	0.88	34.3	0.38
-270	2.26	0.26	0.01	1.02	25.6	0.31
-300	1.69	0.22	0.01	0.88	29.1	0.28
-330	1.25	0.20	0.04	0.90	28.5	0.21
-360	1.86	0.24	0.00	0.91	44.0	0.39

Sample	95Mo/Zr	107Ag/Zr	112Cd/Zr	118Sn/Zr	121Sb/Zr	133Cs/Zr
1020	0.12	0.006	0.011	0.000	0.017	0.04
970	0.25	0.005	0.015	0.009	0.017	0.04
920	0.21	0.004	0.012	0.017	0.012	0.04
870	0.19	0.006	0.013	0.000	0.017	0.03
820	0.30	0.006	0.017	0.002	0.016	0.05
770	0.68	0.010	0.022	0.000	0.008	0.05
720	0.22	0.005	0.017	0.000	0.048	0.05
670	0.39	0.005	0.020	0.014	0.025	0.05
620	0.21	0.005	0.016	0.016	0.022	0.05
570	0.01	0.004	0.008	0.045	0.026	0.03
520	0.03	0.004	0.006	0.012	0.013	0.04
470	0.06	0.005	0.008	0.004	0.018	0.04
420	0.02	0.004	0.006	0.009	0.006	0.03
410	0.01	0.010	0.012	0.007	0.003	0.05
400	0.03	0.003	0.007	0.010	0.008	0.04
390	0.07	0.012	0.016	0.000	0.019	0.05
380	0.07	0.005	0.005	0.000	0.008	0.03
370	0.04	0.010	0.015	0.012	0.018	0.05
360	0.05	0.005	0.012	0.007	0.016	0.04
350	0.01	0.011	0.010	0.011	0.003	0.04
340	0.06	0.005	0.014	0.017	0.031	0.03
330	0.03	0.003	0.006	0.014	0.007	0.02
304	0.07	0.004	0.028	0.015	0.005	0.02
300.5	0.04	0.009	0.008	0.000	0.005	0.04
297.5	0.05	0.004	0.009	0.005	0.004	0.03
294.5	0.03	0.009	0.008	0.000	0.003	0.03
291	0.09	0.005	0.014	0.041	0.006	0.03
288	0.02	0.009	0.011	0.020	0.005	0.04
286.5	0.02	0.005	0.006	0.011	0.006	0.04
285	0.01	0.009	0.011	0.011	0.003	0.05
282	0.01	0.003	0.004	0.014	0.006	0.05
279	0.01	0.009	0.010	0.012	0.003	0.05
275.5	0.01	0.003	0.004	0.015	0.005	0.05
273	0.01	0.009	0.010	0.011	0.004	0.05
270	0.01	0.011	0.005	0.018	0.004	0.06
267	0.02	0.010	0.012	0.010	0.007	0.05
263	0.01	0.003	0.007	0.020	0.014	0.05
260	0.02	0.009	0.011	0.008	0.011	0.05
258	0.02	0.004	0.006	0.013	0.010	0.05
255	0.01	0.009	0.011	0.000	0.001	0.05
235	0.01	0.004	0.007	0.015	0.004	0.05
234	0.01	0.009	0.008	0.000	0.000	0.06
231	0.01	0.004	0.006	0.012	0.004	0.05
226	0.02	0.009	0.009	0.003	0.010	0.05
221.5	0.02	0.003	0.006	0.011	0.007	0.04

Sample	95Mo/Zr	107Ag/Zr	112Cd/Zr	118Sn/Zr	121Sb/Zr	133Cs/Zr
218	0.01	0.008	0.009	0.004	0.003	0.03
216	0.03	0.003	0.005	0.017	0.006	0.05
212	0.02	0.004	0.006	0.039	0.023	0.03
211	0.03	0.005	0.010	0.000	0.002	0.02
205	0.01	0.008	0.010	0.000	0.004	0.05
204	0.01	0.003	0.005	0.010	0.006	0.03
202	0.02	0.008	0.009	0.000	0.004	0.05
201	0.02	0.006	0.006	0.010	0.006	0.05
197.5	0.01	0.009	0.010	0.009	0.004	0.06
195	0.01	0.004	0.005	0.012	0.005	0.06
193	0.02	0.009	0.010	0.007	0.007	0.04
188.5	0.03	0.004	0.007	0.010	0.010	0.05
186	0.01	0.009	0.011	0.014	0.003	0.03
183	0.01	0.003	0.005	0.014	0.005	0.03
178	0.03	0.012	0.006	0.000	0.002	0.01
177	0.01	0.009	0.007	0.000	0.000	0.02
176.5	0.01	0.006	0.005	0.013	0.009	0.04
171	0.01	0.009	0.010	0.006	0.004	0.04
169	0.02	0.014	0.009	0.003	0.005	0.02
166.5	0.01	0.009	0.009	0.006	0.002	0.04
164	0.01	0.006	0.005	0.013	0.006	0.04
150	0.06	0.009	0.012	0.000	0.002	0.03
140	0.02	0.022	0.008	0.000	0.000	0.02
140	0.03	0.016	0.006	0.001	0.001	0.02
130	0.02	0.008	0.009	0.000	0.000	0.03
120	0.03	0.015	0.011	0.018	0.008	0.03
110	0.01	0.012	0.012	0.003	0.003	0.05
100	0.01	0.004	0.007	0.031	0.005	0.05
90	0.01	0.009	0.012	0.009	0.002	0.05
80	0.04	0.008	0.013	0.013	0.009	0.04
70	0.01	0.010	0.013	0.008	0.001	0.03
60	0.02	0.005	0.008	0.020	0.004	0.05
50	0.01	0.010	0.011	0.013	0.006	0.05
40	0.05	0.005	0.011	0.032	0.013	0.04
30	0.03	0.009	0.008	0.000	0.000	0.02
20	0.03	0.005	0.007	0.018	0.008	0.05
10	0.05	0.009	0.012	0.000	0.000	0.02
0	0.08	0.011	0.032	0.013	0.000	0.03
-30	0.06	0.003	0.007	0.012	0.010	0.05
-60	0.11	0.004	0.011	0.023	0.010	0.09
-90	0.25	0.004	0.015	0.014	0.016	0.07
-120	0.41	0.003	0.011	0.015	0.013	0.08
-150	0.37	0.004	0.012	0.014	0.014	0.08
-180	0.29	0.004	0.013	0.015	0.013	0.09
-210	0.32	0.004	0.014	0.015	0.013	0.08
-240	0.56	0.006	0.023	0.026	0.019	0.11
-270	0.56	0.006	0.022	0.024	0.024	0.13
-300	0.44	0.006	0.022	0.020	0.020	0.11
-330	0.29	0.004	0.016	0.016	0.018	0.08
-360	0.39	0.007	0.022	0.022	0.020	0.11

Sample	137Ba/Zr	182W/Zr	197Au/Zr	205Tl/Zr	208Pb/Zr	209Bi/Zr
1020	21.8	0.005	0.0019	0.013	0.25	0.006
970	4.0	0.007	0.0004	0.010	0.16	0.004
920	2.2	0.007	0.0005	0.007	0.11	0.004
870	17.6	0.006	0.0000	0.012	0.11	0.004
820	3.8	0.009	0.0000	0.012	0.17	0.004
770	8.0	0.006	0.0000	0.021	0.13	0.005
720	5.0	0.008	0.0006	0.027	0.18	0.005
670	5.1	0.009	0.0005	0.018	0.20	0.006
620	2.5	0.010	0.0007	0.013	0.18	0.005
570	2.7	0.005	0.0017	0.012	0.26	0.010
520	2.8	0.015	0.0005	0.005	0.19	0.006
470	13.2	0.014	0.0000	0.007	0.19	0.006
420	2.9	0.015	0.0005	0.006	0.15	0.006
410	2.9	0.023	0.0005	0.005	0.08	0.007
400	3.5	0.016	0.0003	0.006	0.15	0.007
390	6.0	0.027	0.0005	0.011	0.21	0.008
380	4.1	0.009	0.0000	0.003	0.05	0.006
370	8.3	0.021	0.0009	0.006	0.17	0.007
360	5.4	0.010	0.0004	0.005	0.21	0.006
350	2.8	0.019	0.0005	0.006	0.07	0.010
340	2.6	0.011	0.0008	0.006	0.39	0.007
330	2.0	0.006	0.0006	0.005	0.17	0.005
304	3.1	0.007	0.0011	0.004	0.19	0.006
300.5	9.4	0.035	0.0009	0.009	0.20	0.009
297.5	7.9	0.011	0.0000	0.004	0.14	0.005
294.5	9.2	0.032	0.0000	0.007	0.14	0.006
291	6.7	0.014	0.0008	0.005	0.17	0.005
288	4.5	0.022	0.0006	0.004	0.11	0.006
286.5	3.0	0.014	0.0002	0.003	0.17	0.006
285	2.5	0.018	0.0007	0.004	0.10	0.007
282	2.5	0.014	0.0006	0.004	0.13	0.005
279	5.1	0.018	0.0007	0.005	0.07	0.007
275.5	4.5	0.015	0.0005	0.004	0.13	0.006
273	4.2	0.018	0.0008	0.004	0.14	0.008
270	3.7	0.017	0.0019	0.004	0.08	0.006
267	4.5	0.025	0.0008	0.005	0.15	0.007
263	4.1	0.020	0.0007	0.007	0.15	0.008
260	4.4	0.015	0.0007	0.007	0.19	0.006
258	4.7	0.014	0.0006	0.005	0.17	0.006
255	4.9	0.016	0.0008	0.004	0.06	0.008
235	3.9	0.019	0.0003	0.004	0.10	0.007
234	5.0	0.017	0.0005	0.007	0.08	0.008
231	4.0	0.019	0.0000	0.004	0.09	0.006
226	3.9	0.023	0.0008	0.011	0.13	0.007
221.5	2.6	0.029	0.0003	0.006	0.12	0.005

Sample	137Ba/Zr	182W/Zr	197Au/Zr	205Tl/Zr	208Pb/Zr	209Bi/Zr
218	1.9	0.051	0.0005	0.004	0.07	0.003
216	4.4	0.016	0.0003	0.005	0.13	0.006
212	2.5	0.004	0.0012	0.009	0.23	0.007
211	1.8	0.021	0.0000	0.002	0.04	0.016
205	3.4	0.021	0.0004	0.005	0.08	0.005
204	1.4	0.017	0.0004	0.005	0.11	0.003
202	3.5	0.024	0.0004	0.005	0.08	0.006
201	3.7	0.019	0.0000	0.004	0.08	0.005
197.5	3.4	0.014	0.0008	0.006	0.08	0.005
195	3.4	0.014	0.0002	0.007	0.10	0.004
193	2.1	0.024	0.0005	0.008	0.11	0.004
188.5	3.5	0.022	0.0004	0.006	0.12	0.005
186	1.4	0.013	0.0008	0.005	0.10	0.004
183	1.8	0.011	0.0004	0.005	0.11	0.004
178	15.4	0.007	0.0005	0.001	0.05	0.001
177	1.0	0.016	0.0000	0.002	0.06	0.001
176.5	2.6	0.012	0.0007	0.004	0.23	0.004
171	2.1	0.015	0.0006	0.004	0.14	0.005
169	1.3	0.017	0.0005	0.002	0.07	0.002
166.5	1.7	0.015	0.0006	0.004	0.09	0.004
164	2.1	0.012	0.0006	0.003	0.16	0.004
150	4.8	0.010	0.0005	0.004	0.13	0.009
140	3.0	0.006	0.0007	0.001	0.07	0.004
140	2.9	0.004	0.0014	0.001	0.06	0.005
130	35.8	0.008	0.0000	0.004	0.10	0.007
120	6.3	0.007	0.0024	0.004	0.22	0.006
110	3.4	0.011	0.0008	0.006	0.12	0.009
100	2.5	0.010	0.0011	0.005	0.13	0.007
90	2.6	0.015	0.0008	0.005	0.14	0.008
80	2.7	0.014	0.0006	0.005	0.12	0.004
70	2.4	0.016	0.0000	0.003	0.09	0.004
60	2.6	0.013	0.0005	0.004	0.14	0.005
50	2.9	0.011	0.0007	0.007	0.22	0.011
40	3.4	0.010	0.0020	0.009	0.29	0.008
30	4.6	0.006	0.0000	0.004	0.12	0.006
20	3.1	0.014	0.0005	0.005	0.11	0.004
10	19.1	0.009	0.0000	0.004	0.10	0.012
0	21.2	0.003	0.0026	0.003	0.10	0.005
-30	8.0	0.008	0.0005	0.015	0.20	0.004
-60	4.4	0.013	0.0011	0.019	0.17	0.008
-90	4.6	0.008	0.0006	0.019	0.16	0.003
-120	3.7	0.009	0.0007	0.015	0.16	0.003
-150	2.1	0.009	0.0007	0.013	0.17	0.003
-180	7.7	0.010	0.0006	0.012	0.16	0.003
-210	3.8	0.010	0.0006	0.010	0.16	0.003
-240	3.5	0.014	0.0010	0.020	0.24	0.005
-270	4.9	0.016	0.0011	0.028	0.29	0.006
-300	3.9	0.015	0.0011	0.026	0.25	0.006
-330	4.2	0.010	0.0006	0.020	0.17	0.004
-360	4.5	0.015	0.0009	0.020	0.23	0.006

Sample	232Th/Zr	238U/Zr	Al/Zr	Ba/Zr	Ca/Zr	Fe/Zr
1020	0.05	0.13	479.3	16.4	17648	205.5
970	0.06	0.14	302.1	2.9	2920	141.7
920	0.07	0.14	219.3	1.6	2703	109.7
870	0.05	0.54	519.0	14.2	24400	259.8
820	0.06	0.27	651.7	3.7	13002	339.7
770	0.06	0.28	243.2	4.8	24651	257.7
720	0.06	0.16	437.8	4.1	17039	269.9
670	0.11	0.17	321.0	3.9	3611	172.9
620	0.07	0.12	267.0	2.0	2497	153.6
570	0.27	0.11	81.7	0.0	3842	39.0
520	0.10	0.07	394.6	1.9	3541	216.4
470	0.07	0.07	592.4	10.0	14033	321.5
420	0.06	0.04	375.8	2.3	6747	199.2
410	0.07	0.04	281.5	2.2	7232	157.3
400	0.07	0.06	473.3	2.0	9005	226.0
390	0.07	0.13	736.9	4.6	15343	335.0
380	0.04	0.06	380.8	2.1	20854	243.1
370	0.10	0.05	535.6	7.4	5313	257.9
360	0.08	0.11	473.2	4.5	10135	249.8
350	0.08	0.04	317.4	2.4	6402	136.7
340	0.08	0.09	468.0	1.8	6780	254.9
330	0.12	0.09	262.1	1.5	6340	144.7
304	0.10	0.24	235.7	2.3	10376	116.1
300.5	0.08	0.16	575.4	8.0	21980	273.4
297.5	0.05	0.20	130.3	6.3	19822	179.7
294.5	0.05	0.21	370.0	7.7	22640	181.5
291	0.04	0.20	285.4	4.8	19671	169.7
288	0.06	0.07	237.8	4.2	7876	132.7
286.5	0.06	0.06	239.4	2.1	6426	148.9
285	0.07	0.03	234.3	2.1	2657	124.4
282	0.07	0.03	223.0	2.0	1561	119.0
279	0.07	0.03	221.0	4.9	1807	112.2
275.5	0.07	0.03	268.6	3.5	1968	129.7
273	0.07	0.03	272.5	3.8	2063	145.2
270	0.07	0.03	188.9	2.9	2621	105.4
267	0.08	0.03	397.9	3.8	4528	214.0
263	0.09	0.03	148.4	0.2	5853	71.6
260	0.07	0.04	411.7	3.8	5163	241.0
258	0.07	0.04	313.1	3.4	4394	163.4
255	0.06	0.04	351.4	3.8	10667	166.3
235	0.06	0.03	382.1	2.8	7634	202.4
234	0.07	0.04	294.4	4.6	11977	190.7
231	0.05	0.03	323.0	3.3	9022	192.4
226	0.08	0.04	987.3	3.3	8513	503.9
221.5	0.06	0.02	1385.5	1.9	5552	726.1

Sample	232Th/Zr	238U/Zr	Al/Zr	Ba/Zr	Ca/Zr	Fe/Zr
218	0.04	0.01	482.1	1.7	4997	254.9
216	0.07	0.03	318.2	3.4	3054	162.9
212	0.25	0.11	250.2	2.2	1587	123.5
211	0.03	0.08	726.8	0.0	33590	333.7
205	0.06	0.03	618.9	2.4	9206	367.1
204	0.04	0.02	577.0	1.1	2084	279.3
202	0.06	0.03	630.2	3.4	9550	355.8
201	0.05	0.03	768.0	3.3	10793	400.1
197.5	0.07	0.03	368.9	2.9	2496	212.1
195	0.06	0.04	437.7	2.9	3414	239.1
193	0.04	0.03	812.2	1.8	2379	431.9
188.5	0.05	0.03	623.3	2.4	7824	376.6
186	0.07	0.02	383.3	1.1	1500	200.4
183	0.06	0.02	535.3	1.6	1965	272.1
178	0.01	0.02	440.7	1.2	1867	218.1
177	0.02	0.03	294.1	12.5	13107	200.8
176.5	0.07	0.05	378.4	1.4	19061	230.4
171	0.05	0.05	461.2	2.3	2586	256.6
169	0.01	0.02	436.2	2.0	2335	230.0
166.5	0.05	0.02	363.6	0.8	13655	207.2
164	0.06	0.04	336.4	1.4	1787	169.5
150	0.06	0.04	363.8	1.7	1948	192.8
140	0.03	0.02	543.9	4.1	13257	242.6
140	0.03	0.02	403.2	0.7	20383	182.6
130	0.04	0.04	359.9	31.0	43825	284.5
120	0.04	0.03	407.3	4.0	15559	238.4
110	0.07	0.08	402.0	2.8	8745	219.7
100	0.08	0.05	310.1	2.0	2146	158.6
90	0.07	0.03	262.0	2.2	4231	147.4
80	0.04	0.20	803.0	1.8	15885	363.4
70	0.04	0.24	101.1	2.2	17772	166.0
60	0.06	0.03	413.9	2.2	5607	208.5
50	0.09	0.06	451.2	2.1	3429	250.0
40	0.07	0.08	1038.8	2.7	9756	550.3
30	0.04	0.04	309.6	2.9	24073	277.9
20	0.07	0.03	434.0	2.0	2947	215.0
10	0.04	0.03	525.0	17.6	28221	312.7
0	0.05	0.03	18.3	18.1	37437	104.8
-30	0.09	0.11	426.9	8.2	3707	228.1
-60	0.14	0.13	499.6	7.2	4418	264.0
-90	0.08	0.15	424.5	4.7	3394	227.5
-120	0.09	0.15	443.9	3.7	2481	240.4
-150	0.09	0.16	457.5	3.4	2850	245.1
-180	0.08	0.15	480.1	8.3	2366	254.4
-210	0.09	0.16	408.2	3.9	1925	221.4
-240	0.12	0.30	608.9	5.3	5224	337.4
-270	0.15	0.23	662.0	7.9	3595	350.2
-300	0.13	0.20	599.5	6.2	4022	310.5
-330	0.09	0.16	448.6	4.4	4073	240.7
-360	0.14	0.28	632.4	7.2	6505	336.5

Sample	Mg/Zr	Mn/Zr	Na/Zr	Ti/Zr
1020	133.8	13.2	40.3	16.0
970	59.7	1.6	34.6	14.9
920	84.4	1.7	26.5	17.2
870	226.1	14.7	97.8	12.2
820	143.5	9.2	28.7	28.5
770	161.4	15.6	85.2	17.3
720	130.5	12.4	34.7	17.5
670	96.8	2.8	25.8	17.4
620	84.9	1.4	22.2	18.4
570	33.1	11.6	13.6	5.8
520	91.5	2.9	57.2	21.3
470	132.2	10.6	61.3	19.2
420	93.4	5.0	45.3	18.1
410	124.0	9.2	49.2	21.7
400	135.3	6.8	72.5	20.4
390	162.0	9.8	54.7	23.0
380	124.6	26.8	0.0	12.5
370	110.6	3.6	63.0	25.2
360	115.8	6.9	31.3	18.8
350	108.7	6.6	65.8	21.6
340	106.8	4.6	85.0	16.9
330	104.6	5.1	28.7	14.7
304	111.8	10.7	17.6	12.7
300.5	171.9	24.0	16.8	24.0
297.5	141.9	20.6	36.3	18.6
294.5	158.0	23.7	44.9	22.3
291	140.5	20.3	31.2	19.6
288	97.9	7.1	35.1	21.8
286.5	106.0	5.7	38.9	24.1
285	97.1	1.8	36.4	24.5
282	88.2	1.1	38.8	22.5
279	100.0	1.1	31.8	25.1
275.5	89.2	1.2	34.9	21.8
273	100.1	1.6	37.6	25.2
270	97.0	1.8	35.7	25.0
267	129.1	3.3	44.0	26.8
263	47.5	17.2	5.2	9.1
260	122.7	3.9	64.1	23.3
258	101.4	3.8	53.3	22.0
255	155.7	12.0	50.0	25.3
235	144.1	9.9	77.6	29.8
234	179.1	14.9	171.5	29.1
231	149.2	11.9	108.6	29.8
226	164.4	7.5	389.3	37.8
221.5	134.9	8.5	127.4	41.8

Sample	Mg/Zr	Mn/Zr	Na/Zr	Ti/Zr
218	166.4	7.3	150.3	60.2
216	103.6	2.4	56.6	25.3
212	91.6	2.4	20.5	12.7
211	287.7	98.5	137.6	41.3
205	181.5	14.3	93.6	35.7
204	106.6	3.1	74.0	45.4
202	217.9	11.2	110.3	49.5
201	221.1	15.7	167.7	45.1
197.5	122.7	2.4	64.2	29.6
195	117.4	5.2	94.8	35.2
193	129.6	4.3	78.5	53.7
188.5	184.4	9.5	121.2	44.6
186	109.6	1.8	57.3	35.8
183	106.3	2.6	62.4	31.2
178	129.9	3.6	85.3	48.7
177	132.5	30.5	54.1	31.9
176.5	229.6	45.2	150.2	51.5
171	109.7	3.4	60.1	32.4
169	122.9	2.8	108.4	36.6
166.5	206.4	32.4	3.9	52.7
164	144.0	2.3	63.3	42.6
150	111.5	2.5	54.5	34.1
140	104.6	14.2	1.9	20.6
140	106.5	35.6	0.0	10.5
130	235.7	94.7	100.5	13.6
120	111.3	18.0	10.6	20.4
110	123.2	9.9	65.4	20.5
100	95.5	2.6	31.6	26.2
90	117.4	7.8	36.9	26.4
80	158.7	43.9	54.4	26.7
70	153.8	48.3	10.8	20.0
60	108.5	10.4	22.5	23.0
50	114.8	4.0	48.1	25.1
40	123.0	11.2	77.3	30.6
30	135.1	35.4	9.7	12.7
20	103.3	3.4	39.4	28.9
10	151.3	51.8	0.0	16.9
0	183.6	87.8	64.3	6.5
-30	81.6	2.2	34.9	25.1
-60	125.5	2.6	36.7	40.5
-90	87.2	1.6	22.4	25.9
-120	89.6	1.3	21.3	26.0
-150	99.2	1.6	22.7	26.9
-180	99.0	1.4	29.9	28.8
-210	99.4	1.0	26.9	28.5
-240	159.4	3.0	53.9	40.8
-270	160.0	2.0	60.2	46.5
-300	154.7	2.5	47.0	41.2
-330	118.0	2.1	44.9	29.0
-360	188.3	3.9	63.6	42.9

The following are the Zr-normalized data for the Rock Creek Canyon Section.

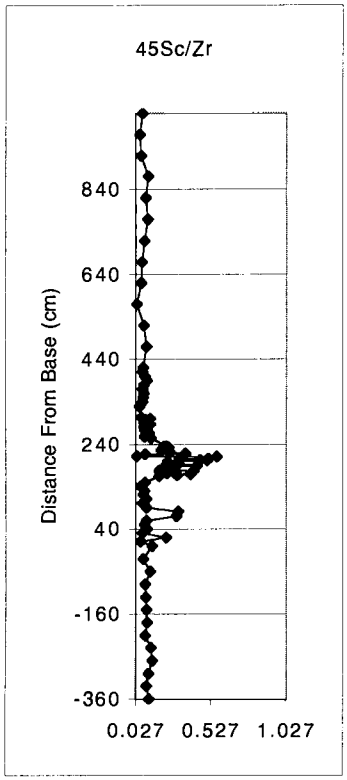

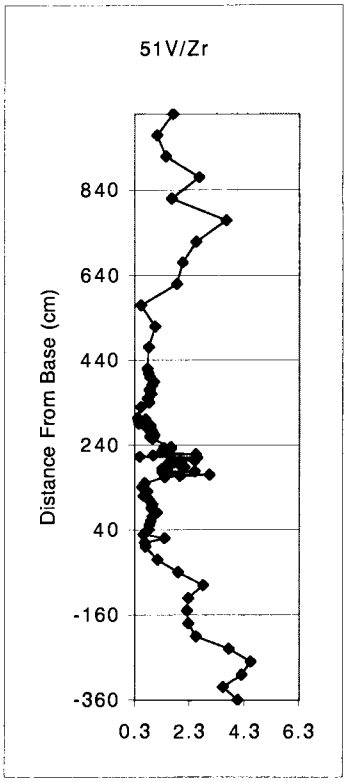

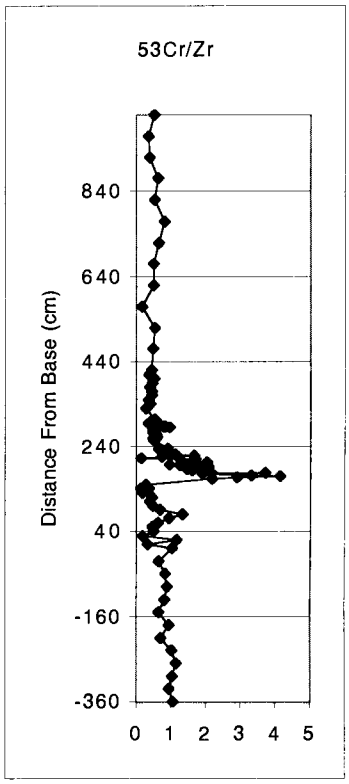

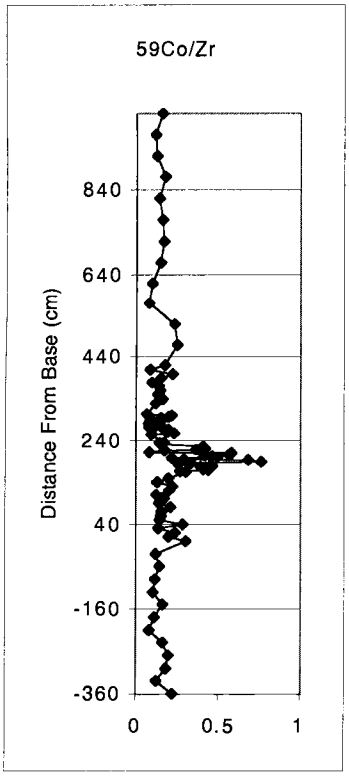

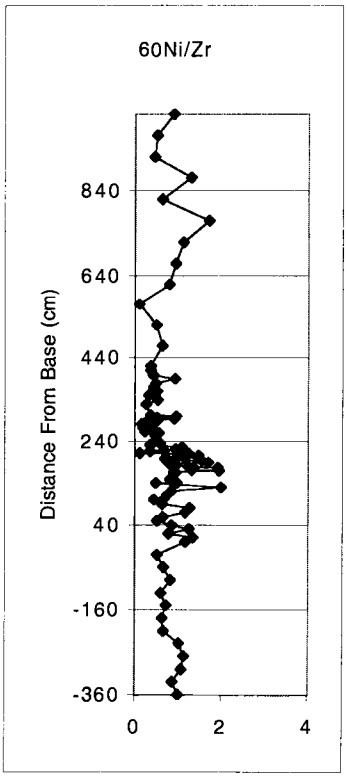

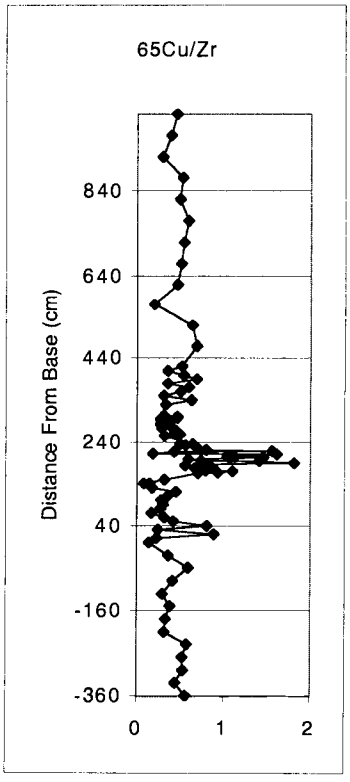

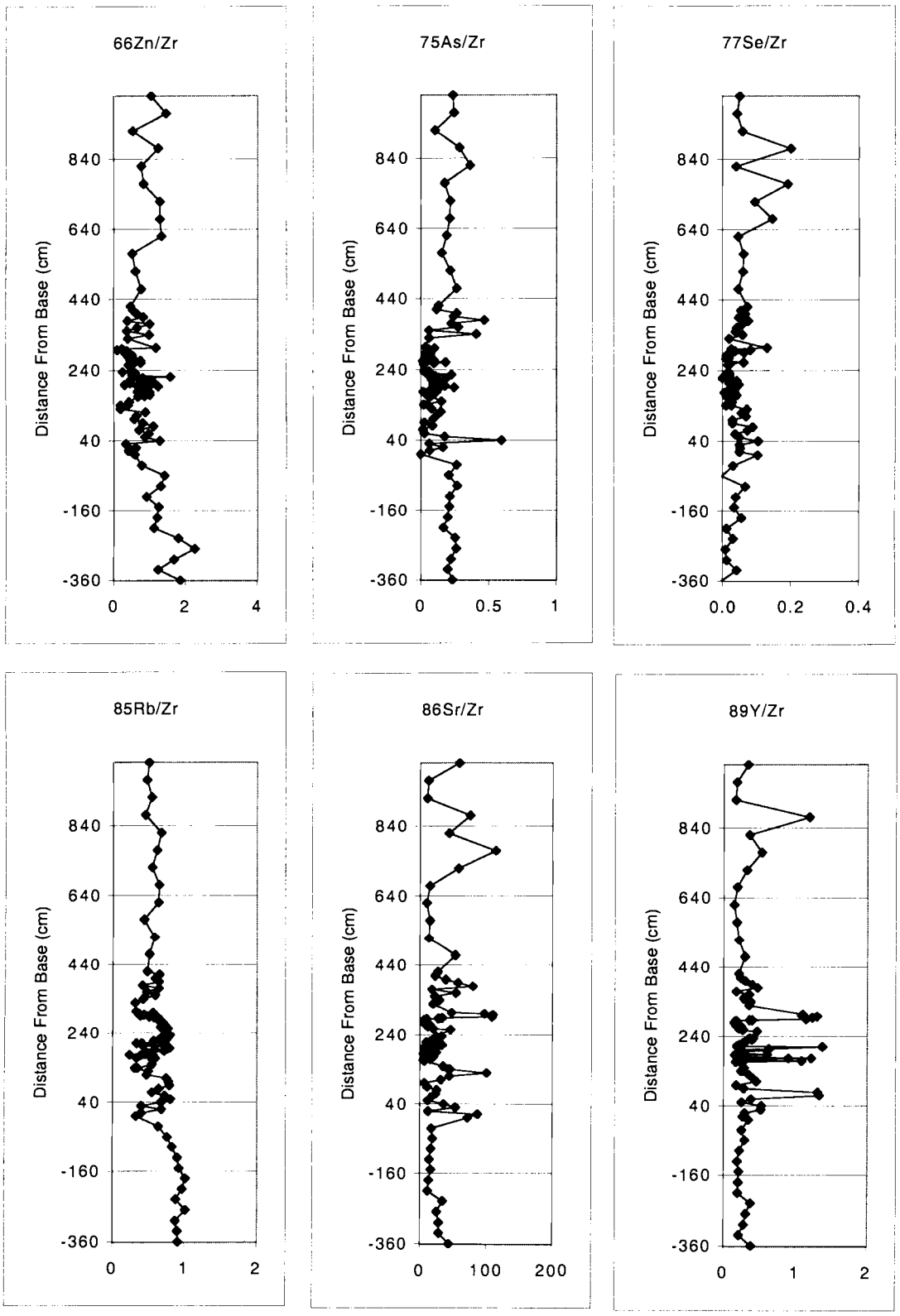
66Zn/Zr
75As/Zr
77Se/Zr
85Rb/Zr
86Sr/Zr
89Y/Zr
Distance From Base (cm)
840
640
440
240
40
-160
-360
0
2
4
0.5
1
0.0
0.2
0.4
100
200

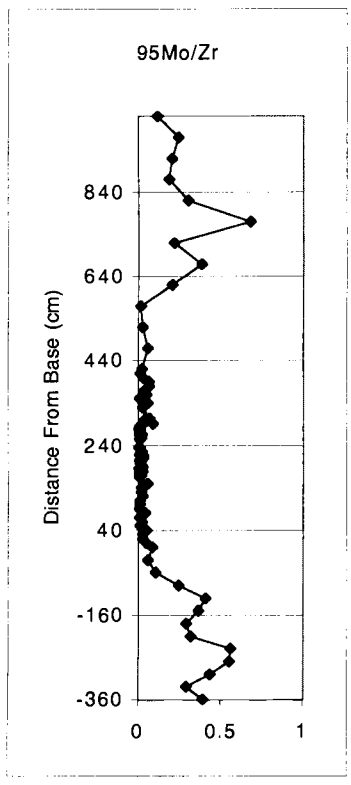
95Mo/Zr
Distance From Base (cm)
840
640
440
240
40
-160
-360
0
0.5
1

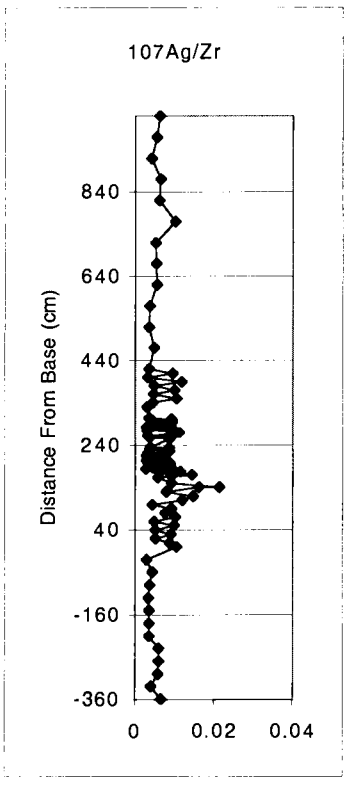
107Ag/Zr
Distance From Base (cm)
840
640
440
240
40
-160
-360
0
0.02
0.04

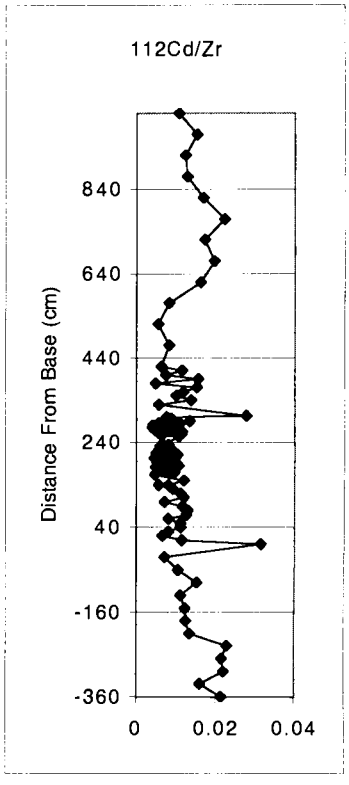
112Cd/Zr
Distance From Base (cm)
840
640
440
240
40
-160
-360
0
0.02
0.04

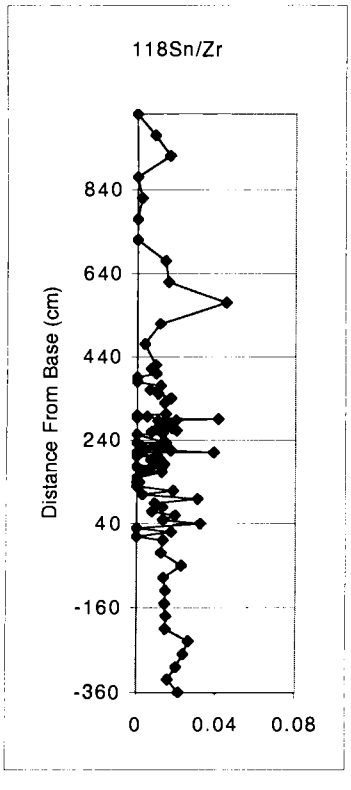
118Sn/Zr
Distance From Base (cm)
840
640
440
240
40
-160
-360
0
0.04
0.08

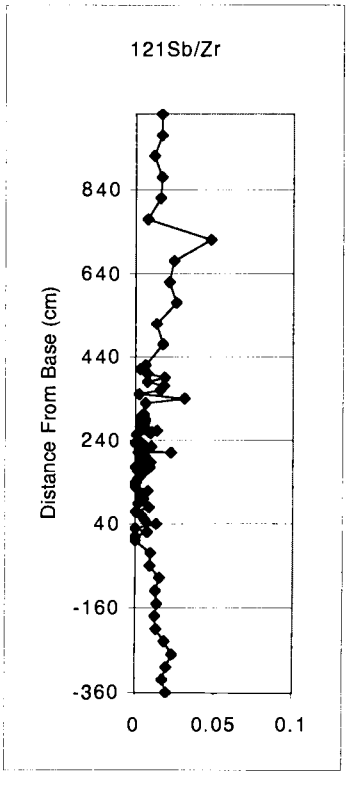
121Sb/Zr
Distance From Base (cm)
840
640
440
240
40
-160
-360
0
0.05
0.1

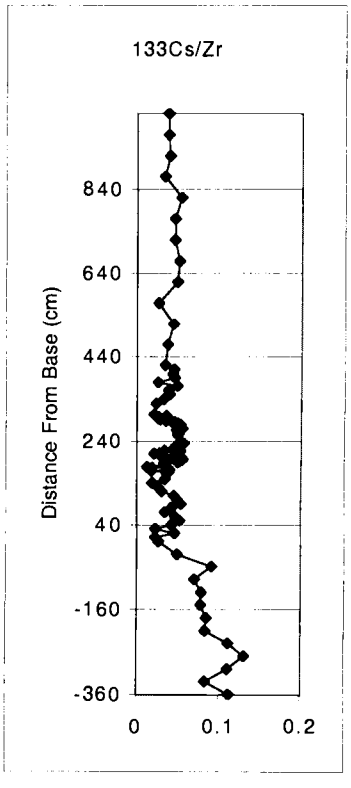
133Cs/Zr
Distance From Base (cm)
840
640
440
240
40
-160
-360
0
0.1
0.2

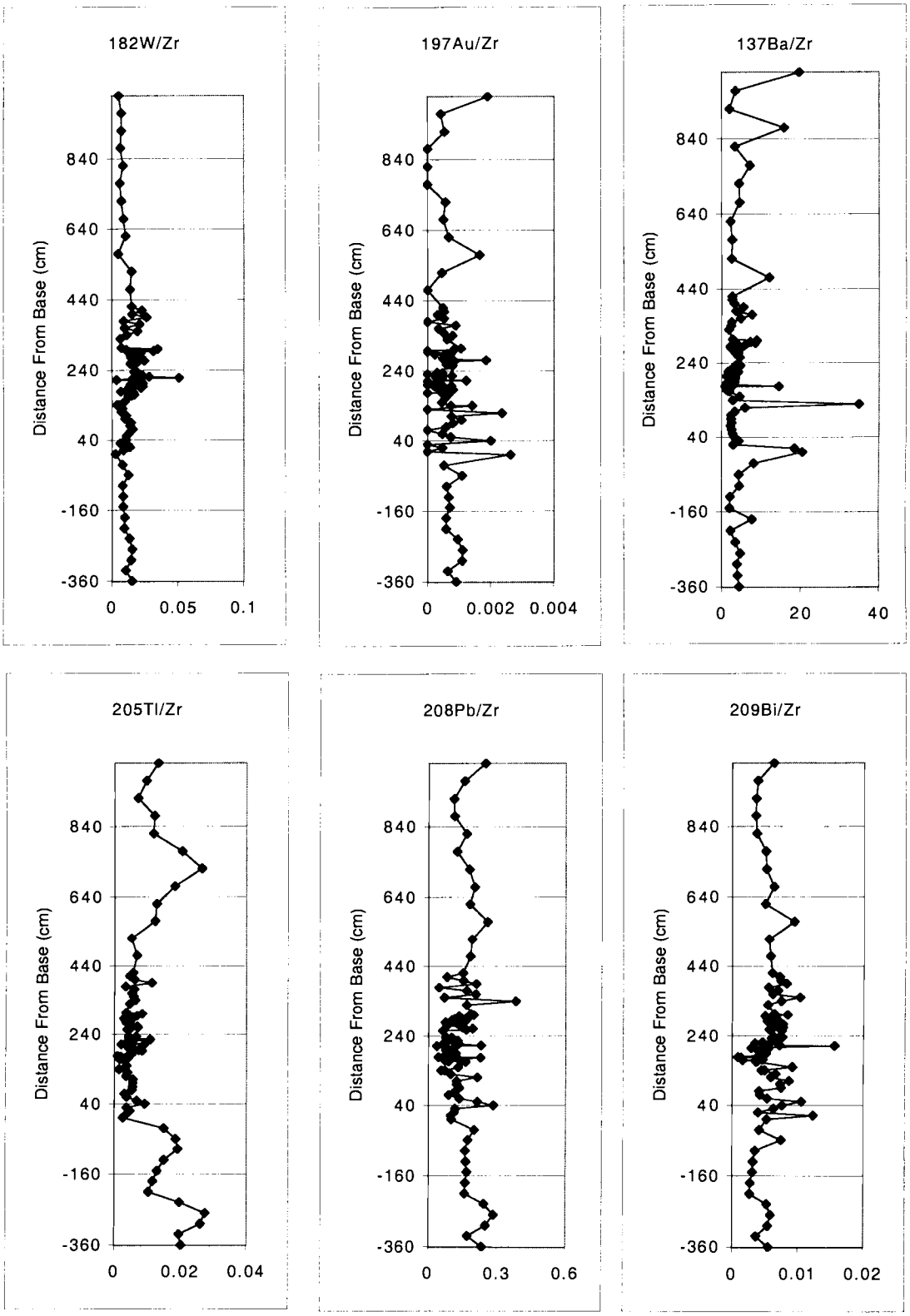
182W/Zr
197Au/Zr
137Ba/Zr
205Tl/Zr
208Pb/Zr
209Bi/Zr
Distance From Base (cm)
840
640
440
240
40
-160
-360
0
0.05
0.1
0.002
0.004
20
40
0.02
0.04
0.3
0.6
0.01
0.02

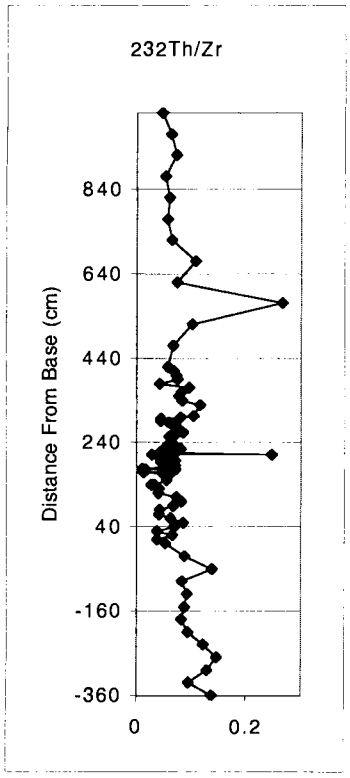
232Th/Zr
Distance From Base (cm)
840
640
440
240
40
-160
-360
0
0.2

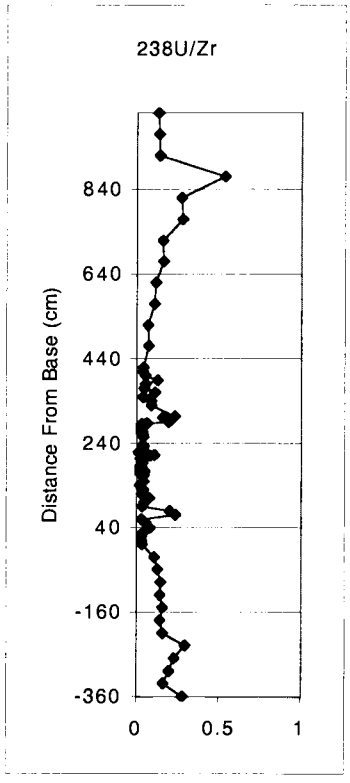
238U/Zr
Distance From Base (cm)
840
640
440
240
40
-160
-360
0
0.5
1

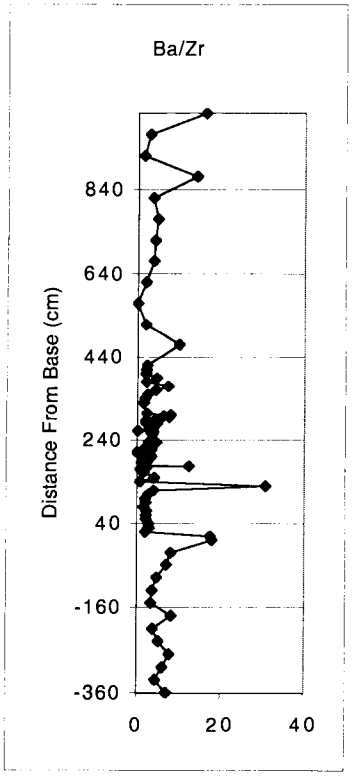
Ba/Zr
Distance From Base (cm)
840
640
440
240
40
-160
-360
0
20
40

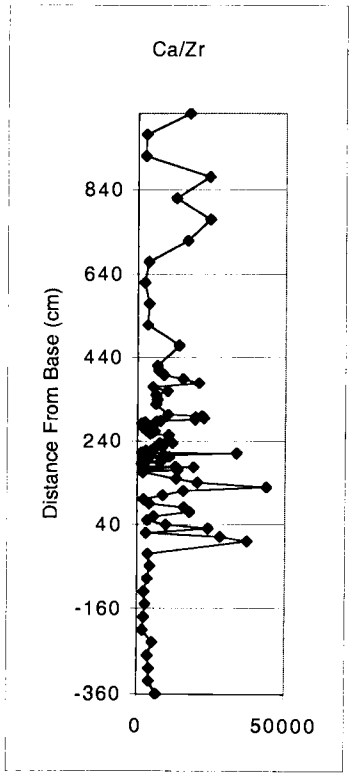
Ca/Zr
Distance From Base (cm)
840
640
440
240
40
-160
-360
0
50000

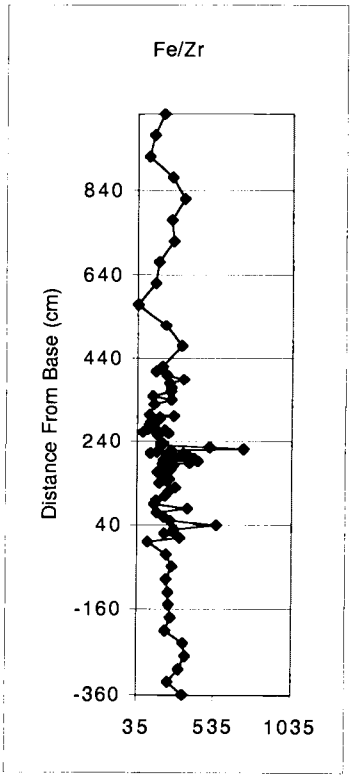
Fe/Zr
Distance From Base (cm)
840
640
440
240
40
-160
-360
35
535
1035

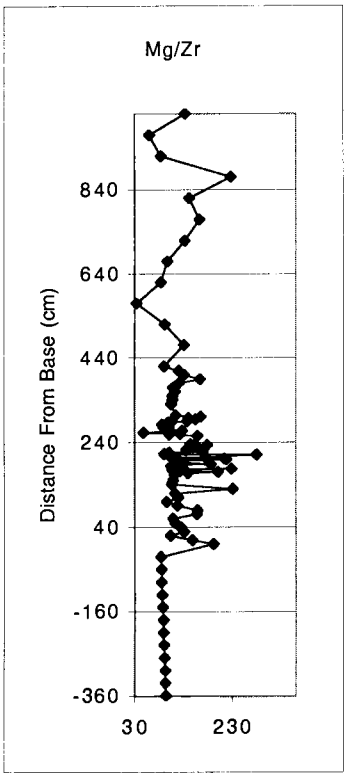
Mg/Zr
Distance From Base (cm)
840
640
440
240
40
-160
-360
30
230

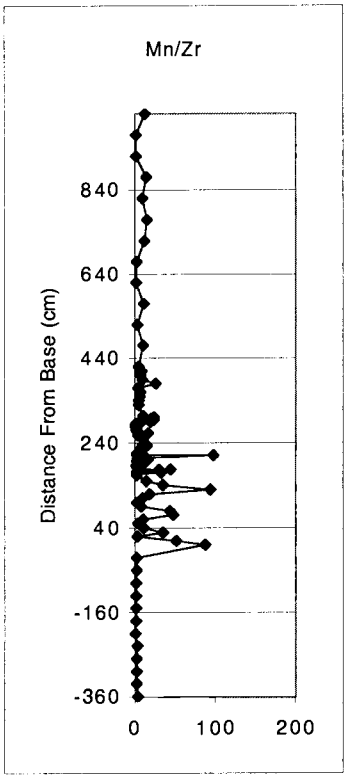
Mn/Zr
Distance From Base (cm)
840
640
440
240
40
-160
-360
0
100
200

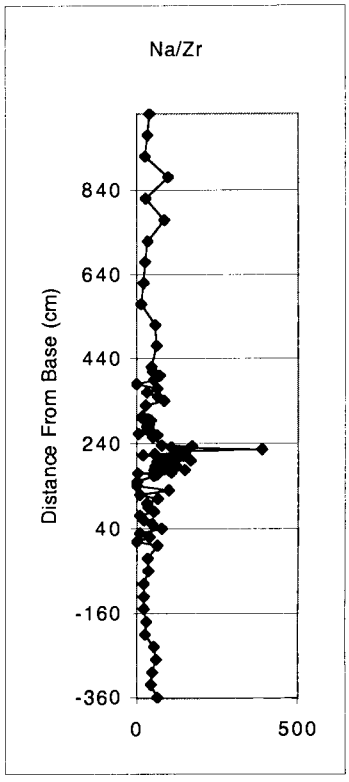
Na/Zr
Distance From Base (cm)
840
640
440
240
40
-160
-360
0
500

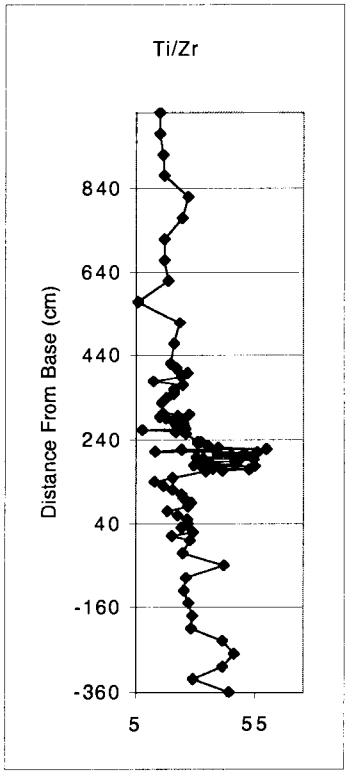
Ti/Zr
Distance From Base (cm)
840
640
440
240
40
-160
-360
5
55

APPENDIX 3

The following are Zr-normalized data for the Bass River Borehole. Samples are feet below sea floor.

Sample	45Sc/Zr	51V/Zr	53Cr/Zr	59Co/Zr	60Ni/Zr
1925.6	0.087	0.41	0.51	0.066	0.21
1926	0.101	0.45	0.57	0.074	0.23
1926.3	0.096	0.42	0.54	0.067	0.21
1926.6	0.096	0.43	0.56	0.069	0.22
1927	0.093	0.38	0.47	0.062	0.19
1927.3	0.083	0.38	0.47	0.062	0.18
1927.6	0.107	0.56	0.68	0.096	0.27
1928	0.092	0.49	0.57	0.069	0.21
1928.3	0.109	0.60	0.67	0.086	0.26
1928.6	0.105	0.56	0.63	0.085	0.26
1929	0.099	0.52	0.61	0.075	0.25
1929.3	0.098	0.51	0.59	0.074	0.24
1929.6	0.101	0.51	0.60	0.078	0.25
1930	0.084	0.40	0.52	0.056	0.19
1930.3	0.095	0.44	0.56	0.062	0.20
1930.6	0.104	0.47	0.61	0.069	0.22
1931	0.106	0.50	0.64	0.078	0.24
1931.3	0.115	0.54	0.68	0.085	0.27
1931.6	0.110	0.54	0.66	0.081	0.26
1932	0.104	0.52	0.62	0.076	0.24
1932.3	0.100	0.49	0.59	0.090	0.29
1932.6	0.100	0.48	0.58	0.076	0.22
1933.7	0.106	0.50	0.63	0.080	0.27
1934	0.105	0.51	0.62	0.078	0.26
1934.3	0.117	0.54	0.67	0.089	0.27
1934.6	0.123	0.56	0.71	0.095	0.30
1935	0.124	0.55	0.72	0.091	0.30
1935.3	0.127	0.58	0.76	0.098	0.32
1935.6	0.120	0.55	0.74	0.084	0.28
1936	0.102	0.43	0.60	0.072	0.24
1936.3	0.094	0.41	0.55	0.071	0.22
1936.6	0.110	0.47	0.62	0.090	0.26
1937	0.093	0.42	0.54	0.078	0.20
1937.3	0.100	0.47	0.58	0.085	0.22
1937.6	0.103	0.49	0.62	0.105	0.25
1938	0.105	0.50	0.74	0.093	0.20
1938.3	0.100	0.49	0.66	0.088	0.20
1938.6	0.074	0.39	0.45	0.071	0.18
1939	0.057	0.35	0.45	0.055	0.17
1939.3	0.073	0.36	0.44	0.066	0.16
1939.6	0.082	0.39	0.46	0.066	0.16
1940	0.068	0.33	0.38	0.062	0.15
1940.3	0.078	0.38	0.42	0.070	0.18
1940.6	0.100	0.50	0.54	0.096	0.23
1940.8	0.105	0.50	0.56	0.090	0.24

Sample	45Sc/Zr	51V/Zr	53Cr/Zr	59Co/Zr	60Ni/Zr
1941	0.075	0.33	0.38	0.059	0.15
1941.5	0.091	0.45	0.55	0.080	0.25
1941.9	0.111	0.55	0.63	0.095	0.27
1942.5	0.090	0.40	0.44	0.071	0.19
1943	0.104	0.45	0.52	0.087	0.23
1943.5	0.092	0.41	0.47	0.076	0.23
1944	0.102	0.49	0.56	0.088	0.25
1944.5	0.106	0.50	0.55	0.088	0.25
1945	0.117	0.60	0.61	0.108	0.34
1945.5	0.086	0.69	0.60	0.097	0.26
1946	0.093	0.58	0.54	0.074	0.23
1946.5	0.081	0.49	0.46	0.061	0.20
1947	0.081	0.46	0.46	0.062	0.19
1947.5	0.068	0.38	0.37	0.048	0.15
1948	0.074	0.39	0.41	0.055	0.19
1948.5	0.078	0.38	0.43	0.058	0.23
1949	0.091	0.49	0.53	0.078	0.28
1949.5	0.062	0.38	0.37	0.022	0.12
1950	0.096	0.50	0.50	0.069	0.22

Sample	65Cu/Zr	66Zn/Zr	75As/Zr	77Se/Zr	85Rb/Zr
1925.6	0.10	0.63	0.045	0.017	0.77
1926	0.12	0.66	0.063	0.014	0.84
1926.3	0.11	0.64	0.044	0.016	0.80
1926.6	0.11	0.65	0.055	0.015	0.80
1927	0.10	0.58	0.072	0.018	0.70
1927.3	0.09	0.56	0.077	0.014	0.70
1927.6	0.15	0.80	0.102	0.018	0.89
1928	0.10	0.69	0.069	0.017	0.84
1928.3	0.13	0.85	0.068	0.019	0.95
1928.6	0.14	0.84	0.099	0.016	0.86
1929	0.12	0.70	0.070	0.017	0.79
1929.3	0.12	0.69	0.060	0.017	0.78
1929.6	0.13	0.70	0.078	0.017	0.79
1930	0.08	0.53	0.060	0.014	0.70
1930.3	0.10	0.60	0.037	0.017	0.76
1930.6	0.10	0.64	0.059	0.020	0.83
1931	0.12	0.74	0.076	0.018	0.85
1931.3	0.13	0.84	0.088	0.019	0.92
1931.6	0.13	0.79	0.054	0.018	0.91
1932	0.11	0.72	0.057	0.017	0.87
1932.3	0.11	0.81	0.049	0.017	0.86
1932.6	0.11	0.69	0.061	0.016	0.86
1933.7	0.13	0.73	0.069	0.019	0.80
1934	0.12	0.75	0.074	0.018	0.80
1934.3	0.14	0.79	0.061	0.019	0.85
1934.6	0.15	0.83	0.091	0.021	0.90
1935	0.16	0.83	0.059	0.020	0.90
1935.3	0.16	0.83	0.156	0.024	0.90
1935.6	0.14	0.80	0.086	0.021	0.88
1936	0.11	0.64	0.061	0.016	0.79
1936.3	0.11	0.68	0.059	0.015	0.74
1936.6	0.13	0.71	0.105	0.016	0.81
1937	0.11	0.65	0.090	0.015	0.78
1937.3	0.12	0.94	0.070	0.016	0.81
1937.6	0.14	0.69	0.114	0.017	0.81
1938	0.11	0.54	0.121	0.020	0.74
1938.3	0.10	0.62	0.083	0.018	0.71
1938.6	0.08	0.52	0.125	0.013	0.65
1939	0.08	0.30	0.031	0.025	0.51
1939.3	0.07	0.52	0.079	0.014	0.64
1939.6	0.08	0.58	0.046	0.015	0.77
1940	0.07	0.57	0.063	0.016	0.68
1940.3	0.09	0.59	0.048	0.014	0.71
1940.6	0.12	0.92	0.053	0.018	0.93
1940.8	0.15	0.80	0.047	0.019	0.80

Sample	65Cu/Zr	66Zn/Zr	75As/Zr	77Se/Zr	85Rb/Zr
1941	0.08	0.58	0.028	0.014	0.73
1941.5	0.11	0.72	0.050	0.018	0.80
1941.9	0.14	0.94	0.062	0.018	0.93
1942.5	0.10	0.69	0.045	0.017	0.82
1943	0.13	0.76	0.061	0.019	0.89
1943.5	0.11	0.72	0.055	0.017	0.85
1944	0.14	0.85	0.081	0.018	0.77
1944.5	0.14	0.86	0.095	0.019	0.94
1945	0.17	0.83	0.148	0.024	0.70
1945.5	0.18	0.93	0.130	0.019	0.52
1946	0.12	0.77	0.140	0.020	0.82
1946.5	0.09	0.65	0.097	0.017	0.75
1947	0.10	0.63	0.073	0.015	0.73
1947.5	0.08	0.50	0.086	0.014	0.63
1948	0.08	0.58	0.085	0.015	0.68
1948.5	0.09	0.64	0.081	0.014	0.73
1949	0.12	0.71	0.095	0.018	0.62
1949.5	0.05	0.27	0.067	0.007	0.49
1950	0.11	0.71	0.114	0.019	0.83

Sample	86Sr/Zr	89Y/Zr	95Mo/Zr	107Ag/Zr	112Cd/Zr
1925.6	3.7	0.14	0.005	0.001	0.003
1926	5.1	0.16	0.002	0.001	0.003
1926.3	5.0	0.15	0.002	0.001	0.003
1926.6	4.9	0.15	0.005	0.002	0.003
1927	5.2	0.20	0.004	0.001	0.003
1927.3	4.6	0.15	0.003	0.001	0.003
1927.6	2.6	0.14	0.005	0.002	0.003
1928	2.1	0.13	0.005	0.002	0.003
1928.3	2.1	0.15	0.006	0.002	0.004
1928.6	2.1	0.15	0.005	0.002	0.004
1929	2.0	0.15	0.006	0.002	0.003
1929.3	2.0	0.15	0.005	0.002	0.003
1929.6	2.3	0.15	0.007	0.002	0.003
1930	2.2	0.13	0.007	0.001	0.003
1930.3	2.7	0.15	0.002	0.002	0.003
1930.6	2.8	0.19	0.004	0.002	0.003
1931	2.7	0.16	0.004	0.002	0.003
1931.3	3.0	0.17	0.005	0.002	0.003
1931.6	3.3	0.16	0.002	0.002	0.003
1932	3.4	0.16	0.001	0.001	0.003
1932.3	2.5	0.17	0.001	0.002	0.003
1932.6	3.3	0.16	0.001	0.002	0.003
1933.7	3.3	0.15	0.007	0.002	0.003
1934	3.0	0.16	0.007	0.002	0.003
1934.3	3.6	0.17	0.003	0.002	0.003
1934.6	3.7	0.17	0.004	0.001	0.003
1935	3.6	0.17	0.004	0.002	0.004
1935.3	4.4	0.18	0.007	0.002	0.004
1935.6	3.7	0.16	0.004	0.002	0.004
1936	4.3	0.13	0.004	0.001	0.003
1936.3	4.6	0.14	0.003	0.001	0.004
1936.6	7.8	0.16	0.006	0.002	0.003
1937	5.0	0.13	0.006	0.002	0.003
1937.3	5.2	0.14	0.004	0.002	0.004
1937.6	4.4	0.14	0.003	0.002	0.003
1938	4.6	0.15	0.002	0.002	0.003
1938.3	4.5	0.16	0.002	0.002	0.003
1938.6	4.9	0.14	0.001	0.001	0.003
1939	4.3	0.10	0.008	0.002	0.003
1939.3	6.9	0.13	0.002	0.001	0.003
1939.6	4.4	0.13	0.001	0.001	0.003
1940	2.2	0.13	0.002	0.001	0.003
1940.3	1.6	0.13	0.006	0.001	0.003
1940.6	2.1	0.16	0.004	0.001	0.004
1940.8	2.4	0.17	0.003	0.001	0.003

Sample	86Sr/Zr	89Y/Zr	95Mo/Zr	107Ag/Zr	112Cd/Zr
1941	2.6	0.14	0.002	0.001	0.003
1941.5	2.8	0.15	0.010	0.001	0.003
1941.9	2.7	0.17	0.006	0.001	0.003
1942.5	3.6	0.17	0.003	0.001	0.003
1943	4.1	0.19	0.003	0.001	0.003
1943.5	3.7	0.17	0.002	0.001	0.003
1944	2.1	0.17	0.003	0.001	0.003
1944.5	3.3	0.17	0.002	0.001	0.003
1945	3.2	0.21	0.005	0.001	0.003
1945.5	1.4	0.17	0.001	0.001	0.003
1946	2.8	0.16	0.001	0.001	0.003
1946.5	2.0	0.15	0.001	0.001	0.003
1947	1.8	0.13	0.001	0.001	0.003
1947.5	1.6	0.13	0.001	0.001	0.002
1948	1.6	0.13	0.002	0.001	0.003
1948.5	1.8	0.13	0.003	0.001	0.003
1949	1.6	0.15	0.003	0.001	0.003
1949.5	0.3	0.08	0.001	0.001	0.002
1950	2.9	0.16	0.001	0.001	0.003

Sample	118Sn/Zr	121Sb/Zr	133Cs/Zr	137Ba/Zr	182W/Zr
1925.6	0.025	0.002	0.042	2.3	0.012
1926	0.028	0.003	0.047	2.5	0.014
1926.3	0.028	0.002	0.045	2.4	0.014
1926.6	0.029	0.003	0.045	2.5	0.014
1927	0.026	0.004	0.038	2.2	0.011
1927.3	0.024	0.003	0.037	2.2	0.011
1927.6	0.028	0.003	0.048	2.8	0.014
1928	0.027	0.003	0.045	2.7	0.014
1928.3	0.030	0.003	0.051	3.0	0.015
1928.6	0.036	0.003	0.047	2.8	0.015
1929	0.027	0.003	0.044	2.6	0.014
1929.3	0.026	0.002	0.042	2.6	0.013
1929.6	0.027	0.003	0.043	2.6	0.013
1930	0.025	0.003	0.039	2.2	0.012
1930.3	0.027	0.002	0.043	2.4	0.013
1930.6	0.029	0.003	0.047	2.6	0.014
1931	0.030	0.003	0.047	2.6	0.014
1931.3	0.031	0.004	0.052	2.8	0.016
1931.6	0.030	0.003	0.050	2.8	0.015
1932	0.028	0.002	0.047	2.6	0.015
1932.3	0.026	0.002	0.045	2.7	0.014
1932.6	0.027	0.002	0.046	2.5	0.014
1933.7	0.029	0.003	0.044	2.6	0.014
1934	0.027	0.003	0.043	2.6	0.014
1934.3	0.030	0.003	0.047	2.8	0.015
1934.6	0.031	0.004	0.049	2.9	0.015
1935	0.032	0.003	0.050	2.8	0.015
1935.3	0.031	0.004	0.050	2.9	0.015
1935.6	0.031	0.003	0.048	2.7	0.014
1936	0.029	0.002	0.045	2.3	0.014
1936.3	0.027	0.002	0.042	2.2	0.013
1936.6	0.028	0.003	0.045	2.6	0.014
1937	0.024	0.003	0.041	2.2	0.013
1937.3	0.025	0.003	0.044	2.2	0.013
1937.6	0.026	0.003	0.043	2.2	0.013
1938	0.020	0.002	0.029	1.8	0.010
1938.3	0.020	0.002	0.032	1.8	0.010
1938.6	0.020	0.002	0.032	1.8	0.010
1939	0.015	0.002	0.027	1.5	0.008
1939.3	0.018	0.002	0.030	1.8	0.010
1939.6	0.025	0.002	0.039	2.2	0.011
1940	0.022	0.002	0.034	2.1	0.010
1940.3	0.022	0.002	0.035	2.3	0.012
1940.6	0.030	0.002	0.049	2.7	0.014
1940.8	0.028	0.002	0.045	2.6	0.015

Sample	118Sn/Zr	121Sb/Zr	133Cs/Zr	137Ba/Zr	182W/Zr
1941	0.023	0.001	0.036	2.2	0.012
1941.5	0.025	0.002	0.041	2.4	0.013
1941.9	0.030	0.002	0.048	2.9	0.015
1942.5	0.025	0.002	0.042	2.5	0.013
1943	0.028	0.002	0.046	2.6	0.014
1943.5	0.027	0.002	0.044	2.5	0.014
1944	0.031	0.002	0.048	2.6	0.016
1944.5	0.031	0.002	0.048	2.8	0.016
1945	0.033	0.003	0.049	2.5	0.017
1945.5	0.029	0.002	0.042	1.9	0.016
1946	0.028	0.002	0.044	2.4	0.014
1946.5	0.025	0.002	0.039	2.2	0.013
1947	0.027	0.002	0.040	2.1	0.014
1947.5	0.022	0.002	0.033	1.8	0.011
1948	0.024	0.002	0.036	2.0	0.012
1948.5	0.025	0.002	0.038	2.1	0.013
1949	0.030	0.003	0.044	2.2	0.016
1949.5	0.023	0.002	0.030	1.9	0.015
1950	0.029	0.002	0.045	2.4	0.015

Sample	197Au/Zr	205Tl/Zr	208Pb/Zr	209Bi/Zr	232Th/Zr
1925.6	0.0006	0.004	0.11	0.001	0.078
1926	0.0007	0.004	0.13	0.002	0.085
1926.3	0.0006	0.004	0.10	0.002	0.081
1926.6	0.0007	0.004	0.12	0.002	0.096
1927	0.0006	0.004	0.12	0.002	0.099
1927.3	0.0006	0.004	0.09	0.001	0.074
1927.6	0.0006	0.005	0.14	0.002	0.087
1928	0.0007	0.005	0.10	0.001	0.076
1928.3	0.0008	0.005	0.13	0.002	0.093
1928.6	0.0007	0.005	0.14	0.002	0.089
1929	0.0006	0.005	0.13	0.002	0.087
1929.3	0.0007	0.004	0.12	0.002	0.085
1929.6	0.0008	0.005	0.13	0.002	0.092
1930	0.0006	0.004	0.09	0.001	0.070
1930.3	0.0007	0.004	0.08	0.001	0.084
1930.6	0.0007	0.004	0.09	0.001	0.090
1931	0.0008	0.005	0.12	0.002	0.090
1931.3	0.0007	0.005	0.15	0.002	0.098
1931.6	0.0007	0.005	0.13	0.002	0.093
1932	0.0007	0.004	0.12	0.002	0.087
1932.3	0.0008	0.004	0.11	0.002	0.089
1932.6	0.0007	0.004	0.11	0.002	0.088
1933.7	0.0007	0.004	0.14	0.002	0.088
1934	0.0007	0.004	0.13	0.002	0.087
1934.3	0.0007	0.004	0.14	0.002	0.095
1934.6	0.0007	0.005	0.16	0.002	0.097
1935	0.0008	0.005	0.13	0.002	0.098
1935.3	0.0007	0.005	0.16	0.002	0.100
1935.6	0.0007	0.005	0.12	0.002	0.094
1936	0.0008	0.004	0.11	0.002	0.089
1936.3	0.0007	0.004	0.10	0.002	0.078
1936.6	0.0008	0.004	0.13	0.002	0.090
1937	0.0006	0.003	0.12	0.001	0.074
1937.3	0.0006	0.004	0.14	0.001	0.074
1937.6	0.0007	0.004	0.14	0.002	0.090
1938	0.0005	0.003	0.09	0.001	0.116
1938.3	0.0004	0.003	0.09	0.001	0.070
1938.6	0.0005	0.003	0.09	0.001	0.064
1939	0.0005	0.003	0.08	0.001	0.056
1939.3	0.0006	0.003	0.08	0.001	0.068
1939.6	0.0006	0.004	0.09	0.001	0.072
1940	0.0006	0.004	0.11	0.001	0.074
1940.3	0.0006	0.004	0.11	0.001	0.067
1940.6	0.0007	0.005	0.14	0.001	0.076
1940.8	0.0008	0.005	0.16	0.003	0.080

Sample	197Au/Zr	205Tl/Zr	208Pb/Zr	209Bi/Zr	232Th/Zr
1941	0.0008	0.004	0.11	0.002	0.056
1941.5	0.0007	0.004	0.12	0.001	0.073
1941.9	0.0008	0.005	0.14	0.002	0.090
1942.5	0.0007	0.005	0.14	0.002	0.063
1943	0.0008	0.005	0.16	0.003	0.077
1943.5	0.0008	0.005	0.14	0.003	0.068
1944	0.0007	0.006	0.18	0.003	0.079
1944.5	0.0008	0.006	0.17	0.003	0.081
1945	0.0008	0.007	0.25	0.004	0.089
1945.5	0.0007	0.005	0.19	0.003	0.070
1946	0.0008	0.005	0.15	0.003	0.070
1946.5	0.0007	0.004	0.14	0.002	0.067
1947	0.0008	0.005	0.13	0.002	0.065
1947.5	0.0006	0.004	0.10	0.002	0.058
1948	0.0007	0.004	0.14	0.002	0.064
1948.5	0.0007	0.005	0.16	0.002	0.064
1949	0.0008	0.005	0.21	0.003	0.073
1949.5	0.0008	0.003	0.06	0.000	0.024
1950	0.0008	0.005	0.16	0.003	0.080

Sample	238U/Zr	Al/Zr	Ba/Zr	Ca/Zr	Fe/Zr
1925.6	0.017	462.9	2.3	445.5	211.3
1926	0.018	537.0	2.6	616.2	261.0
1926.3	0.019	478.7	2.4	561.9	200.2
1926.6	0.022	516.6	2.4	567.8	198.9
1927	0.022	478.9	2.2	952.1	189.7
1927.3	0.020	457.9	2.1	679.6	172.3
1927.6	0.023	571.8	3.0	237.6	249.8
1928	0.018	465.6	2.6	176.6	198.2
1928.3	0.021	565.6	3.0	165.9	233.1
1928.6	0.020	609.7	2.8	156.8	263.1
1929	0.020	502.2	2.5	167.7	216.0
1929.3	0.019	521.7	2.7	154.7	208.1
1929.6	0.021	528.7	2.5	184.6	228.3
1930	0.018	409.1	2.1	233.1	167.0
1930.3	0.019	490.8	2.3	301.7	166.3
1930.6	0.021	535.5	2.5	320.3	187.8
1931	0.020	561.5	2.6	236.5	218.5
1931.3	0.019	598.5	2.7	261.5	274.4
1931.6	0.018	595.6	2.7	277.8	232.9
1932	0.016	541.5	2.6	291.9	237.6
1932.3	0.016	529.6	2.7	241.2	278.0
1932.6	0.015	499.6	2.4	329.7	214.2
1933.7	0.018	524.7	2.6	293.9	226.4
1934	0.019	534.1	2.4	280.2	223.7
1934.3	0.020	609.5	2.7	302.1	244.5
1934.6	0.020	619.2	2.8	338.6	278.0
1935	0.021	631.0	2.8	384.3	231.3
1935.3	0.022	625.8	2.9	480.5	324.5
1935.6	0.022	604.6	2.6	444.4	240.0
1936	0.020	525.2	2.2	426.0	222.2
1936.3	0.019	494.7	2.2	482.2	191.2
1936.6	0.022	554.8	2.5	788.6	237.3
1937	0.015	464.4	2.2	611.8	282.7
1937.3	0.015	486.0	2.2	567.5	314.5
1937.6	0.017	546.0	2.2	462.1	326.6
1938	0.020	372.8	1.7	826.9	344.6
1938.3	0.016	389.5	1.7	708.9	263.7
1938.6	0.012	381.1	1.7	489.9	206.5
1939	0.011	333.1	1.6	516.3	169.2
1939.3	0.013	377.8	1.8	687.7	193.7
1939.6	0.014	418.3	2.2	362.7	164.8
1940	0.014	361.2	2.0	206.8	196.3
1940.3	0.014	375.4	2.2	134.0	359.9
1940.6	0.015	492.1	2.7	161.4	350.8
1940.8	0.021	737.6	2.8	179.4	387.1

Sample	238U/Zr	Al/Zr	Ba/Zr	Ca/Zr	Fe/Zr
1941	0.017	462.1	2.4	275.2	241.2
1941.5	0.016	478.2	2.4	232.5	215.9
1941.9	0.017	561.2	2.8	193.5	251.6
1942.5	0.019	461.6	2.6	351.6	244.9
1943	0.021	517.0	2.8	394.8	268.4
1943.5	0.021	490.6	2.7	348.3	245.4
1944	0.023	607.5	2.8	164.7	310.9
1944.5	0.023	588.9	3.0	311.5	311.8
1945	0.025	707.7	2.8	255.6	378.5
1945.5	0.023	627.9	2.4	80.5	326.8
1946	0.021	444.7	2.6	326.9	235.8
1946.5	0.019	385.4	2.4	254.3	202.8
1947	0.019	343.0	2.3	213.3	185.8
1947.5	0.017	292.2	2.0	204.8	151.7
1948	0.018	413.5	2.2	182.7	215.7
1948.5	0.020	423.8	2.4	212.6	225.7
1949	0.023	561.7	2.7	147.9	296.3
1949.5	0.016	180.3	2.1	0.0	101.0
1950	0.021	412.3	2.5	365.2	223.5

Sample	Mg/Zr	Mn/Zr	Na/Zr	Ti/Zr
1925.6	56.4	1.4	26.6	27.8
1926	65.4	1.7	28.3	31.3
1926.3	59.4	1.5	28.0	27.9
1926.6	57.6	1.5	26.8	28.0
1927	63.3	2.2	27.0	24.7
1927.3	48.8	1.9	24.0	25.8
1927.6	60.1	1.6	27.5	32.1
1928	52.0	1.5	29.6	30.1
1928.3	61.0	1.7	30.1	32.1
1928.6	57.7	1.6	26.3	31.0
1929	50.6	1.3	24.3	28.6
1929.3	52.8	1.2	24.8	28.1
1929.6	52.7	1.3	24.4	28.0
1930	42.9	1.2	21.5	25.3
1930.3	48.3	1.1	22.2	26.5
1930.6	54.1	1.4	24.5	28.5
1931	54.6	1.4	25.0	28.6
1931.3	59.5	1.2	23.7	29.3
1931.6	58.7	1.3	25.1	30.2
1932	57.0	1.3	25.7	28.4
1932.3	58.0	1.5	26.5	29.5
1932.6	57.3	1.5	24.4	27.9
1933.7	52.6	1.3	24.8	28.8
1934	53.3	1.3	23.9	28.4
1934.3	58.3	1.4	24.3	30.2
1934.6	62.5	1.6	28.0	31.7
1935	62.0	1.4	26.7	30.7
1935.3	65.6	1.5	28.0	31.3
1935.6	61.1	1.4	25.9	29.7
1936	52.0	1.3	23.6	30.0
1936.3	48.4	1.5	21.8	27.9
1936.6	57.2	2.0	23.8	29.9
1937	54.4	1.8	24.6	26.2
1937.3	56.6	1.5	25.4	27.7
1937.6	55.1	1.5	23.3	28.6
1938	53.4	2.2	24.0	25.8
1938.3	49.2	2.0	20.5	23.9
1938.6	41.4	1.2	19.6	22.1
1939	35.2	1.2	17.6	21.3
1939.3	41.1	1.4	21.6	23.4
1939.6	39.0	1.5	23.7	25.5
1940	37.1	1.6	21.9	24.2
1940.3	55.9	2.0	21.1	26.7
1940.6	66.1	2.4	24.6	29.6
1940.8	72.9	2.5	24.7	35.6

Sample	Mg/Zr	Mn/Zr	Na/Zr	Ti/Zr
1941	49.3	1.9	20.4	30.2
1941.5	47.2	1.6	24.1	28.0
1941.9	57.8	1.8	26.3	30.9
1942.5	57.9	1.8	23.8	31.5
1943	63.4	1.9	27.5	32.0
1943.5	58.8	1.9	22.5	32.6
1944	59.0	1.8	22.9	36.0
1944.5	64.7	1.9	27.4	36.8
1945	59.6	1.8	22.9	36.5
1945.5	54.3	2.1	36.0	37.1
1946	50.9	1.5	21.9	33.8
1946.5	45.6	1.4	23.0	31.1
1947	39.5	1.3	19.0	32.0
1947.5	37.4	1.1	18.9	26.9
1948	42.2	1.2	18.4	29.3
1948.5	48.5	1.4	20.6	30.0
1949	53.5	1.4	20.7	33.7
1949.5	24.5	0.6	15.0	29.3
1950	53.4	1.5	25.1	33.0

The following are the Zr-normalized data for the Bass River Borehole.

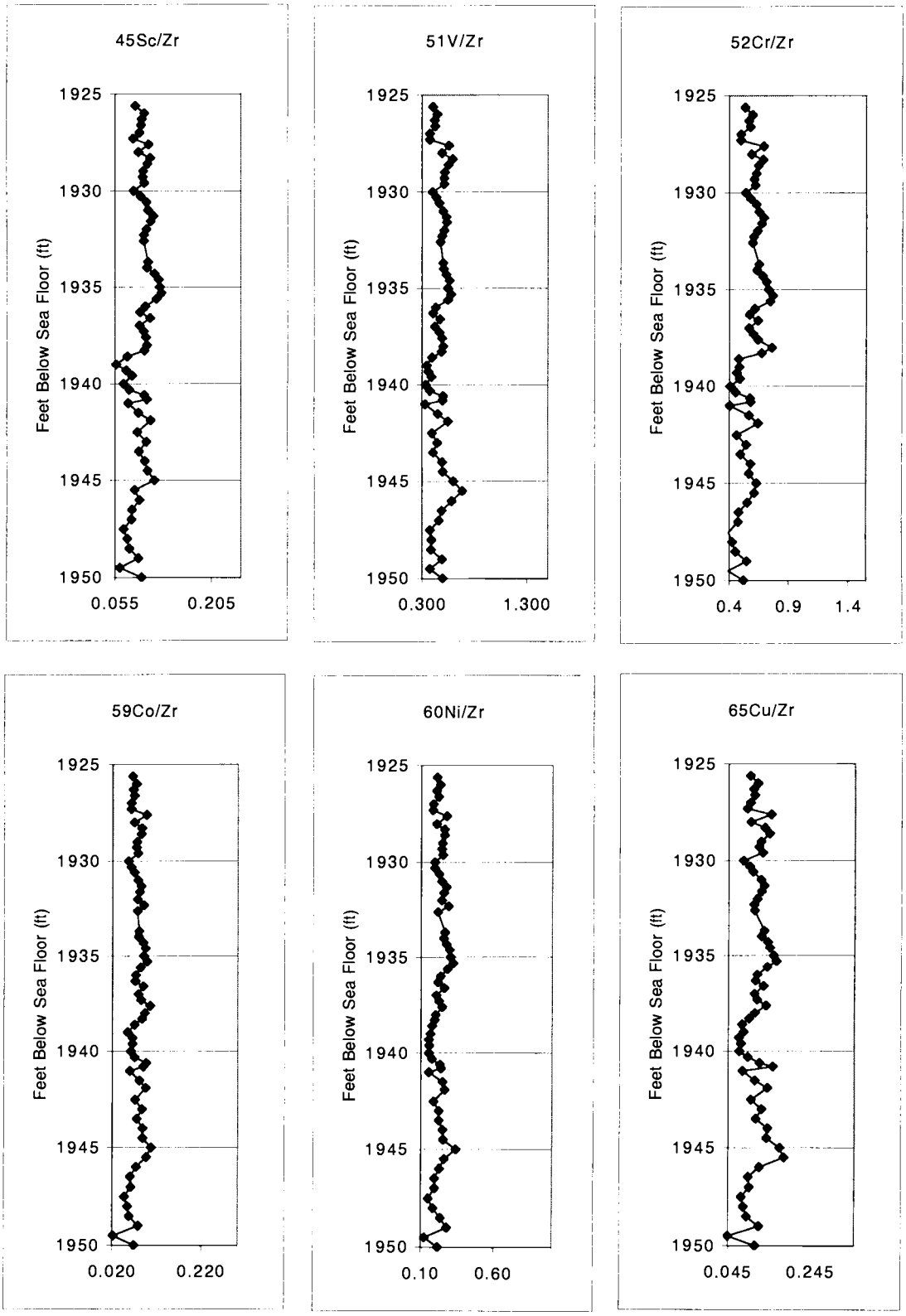

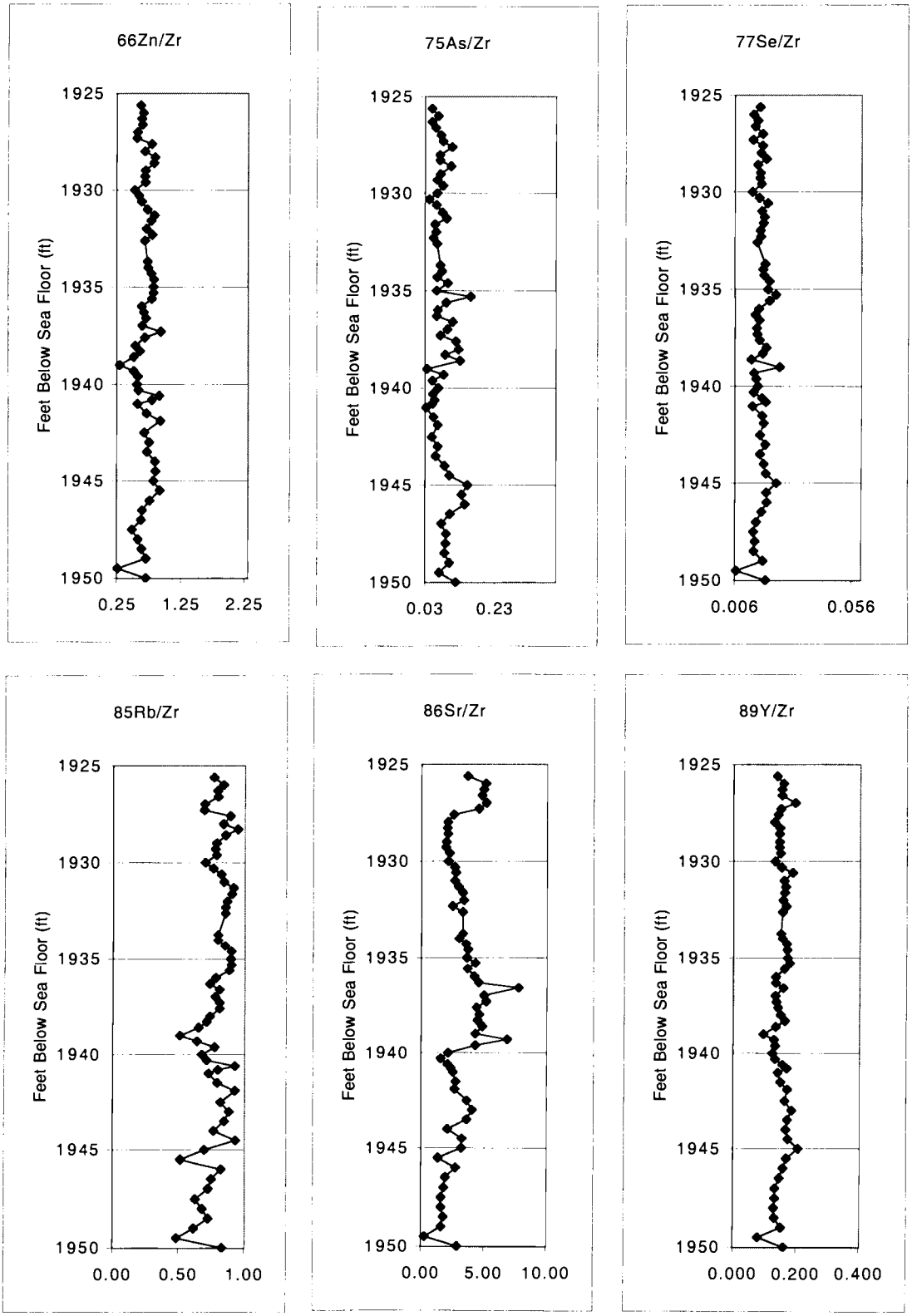
66Zn/Zr
75As/Zr
77Se/Zr
85Rb/Zr
86Sr/Zr
89Y/Zr
Feet Below Sea Floor (ft)
1925
1930
1935
1940
1945
1950
0.25
1.25
2.25
0.03
0.23
0.006
0.056
0.00
0.50
1.00
0.00
5.00
10.00
0.000
0.200
0.400

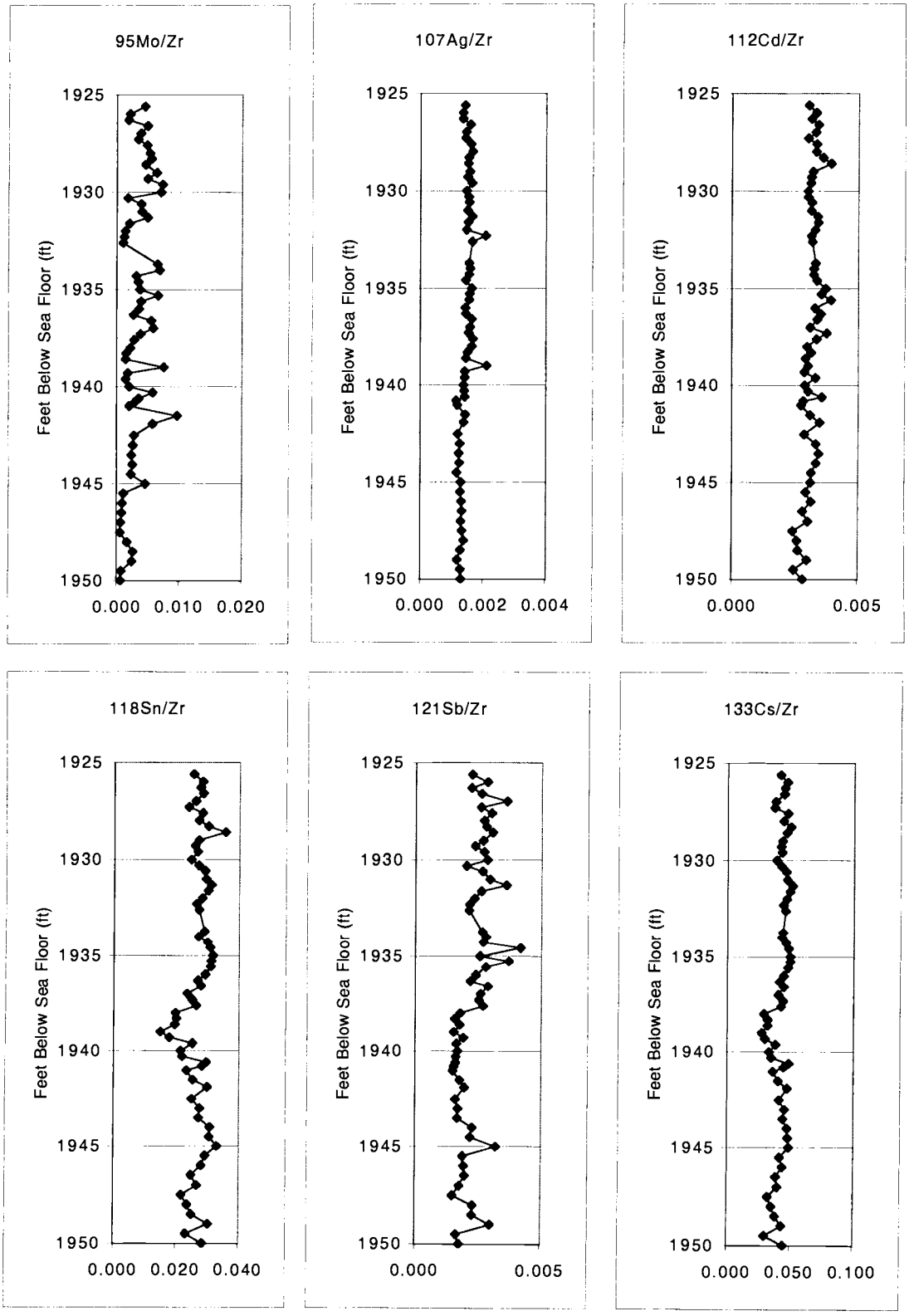
95Mo/Zr
107Ag/Zr
112Cd/Zr
118Sn/Zr
121Sb/Zr
133Cs/Zr
Feet Below Sea Floor (ft)
1925
1930
1935
1940
1945
1950
0.000
0.010
0.020
0.002
0.004
0.005
0.020
0.040
0.050
0.100

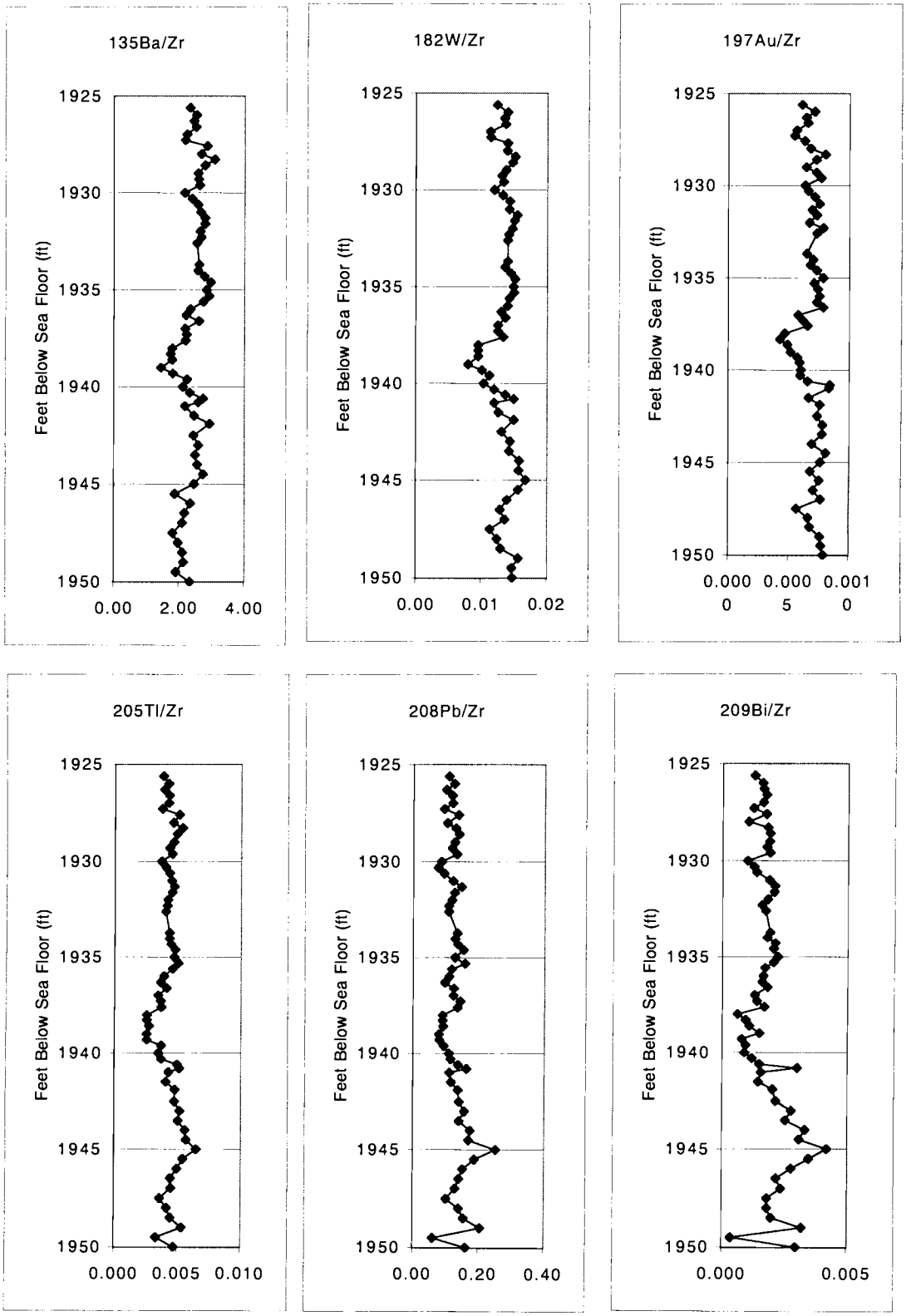
135Ba/Zr
182W/Zr
197Au/Zr
205Tl/Zr
208Pb/Zr
209Bi/Zr
Feet Below Sea Floor (ft)
1925
1930
1935
1940
1945
1950
0.00 2.00 4.00
0.00 0.01 0.02
0.000 0.000 0.001
0 5 0
0.000 0.005 0.010
0.00 0.20 0.40
0.000 0.005

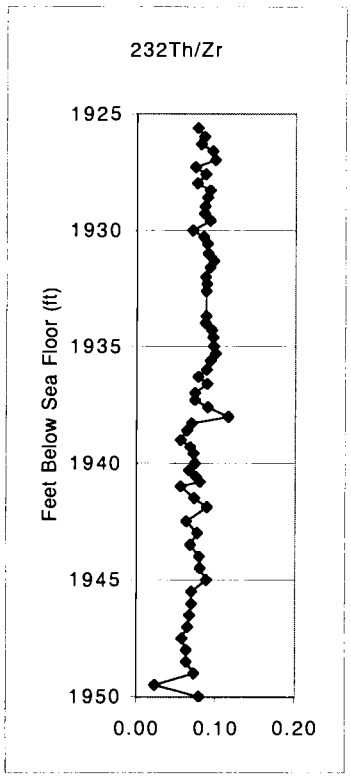
232Th/Zr
Feet Below Sea Floor (ft)
1925
1930
1935
1940
1945
1950
0.00
0.10
0.20

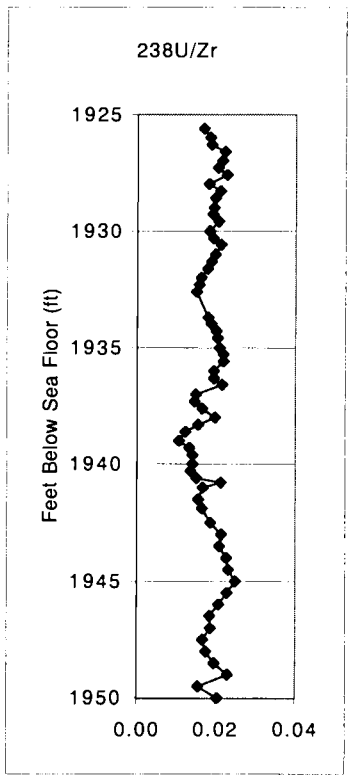
238U/Zr
Feet Below Sea Floor (ft)
1925
1930
1935
1940
1945
1950
0.00
0.02
0.04

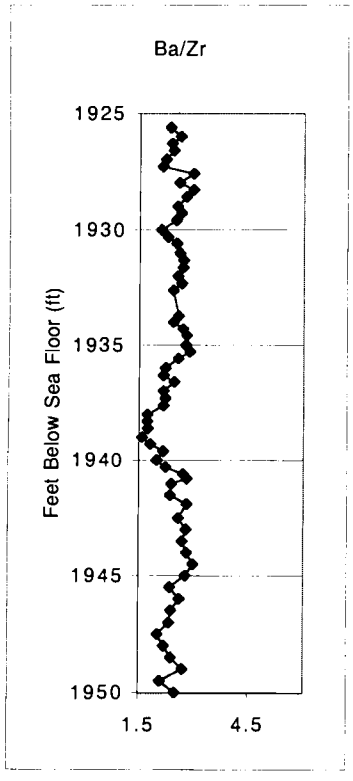
Ba/Zr
Feet Below Sea Floor (ft)
1925
1930
1935
1940
1945
1950
1.5
4.5

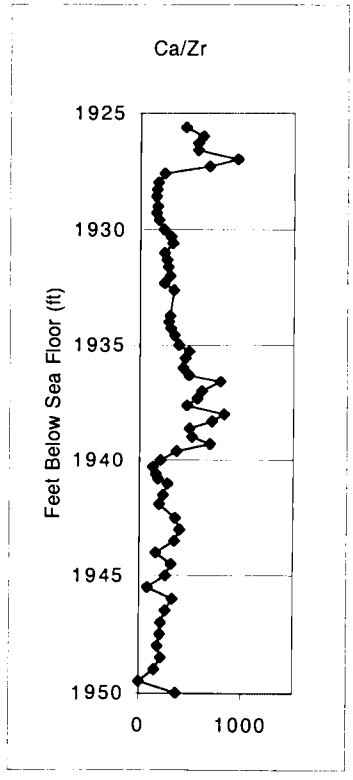
Ca/Zr
Feet Below Sea Floor (ft)
1925
1930
1935
1940
1945
1950
0
1000

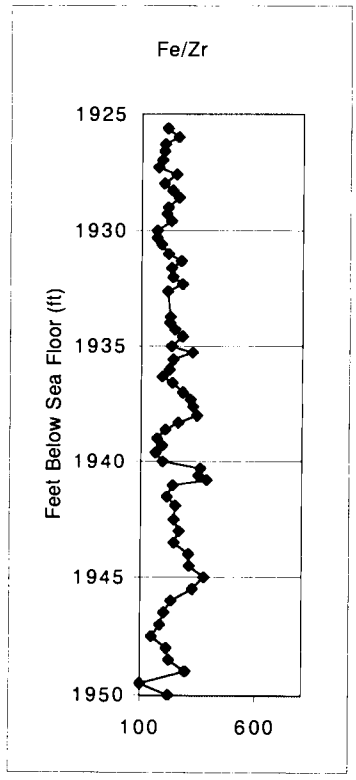
Fe/Zr
Feet Below Sea Floor (ft)
1925
1930
1935
1940
1945
1950
100
600

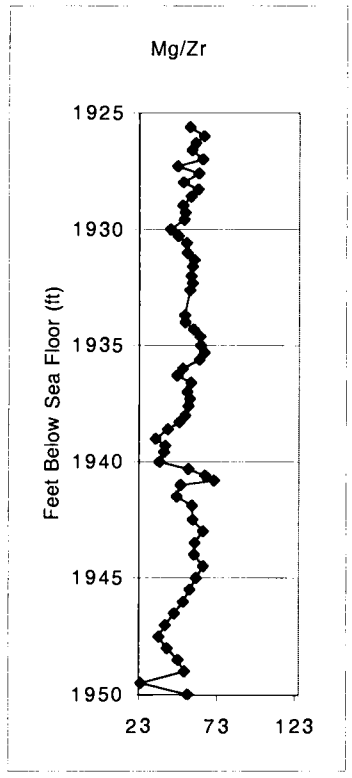
Mg/Zr
Feet Below Sea Floor (ft)
1925
1930
1935
1940
1945
1950
23
73
123

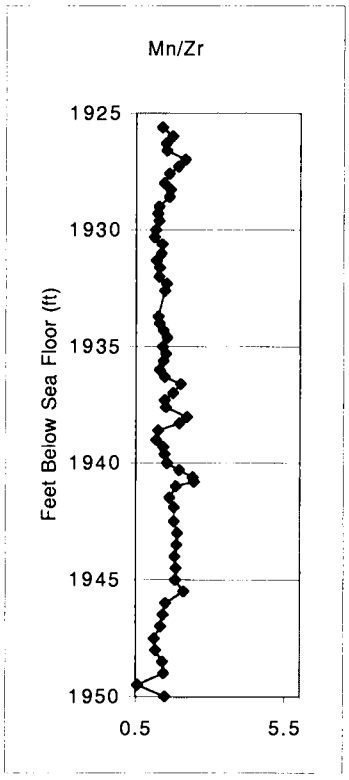
Mn/Zr
Feet Below Sea Floor (ft)
1925
1930
1935
1940
1945
1950
0.5
5.5

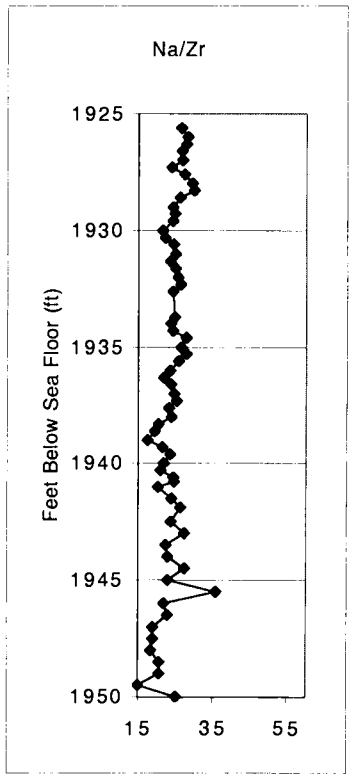
Na/Zr
Feet Below Sea Floor (ft)
1925
1930
1935
1940
1945
1950
15
35
55

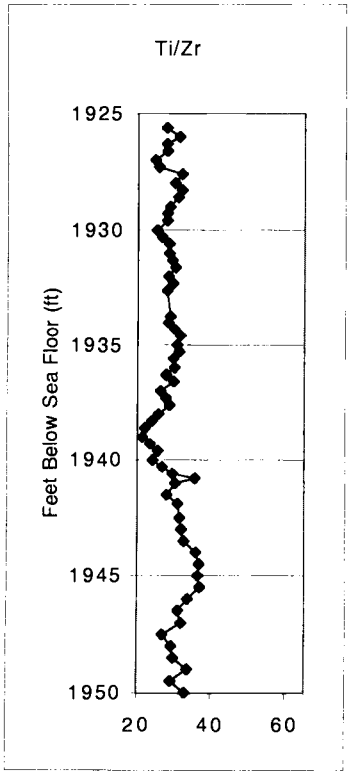
Ti/Zr
Feet Below Sea Floor (ft)
1925
1930
1935
1940
1945
1950
20
40
60

The following are Zr-normalized data for ODP Site 1138.
Core positions are meters below sea level.

Core Position	45Sc/Zr	51V/Zr	53Cr/Zr	59Co/Zr	60Ni/Zr
652.13	0.20	0.78	1.71	0.13	1.21
652.38	0.19	0.85	2.16	0.12	1.39
653.2	0.17	1.07	0.84	0.15	0.84
653.42	0.20	0.95	0.89	0.14	0.65
653.72	0.16	0.89	0.85	0.10	0.41
653.91	0.15	0.87	0.83	0.10	0.40
654.08	0.16	0.87	0.93	0.12	0.55
654.3	0.08	0.54	0.41	0.08	0.22
654.5	0.17	0.99	1.15	0.22	0.88
654.7	0.16	0.94	1.06	0.10	0.37
654.9	0.21	1.23	1.34	0.24	0.76
655.1	0.20	1.01	1.09	0.17	0.66
655.3	0.21	4.97	1.75	0.28	1.66
655.5	0.20	13.72	3.19	0.29	2.13
655.72	0.22	1.59	1.75	0.21	1.17
655.9	0.23	1.20	1.24	0.21	1.02
656.1	0.22	1.48	1.24	0.21	1.07
656.3	0.20	1.77	2.41	0.35	1.68
656.42	0.16	0.75	0.80	0.13	0.55
656.52	0.21	1.34	1.84	0.23	1.36
656.58	0.22	1.11	1.26	0.19	1.07
656.6	0.22	1.08	1.23	0.19	1.17
656.7	0.22	1.08	1.24	0.21	0.96
656.78	0.22	1.25	1.32	0.27	0.84
656.88	0.15	1.35	1.20	0.09	0.61
656.98	0.21	6.28	3.07	0.20	1.88
657.08	0.13	2.26	1.23	0.11	0.66
657.1	0.07	1.80	0.93	0.93	31.86
657.18	0.14	1.74	1.67	0.10	0.96
657.2	0.21	3.35	3.37	0.18	1.92
657.28	0.15	1.52	1.52	0.09	0.84
657.38	0.15	7.91	2.83	0.16	1.64
657.48	0.13	0.51	0.74	0.17	0.47
657.58	0.13	0.45	0.65	0.24	0.51
657.68	0.17	0.63	1.26	0.21	0.38
657.78	0.29	1.95	2.77	0.52	0.80
657.88	0.13	0.63	1.41	0.27	0.44
657.98	0.47	2.01	4.49	1.16	1.79
658.06	0.49	2.12	4.74	1.77	2.33
658.09	0.38	1.67	3.48	0.72	1.11
658.18	0.44	1.87	4.09	0.63	0.86
658.28	0.41	2.39	2.72	0.60	0.77
658.38	0.46	2.43	2.60	0.90	0.98
658.48	0.15	1.02	0.77	0.46	0.47
658.59	0.30	2.14	1.60	0.63	0.73
658.68	0.28	2.13	1.71	1.98	1.35
658.78	0.28	1.46	1.80	0.54	0.60

Core Position	45Sc/Zr	51V/Zr	53Cr/Zr	59Co/Zr	60Ni/Zr
658.88	0.36	1.99	2.56	0.45	0.50
659	0.31	3.03	2.86	0.33	0.48
659.08	0.29	2.61	2.48	0.73	0.72
659.17	0.31	3.10	2.48	2.21	0.95
659.35	0.39	2.72	1.93	0.44	1.12
659.43	0.42	3.21	2.31	0.54	1.22
659.51	0.45	3.28	2.48	0.59	1.32
659.62	0.44	3.04	2.47	0.56	1.19

Core Position	65Cu/Zr	66Zn/Zr	75As/Zr	77Se/Zr	85Rb/Zr
652.13	0.57	0.93	0.08	0.01	0.36
652.38	0.71	1.42	0.05	0.02	0.34
653.2	0.72	1.48	0.48	0.05	0.29
653.42	0.57	0.94	0.06	0.02	0.34
653.72	0.61	0.98	0.04	0.03	0.28
653.91	0.46	0.71	0.04	0.02	0.29
654.08	0.59	0.76	0.07	0.02	0.30
654.3	0.27	0.54	0.01	0.04	0.20
654.5	0.71	1.45	0.18	0.06	0.30
654.7	0.46	0.93	0.07	0.05	0.32
654.9	0.69	1.33	0.11	0.06	0.36
655.1	0.56	1.07	0.17	0.07	0.33
655.3	1.12	1.88	0.62	0.07	0.36
655.5	1.49	4.22	0.59	0.24	0.32
655.72	1.20	1.96	0.25	0.13	0.36
655.9	0.74	1.55	0.40	0.13	0.33
656.1	0.75	2.15	0.32	0.07	0.32
656.3	1.46	2.53	0.49	0.19	0.36
656.42	0.44	0.85	0.23	0.04	0.23
656.52	1.38	2.44	0.30	0.16	0.37
656.58	0.88	1.61	2.07	0.08	0.32
656.6	0.79	2.09	0.69	0.06	0.33
656.7	0.85	0.99	0.85	0.06	0.34
656.78	0.79	0.97	0.24	0.07	0.32
656.88	0.81	1.80	0.10	0.09	0.22
656.98	1.69	3.66	0.36	0.35	0.36
657.08	0.76	0.74	0.28	0.10	0.21
657.1	0.70	0.84	542.36	1.48	0.28
657.18	1.04	2.28	0.16	0.15	0.25
657.2	1.73	9.62	0.37	0.31	0.38
657.28	0.97	2.04	0.14	0.16	0.25
657.38	1.35	3.94	0.30	0.33	0.37
657.48	0.49	0.96	0.45	0.03	0.19
657.58	0.37	0.71	0.16	0.01	0.19
657.68	0.34	0.69	0.14	0.03	0.94
657.78	0.72	1.40	0.13	0.09	1.81
657.88	0.19	0.58	0.09	0.05	1.00
657.98	0.30	1.65	0.45	0.13	4.69
658.06	0.29	1.87	0.53	0.08	5.00
658.09	0.41	1.34	0.47	0.06	3.11
658.18	0.26	1.26	0.42	0.06	3.94
658.28	0.29	1.39	0.35	0.03	3.07
658.38	0.23	1.31	0.42	0.02	3.62
658.48	0.20	0.48	0.35	0.01	0.78
658.59	0.40	4.29	0.63	0.02	1.76
658.68	0.39	1.81	0.85	0.02	1.53
658.78	0.40	2.28	0.75	0.02	1.62

Core Position	65Cu/Zr	66Zn/Zr	75As/Zr	77Se/Zr	85Rb/Zr
658.88	0.30	2.42	0.39	0.04	3.02
659	0.89	0.73	0.24	0.03	2.28
659.08	0.42	0.76	0.30	0.03	2.05
659.17	0.22	0.75	0.30	0.02	2.35
659.35	0.43	1.12	0.58	0.04	0.37
659.43	0.50	1.25	0.69	0.05	0.41
659.51	0.46	1.26	0.69	0.06	0.44
659.62	0.46	1.17	0.65	0.05	0.42

Core Position	86Sr/Zr	89Y/Zr	95Mo/Zr	107Ag/Zr	112Cd/Zr
652.13	69.3	1.20	0.153	0.008	0.018
652.38	49.5	0.84	0.271	0.007	0.007
653.2	25.3	0.61	0.027	0.013	0.008
653.42	36.3	0.82	0.011	0.005	0.006
653.72	15.4	0.39	0.008	0.007	0.006
653.91	16.3	0.38	0.008	0.004	0.005
654.08	15.9	0.40	0.009	0.005	0.005
654.3	5.1	0.17	0.001	0.003	0.008
654.5	16.6	0.44	0.022	0.005	0.005
654.7	18.7	0.62	0.010	0.004	0.005
654.9	21.6	0.82	0.016	0.005	0.005
655.1	21.7	1.81	0.012	0.005	0.005
655.3	39.6	0.83	0.179	0.007	0.020
655.5	32.2	1.19	0.367	0.012	0.046
655.72	22.0	0.52	0.040	0.007	0.008
655.9	16.8	0.37	0.053	0.005	0.005
656.1	18.6	0.38	0.020	0.005	0.008
656.3	22.2	0.58	0.066	0.009	0.007
656.42	9.2	0.24	0.013	0.003	0.004
656.52	23.3	0.65	0.048	0.007	0.005
656.58	14.6	0.42	0.023	0.006	0.011
656.6	15.6	0.41	0.019	0.005	0.008
656.7	16.9	0.38	0.028	0.005	0.007
656.78	15.2	0.44	0.028	0.006	0.006
656.88	9.7	0.32	0.024	0.004	0.004
656.98	23.4	2.19	0.127	0.012	0.013
657.08	10.8	0.36	0.068	0.003	0.004
657.1	4.3	0.24	1.189	0.007	0.051
657.18	12.2	0.34	0.041	0.008	0.004
657.2	21.8	0.52	0.108	0.016	0.010
657.28	12.0	0.98	0.038	0.006	0.004
657.38	9.6	0.88	0.114	0.024	0.030
657.48	6.2	0.11	0.018	0.004	0.003
657.58	2.7	0.10	0.011	0.003	0.003
657.68	2.7	0.28	0.012	0.003	0.003
657.78	5.2	0.72	0.025	0.008	0.017
657.88	2.3	0.78	0.006	0.003	0.003
657.98	8.4	1.31	0.015	0.005	0.017
658.06	8.3	0.91	0.030	0.005	0.049
658.09	7.7	0.71	0.018	0.005	0.008
658.18	7.8	0.66	0.014	0.005	0.006
658.28	5.6	0.29	0.011	0.005	0.011
658.38	3.5	0.16	0.009	0.004	0.007
658.48	3.0	0.06	0.005	0.002	0.003
658.59	6.4	0.14	0.009	0.004	0.007
658.68	5.6	0.13	0.009	0.004	0.006
658.78	6.6	0.14	0.009	0.004	0.011

Core Position	86Sr/Zr	89Y/Zr	95Mo/Zr	107Ag/Zr	112Cd/Zr
658.88	3.9	0.25	0.008	0.004	0.020
659	3.5	0.16	0.009	0.003	0.005
659.08	3.3	0.15	0.008	0.004	0.006
659.17	2.3	0.22	0.007	0.003	0.004
659.35	14.0	0.68	0.036	0.004	0.016
659.43	15.4	0.78	0.037	0.005	0.042
659.51	17.1	0.85	0.037	0.005	0.022
659.62	15.3	0.74	0.032	0.003	0.021

Core Position	118Sn/Zr	121Sb/Zr	133Cs/Zr	137Ba/Zr	182W/Zr
652.13	0.209	0.005	0.010	78.6	0.014
652.38	0.023	0.007	0.017	46.8	0.011
653.2	0.015	0.010	0.017	63.0	0.011
653.42	0.017	0.005	0.019	51.0	0.012
653.72	0.016	0.005	0.017	78.8	0.008
653.91	0.015	0.003	0.017	47.9	0.008
654.08	0.015	0.005	0.018	71.1	0.011
654.3	0.013	0.003	0.009	32.5	0.005
654.5	0.016	0.004	0.018	61.5	0.007
654.7	0.017	0.003	0.020	41.9	0.008
654.9	0.014	0.005	0.024	72.2	0.011
655.1	0.016	0.005	0.022	53.0	0.011
655.3	0.017	0.010	0.017	129.0	0.007
655.5	0.015	0.016	0.014	214.7	0.005
655.72	0.014	0.009	0.020	137.7	0.007
655.9	0.013	0.006	0.022	90.0	0.010
656.1	0.014	0.008	0.021	71.0	0.009
656.3	0.013	0.014	0.019	183.1	0.006
656.42	0.008	0.004	0.016	37.6	0.008
656.52	0.014	0.012	0.022	202.1	0.007
656.58	0.013	0.011	0.022	93.2	0.011
656.6	0.014	0.006	0.023	83.2	0.011
656.7	0.013	0.007	0.024	100.5	0.009
656.78	0.013	0.006	0.023	77.8	0.009
656.88	0.009	0.006	0.014	82.2	0.004
656.98	0.015	0.022	0.021	253.2	0.005
657.08	0.008	0.006	0.013	81.6	0.004
657.1	0.009	2.494	0.008	27.7	0.006
657.18	0.010	0.008	0.015	145.5	0.004
657.2	0.015	0.021	0.021	279.4	0.005
657.28	0.010	0.008	0.016	154.0	0.004
657.38	0.012	0.031	0.017	229.6	0.004
657.48	0.010	0.005	0.015	45.8	0.005
657.58	0.009	0.002	0.016	33.5	0.006
657.68	0.008	0.003	0.035	26.4	0.005
657.78	0.014	0.006	0.068	19.7	0.008
657.88	0.006	0.002	0.038	14.6	0.003
657.98	0.014	0.008	0.141	40.7	0.005
658.06	0.015	0.008	0.149	8.8	0.006
658.09	0.014	0.005	0.097	33.3	0.007
658.18	0.013	0.003	0.122	0.5	0.005
658.28	0.011	0.004	0.087	0.9	0.006
658.38	0.010	0.004	0.090	0.2	0.005
658.48	0.006	0.002	0.021	0.1	0.004
658.59	0.011	0.005	0.049	0.6	0.008
658.68	0.011	0.004	0.042	1.2	0.008
658.78	0.028	0.004	0.049	0.3	0.009

Core Position	118Sn/Zr	121Sb/Zr	133Cs/Zr	137Ba/Zr	182W/Zr
658.88	0.011	0.004	0.072	0.3	0.008
659	0.011	0.004	0.060	0.2	0.008
659.08	0.011	0.003	0.052	1.4	0.009
659.17	0.011	0.003	0.051	0.1	0.007
659.35	0.015	0.009	0.006	0.3	0.012
659.43	0.017	0.010	0.007	0.3	0.014
659.51	0.015	0.009	0.005	0.3	0.013
659.62	0.015	0.009	0.007	0.2	0.013

Core Position	197Au/Zr	205Tl/Zr	208Pb/Zr	209Bi/Zr	232Th/Zr
652.13	0.0026	0.002	0.18	0.003	0.022
652.38	0.0010	0.002	0.16	0.003	0.035
653.2	0.0009	0.001	0.14	0.002	0.029
653.42	0.0008	0.002	0.15	0.003	0.032
653.72	0.0010	0.002	0.11	0.002	0.037
653.91	0.0009	0.002	0.10	0.002	0.039
654.08	0.0008	0.001	0.12	0.003	0.032
654.3	0.0007	0.002	0.06	0.002	0.026
654.5	0.0013	0.003	0.12	0.002	0.042
654.7	0.0007	0.002	0.11	0.002	0.043
654.9	0.0008	0.003	0.13	0.002	0.039
655.1	0.0007	0.002	0.13	0.001	0.036
655.3	0.0008	0.010	0.15	0.002	0.043
655.5	0.0007	0.026	0.14	0.002	0.039
655.72	0.0013	0.003	0.12	0.002	0.042
655.9	0.0008	0.003	0.13	0.001	0.035
656.1	0.0008	0.002	0.15	0.001	0.037
656.3	0.0013	0.005	0.12	0.001	0.041
656.42	0.0006	0.001	0.09	0.001	0.027
656.52	0.0009	0.004	0.13	0.002	0.044
656.58	0.0008	0.002	0.17	0.001	0.037
656.6	0.0007	0.002	0.14	0.001	0.038
656.7	0.0008	0.003	0.13	0.002	0.040
656.78	0.0010	0.003	0.12	0.001	0.037
656.88	0.0006	0.002	0.07	0.001	0.030
656.98	0.0011	0.008	0.14	0.002	0.052
657.08	0.0006	0.005	0.06	0.001	0.025
657.1	0.0013	0.142	0.24	0.001	0.043
657.18	0.0008	0.003	0.07	0.001	0.033
657.2	0.0010	0.006	0.12	0.002	0.048
657.28	0.0007	0.003	0.08	0.001	0.037
657.38	0.0008	0.011	0.08	0.002	0.037
657.48	0.0006	0.002	0.08	0.002	0.026
657.58	0.0006	0.001	0.07	0.001	0.024
657.68	0.0006	0.001	0.06	0.001	0.023
657.78	0.0011	0.004	0.10	0.002	0.041
657.88	0.0004	0.003	0.03	0.001	0.019
657.98	0.0008	0.007	0.08	0.001	0.021
658.06	0.0007	0.008	0.08	0.001	0.019
658.09	0.0009	0.007	0.07	0.001	0.029
658.18	0.0010	0.003	0.04	0.001	0.024
658.28	0.0007	0.004	0.05	0.001	0.023
658.38	0.0006	0.003	0.07	0.000	0.017
658.48	0.0004	0.003	0.03	0.000	0.013
658.59	0.0007	0.003	0.06	0.001	0.025
658.68	0.0007	0.004	0.06	0.001	0.024
658.78	0.0008	0.005	0.05	0.001	0.023

Core Position	197Au/Zr	205Tl/Zr	208Pb/Zr	209Bi/Zr	232Th/Zr
658.88	0.0006	0.003	0.04	0.000	0.017
659	0.0009	0.001	0.05	0.000	0.023
659.08	0.0007	0.001	0.06	0.000	0.022
659.17	0.0006	0.000	0.06	0.000	0.022
659.35	0.0006	0.000	0.04	0.001	0.024
659.43	0.0007	0.000	0.05	0.001	0.029
659.51	0.0000	0.000	0.04	0.000	0.027
659.62	0.0007	0.000	0.05	0.000	0.030

Core Position	238U/Zr	Al/Zr	Ba/Ar	Ca/Ar	Fe/Ar
652.13	0.000	674.8	69.5	19143	326.7
652.38	0.004	710.6	41.7	12766	362.6
653.2	0.014	641.2	59.9	8077	342.1
653.42	0.014	779.9	48.0	9250	377.7
653.72	0.015	549.8	76.1	3410	303.9
653.91	0.011	579.3	45.9	3767	314.5
654.08	0.016	581.2	68.4	4079	298.5
654.3	0.010	328.6	26.6	1841	177.6
654.5	0.028	949.2	59.2	3475	508.0
654.7	0.019	595.0	39.3	4612	334.7
654.9	0.031	881.6	69.6	5997	441.9
655.1	0.068	703.2	49.8	5516	397.1
655.3	0.069	1219.5	121.8	10011	681.6
655.5	0.147	1675.9	213.5	7425	665.7
655.72	0.061	997.3	131.8	3671	538.2
655.9	0.040	657.5	85.3	3178	569.0
656.1	0.049	681.4	59.1	3350	400.5
656.3	0.081	1399.9	174.8	2811	709.1
656.42	0.036	531.6	35.0	1460	284.9
656.52	0.067	1296.6	193.2	3633	655.4
656.58	0.042	782.6	84.8	2813	433.9
656.6	0.042	758.6	76.6	2952	406.4
656.7	0.044	942.1	92.4	3145	494.1
656.78	0.055	907.8	71.1	2189	460.3
656.88	0.051	547.3	78.3	207	294.8
656.98	0.211	1044.6	238.6	759	586.8
657.08	0.082	606.1	75.2	233	335.3
657.1	0.035	13741.2	8.7	59	7328.7
657.18	0.068	552.5	133.1	138	285.8
657.2	0.128	1062.8	261.0	188	574.5
657.28	0.082	487.6	137.1	230	261.8
657.38	0.112	795.1	188.9	263	416.0
657.48	0.029	635.7	40.2	146	354.3
657.58	0.023	541.1	29.7	76	300.3
657.68	0.033	1036.0	23.0	110	545.4
657.78	0.059	1747.8	16.5	1054	962.7
657.88	0.031	958.2	12.8	381	518.0
657.98	0.073	4284.5	34.8	2734	2303.9
658.06	0.065	4259.8	13.5	4803	2446.4
658.09	0.064	3118.8	27.6	2341	1637.3
658.18	0.052	3838.6	0.9	2560	2031.5
658.28	0.059	3061.1	1.3	1407	1633.3
658.38	0.039	3325.2	0.2	599	1904.5
658.48	0.027	904.0	0.3	445	514.1
658.59	0.051	1988.6	1.0	804	1059.4
658.68	0.041	1917.5	1.9	772	1037.0
658.78	0.046	2098.8	0.6	923	1107.4

Core Position	238U/Zr	Al/Zr	Ba/Ar	Ca/Ar	Fe/Ar
658.88	0.047	3435.5	0.3	484	1838.3
659	0.019	2715.1	0.3	755	1484.3
659.08	0.020	2605.8	2.2	615	1411.3
659.17	0.008	3282.6	0.3	398	1750.0
659.35	0.000	2475.4	0.6	17149	1284.9
659.43	0.000	2984.5	0.0	19223	1552.9
659.51	0.000	2662.4	0.1	21770	1543.8
659.62	0.000	2865.5	0.5	16783	1432.1

Core Position	Mg/Zr	Mn/Zr	Na/Zr	Ti/Zr
652.13	154.9	51.0	288.7	74.9
652.38	155.7	31.2	156.7	68.4
653.2	134.1	18.1	128.3	70.2
653.42	150.6	23.5	128.6	77.4
653.72	117.0	5.1	114.8	67.5
653.91	120.7	6.4	129.0	64.7
654.08	116.8	6.3	153.9	75.9
654.3	65.2	3.0	69.4	36.0
654.5	118.9	5.4	155.3	78.2
654.7	120.0	7.2	113.8	70.1
654.9	147.4	10.5	156.8	82.7
655.1	134.3	10.7	118.8	78.9
655.3	128.1	22.8	217.2	78.8
655.5	113.9	16.7	218.5	76.0
655.72	126.2	5.6	176.4	82.5
655.9	134.0	5.1	136.0	88.0
656.1	120.6	5.4	144.4	71.7
656.3	115.5	5.8	197.7	76.2
656.42	95.2	2.4	93.5	56.3
656.52	122.8	6.2	176.6	80.3
656.58	142.7	4.1	128.4	84.2
656.6	138.6	4.6	127.4	84.9
656.7	142.2	4.3	142.5	83.8
656.78	132.4	3.4	150.5	88.8
656.88	80.5	1.0	106.8	53.0
656.98	105.6	1.8	188.4	66.0
657.08	72.1	1.0	112.2	54.9
657.1	16.4	0.6	45.0	12.7
657.18	74.4	1.0	110.3	47.3
657.2	111.1	1.6	183.9	75.5
657.28	72.4	1.1	100.6	42.3
657.38	78.9	1.0	137.1	43.3
657.48	85.0	0.8	98.3	49.8
657.58	85.8	0.8	71.7	49.0
657.68	134.6	0.8	75.3	43.5
657.78	236.5	2.5	127.7	75.8
657.88	115.4	1.1	48.6	30.9
657.98	454.2	8.4	107.0	54.8
658.06	468.6	18.7	97.9	64.2
658.09	334.7	7.8	109.3	70.0
658.18	384.5	7.4	128.4	68.2
658.28	306.8	2.7	93.0	72.4
658.38	313.8	1.9	99.9	58.5
658.48	101.2	0.8	63.8	49.7
658.59	191.3	1.6	123.3	88.4
658.68	193.0	1.5	120.9	93.9
658.78	197.2	1.6	136.8	97.4

Core Position	Mg/Zr	Mn/Zr	Na/Zr	Ti/Zr
658.88	270.4	1.8	119.1	74.9
659	255.6	1.7	109.6	85.7
659.08	236.1	1.5	112.7	86.8
659.17	254.2	1.6	101.9	77.3
659.35	212.9	53.3	213.4	84.5
659.43	224.1	61.8	244.7	94.3
659.51	245.1	69.5	238.7	98.6
659.62	219.0	47.8	254.9	93.1

The following are the Zr-normalized data for ODP Site 1138.

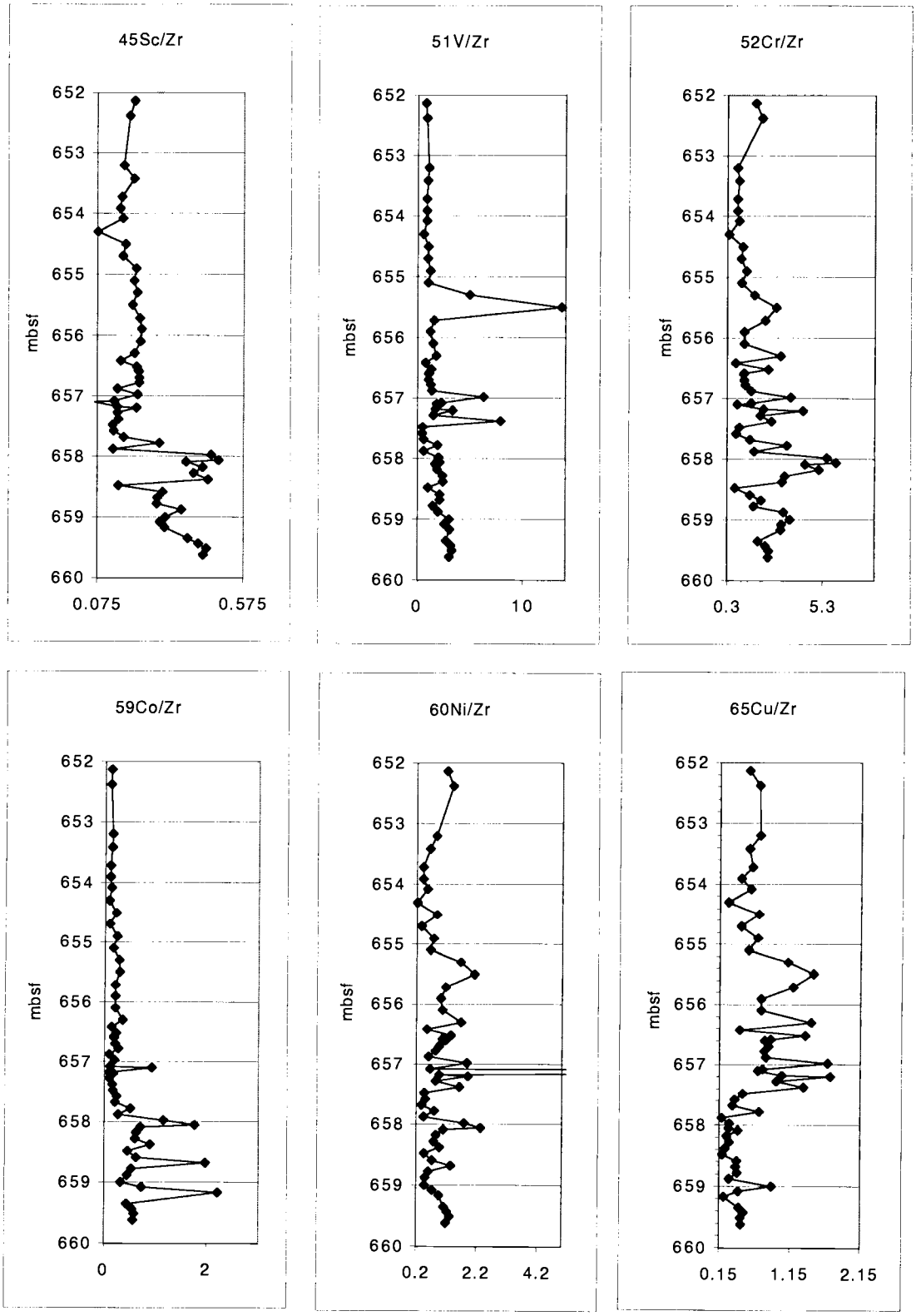

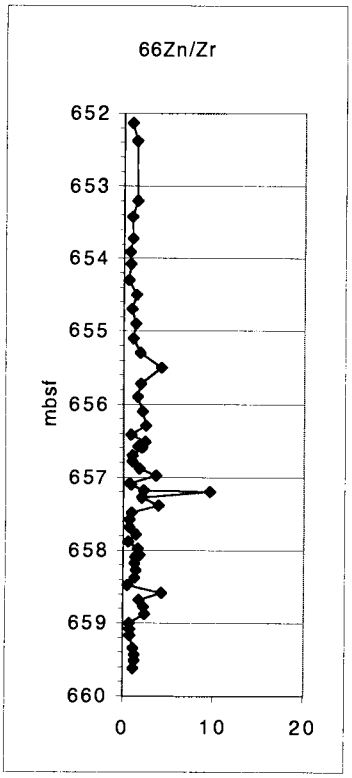
66Zn/Zr
mbsf
652
653
654
655
656
657
658
659
660
0
10
20

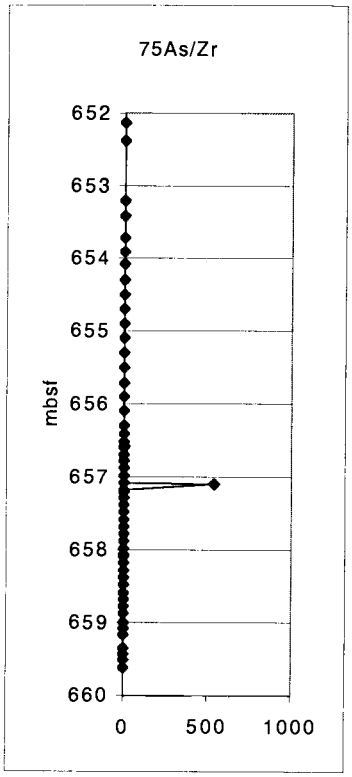
75As/Zr
mbsf
652
653
654
655
656
657
658
659
660
0
500
1000

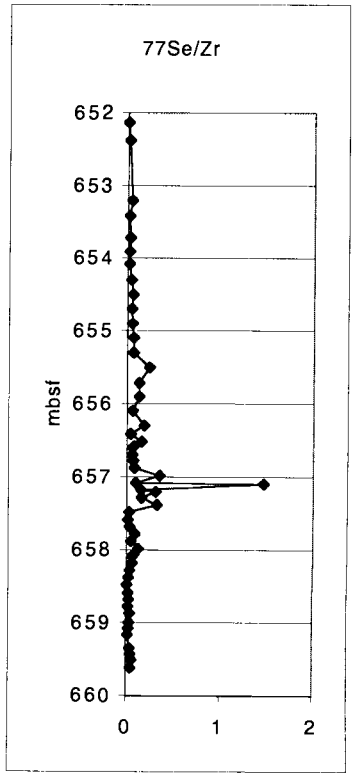
77Se/Zr
mbsf
652
653
654
655
656
657
658
659
660
0
1
2

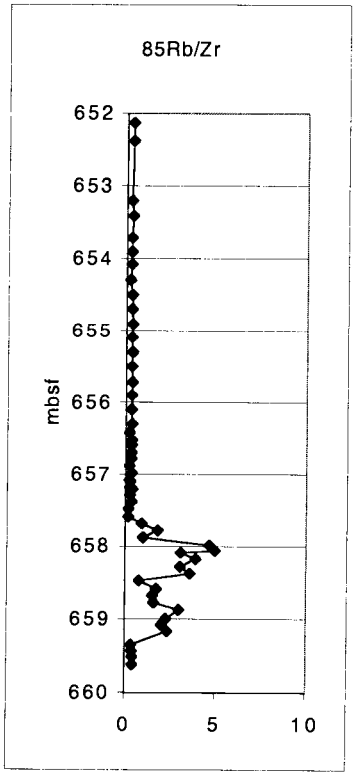
85Rb/Zr
mbsf
652
653
654
655
656
657
658
659
660
0
5
10

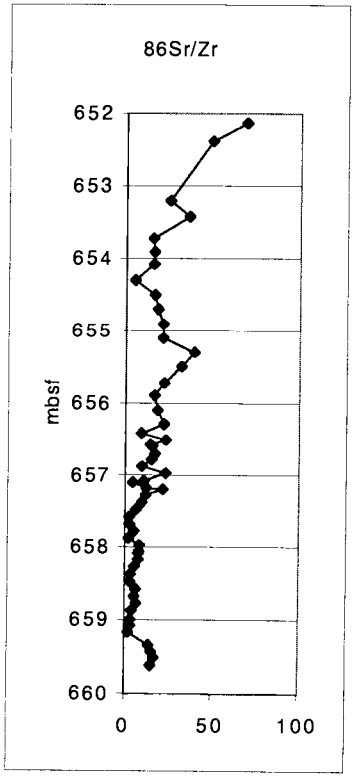
86Sr/Zr
mbsf
652
653
654
655
656
657
658
659
660
0
50
100

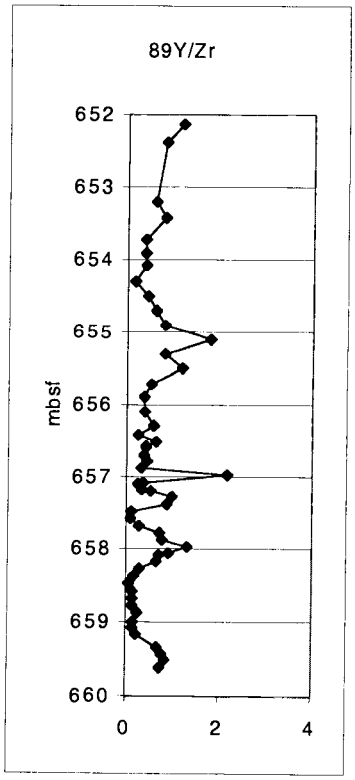
89Y/Zr
mbsf
652
653
654
655
656
657
658
659
660
0
2
4

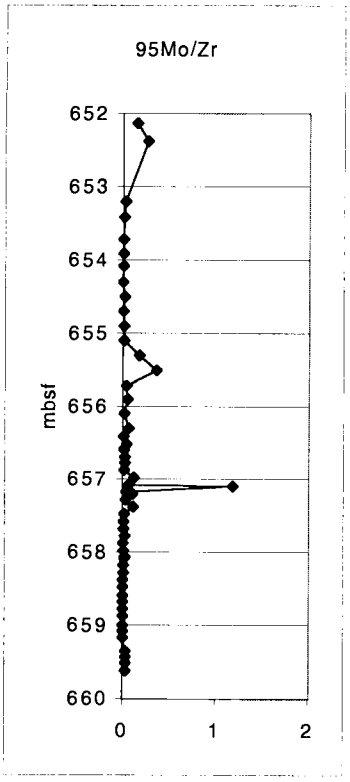
95Mo/Zr
mbsf
652
653
654
655
656
657
658
659
660
0
1
2

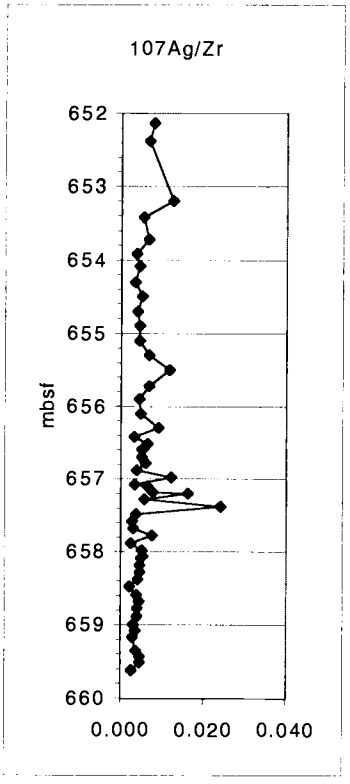
107Ag/Zr
mbsf
652
653
654
655
656
657
658
659
660
0.000
0.020
0.040

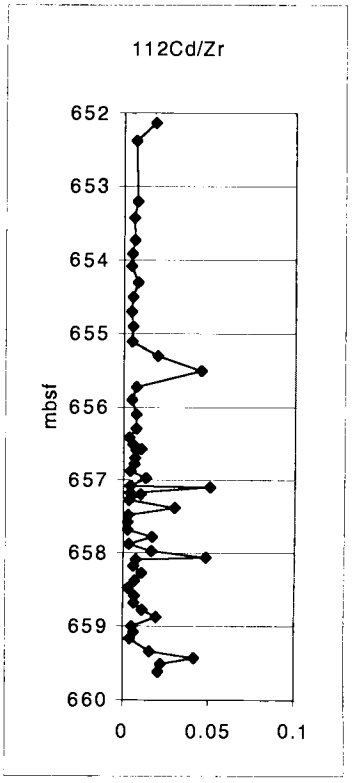
112Cd/Zr
mbsf
652
653
654
655
656
657
658
659
660
0
0.05
0.1

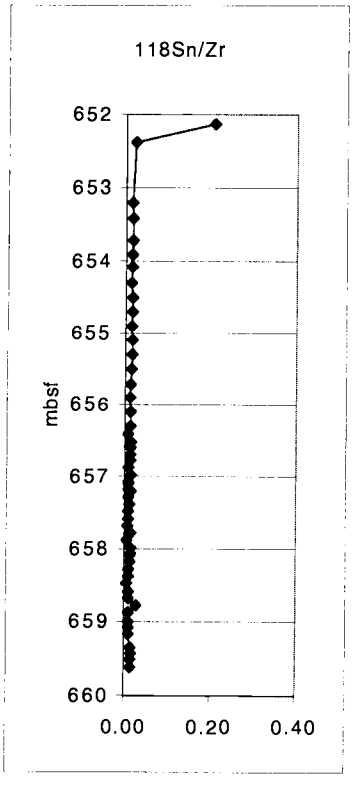
118Sn/Zr
mbsf
652
653
654
655
656
657
658
659
660
0.00
0.20
0.40

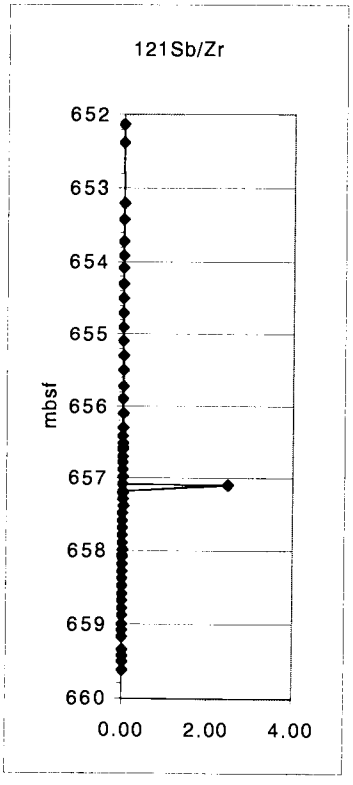
121Sb/Zr
mbsf
652
653
654
655
656
657
658
659
660
0.00
2.00
4.00

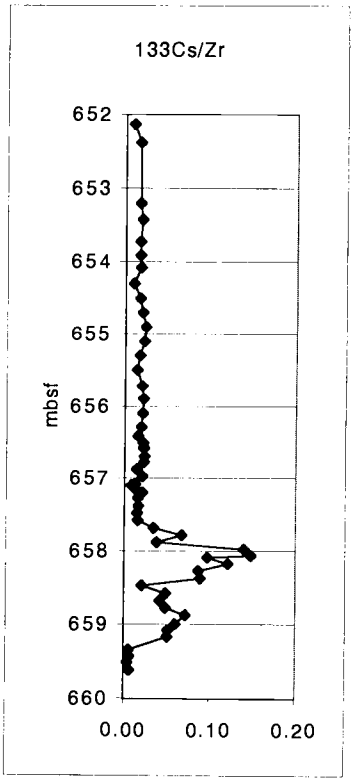
133Cs/Zr
mbsf
652
653
654
655
656
657
658
659
660
0.00
0.10
0.20

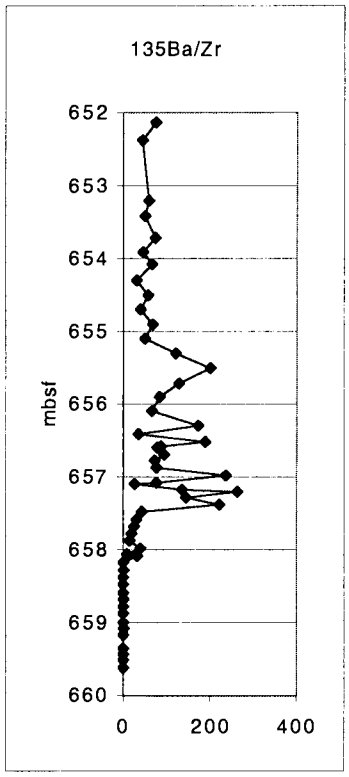
135Ba/Zr
mbsf
652
653
654
655
656
657
658
659
660
0
200
400

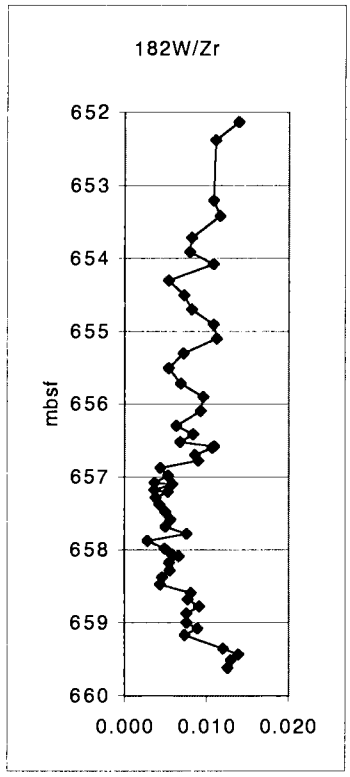
182W/Zr
mbsf
652
653
654
655
656
657
658
659
660
0.000
0.010
0.020

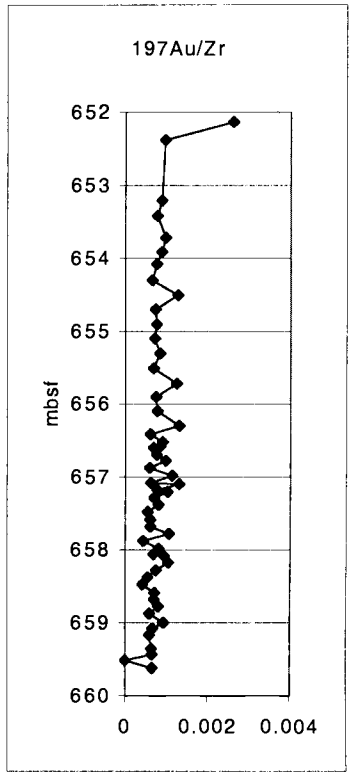
197Au/Zr
mbsf
652
653
654
655
656
657
658
659
660
0
0.002
0.004

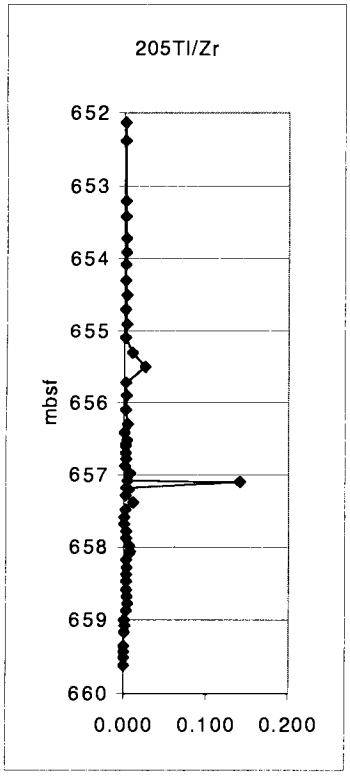
205Tl/Zr
mbsf
652
653
654
655
656
657
658
659
660
0.000
0.100
0.200

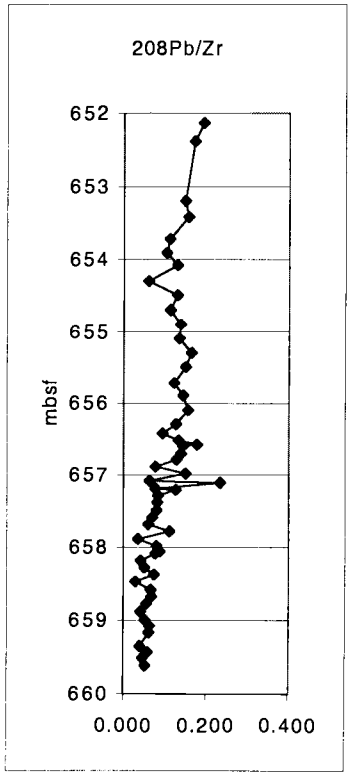
208Pb/Zr
mbsf
652
653
654
655
656
657
658
659
660
0.000
0.200
0.400

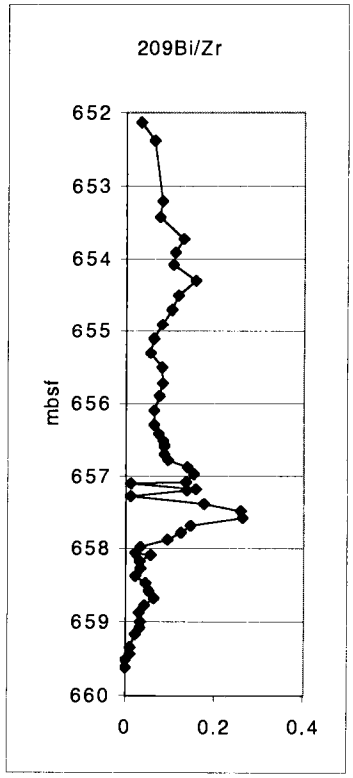
209Bi/Zr
mbsf
652
653
654
655
656
657
658
659
660
0
0.2
0.4

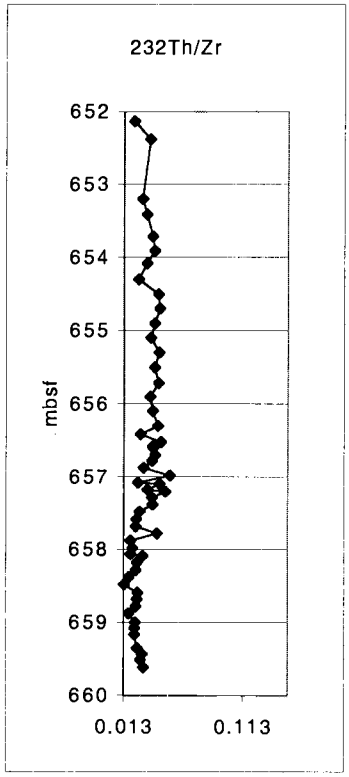
232Th/Zr
652
653
654
655
656
657
658
659
660
mbsf
0.013
0.113

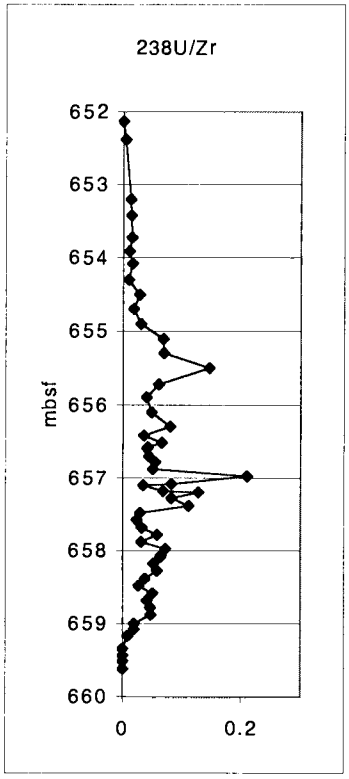
238U/Zr
652
653
654
655
656
657
658
659
660
mbsf
0
0.2

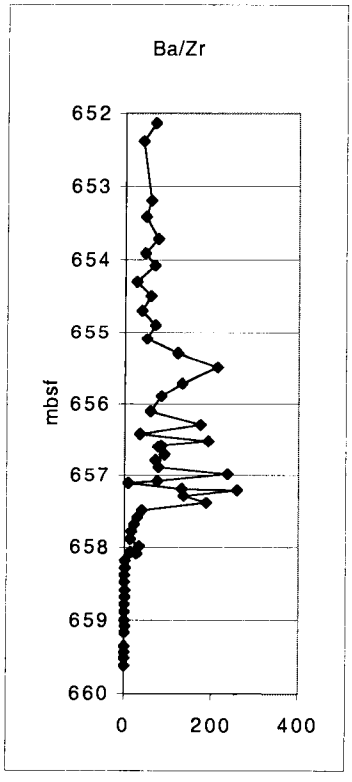
Ba/Zr
652
653
654
655
656
657
658
659
660
mbsf
0
200
400

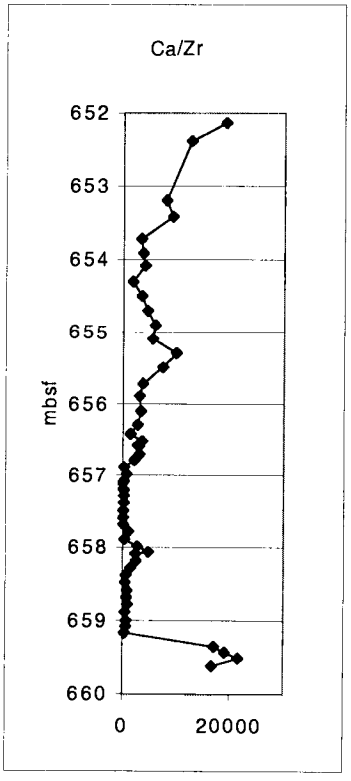
Ca/Zr
652
653
654
655
656
657
658
659
660
mbsf
0
20000

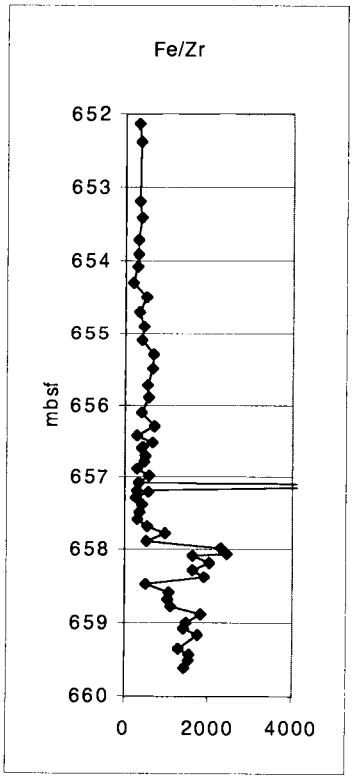
Fe/Zr
652
653
654
655
656
657
658
659
660
mbsf
0
2000
4000

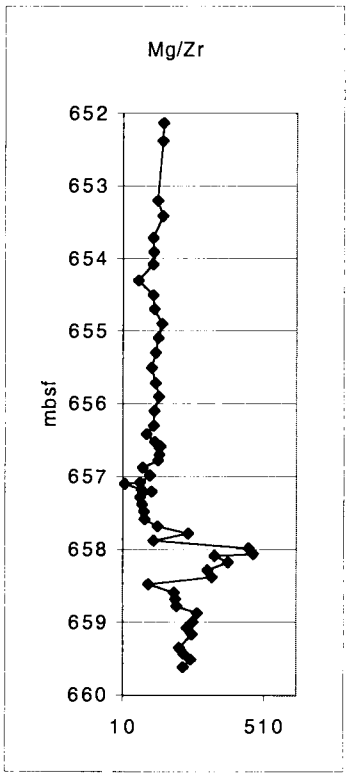
Mg/Zr
652
653
654
655
656
657
658
659
660
mbsf
10
510

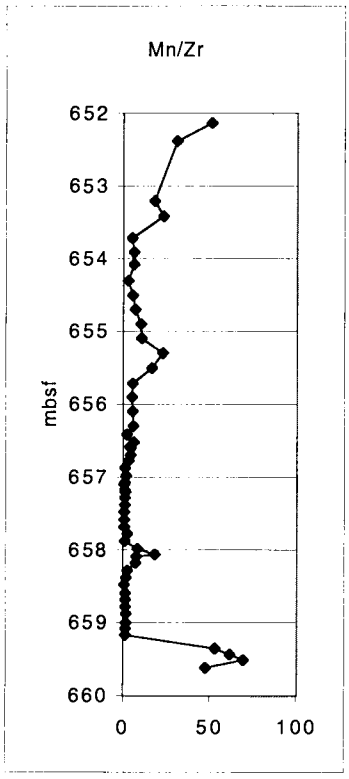
Mn/Zr
652
653
654
655
656
657
658
659
660
mbsf
0
50
100

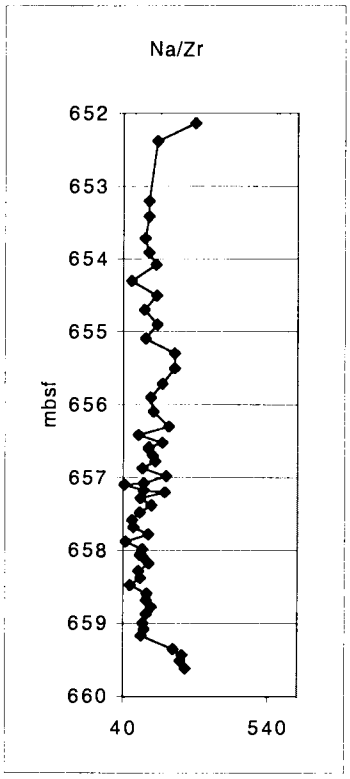
Na/Zr
652
653
654
655
656
657
658
659
660
mbsf
40
540

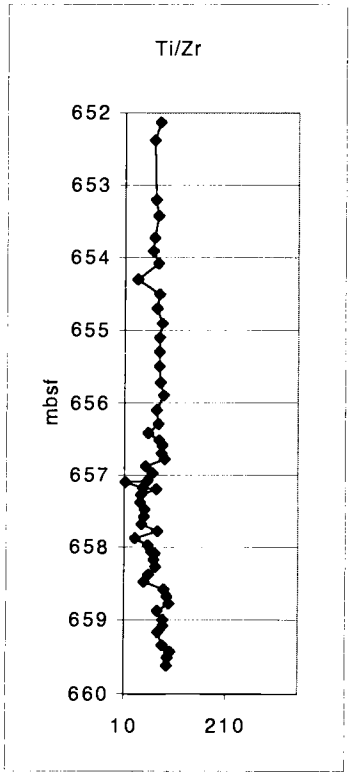
Ti/Zr
652
653
654
655
656
657
658
659
660
mbsf
10
210

The following are the Zr-normalized data for the Baranca el Canon section. Samples are meters above base.

Sample	45Sc/Zr	51V/Zr	53Cr/Zr	59Co/Zr	60Ni/Zr
82.4	0.083	0.49	2.68	0.28	1.82
81.6	0.170	1.47	1.80	0.49	1.94
81	0.356	2.16	4.90	2.34	7.52
80.6	0.118	0.67	2.83	0.46	3.22
80	0.153	0.85	10.33	0.64	5.89
79.4	0.094	0.79	0.71	0.20	1.18
79	0.062	0.59	0.55	0.08	0.60
78.5	0.084	0.60	1.18	0.13	1.16
77.8	0.113	1.00	1.05	0.18	2.32
77.3	0.063	0.78	0.83	0.46	1.27
76.8	0.050	0.53	1.63	0.53	1.52
76.3	0.060	0.54	0.68	0.25	0.76
75.9	0.059	0.53	0.70	0.34	1.24
75.3	0.038	0.36	0.37	0.26	0.97
75	0.045	0.73	1.88	0.45	2.33
74.5	0.027	0.93	1.91	0.55	4.84
73.8	0.091	0.79	0.34	0.12	1.56
73.4	0.102	0.65	0.46	0.23	2.66
73	0.077	0.44	0.27	0.19	2.38
72.5	0.210	1.33	1.10	0.70	5.30
71.7	0.102	0.64	5.54	0.25	4.64
70.4	0.092	0.57	0.55	0.14	0.83
69.7	0.057	0.47	0.45	0.17	0.80
69	0.136	0.89	1.20	0.36	2.37
68.6	0.178	1.04	0.78	0.45	2.43
68	0.047	0.67	0.81	0.16	1.17
67.5	0.147	1.49	1.64	0.50	3.24
67	0.135	1.23	2.02	0.51	3.19
66.6	0.089	0.49	1.47	0.23	0.81
65.6	0.191	0.55	2.18	0.52	2.23
65	0.126	0.79	0.62	0.23	0.77
64.5	0.074	0.52	0.62	0.23	1.05
64	0.129	0.56	0.71	0.56	2.96
63.4	0.075	0.55	1.17	0.30	1.70
63	0.091	0.39	0.41	0.19	0.64
62.5	0.119	0.53	2.56	0.24	1.53
62.1	0.086	0.36	0.32	0.10	0.16
61.5	0.096	0.49	0.49	0.17	0.39
60.8	0.117	0.50	0.78	0.09	0.25
60.5	0.123	1.21	2.08	0.47	2.94
59.8	0.028	0.18	0.39	0.09	0.49
59.5	0.357	1.44	3.57	1.87	6.19
58.9	0.374	2.84	3.40	1.01	2.74
58.5	0.188	1.26	1.27	0.36	1.66
57.3	0.714	4.83	3.76	1.40	7.06
56.9	0.314	3.79	1.64	1.06	4.24

Sample	45Sc/Zr	51V/Zr	53Cr/Zr	59Co/Zr	60Ni/Zr
56.6	0.215	2.70	0.98	0.46	2.05
56.2	0.163	2.00	3.37	0.99	5.63
55.8	0.182	2.66	2.30	1.08	3.23
55.5	0.210	1.62	13.16	0.60	3.94
55	0.150	1.07	0.58	0.43	1.12
54.5	0.115	0.51	2.86	0.30	1.55
54	0.185	0.57	1.08	0.46	1.08
53.5	0.211	1.19	2.09	0.43	1.55
53	0.286	1.43	1.79	0.50	1.04
52.2	0.254	1.08	3.11	0.31	1.18
51.5	0.692	4.09	7.11	0.46	1.99
51	0.783	8.42	10.01	1.07	4.59
50.6	0.096	1.64	0.48	0.09	0.47
50.3	0.123	1.06	0.68	0.19	0.44
49.7	0.114	1.62	0.44	0.17	0.36
48.8	0.201	1.86	1.01	0.62	2.19
47.5	0.236	1.61	0.84	0.85	3.36

Sample	65Cu/Zr	66Zn/Zr	75As/Zr	77Se/Zr	85Rb/Zr
82.4	0.45	0.2	0.11	0.007	0.18
81.6	0.39	0.4	0.42	0.020	0.44
81	5.60	1.1	1.14	0.080	0.38
80.6	0.46	0.8	0.52	0.022	0.18
80	3.84	2.7	0.38	0.032	0.13
79.4	0.21	0.0	0.20	0.012	0.32
79	0.10	0.6	2.02	0.003	0.24
78.5	0.10	0.1	0.36	0.013	0.21
77.8	0.41	8.3	0.39	0.020	0.38
77.3	1.14	2.2	0.34	0.180	0.24
76.8	1.56	2.2	0.88	0.201	0.23
76.3	0.73	0.7	1.23	0.002	0.32
75.9	1.09	9.8	0.49	0.038	0.37
75.3	0.84	1.9	0.52	0.056	0.18
75	1.63	5.7	0.60	0.031	0.31
74.5	2.58	5.7	0.44	0.223	0.52
73.8	0.35	2.9	0.41	0.016	0.28
73.4	0.24	2.1	0.06	0.027	0.25
73	0.42	5.4	0.32	0.015	0.23
72.5	0.51	6.3	2.76	0.067	0.59
71.7	5.88	3.4	0.45	0.025	0.36
70.4	0.14	0.9	0.61	0.013	0.28
69.7	0.25	1.0	0.46	0.011	0.23
69	0.57	4.6	7.78	0.024	0.36
68.6	0.44	1.6	0.96	0.036	0.31
68	0.11	0.4	0.35	0.010	0.10
67.5	0.43	3.8	1.57	0.019	0.48
67	0.79	1.6	0.51	0.131	0.44
66.6	0.18	0.8	0.37	0.053	0.39
65.6	1.55	2.5	0.69	0.038	0.35
65	0.97	1.2	0.62	0.125	0.24
64.5	0.32	0.3	9.84	0.001	0.12
64	0.81	18.9	3.76	0.004	0.49
63.4	0.30	6.4	2.73	0.017	0.19
63	0.21	1.6	1.92	0.008	0.14
62.5	0.93	0.9	0.38	0.031	0.17
62.1	0.18	0.2	0.13	0.014	0.20
61.5	0.32	0.3	0.42	0.009	0.20
60.8	0.35	0.1	1.24	0.059	0.18
60.5	0.78	2.6	1.40	0.026	0.26
59.8	0.18	0.0	1.00	0.046	0.06
59.5	0.62	1.8	2.33	0.048	0.55
58.9	0.56	1.3	3.76	0.098	0.61
58.5	0.44	2.1	7.27	0.039	0.22
57.3	0.92	0.9	5.87	0.076	0.45
56.9	1.03	1.3	4.67	0.071	0.28

Sample	65Cu/Zr	66Zn/Zr	75As/Zr	77Se/Zr	85Rb/Zr
56.6	0.66	2.6	2.86	0.043	0.28
56.2	0.75	2.0	6.26	0.047	0.34
55.8	1.10	3.3	1.62	0.063	0.30
55.5	1.66	0.7	3.44	0.044	0.26
55	0.30	0.1	1.51	0.042	0.22
54.5	0.66	5.0	0.84	0.103	0.28
54	0.42	0.1	1.67	0.125	0.33
53.5	0.87	1.3	0.12	0.044	0.42
53	0.99	1.0	0.33	0.029	0.49
52.2	0.66	4.0	0.15	0.004	0.24
51.5	0.81	1.1	0.26	0.062	0.98
51	2.15	4.0	1.80	0.912	0.63
50.6	0.16	0.3	0.52	0.023	0.55
50.3	0.47	0.5	0.32	0.038	0.70
49.7	0.26	0.7	0.15	0.029	0.52
48.8	0.19	2.5	1.04	0.134	0.94
47.5	0.84	3.5	0.19	0.186	1.60

Sample	86Sr/Zr	89Y/Zr	95Mo/Zr	107Ag/Zr	118Sn/Zr
82.4	44.3	0.22	0.09	0.004	0.006
81.6	84.2	0.45	0.16	0.003	0.020
81	339.1	1.29	0.33	0.011	0.023
80.6	110.1	0.39	0.13	0.003	0.016
80	167.7	0.62	0.25	0.000	0.039
79.4	66.9	0.33	0.05	0.004	0.007
79	28.5	0.30	0.24	0.008	0.006
78.5	51.6	0.33	0.13	0.003	0.010
77.8	105.9	0.51	0.10	0.006	0.074
77.3	66.4	0.96	0.04	0.005	0.043
76.8	74.5	0.39	0.43	0.006	0.042
76.3	30.7	0.11	0.09	0.004	0.041
75.9	51.2	0.18	0.07	0.006	0.047
75.3	45.5	0.29	0.05	0.005	0.036
75	74.3	0.24	0.12	0.009	0.078
74.5	128.0	0.28	0.14	0.016	0.074
73.8	73.3	0.24	0.13	0.002	0.037
73.4	133.7	0.93	0.09	0.008	0.094
73	105.1	0.22	0.05	0.012	0.084
72.5	309.0	0.55	0.61	0.010	0.086
71.7	144.9	0.20	0.11	0.006	0.025
70.4	50.6	0.17	0.04	0.003	0.010
69.7	33.1	0.23	0.03	0.004	0.055
69	95.6	0.55	0.35	0.008	0.054
68.6	109.9	0.28	0.10	0.004	0.036
68	33.4	0.09	0.01	0.003	0.010
67.5	121.7	0.49	0.10	0.005	0.185
67	112.6	0.44	0.03	0.008	0.019
66.6	35.8	0.19	0.03	0.002	0.015
65.6	84.8	0.69	0.06	0.003	0.074
65	24.6	1.07	0.02	0.002	0.035
64.5	43.8	0.11	0.05	0.004	0.017
64	138.6	0.33	0.07	0.007	0.107
63.4	75.3	0.23	0.19	0.006	0.179
63	26.9	0.27	0.03	0.003	0.015
62.5	25.0	0.39	0.04	0.003	0.019
62.1	5.1	0.17	0.01	0.003	0.012
61.5	8.0	0.26	0.01	0.003	0.013
60.8	28.7	0.65	0.02	0.005	0.014
60.5	107.7	0.99	0.23	0.003	0.023
59.8	19.9	0.45	0.09	0.003	0.003
59.5	310.6	2.14	0.43	0.107	0.000
58.9	159.8	0.76	0.11	0.006	0.034
58.5	61.3	0.34	0.49	0.002	0.009
57.3	302.0	1.74	1.28	0.010	0.010
56.9	222.7	1.15	0.09	0.093	0.007

Sample	86Sr/Zr	89Y/Zr	95Mo/Zr	107Ag/Zr	118Sn/Zr
56.6	83.3	0.42	0.04	0.013	0.028
56.2	177.2	0.48	0.48	0.017	0.035
55.8	172.2	0.68	0.17	0.000	-0.006
55.5	71.8	0.54	0.17	0.005	0.028
55	44.1	0.29	0.05	0.050	0.002
54.5	21.5	0.18	0.06	0.004	0.013
54	42.4	1.00	0.04	0.005	0.004
53.5	25.4	0.37	0.03	0.004	0.017
53	33.6	0.35	0.02	0.005	0.020
52.2	16.3	0.17	0.01	0.003	0.012
51.5	34.7	0.96	0.02	0.004	0.009
51	42.4	9.08	0.05	0.010	0.041
50.6	7.0	0.30	0.00	0.004	0.011
50.3	7.0	0.24	0.01	0.004	0.011
49.7	6.1	0.21	0.01	0.003	0.012
48.8	105.0	0.93	0.15	0.007	0.045
47.5	187.0	0.66	0.11	0.012	0.093

Sample	121Sb/Zr	133Cs/Zr	137Ba/Zr	182W/Zr	197Au/Zr
82.4	0.006	0.020	0.8	0.014	0.0010
81.6	0.023	0.043	1.8	0.099	0.0020
81	0.034	0.046	3.9	0.023	0.0115
80.6	0.022	0.019	2.0	0.016	0.0032
80	0.079	0.025	1.8	0.020	0.0049
79.4	0.011	0.030	1.3	0.012	0.0012
79	0.015	0.023	0.7	0.012	0.0008
78.5	0.010	0.020	1.0	0.014	0.0013
77.8	0.023	0.031	2.1	0.023	0.0028
77.3	0.007	0.018	3.3	0.013	0.0036
76.8	0.014	0.014	2.4	0.016	0.0020
76.3	0.030	0.027	2.6	0.019	0.0008
75.9	0.018	0.024	2.1	0.017	0.0014
75.3	0.006	0.013	1.5	0.004	0.0026
75	0.018	0.020	2.0	0.013	0.0022
74.5	0.016	0.020	3.2	0.020	0.0000
73.8	0.020	0.028	1.7	0.014	0.0014
73.4	0.020	0.031	2.9	0.031	0.0039
73	0.025	0.022	17.6	0.012	0.0155
72.5	0.048	0.067	11.9	0.038	0.0076
71.7	0.019	0.031	2.6	0.019	0.0028
70.4	0.007	0.025	1.0	0.013	0.0005
69.7	0.006	0.019	0.7	0.011	0.0006
69	0.269	0.030	1.5	0.027	0.0027
68.6	0.020	0.028	1.7	0.032	0.0020
68	0.007	0.009	1.0	0.006	0.0008
67.5	0.019	0.043	2.8	0.024	0.0024
67	0.019	0.039	16.5	0.019	0.0023
66.6	0.006	0.031	4.9	0.014	0.0006
65.6	0.011	0.038	3.6	0.025	0.0005
65	0.006	0.023	1.5	0.013	0.0008
64.5	0.066	0.012	1.7	0.011	0.0008
64	0.021	0.043	6.8	0.025	0.0029
63.4	0.012	0.021	2.2	0.012	0.0010
63	0.011	0.016	3.2	0.010	0.0009
62.5	0.004	0.022	2.5	0.015	0.0009
62.1	0.002	0.031	0.5	0.010	0.0002
61.5	0.048	0.031	3.5	0.016	0.0004
60.8	0.007	0.018	1.0	0.015	0.0005
60.5	0.049	0.032	12.9	0.013	0.0032
59.8	0.005	0.008	0.5	0.002	0.0003
59.5	0.024	0.071	3.1	0.048	0.0060
58.9	0.080	0.057	8.6	0.052	0.0029
58.5	0.046	0.028	4.0	0.026	0.0021
57.3	0.057	0.086	4.0	0.057	0.0048
56.9	0.050	0.043	18.4	0.057	0.0036

Sample	121Sb/Zr	133Cs/Zr	137Ba/Zr	182W/Zr	197Au/Zr
56.6	0.055	0.030	1.7	0.025	0.0125
56.2	0.070	0.041	2.7	0.047	0.0029
55.8	0.040	0.040	3.2	0.011	0.0057
55.5	0.225	0.034	1.6	0.036	0.0026
55	0.009	0.024	1.0	0.014	0.0017
54.5	0.036	0.029	1.2	0.018	0.0320
54	0.018	0.040	0.8	0.018	0.0018
53.5	0.005	0.071	0.9	0.015	0.0011
53	0.003	0.087	1.3	0.019	0.0011
52.2	0.003	0.048	0.5	0.008	0.0005
51.5	0.006	0.123	1.1	0.009	0.0015
51	0.033	0.107	3.0	0.021	0.0024
50.6	0.003	0.064	0.7	0.010	0.0005
50.3	0.003	0.090	2.9	0.012	0.0005
49.7	0.005	0.049	0.9	0.015	0.0008
48.8	0.022	0.115	2.0	0.026	0.0037
47.5	0.019	0.143	5.0	0.043	0.0037

Sample	205Tl/Zr	208Pb/Zr	209Bi/Zr	232Th/Zr	238U/Zr
82.4	0.001	0.11	0.0014	0.014	0.06
81.6	0.005	0.26	0.0000	0.036	0.14
81	0.000	0.82	0.0000	0.011	0.46
80.6	0.003	0.28	0.0000	0.022	0.16
80	0.000	0.47	0.0000	0.025	0.23
79.4	0.004	0.18	0.0000	0.034	0.12
79	0.002	0.09	0.0000	0.024	0.06
78.5	0.001	0.13	0.0000	0.027	0.08
77.8	0.003	0.25	0.0057	0.031	0.10
77.3	0.002	0.24	0.0018	0.034	0.08
76.8	0.002	0.28	0.0020	0.034	0.07
76.3	0.013	0.15	0.0016	0.035	0.05
75.9	0.011	0.24	0.0028	0.035	0.05
75.3	0.003	0.19	0.0026	0.018	0.06
75	0.002	0.32	0.0067	0.042	0.10
74.5	0.004	0.52	0.0039	0.039	0.13
73.8	0.002	0.21	0.0020	0.028	0.09
73.4	0.004	0.30	0.0039	0.027	0.16
73	0.003	0.27	0.0031	0.015	0.08
72.5	0.010	0.68	0.0000	0.038	0.32
71.7	0.003	0.29	0.0031	0.015	0.08
70.4	0.002	0.14	0.0000	0.023	0.05
69.7	0.001	0.12	0.0013	0.015	0.05
69	0.003	0.29	0.0082	0.019	0.10
68.6	0.000	0.34	0.0000	0.028	0.11
68	0.000	0.10	0.0011	0.007	0.04
67.5	0.000	0.69	0.0000	0.043	0.17
67	0.004	0.37	0.0000	0.027	0.19
66.6	0.006	0.11	0.0442	0.024	0.07
65.6	0.011	0.44	0.0000	0.035	0.05
65	0.011	0.12	0.0012	0.026	0.05
64.5	0.001	0.15	0.0012	0.018	0.05
64	0.007	0.48	0.0071	0.029	0.09
63.4	0.000	0.28	0.0000	0.017	0.07
63	0.001	0.12	0.0010	0.033	0.06
62.5	0.002	0.11	0.0036	0.029	0.04
62.1	0.002	0.06	0.0005	0.025	0.01
61.5	0.005	0.06	0.0008	0.030	0.03
60.8	0.002	0.07	0.0006	0.056	0.04
60.5	0.003	0.36	0.0325	0.133	0.24
59.8	0.001	0.07	0.0026	0.006	0.06
59.5	0.000	0.88	0.0000	0.036	0.71
58.9	0.006	0.45	0.0000	0.057	0.37
58.5	0.002	0.23	0.0023	0.028	0.18
57.3	0.000	0.85	0.0000	0.057	0.61
56.9	0.000	0.69	-0.0071	0.057	0.48

Sample	205Tl/Zr	208Pb/Zr	209Bi/Zr	232Th/Zr	238U/Zr
56.6	0.003	0.87	-0.0025	0.025	0.36
56.2	0.006	0.48	-0.0058	0.012	0.49
55.8	0.000	0.48	-0.0057	0.023	0.27
55.5	0.003	0.21	-0.0026	0.044	0.15
55	0.003	0.15	-0.0017	0.019	0.08
54.5	0.005	0.12	0.0000	0.020	0.05
54	0.004	0.16	-0.0018	0.025	0.06
53.5	0.009	0.12	-0.0011	0.024	0.03
53	0.005	0.14	0.0000	0.027	0.03
52.2	0.002	0.08	0.0000	0.012	0.01
51.5	0.003	0.10	-0.0015	0.010	0.02
51	0.007	0.25	-0.0024	0.017	0.03
50.6	0.002	0.08	0.0003	0.027	0.02
50.3	0.003	0.08	0.0003	0.029	0.02
49.7	0.004	0.09	0.0004	0.036	0.02
48.8	0.007	0.35	-0.0037	0.052	0.23
47.5	0.012	0.69	-0.0062	0.043	0.14

Sample	Ba/Zr	Ca/Zr	Fe/Zr	Mg/Zr	Mn/Zr
82.4	1.3	50258	61.8	389.6	6.1
81.6	1.0	86989	162.6	686.8	11.7
81	0.9	407797	-7.8	2552.8	38.3
80.6	4.0	107088	58.8	757.1	15.3
80	4.8	171193	-11.8	1157.5	14.7
79.4	2.8	61186	75.2	552.9	6.9
79	1.2	26344	112.0	240.9	2.6
78.5	1.2	47277	83.6	437.5	5.0
77.8	3.7	96903	111.5	875.3	12.5
77.3	3.8	62804	85.8	582.8	11.6
76.8	4.4	69471	118.6	593.6	11.4
76.3	3.3	26232	132.9	278.2	3.8
75.9	3.6	48057	141.9	466.4	7.0
75.3	2.5	46474	33.6	414.7	5.3
75	3.3	78184	83.0	655.7	9.9
74.5	6.7	134598	13.2	1070.0	16.3
73.8	3.2	69607	94.8	595.4	6.9
73.4	1.8	132597	57.8	1962.6	15.8
73	20.4	110274	-0.2	897.4	10.8
72.5	19.9	331347	30.1	2465.9	35.3
71.7	2.2	109804	64.7	1017.0	9.9
70.4	1.6	54777	125.7	524.1	7.2
69.7	1.5	44613	141.8	428.6	6.2
69	2.2	104042	163.9	731.7	15.2
68.6	3.5	134469	301.3	983.9	17.0
68	1.9	42556	27.8	318.2	5.4
67.5	5.6	161447	126.4	1218.9	26.2
67	19.6	140093	61.4	1362.0	20.3
66.6	5.9	38285	110.9	430.7	7.5
65.6	4.6	97744	299.1	929.8	24.4
65	2.6	34496	255.8	679.6	13.4
64.5	2.1	41447	240.5	781.8	7.3
64	10.5	123610	163.6	1736.3	20.1
63.4	3.8	75938	34.7	674.4	12.2
63	3.8	32387	157.0	319.2	8.2
62.5	3.0	30654	111.2	325.8	9.5
62.1	0.7	5620	90.2	102.1	3.0
61.5	3.8	10524	640.8	127.5	4.6
60.8	1.4	15868	77.2	163.8	5.0
60.5	15.4	117915	93.6	1104.1	27.6
59.8	0.9	23596	37.6	202.5	4.6
59.5	6.4	403705	11.2	3601.5	64.8
58.9	12.4	192826	389.6	1943.0	34.9
58.5	5.2	86059	258.5	852.3	12.6
57.3	3.8	355572	970.9	3139.8	50.1
56.9	25.0	241448	126.2	2344.9	32.0

Sample	Ba/Zr	Ca/Zr	Fe/Zr	Mg/Zr	Mn/Zr
56.6	3.9	91852	402.0	991.1	14.7
56.2	4.8	184391	343.9	1526.8	27.0
55.8	5.9	197575	57.1	2142.5	29.5
55.5	3.6	85716	405.1	836.2	15.4
55	1.9	58589	280.7	528.6	13.7
54.5	1.6	30831	254.9	263.4	7.0
54	1.8	55966	286.7	495.5	20.1
53.5	1.8	30764	336.2	471.9	16.0
53	2.3	39926	466.9	2314.5	22.8
52.2	0.8	16272	419.3	442.6	7.9
51.5	1.9	48859	574.7	762.7	35.8
51	3.4	64804	1477.0	719.7	55.9
50.6	1.1	7605	223.3	228.8	6.1
50.3	3.2	6464	280.8	306.0	5.1
49.7	1.2	6736	274.8	3334.0	10.1
48.8	4.7	135063	293.0	1508.4	41.3
47.5	5.0	225941	160.9	2963.4	38.3

Sample	Na/Zr	Ti/Zr
82.4	83.8	28.2
81.6	53.8	51.2
81	727.9	174.9
80.6	125.5	51.1
80	190.5	70.4
79.4	64.6	36.2
79	23.1	18.0
78.5	54.5	30.4
77.8	205.1	49.3
77.3	90.1	31.1
76.8	99.5	36.1
76.3	35.5	33.5
75.9	182.6	34.8
75.3	74.9	19.0
75	155.8	36.7
74.5	293.2	49.5
73.8	113.1	41.7
73.4	196.9	57.1
73	163.7	5.8
72.5	438.5	52.9
71.7	155.7	41.5
70.4	104.6	33.9
69.7	63.7	21.2
69	396.8	47.3
68.6	178.0	58.2
68	43.2	20.3
67.5	5606.2	71.1
67	369.4	54.2
66.6	191.1	28.3
65.6	143.2	50.0
65	258.7	35.6
64.5	116.1	26.1
64	1960.3	65.2
63.4	171.0	34.4
63	62.9	30.2
62.5	356.5	38.9
62.1	13.1	20.9
61.5	20.3	26.5
60.8	26.5	29.9
60.5	261.1	54.3
59.8	71.3	1.4
59.5	499.2	58.4
58.9	255.3	115.4
58.5	111.7	56.0
57.3	400.6	158.0
56.9	230.1	102.3

Sample	Na/Zr	Ti/Zr
56.6	108.4	51.0
56.2	261.3	76.7
55.8	2563.4	73.3
55.5	85.3	57.6
55	96.2	35.5
54.5	32.5	34.2
54	83.5	44.8
53.5	63.1	50.8
53	40.9	63.3
52.2	32.0	43.6
51.5	34.6	81.5
51	653.8	104.0
50.6	13.7	28.0
50.3	28.6	32.7
49.7	12.1	44.8
48.8	92.9	62.7
47.5	301.0	110.5

The following are the Zr-normalized data for the Baranca el Canon section.

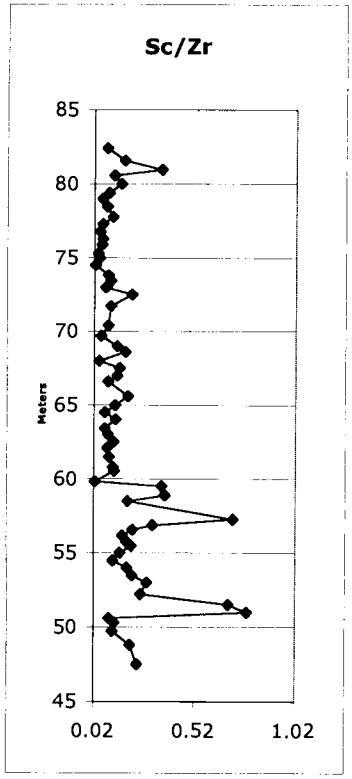

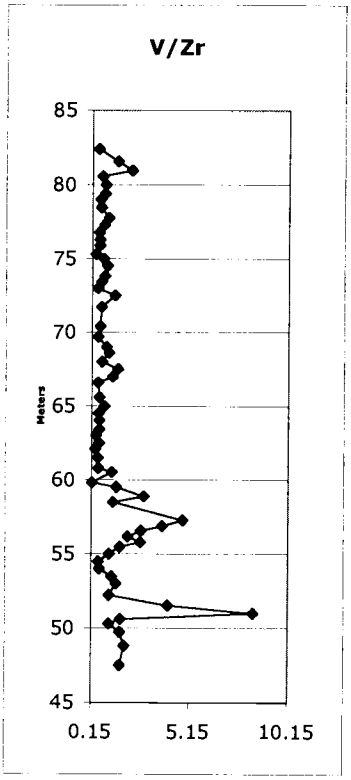

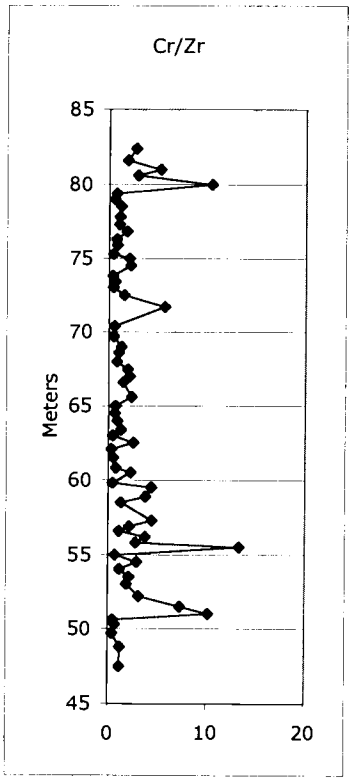

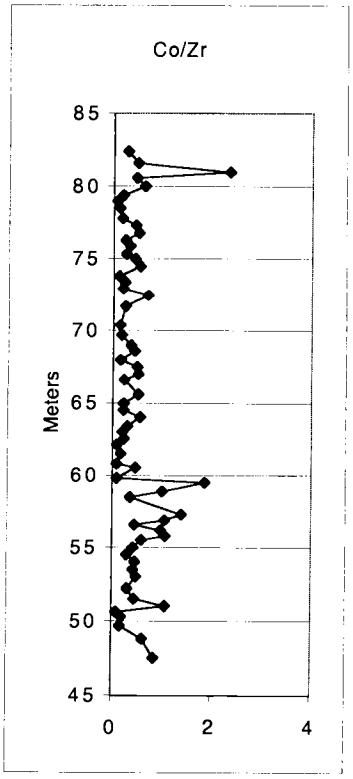

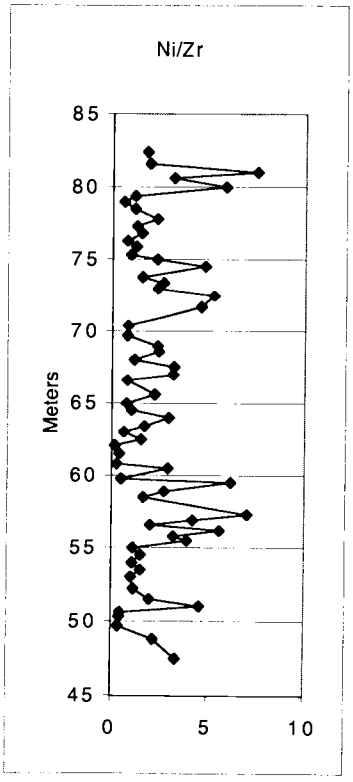

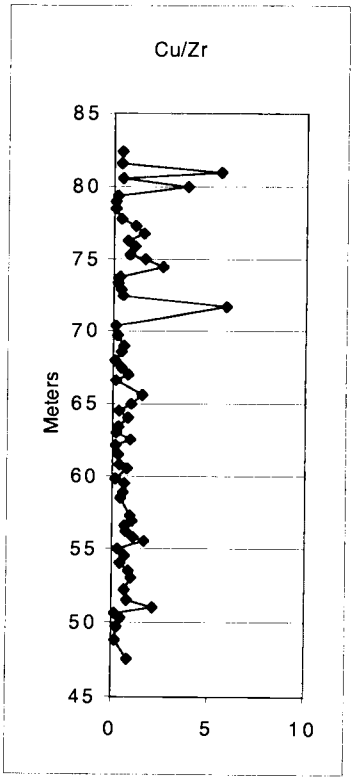

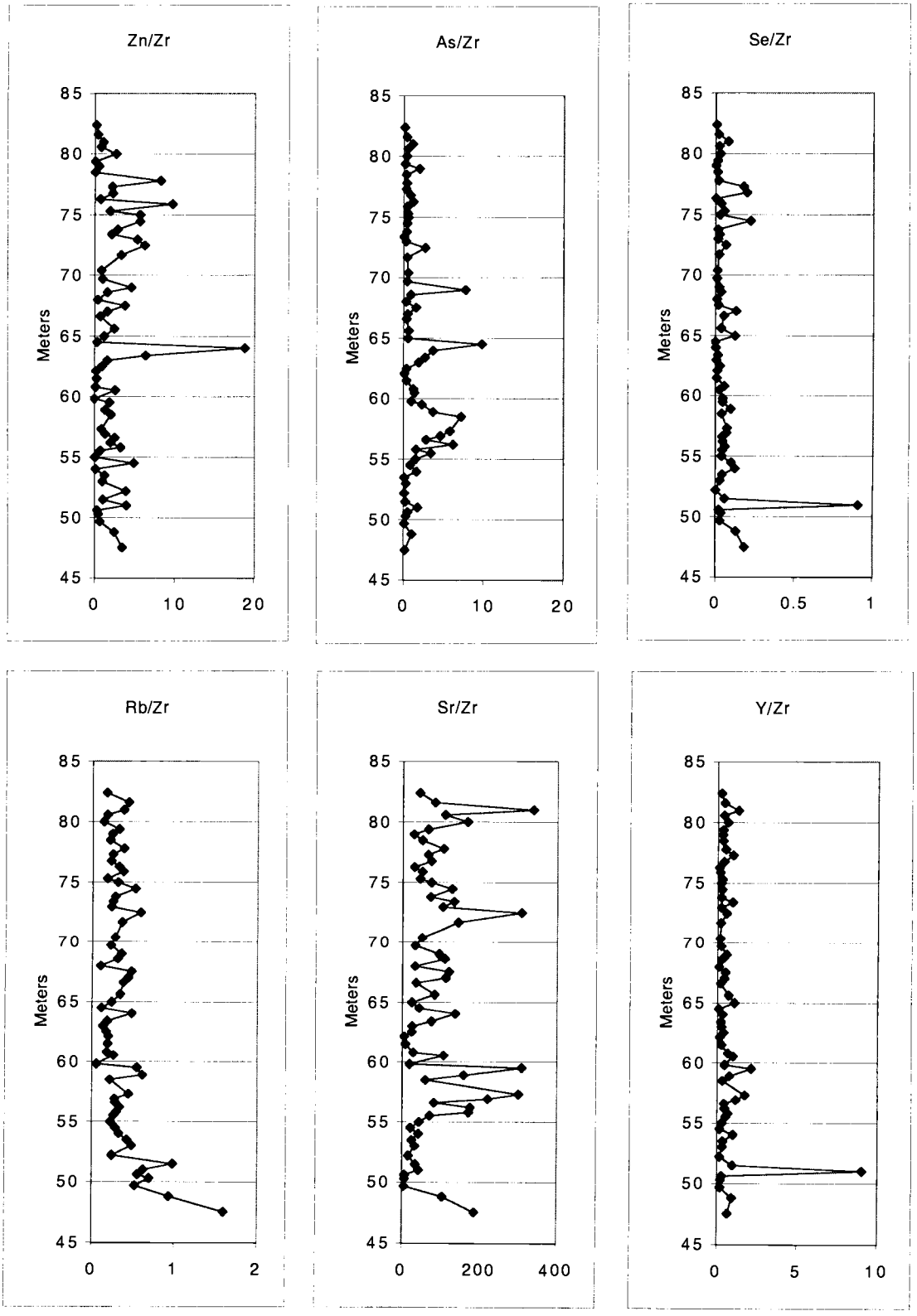
Zn/Zr
As/Zr
Se/Zr
Rb/Zr
Sr/Zr
Y/Zr
Meters
85
80
75
70
65
60
55
50
45
0
10
20
0.5
1
2
200
400
5

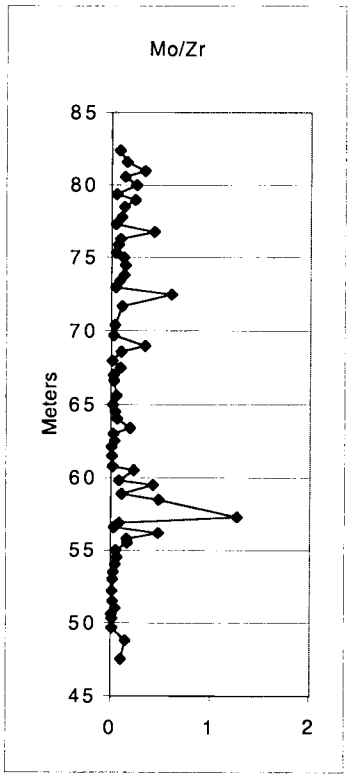
Mo/Zr
Meters
85
80
75
70
65
60
55
50
45
0
1
2

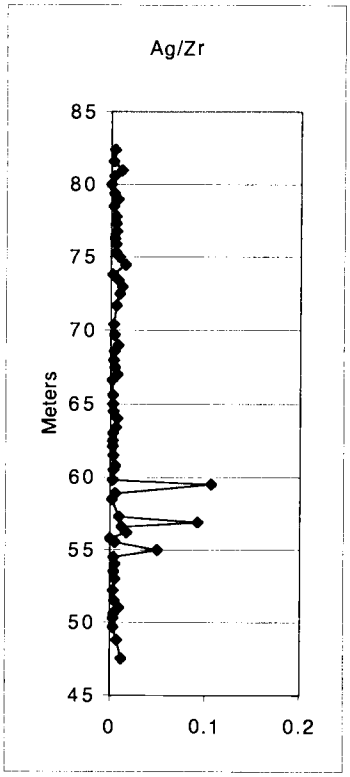
Ag/Zr
Meters
85
80
75
70
65
60
55
50
45
0
0.1
0.2

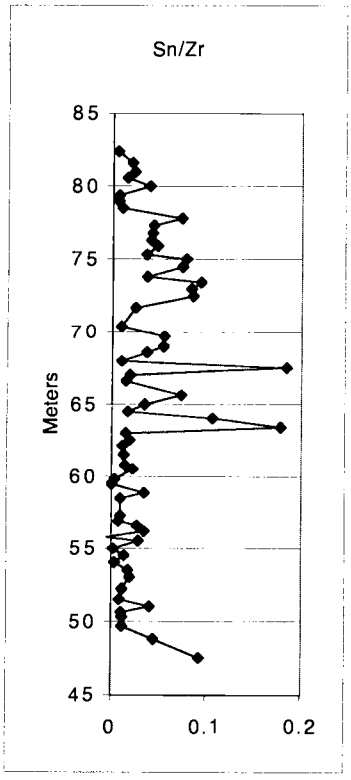
Sn/Zr
Meters
85
80
75
70
65
60
55
50
45
0
0.1
0.2

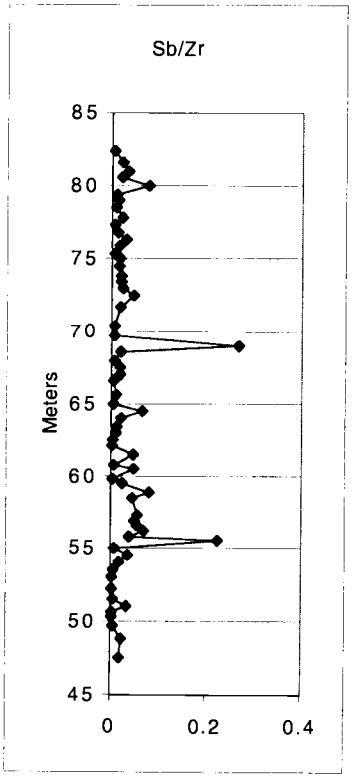
Sb/Zr
Meters
85
80
75
70
65
60
55
50
45
0
0.2
0.4

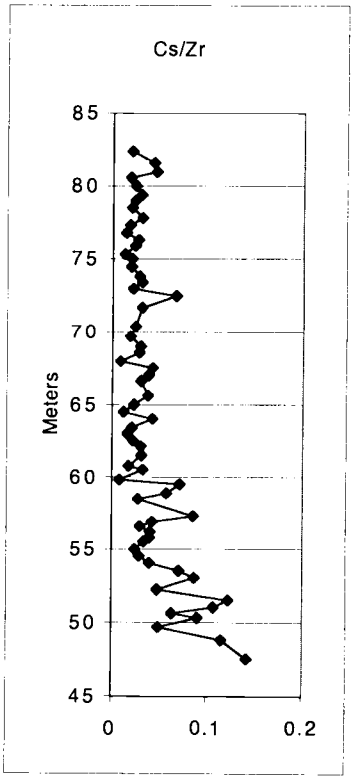
Cs/Zr
Meters
85
80
75
70
65
60
55
50
45
0
0.1
0.2

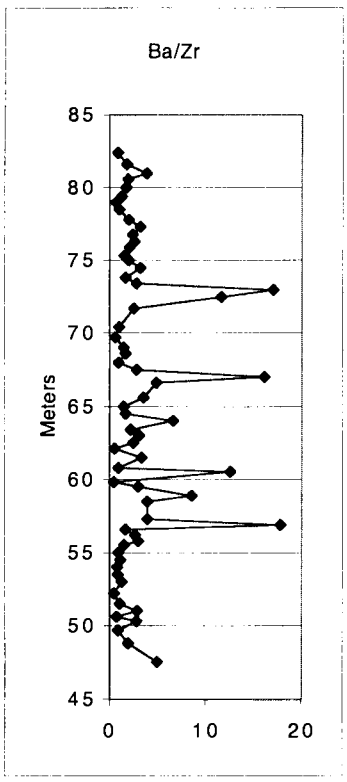
Ba/Zr
Meters
85
80
75
70
65
60
55
50
45
0
10
20

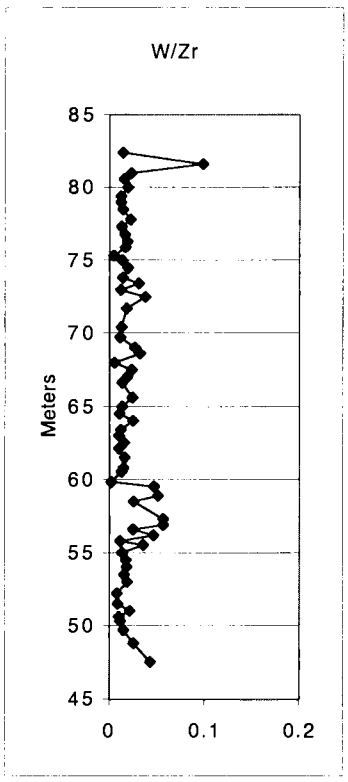
W/Zr
Meters
85
80
75
70
65
60
55
50
45
0
0.1
0.2

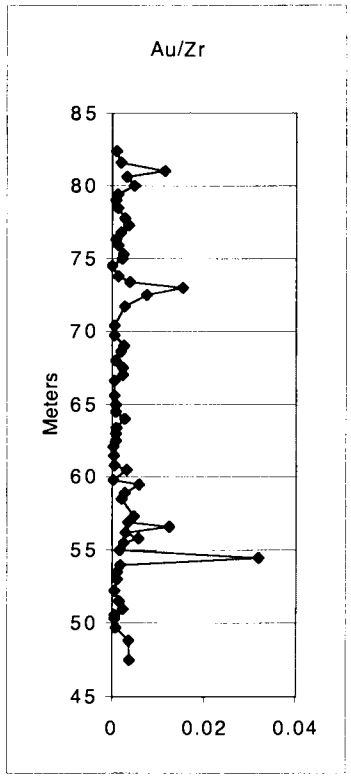
Au/Zr
Meters
85
80
75
70
65
60
55
50
45
0
0.02
0.04

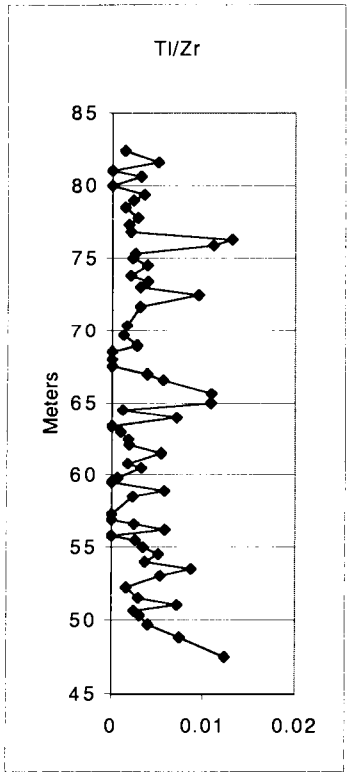
Tl/Zr
Meters
85
80
75
70
65
60
55
50
45
0
0.01
0.02

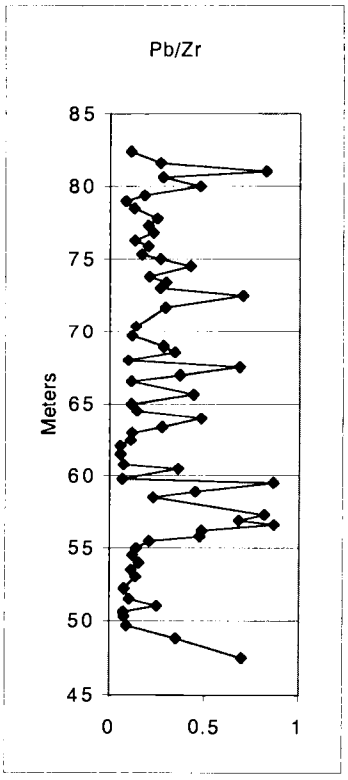
Pb/Zr
Meters
85
80
75
70
65
60
55
50
45
0
0.5
1

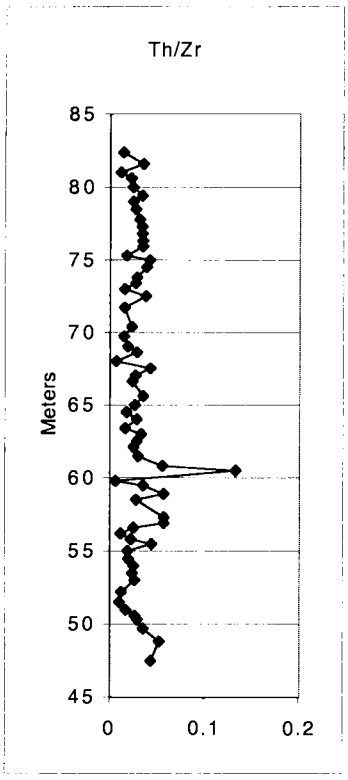
Th/Zr
Meters
85
80
75
70
65
60
55
50
45
0
0.1
0.2

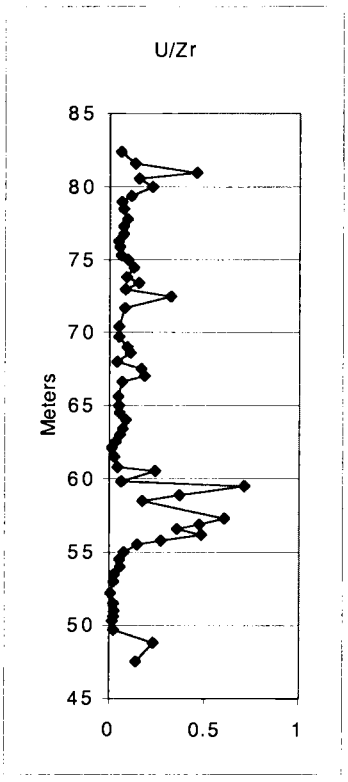
U/Zr
Meters
85
80
75
70
65
60
55
50
45
0
0.5
1

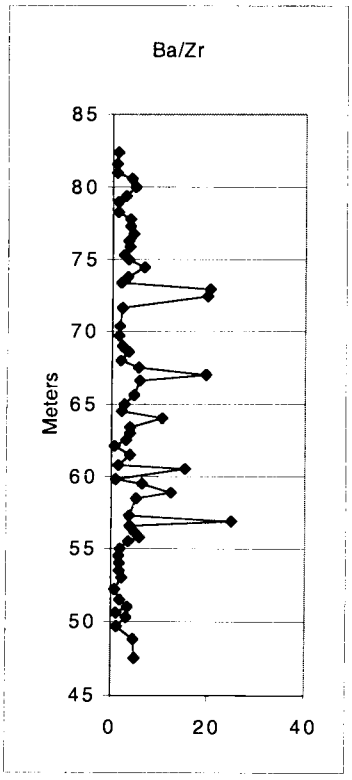
Ba/Zr
Meters
85
80
75
70
65
60
55
50
45
0
20
40

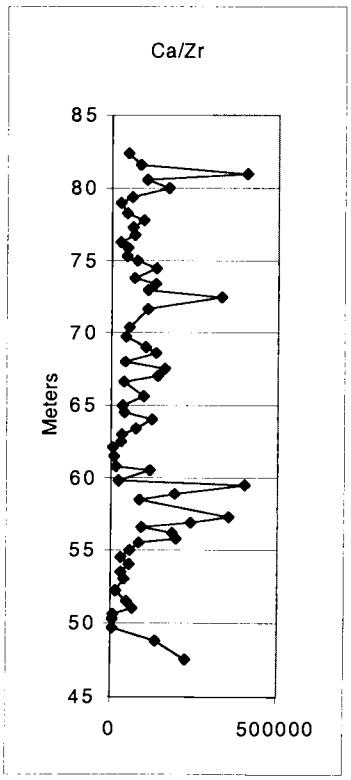
Ca/Zr
Meters
85
80
75
70
65
60
55
50
45
0
500000

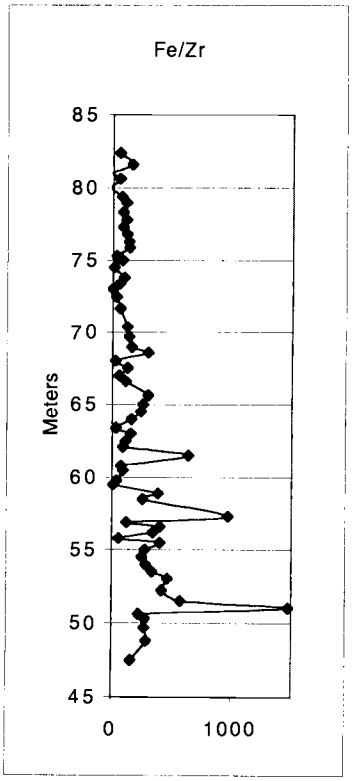
Fe/Zr
Meters
85
80
75
70
65
60
55
50
45
0
1000

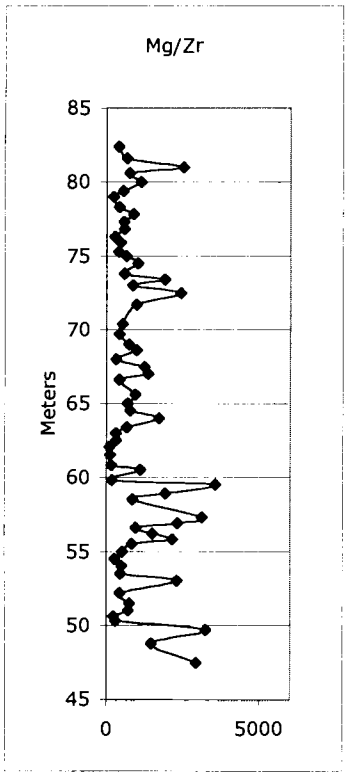
Mg/Zr
Meters
85
80
75
70
65
60
55
50
45
0
5000

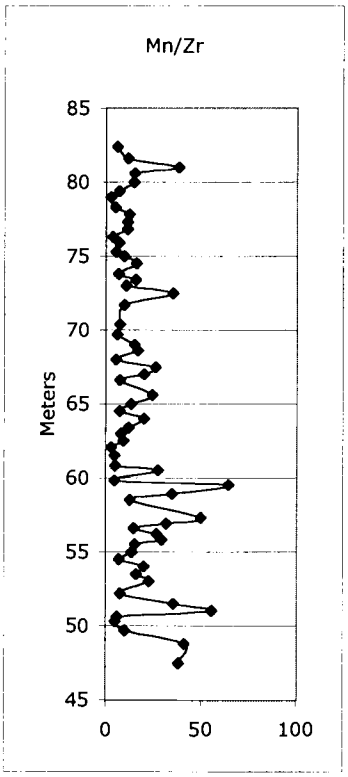
Mn/Zr
Meters
85
80
75
70
65
60
55
50
45
0
50
100

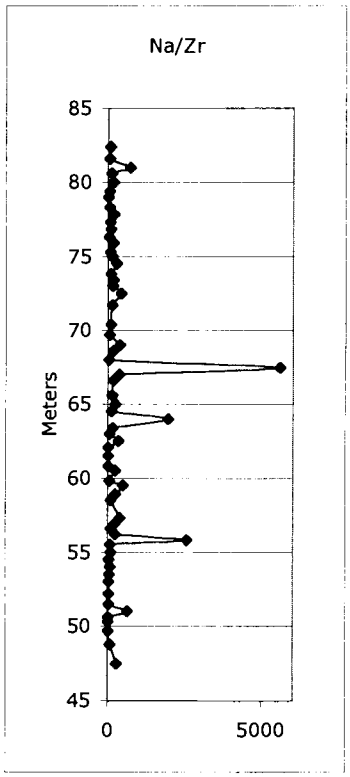
Na/Zr
Meters
85
80
75
70
65
60
55
50
45
0
5000

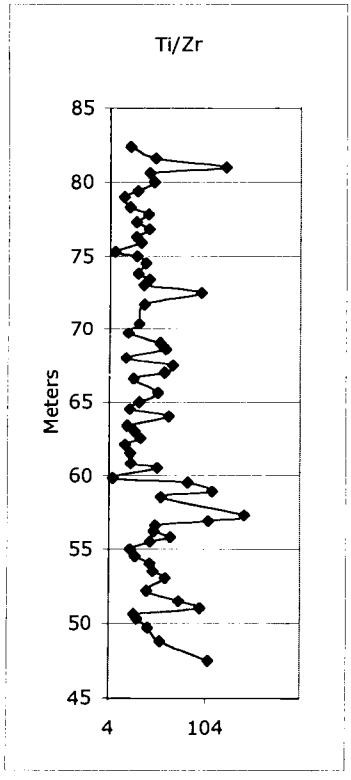
Ti/Zr
Meters
85
80
75
70
65
60
55
50
45
4
104

The following are Zr-normalized data the Totumo-3 Well core.
Depth is meters from La Luna Formation.

Depth	45Sc/Zr	51V/Zr	53Cr/Zr	59Co/Zr	60Ni/Zr
20.48	0.07	18.9	1.4	0.11	3.2
19.74	0.11	13.1	1.0	0.12	1.9
19.56	0.11	9.7	0.9	0.14	1.3
18.75	0.16	6.1	1.3	0.33	1.7
18.39	0.10	16.6	1.1	0.15	2.3
17.61	0.09	6.7	1.5	0.27	1.7
17.15	0.09	15.5	1.0	0.16	2.3
16.59	0.09	10.3	2.7	0.31	4.1
15.96	0.11	3.8	3.1	0.27	2.1
15.42	0.12	2.1	1.3	0.31	2.5
15.02	0.14	7.6	2.4	0.49	3.6
14.84	0.19	2.7	2.2	0.45	3.8
14.48	0.33	20.1	3.8	1.23	4.5
13.95	0.37	9.7	4.4	2.41	9.1
13.85	0.26	4.3	1.4	0.32	4.1
13.62	0.26	31.4	2.9	1.28	9.8
13.09	0.09	22.4	1.8	0.31	11.7
12.55	0.07	9.9	1.1	0.35	4.1
12.02	0.09	89.2	7.7	0.36	17.4
11.48	0.09	123.7	5.8	1.50	23.2
10.93	0.06	68.7	7.8	0.28	17.0
10.34	0.06	47.3	5.9	0.25	13.7
9.83	0.09	84.2	8.8	1.17	11.0
9.4	0.07	42.0	4.8	0.40	10.0
9.07	0.00	196.2	12.5	11.31	42.6
8.67	0.05	41.4	5.1	0.25	7.7
8.03	0.04	65.6	10.3	1.23	9.5
7.55	0.07	150.6	12.4	4.60	21.9
7.07	0.05	46.9	5.0	0.25	7.1
6.73	0.05	35.8	5.0	0.23	10.4
6.28	0.08	167.6	25.2	4.32	29.0
5.82	0.06	59.9	6.4	0.42	11.2
5.34	0.05	41.8	4.9	0.29	7.8
4.83	0.06	85.7	4.8	1.48	9.6
4.32	0.05	45.4	5.6	0.25	9.2
3.84	0.11	86.7	16.8	1.55	11.9
3.41	0.06	37.5	3.3	0.35	6.0
2.85	0.06	30.6	3.1	0.32	4.1
2.37	0.05	29.5	3.0	0.15	4.9
1.93	0.07	36.1	2.1	0.89	4.9
1.55	0.06	50.7	4.8	0.34	11.8
0.77	0.06	40.6	4.1	0.22	13.3
0.41	0.10	107.5	2.8	4.46	18.0

Depth	65Cu/Zr	66Zn/Zr	75As/Zr	77Se/Zr	85Rb/Zr
20.48	0.7	8.0	0.59	0.22	0.68
19.74	0.5	6.7	0.62	0.21	1.00
19.56	0.5	5.0	0.68	0.16	1.11
18.75	0.7	4.2	0.72	0.19	1.28
18.39	0.6	6.1	0.69	0.26	0.97
17.61	1.0	5.0	1.00	0.27	0.95
17.15	0.5	6.7	0.74	0.29	0.89
16.59	1.2	5.4	0.73	0.26	0.58
15.96	0.8	5.6	1.03	0.22	1.16
15.42	1.0	3.1	1.23	0.24	0.77
15.02	1.4	4.7	1.10	0.23	0.76
14.84	1.2	4.7	0.94	0.14	0.75
14.48	2.4	6.3	1.52	0.09	0.88
13.95	13.5	10.5	2.45	0.77	0.33
13.85	1.5	9.2	0.96	0.41	0.52
13.62	2.1	15.5	0.99	0.24	0.76
13.09	2.4	17.1	3.17	1.25	0.66
12.55	1.7	8.5	2.07	0.96	0.71
12.02	3.5	121.7	5.07	1.18	0.93
11.48	2.9	70.0	5.37	1.17	1.09
10.93	3.1	91.0	3.68	1.24	0.78
10.34	2.8	77.1	3.12	1.17	0.68
9.83	2.2	47.3	1.64	0.66	0.74
9.4	2.2	59.8	2.02	0.58	0.57
9.07	9.7	160.1	3.10	2.52	0.87
8.67	2.1	55.3	1.71	0.44	0.56
8.03	1.9	49.9	1.32	0.41	0.52
7.55	5.0	118.5	3.59	1.70	1.95
7.07	2.0	66.0	1.39	0.50	0.55
6.73	1.8	55.0	1.54	0.68	0.58
6.28	9.1	137.4	9.96	3.79	1.61
5.82	2.5	75.0	2.00	0.66	0.67
5.34	2.2	68.3	1.43	0.55	0.52
4.83	2.2	53.4	1.63	0.81	0.99
4.32	2.5	85.1	1.89	0.43	0.50
3.84	2.5	38.6	1.22	0.62	1.02
3.41	1.7	37.5	1.14	0.38	0.57
2.85	1.5	26.2	1.08	0.54	0.61
2.37	1.6	36.4	0.86	0.33	0.45
1.93	1.1	17.5	0.97	0.53	0.82
1.55	2.2	63.9	1.38	0.67	0.61
0.77	2.4	65.3	1.16	0.85	0.54
0.41	4.9	41.2	1.10	1.13	2.16

Depth	86Sr/Zr	89Y/Zr	95Mo/Zr	107Ag/Zr	112Cd/Zr
20.48	10.8	0.44	1.85	0.011	0.08
19.74	9.3	0.48	1.39	0.009	0.05
19.56	9.1	0.38	0.71	0.008	0.05
18.75	51.5	0.62	0.45	0.011	0.04
18.39	14.2	0.50	1.79	0.011	0.06
17.61	35.3	0.48	1.73	0.017	0.09
17.15	19.4	0.39	1.30	0.026	0.05
16.59	40.4	1.00	1.32	0.015	0.09
15.96	13.6	0.53	0.55	0.010	0.04
15.42	18.6	0.42	0.46	0.009	0.04
15.02	51.0	0.74	0.76	0.019	0.07
14.84	34.9	0.73	0.23	0.011	0.03
14.48	268.2	2.24	0.79	0.085	0.10
13.95	5.2	0.50	0.73	0.008	0.08
13.85	11.0	0.76	0.97	0.009	0.06
13.62	211.7	1.79	1.32	0.020	0.10
13.09	14.3	0.72	5.04	0.021	0.23
12.55	39.9	0.47	1.52	0.037	0.28
12.02	70.1	1.71	9.50	0.143	2.14
11.48	388.4	3.01	15.08	0.077	0.87
10.93	50.3	1.59	7.70	0.112	1.19
10.34	40.4	1.61	5.23	0.115	1.06
9.83	237.3	3.08	4.30	0.109	0.74
9.4	66.8	1.59	5.88	0.082	1.02
9.07	2101.9	13.96	14.67	0.250	1.62
8.67	45.5	0.72	4.36	0.066	0.82
8.03	208.6	0.74	4.38	0.083	0.87
7.55	902.7	2.53	7.10	0.268	2.39
7.07	50.7	1.42	3.70	0.068	1.29
6.73	43.5	1.05	3.42	0.073	0.92
6.28	681.7	2.31	12.25	0.438	2.44
5.82	98.0	2.11	6.33	0.094	1.43
5.34	64.5	1.07	4.77	0.081	1.59
4.83	178.2	1.12	3.50	0.118	1.12
4.32	56.8	1.02	7.14	0.079	1.61
3.84	197.8	1.07	3.88	0.085	0.94
3.41	75.2	0.88	3.99	0.051	0.66
2.85	40.7	0.46	2.02	0.058	0.50
2.37	27.8	0.68	3.20	0.045	0.76
1.93	102.7	0.57	1.72	0.051	0.33
1.55	62.0	1.75	5.64	0.081	1.28
0.77	34.4	1.80	5.32	0.088	1.35
0.41	532.4	2.77	2.08	0.125	0.42

Depth	118Sn/Zr	121Sb/Zr	133Cs/Zr	137Ba/Zr	182W/Zr
20.48	0.025	0.142	0.043	2.9	0.021
19.74	0.033	0.088	0.063	6.2	0.027
19.56	0.035	0.068	0.071	6.9	0.025
18.75	0.037	0.049	0.080	12.8	0.025
18.39	0.031	0.093	0.059	37.5	0.026
17.61	0.033	0.100	0.056	38.1	0.028
17.15	0.025	0.076	0.053	7.2	0.020
16.59	0.023	0.098	0.038	59.8	0.026
15.96	0.036	0.045	0.080	12.0	0.024
15.42	0.028	0.041	0.047	3.4	0.017
15.02	0.019	0.052	0.045	9.8	0.021
14.84	0.035	0.032	0.049	26.4	0.017
14.48	0.017	0.065	0.051	124.2	0.027
13.95	0.024	0.175	0.024	1.9	0.034
13.85	0.027	0.077	0.037	5.3	0.020
13.62	0.040	0.076	0.044	184.7	0.028
13.09	0.032	0.346	0.042	1.6	0.028
12.55	0.016	0.132	0.044	39.0	0.020
12.02	0.031	1.080	0.060	3.6	0.018
11.48	0.012	1.411	0.061	8.8	0.033
10.93	0.018	0.819	0.042	3.6	0.018
10.34	0.018	0.613	0.035	4.5	0.014
9.83	0.005	0.424	0.031	22.7	0.023
9.4	0.019	0.568	0.033	31.8	0.016
9.07	0.000	1.077	0.038	193.3	0.058
8.67	0.015	0.519	0.031	2.8	0.015
8.03	0.017	0.391	0.026	83.0	0.022
7.55	0.000	0.732	0.080	338.1	0.045
7.07	0.013	0.416	0.031	2.1	0.012
6.73	0.015	0.347	0.033	3.1	0.014
6.28	0.025	1.826	0.074	24.8	0.074
5.82	0.025	0.574	0.038	4.5	0.015
5.34	0.011	0.485	0.030	11.2	0.014
4.83	0.022	0.304	0.043	5.0	0.022
4.32	0.013	0.829	0.029	3.7	0.014
3.84	0.019	0.327	0.047	5.7	0.038
3.41	0.016	0.391	0.031	2.9	0.014
2.85	0.010	0.217	0.030	2.1	0.012
2.37	0.013	0.309	0.026	1.7	0.011
1.93	0.010	0.173	0.037	2.6	0.018
1.55	0.009	0.511	0.034	3.1	0.012
0.77	0.013	0.476	0.032	2.5	0.015
0.41	0.177	0.260	0.094	11.3	0.073

Depth	197Au/Zr	205Tl/Zr	208Pb/Zr	209Bi/Zr	232Th/Zr
20.48	0.0008	0.06	0.25	0.003	0.13
19.74	0.0013	0.04	0.31	0.004	0.20
19.56	0.0013	0.03	0.39	0.004	0.23
18.75	0.0016	0.05	0.50	0.005	0.19
18.39	0.0015	0.05	0.32	0.004	0.19
17.61	0.0016	0.07	0.52	0.005	0.14
17.15	0.0025	0.07	0.30	0.003	0.16
16.59	0.0013	0.11	0.49	0.004	0.09
15.96	0.0017	0.06	0.53	0.006	0.23
15.42	0.0013	0.11	0.42	0.006	0.13
15.02	0.0016	0.14	0.96	0.004	0.09
14.84	0.0016	0.14	0.58	0.006	0.10
14.48	0.0034	0.14	3.44	0.000	0.11
13.95	0.0022	0.11	0.11	0.003	0.03
13.85	0.0011	0.13	0.28	0.003	0.08
13.62	0.0040	0.16	0.62	0.000	0.08
13.09	0.0021	0.30	0.26	0.007	0.10
12.55	0.0023	0.10	0.58	0.005	0.11
12.02	0.0007	0.25	0.80	0.005	0.16
11.48	0.0772	0.22	0.43	0.000	0.20
10.93	0.0017	0.23	0.41	0.005	0.12
10.34	0.0007	0.27	0.57	0.004	0.09
9.83	0.0026	0.17	1.37	-0.003	0.07
9.4	0.0006	0.13	0.63	0.002	0.10
9.07	0.0385	0.38	3.96	-0.038	0.21
8.67	0.0008	0.09	0.52	0.003	0.11
8.03	0.0022	0.09	2.06	-0.002	0.08
7.55	0.0000	0.39	2.76	-0.018	0.23
7.07	0.0040	0.11	0.32	0.002	0.10
6.73	0.0007	0.17	0.34	0.003	0.11
6.28	0.0083	0.76	1.96	0.000	0.20
5.82	0.0044	0.16	0.49	0.002	0.11
5.34	0.0005	0.11	0.58	0.002	0.09
4.83	0.0031	0.20	0.93	-0.003	0.12
4.32	0.0010	0.09	0.73	0.002	0.09
3.84	0.0000	0.14	0.37	-0.003	0.12
3.41	0.0021	0.07	0.52	0.001	0.10
2.85	0.0000	0.12	0.35	0.001	0.08
2.37	0.0016	0.07	0.24	0.002	0.08
1.93	0.0000	0.14	0.19	-0.002	0.08
1.55	0.0006	0.16	0.38	0.002	0.10
0.77	0.0007	0.16	0.33	0.002	0.09
0.41	0.0104	0.20	0.79	0.000	0.30

Depth	238U/Zr	Ba/Zr	Ca/Zr	Fe/Zr	Mg/Zr
20.48	0.29	3.3	2044	263.3	62.5
19.74	0.19	6.8	1592	375.1	84.0
19.56	0.10	7.9	1204	438.7	90.7
18.75	0.47	14.4	22483	479.3	572.6
18.39	0.21	41.5	2036	376.7	96.6
17.61	0.52	42.9	6085	455.9	102.8
17.15	0.20	7.7	2020	368.8	146.5
16.59	0.84	62.3	7321	431.5	95.0
15.96	0.41	12.8	2311	578.3	87.0
15.42	0.40	3.8	3843	654.3	92.8
15.02	0.48	11.0	11924	590.1	187.1
14.84	0.34	29.1	13145	547.0	240.3
14.48	0.80	132.5	91936	870.1	724.7
13.95	0.13	2.4	1075	2960.6	129.7
13.85	0.26	5.9	2310	461.3	99.2
13.62	0.50	201.0	135524	562.2	2310.1
13.09	0.68	1.9	2659	543.1	65.5
12.55	0.44	41.5	14164	316.8	231.3
12.02	2.42	4.9	16645	338.9	144.4
11.48	6.27	13.9	137610	399.1	780.8
10.93	3.37	4.3	10885	352.7	140.7
10.34	2.24	5.1	9119	426.0	154.1
9.83	4.35	25.7	81803	329.7	537.0
9.4	2.23	33.5	15692	206.1	171.3
9.07	30.04	225.0	653795	477.4	8154.6
8.67	0.96	3.4	11343	169.4	123.2
8.03	1.14	87.9	72076	217.5	532.1
7.55	2.21	360.8	296665	870.1	2964.0
7.07	1.50	2.7	11678	170.7	121.2
6.73	1.42	3.6	9567	243.0	118.0
6.28	3.32	35.6	266964	939.6	1944.8
5.82	2.61	5.2	21596	217.4	166.6
5.34	1.29	12.4	15297	170.6	150.2
4.83	1.22	9.0	99685	384.9	1103.7
4.32	1.50	4.4	14438	154.2	130.1
3.84	1.44	8.5	101571	367.7	1059.1
3.41	1.23	3.6	20819	184.1	193.8
2.85	0.60	2.7	17068	267.6	177.0
2.37	0.87	1.9	7196	134.6	81.2
1.93	0.61	4.5	62544	332.0	673.9
1.55	2.79	3.7	15177	215.1	140.0
0.77	2.67	2.9	8506	195.1	96.8
0.41	1.58	22.4	353329	503.6	3015.5

Depth	Mn/Zr	Na/Zr	Ti/Zr
20.48	12.4	44.6	28.3
19.74	14.4	53.7	36.7
19.56	15.0	57.1	39.6
18.75	35.2	84.4	44.6
18.39	14.9	55.8	38.0
17.61	25.3	93.3	36.5
17.15	14.2	53.2	31.5
16.59	25.1	79.5	25.1
15.96	20.0	70.5	36.1
15.42	17.3	58.9	31.5
15.02	25.8	70.1	38.2
14.84	28.1	83.4	46.0
14.48	109.8	153.2	72.8
13.95	92.3	446.9	143.7
13.85	18.1	73.4	36.8
13.62	126.9	170.2	83.4
13.09	14.5	51.0	63.2
12.55	21.1	39.2	33.2
12.02	23.4	42.1	38.3
11.48	105.0	45.0	88.4
10.93	18.1	41.1	34.5
10.34	15.5	37.9	38.9
9.83	66.1	25.0	59.2
9.4	19.4	29.6	28.2
9.07	465.0	43.4	277.9
8.67	13.6	24.2	24.4
8.03	54.1	11.6	43.8
7.55	210.5	-8.8	179.8
7.07	14.0	18.2	23.9
6.73	12.8	25.4	25.5
6.28	177.0	-103.4	165.0
5.82	21.9	24.1	27.0
5.34	15.2	15.0	23.0
4.83	67.5	-33.4	79.2
4.32	14.6	15.5	22.1
3.84	68.0	-36.1	69.9
3.41	19.5	16.4	29.4
2.85	15.7	11.9	32.0
2.37	8.7	12.6	18.4
1.93	45.3	-5.1	56.1
1.55	17.1	12.5	25.7
0.77	10.9	11.6	21.6
0.41	228.1	-103.7	140.2

The following are the Zr-normalized data for the Totumo-3 Well core.

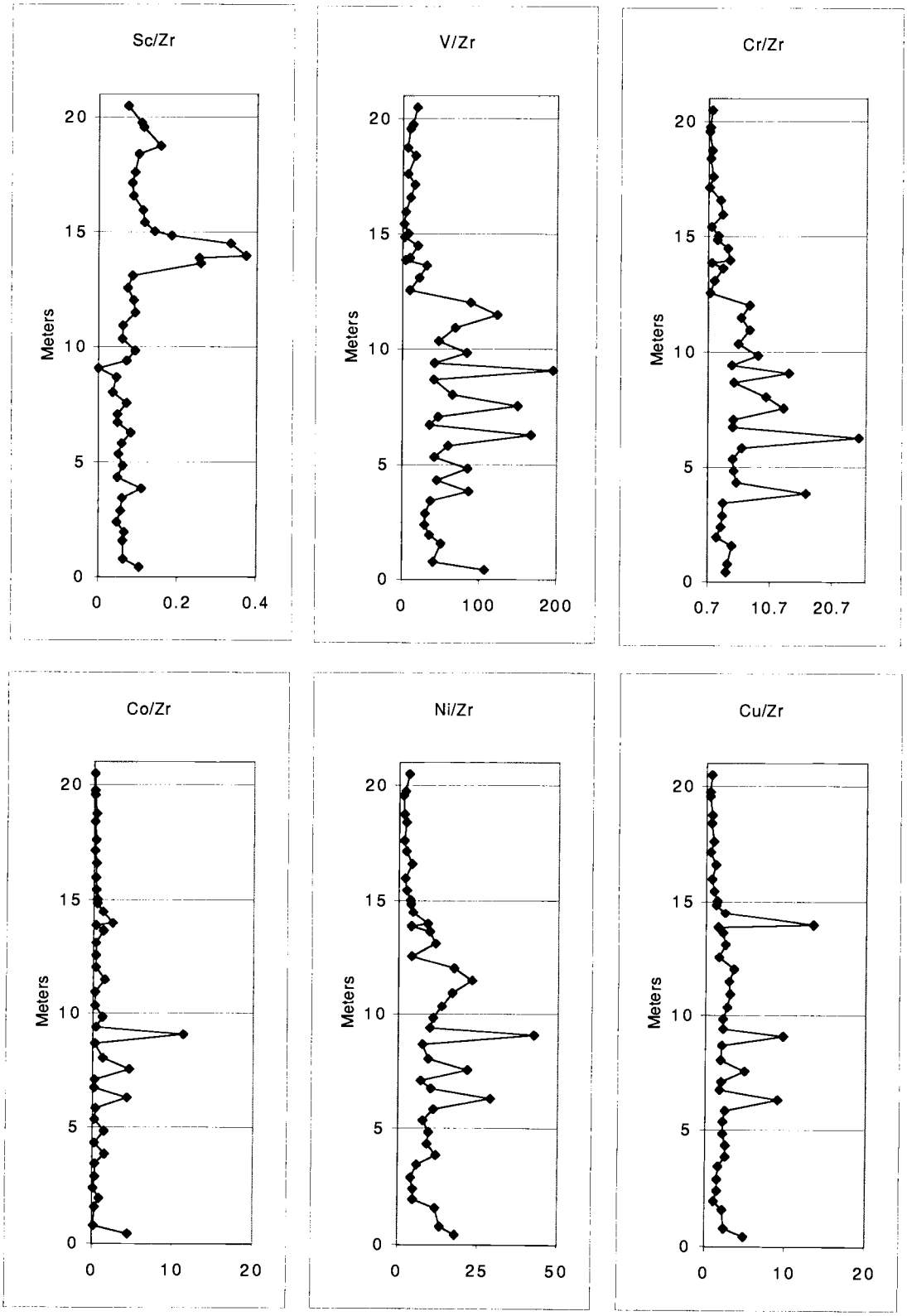

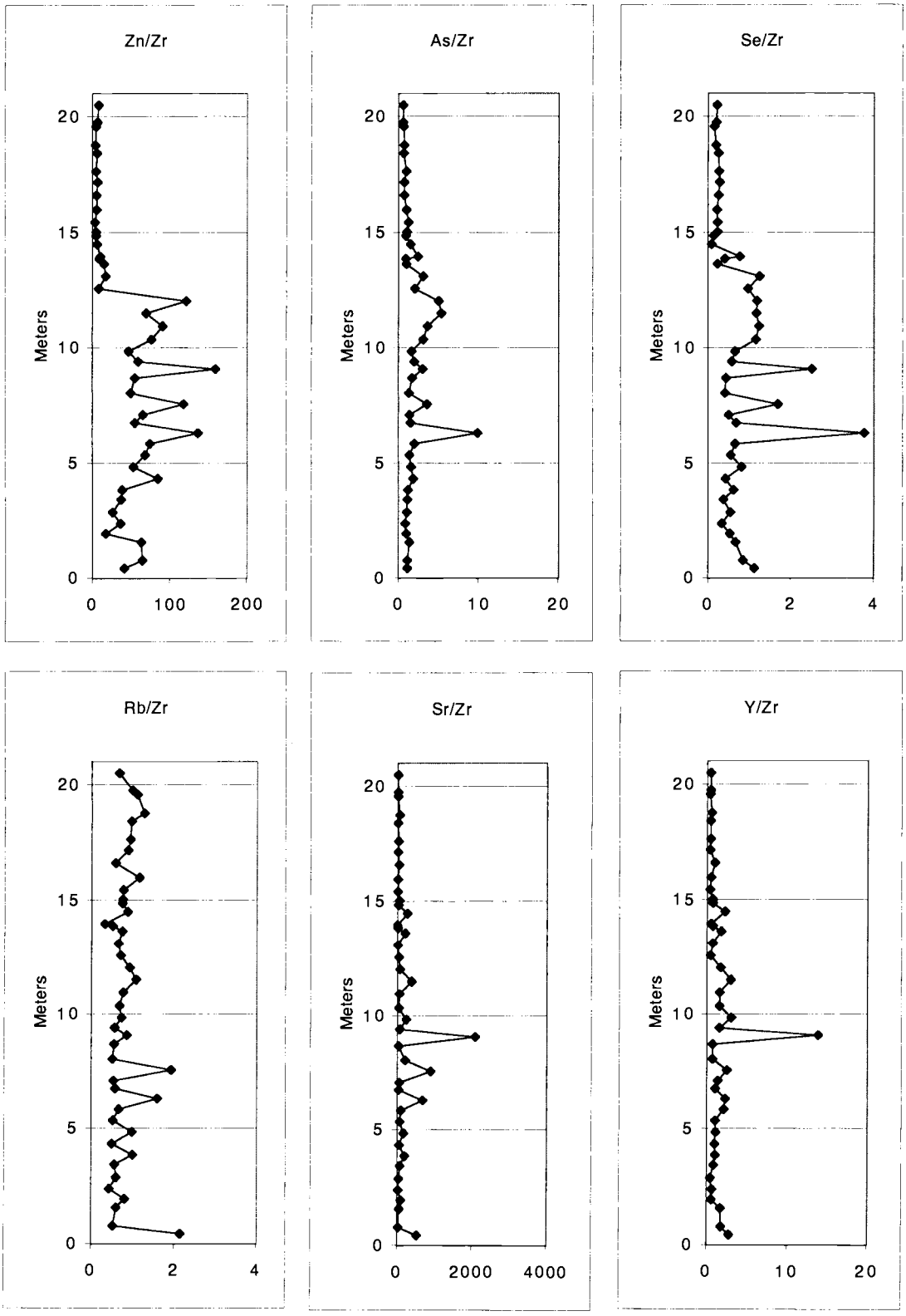
Zn/Zr
Meters
0
5
10
15
20
0
100
200
As/Zr
Meters
0
5
10
15
20
0
10
20
Se/Zr
Meters
0
5
10
15
20
0
2
4
Rb/Zr
Meters
0
5
10
15
20
0
2
4
Sr/Zr
Meters
0
5
10
15
20
0
2000
4000
Y/Zr
Meters
0
5
10
15
20
0
10
20

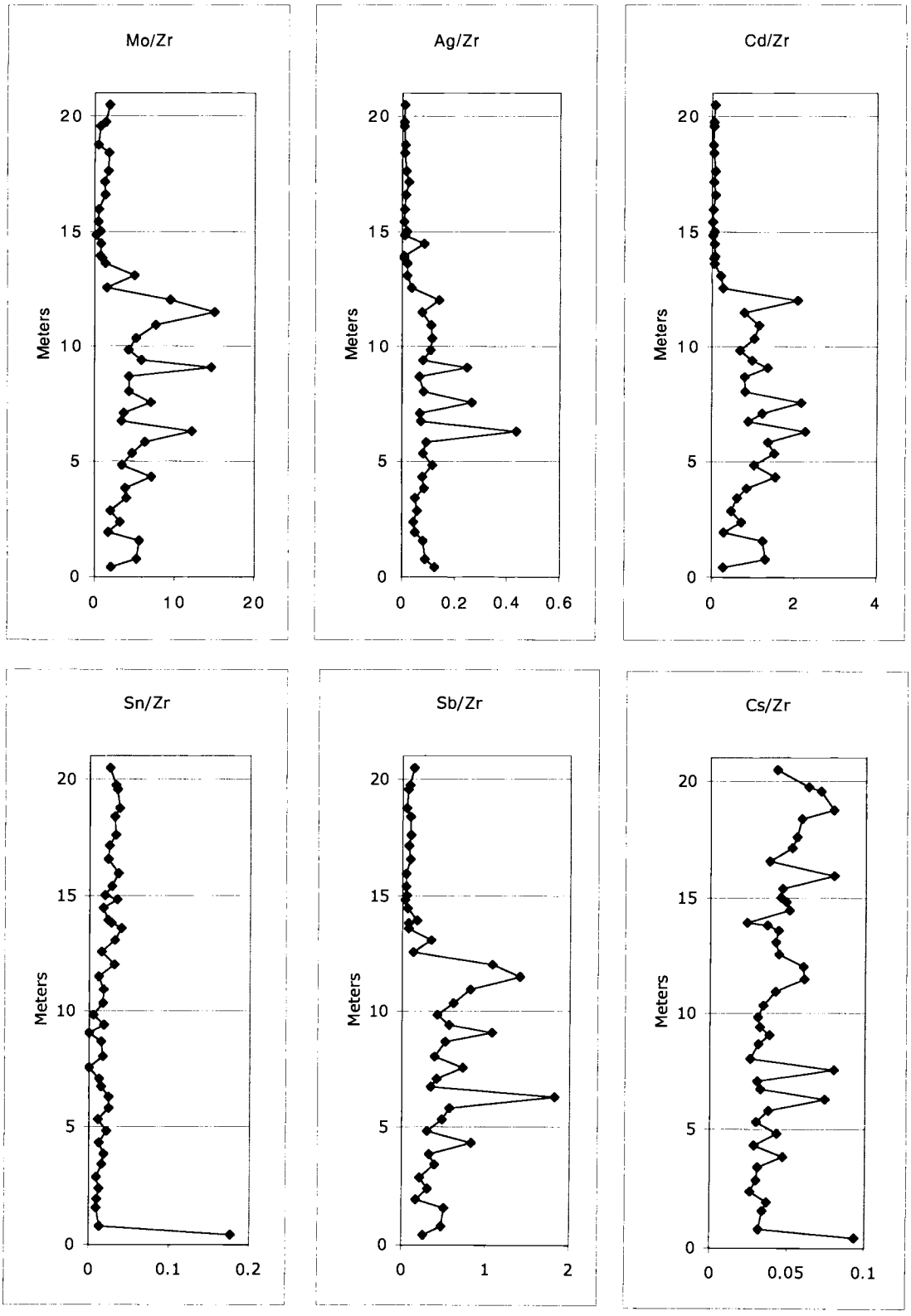
Mo/Zr
Meters
0
5
10
15
20
0
10
20
Ag/Zr
Meters
0
5
10
15
20
0
0.2
0.4
0.6
Cd/Zr
Meters
0
5
10
15
20
0
2
4
Sn/Zr
Meters
0
5
10
15
20
0
0.1
0.2
Sb/Zr
Meters
0
5
10
15
20
0
1
2
Cs/Zr
Meters
0
5
10
15
20
0
0.05
0.1

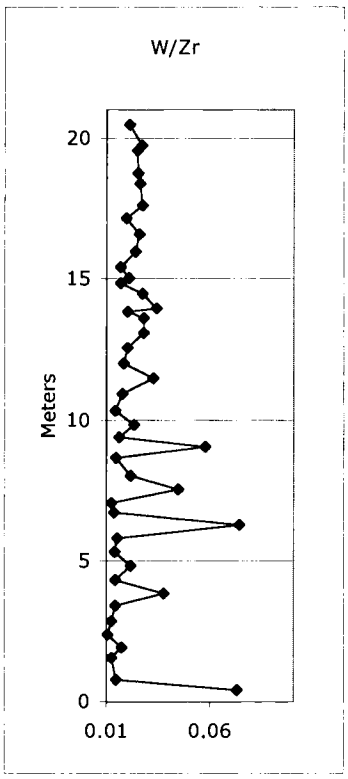
W/Zr
Meters
0
5
10
15
20
0.01
0.06

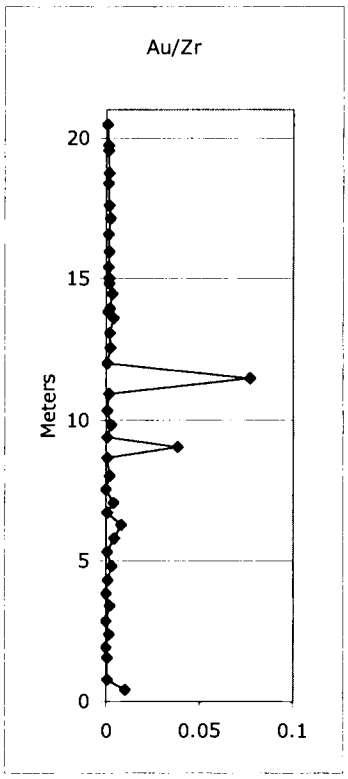
Au/Zr
Meters
0
5
10
15
20
0
0.05
0.1

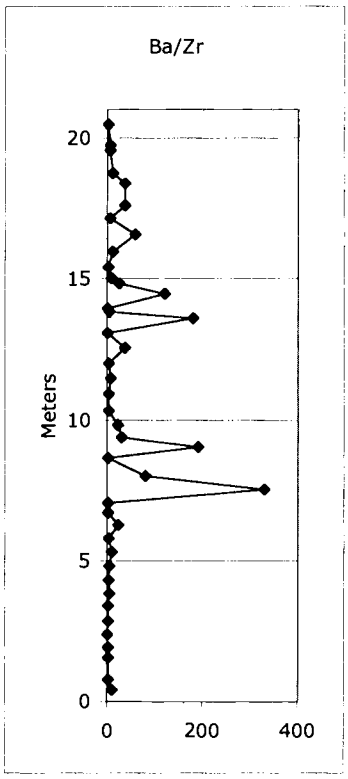
Ba/Zr
Meters
0
5
10
15
20
0
200
400

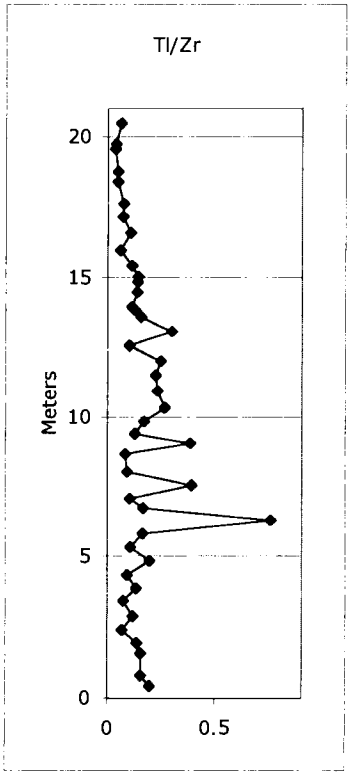
Tl/Zr
Meters
0
5
10
15
20
0
0.5

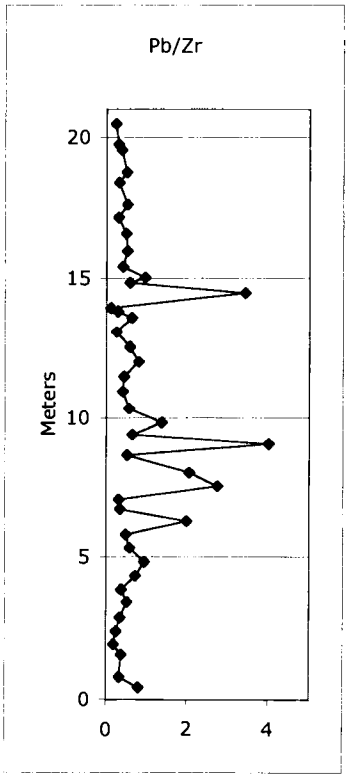
Pb/Zr
Meters
0
5
10
15
20
0
2
4

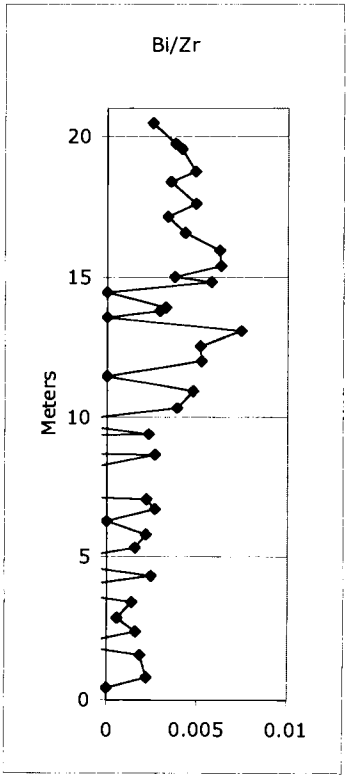
Bi/Zr
Meters
0
5
10
15
20
0
0.005
0.01

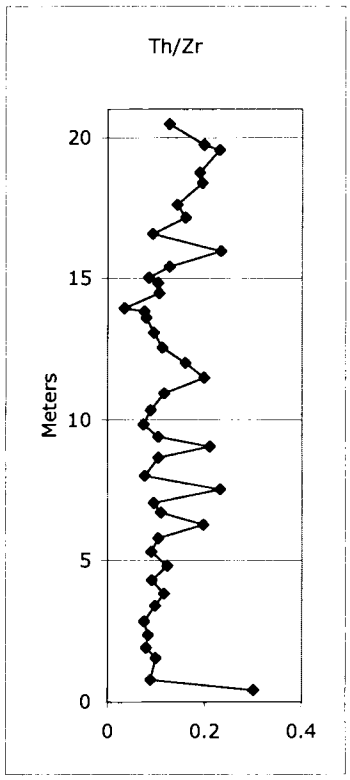
Th/Zr
Meters
0
5
10
15
20
0
0.2
0.4

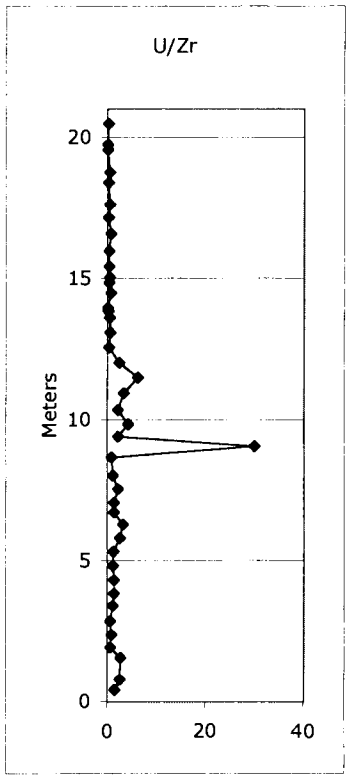
U/Zr
Meters
0
5
10
15
20
0
20
40

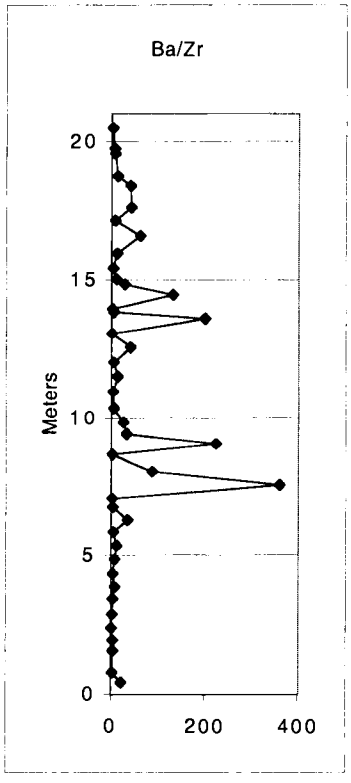
Ba/Zr
Meters
0
5
10
15
20
0
200
400

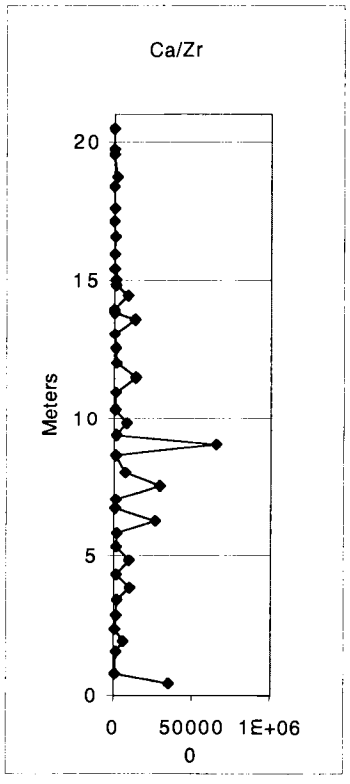
Ca/Zr
Meters
0
5
10
15
20
0
50000
1E+06
0

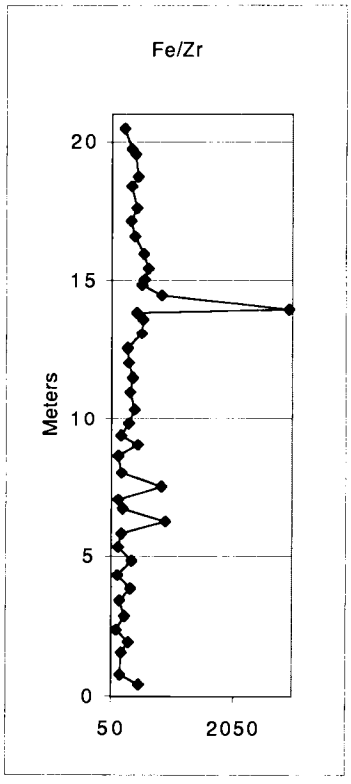
Fe/Zr
Meters
0
5
10
15
20
50
2050

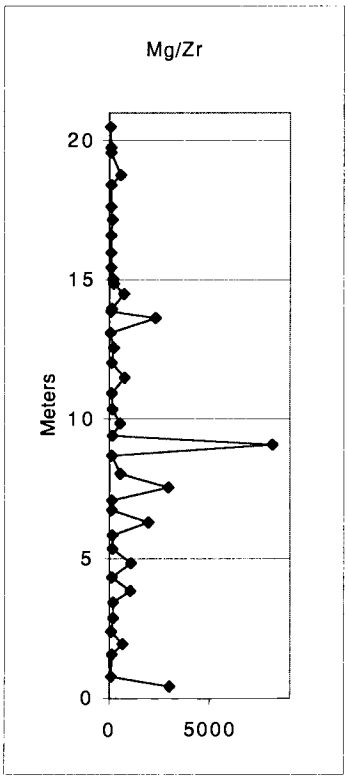
Mg/Zr
Meters
20
15
10
5
0
0
5000

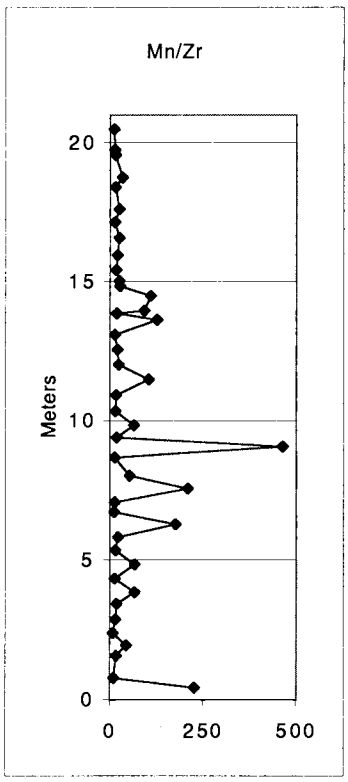
Mn/Zr
Meters
20
15
10
5
0
0
250
500

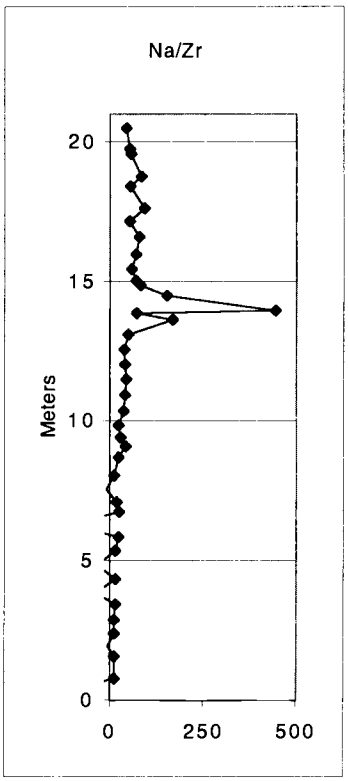
Na/Zr
Meters
20
15
10
5
0
0
250
500

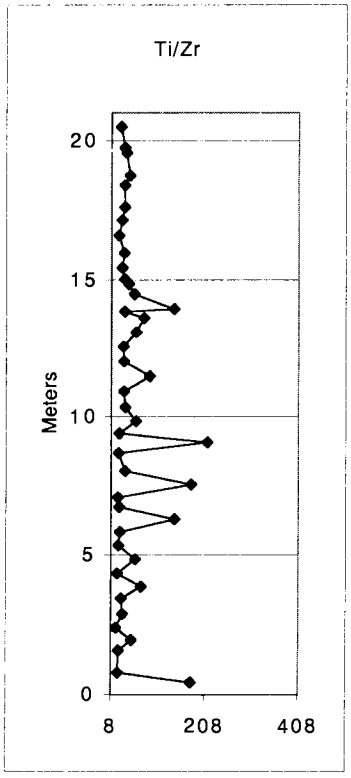
Ti/Zr
Meters
20
15
10
5
0
8
208
408